MEASUREMENT OF NORMAL AND SHEAR STRESSES AT THE BASE OF A RIGID FOOTING FOUNDED ON QUARTZ SAND

by

Samuel Onyeabor Nwabuokei
B.Eng. (Hons)
Ahmadu Bello University
Zaria

Submitted in partial fulfillment of the
requirements for the degree of
Master of Applied Science

Department of Civil Engineering
School of Graduate Studies
University of Ottawa
Ottawa, Canada

ABSTRACT

This study deals with the measurement of normal andsshear stress distribution at the base of a rigid "rough" footing located in sand. The model footing was equipped with six modified Cambridge load cells and the sand was deformed under a plain strain condition. The load cells were calibrated under different loading conditions and load magnitudes after they had been installed in the footing calibration curves for normal point and line loads at different eccentricities and shear loads are presented - Appendix A. The property of the quartz sand was determined by a previous investigator (Hasnain 1974). All footing tests were carried out in a large sand-box and were performed in conjunction with tests to determine the bearing capacity factors of footings on or near slopes. The study presented here deals exclusively with the calibration of the Cambridge load cells and the measurements of normal and shear stress distributions at different load levels.

The experimental results are also compared to available theories. The relationship between the applied load and contact stresses and the relationship between the contact stresses have also been presented graphically.

DEDICATION

I dedicate this thesis for the purpose of

Peace amongst Men

ACKNOWLEDGEMENTS

The writer would like to express his sincere gratitude to his supervisor, Dr. G. E. Bauer, Associate Professor, Department of Civil Engineering, for his helpful suggestions and guidance during the preparation of this thesis.

The writer is extremely grateful to Dr. J. D. Scott and Dr. D. H. Shields, Professors, Department of Civil Engineering, University of Ottawa for their comments and assistance.

Thanks are also due to the Federal Government of Nigeria for financial assistance.

His thanks also go to Mr. J. H. Deschenes, a Ph.D. student engaged in the determination of the bearing capacity of footing on slopes in the sandbox for making the testing facility and the bearing test results available to the writer.

The help given by Mr. P. Lai (graduate student), Mr. Oktai Siret (senior technician responsible for the sandbox project), and the Staff of the Civil Engineering Department Machine Workshop is also acknowledged.

Acknowledgement is extended to Mrs. Wanda Storto who has ably and patiently typed the manuscript.

Finally, the writer extends his most sincere appreciation to his parents, brothers and sisters for their continued encouragement.

TABLE OF CONTENTS

LIST OF TABLES

LIST OF FIGURES

CHAPTER 1

INTRODUCTION

1.1 General

Loads are usually transferred from structures to the supporting soil by means of transition members of which the commonest being employed today is the spread foundation or footing. The dimensioning and the proper calculation of the strength of these transition members cannot be accurately accomplished without a full knowledge of the following:

1. Magnitude of load.
2. Direction and point of application of load.
3. Deformation of underlying soil, and
4. The reaction pressure caused by the load.

In this study, the reaction pressure which is usually the most difficult to determine, will be referred to as the contact stresses which consist of the normal stress, eccentricity of the normal stress and the shear stress.

When a transition member, such as a footing, resting on a soil is loaded, stresses are developed within the soil. An increase in load produces settlements under the structure and heaves around it. The settlement depends on the compressibility characteristics of the soil and as would be anticipated, the shape of the settlement versus load curve and the elastic properties of the soil are essential factors in the contact stress distribution.

Usually in the field, there is always some friction between the footing and the soil. This has been carefully simulated in the footing provided by gluing some sand on the footing's surface. As would be expected, the resultant of the contact stresses would not be vertical and thus would possess horizontal and vertical components referred to in this study as the shear and normal stresses, respectively. However, since there is a large variation in the normal stress distribution an eccentricity would be anticipated.

Consequently, the determination of the magnitude, direction and point of application of the above stresses (contact stresses) has necessitated the construction of a rigid footing with six modified Cambridge cells at the University of Ottawa which will be tested in a steel box filled with sand at different relative densities. The present study is part of a large project on the bearing capacity of sand being undertaken by the Geotechnical Group of the Civil Engineering Department of the University of Ottawa.

Earlier experimental investigations on the stress distribution in the contact layer between a footing and soil has indicated that a number of factors affect their nature and shape. Among these factors are the following:

1) Magnitude of loading under a virgin or reloading condition.
2) Foundation depth.
3) Distance to firm base.
4) Height of groundwater level.
5) Size of foundation.
6) Shape of foundation.

7) Rigidity of foundation.

8) Soil density.

9) Load application rate.

10) Load application time.

Earlier experimental investigations with load as the prime factor indicated that the shape of the normal stress distribution at the interface between a footing and a soil medium gave opposite results depending on the type of soil. The results were predominahtly concave parabolic distributions for clayey soil. On the other hand, the results for tests in sand gave curves which varied from a convex parabolic distribution to w-shaped curves depending on the cohesion in the sand and the depth of embedment of the foundation.

However, the conclusion which can be derived is that, the normal stress distribution under a foundation is not uniform. This might lead to a conservative design in sand and a probable unsafe situation in clay under the presently used design load.

Experimental investigations have also shown that the shear stress has a convex parabolic distribution which increased towards the edges of the footing. These edge stresses also increased as the load increased and decreased as the normal stress decreased.

Theoretical solutions have been proposed by Boussinesq (1885), Schultze (1961), Sedykh (1964), Schweickert (1964) and Salvadurai (1976). Their results are at best valid for cohesive

materials which exhibit a linear elastic rigid plastic characteristics. Thus, any accurate theoretical analysis of the contact stress distribution in a granular medium must wait for a proper clarification of the effects of the above mentioned factors.

1.2 Statement of the Problem

In this study, the six modified Cambridge load cells, already installed in the footing, had to be calibrated in their true operation condition.

The distribution of the contact stresses (normal stress, the eccentricity of the normal stress and shear stress) under the centre segment of a rigid rough strip footing (divided into three-two feet sections) provided with the six modified Cambridge load cells had to be investigated.

The tests were performed in the University of Ottawa sandbox with measurements made at the sand surface in order to study the effects of virgin loading and density variations on the stresses at the base of the footing.

As has been enumerated previously, the contact stress distribution depends on a number of factors. Thus, every effort was made to maintain these factors constant, with the exception of the factor being investigated.

The writer also thought it necessary to obtain the actual load-settlement relationship in order that the effect of the stress-

strain of the granular medium on the contact stress distribution could be deduced.

From an earlier study performed by Doohan (1975), it was found cumbersome and time-consuming to use the Kiethly instrument (model 155) null detector microvoltmeter as a recording device. Thus, a hook-up of the footing to a multichannel digital strain indicator was undertaken. This did almost eliminate the time-lag effect in the strain readings for the six modified Cambridge load cells.

Also, an effort has been made to study and explain the cause for the existence of the net shear forces indicated by Doohan (1975). Thus, as a first step the detrimental factors introduced by the experimental arrangement were eliminated as much as possible. This was brought about by a modified loading system coupled with a system that spreads the sand into the sandbox at constant density.

It was also thought necessary to investigate the conclusions derived by Arthur and Roscoe (1961) on the independence of the values of the Cambridge load cells calibration. Constants on the nature of loading (line load, point load and surface load) and if their conclusions were also valid for the modified Cambridge cells, especially when calibrated as an integral part of the footing.

As a minor section of this thesis, the experimental and theoretical results have been compared. The graphical relationship between contact stresses and applied loads have also been given.

1.3 Outline of Thesis

The thesis consists of eight chapters in which Chapter 2 gives a review of some of the existing experimental and theoretical studies. Chapter 3 describes the model footing and its components. Chapter 4 deals with the calibration of the load cells mounted on the footing for point load, line load and shear load followed by the mathematical operations necessary for the determination of the load cell constants. Also in this chapter, the effects of factors such as load, eccentricity and temperature on the calibration constants have been elucidated.

Chapters 5, 6 and 7 deal with the footing tests in the sand box, the results and finally the analysis of the results and subsequently the computations for the normal stress, shear stress and eccentricity.

The thesis has been concluded by deductions made from the study followed by suggestions for further research on the contact stress distribution between a rigid rough footing and sand.

CHAPTER 2

On account of the mounting interest on the nature and shape of the distribution of contact stresses, a brief review will be given here of some of the model scale and full scale experiments that have been performed.

Some of the available theoretical analysis on contact stress distribution will also be reviewed. This will be followed by a discussion in which the effects of the factors enumerated in Chapter 1 will be scrutinized.

2.1 Experimental Investigations

This review will be subdivided into two sections: (A) model scale tests, (B) full scale tests.

(A) Model Scale Tests

Kogler and Scheidig (1927) investigated the normal stress distribution on a 63 cm diameter concrete footing at various depths in sand. They obtained a convex parabola. They also found out that loading the ground outside the footing, increasing the density of the soil and using greater foundation depths merely flattened the convexity of the distribution.

Faber (1933) made normal stress distribution measurements on a 12" (32.75 cm) diameter footing in sand. He obtained convex parabolae at depths of 0 cm to 90 cm for the normal stress distribution

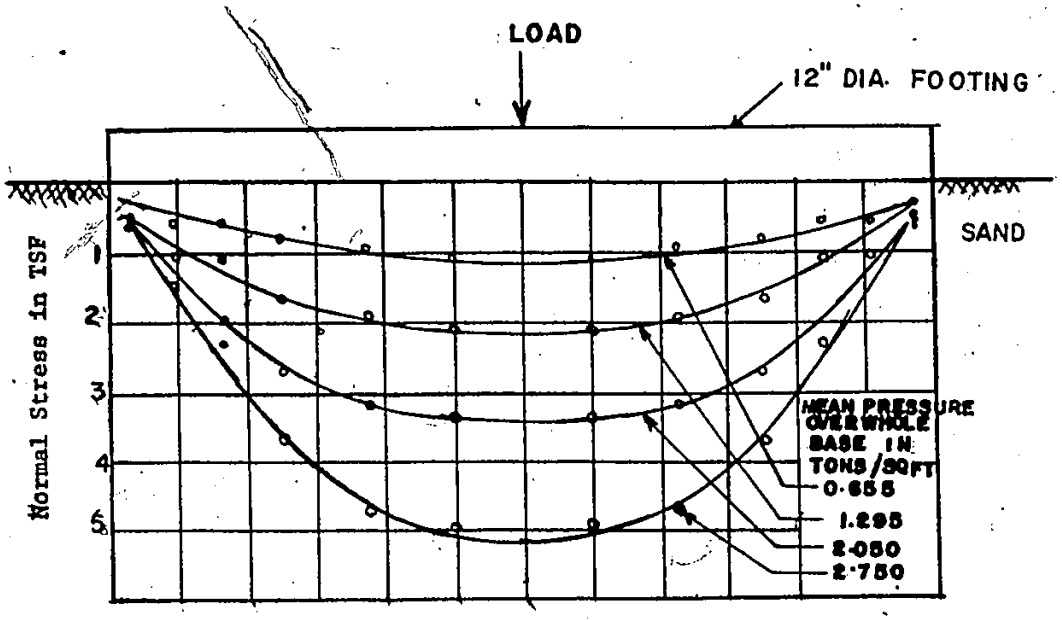

FIGURE 2·1·1 NORMAL STRESS DISTRIBUTION AFTER FABER (1933)

under various magnitudes of load. Some of his results are shown in Figure 2.1.1.

Ohde (1942) measured the normal stress on a 20 cm x 40 cm board footing on sand. He obtained a concave parabola, quite contrary to the results of the researches indicated above.

In 1963, Krivorotov determined the normal stress on 14 cm, 20 cm and 30 cm wide footings on dry river sand. He obtained saddle-shaped distribution whose convexity increased with load. He also found out that a reduction in the density of the sand made the saddle-shape of the curves less pronounced. Typical curves are shown in Figure 2.1.2.

Helenelund (1966), from the work done by Puskala and Schmidt on a 30.5 cm diameter and 30 cm x 30 cm metal footings, he came to the conclusion that normal stresses on rigid footings on sandy soils are fairly uniformly distributed, while in fine sand, the edge stresses are higher because of the apparent cohesion. He also indicated that the normal stresses in the central region of the footing increases faster than the edge stresses with an increase in load. He also pointed out that an increase in foundation depth and subsoil density merely reduces the yielding and thus increases the edge stresses while an increase in water level reduces the edge stresses because of the loss in apparent cohesion.

Koichi, Akai and Hideo Otsuki (1974) made measurements on a 20 cm diameter footing provided with four semi-conductive type pressure cells, on sandy loam and sandy soils.

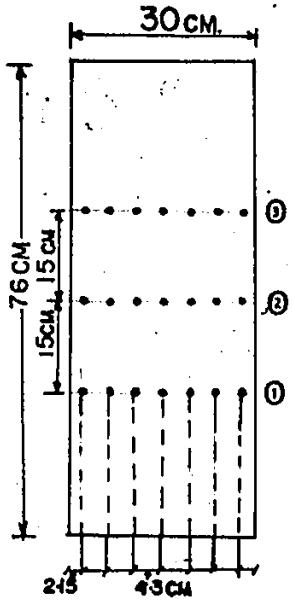

ARRANGEMENT OF DYNAMOMETERS IN SAND TANK IN BOTH CASES

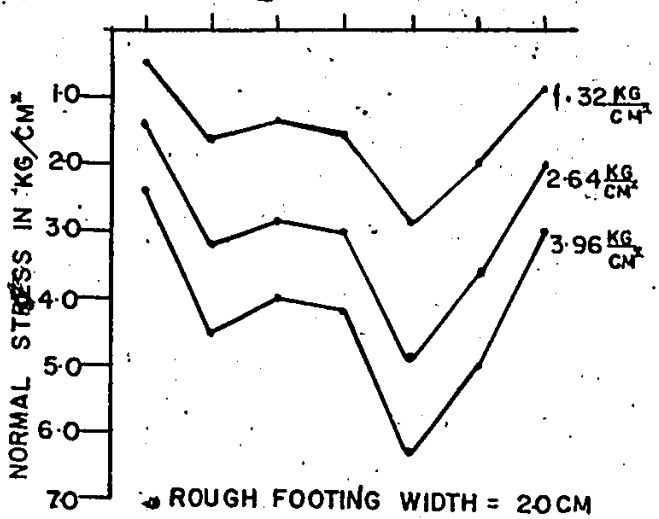

ROUGH FOOTING WIDTH = 20CM

AVERAGE NORMAL STRESS FOR ①, ② & ③

APPLIED STRESS P_N KG/CM²	1·32	2·64	3·96
MEAN REACTIVE STRESS P_r	1·51	3·01	4·20
$\frac{P_r - P_N}{P_N} \times 100$	↑11·4	↑11·4	↓6·0

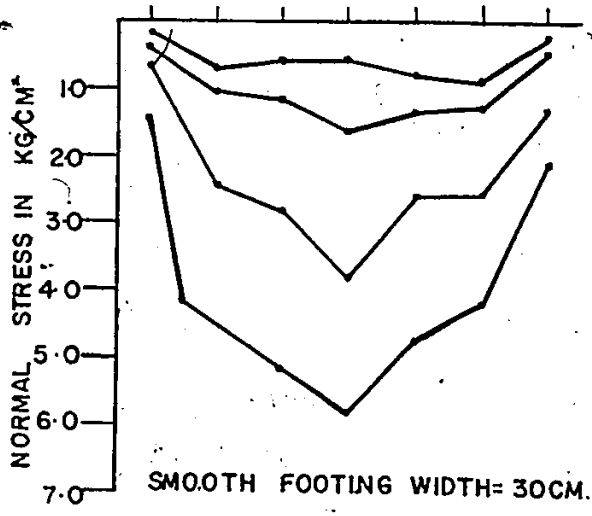

SMOOTH FOOTING WIDTH= 30CM.

AVERAGE NORMAL STRESS FOR ①, ② & ③

P_N KG/CM²	P_r KG/CM²	$\frac{P_r - P_N}{P_N} \times 100$
0·57	0·58	-12·3
1·34	1·04	-22·5
2·58	2·33	-13·2
4·03	3·99	-1·0

FIGURE 2·1·2 NORMAL STRESS DISTRIBUTION AFTER KRIVOROTOV (1963).

In the former soil, for virgin loading they obtained a normal stress distribution that was almost uniform over the central region, and this uniformity increased with load. The fringe stresses which were smaller than the stresses in the central region were found to increase with load levels. However, on repeated loading, the fringe stresses were found to decrease parabolically at lower load levels.

In sandy soil, a nearly uniform normal stress distribution was obtained for lower load levels, while the fringe stresses decreased remarkably at higher load levels near the ultimate load of the sand. Their results are shown in Figure 2.1.3.

In 1972, Hartikainen reported normal stress distribution measurements done at Helsinki University for 112 test loads. The tests were performed in order to determine the effects of load magnitude, ground water table, foundation depth and reloading on the normal stress distribution. Their results indicated that these factors affect the normal stress distribution. It was shown that for virgin loading at the surface of the dry sand that the normal stress distribution changed from concave to convex as the load increased to ultimate load. At reloading, the distribution was convex. In moist sand, they found that the normal stress distribution was concave and hardly changed with load.

He also reported that, at lower load levels the shear stresses are higher at reloading than at virgin loading while at their highest

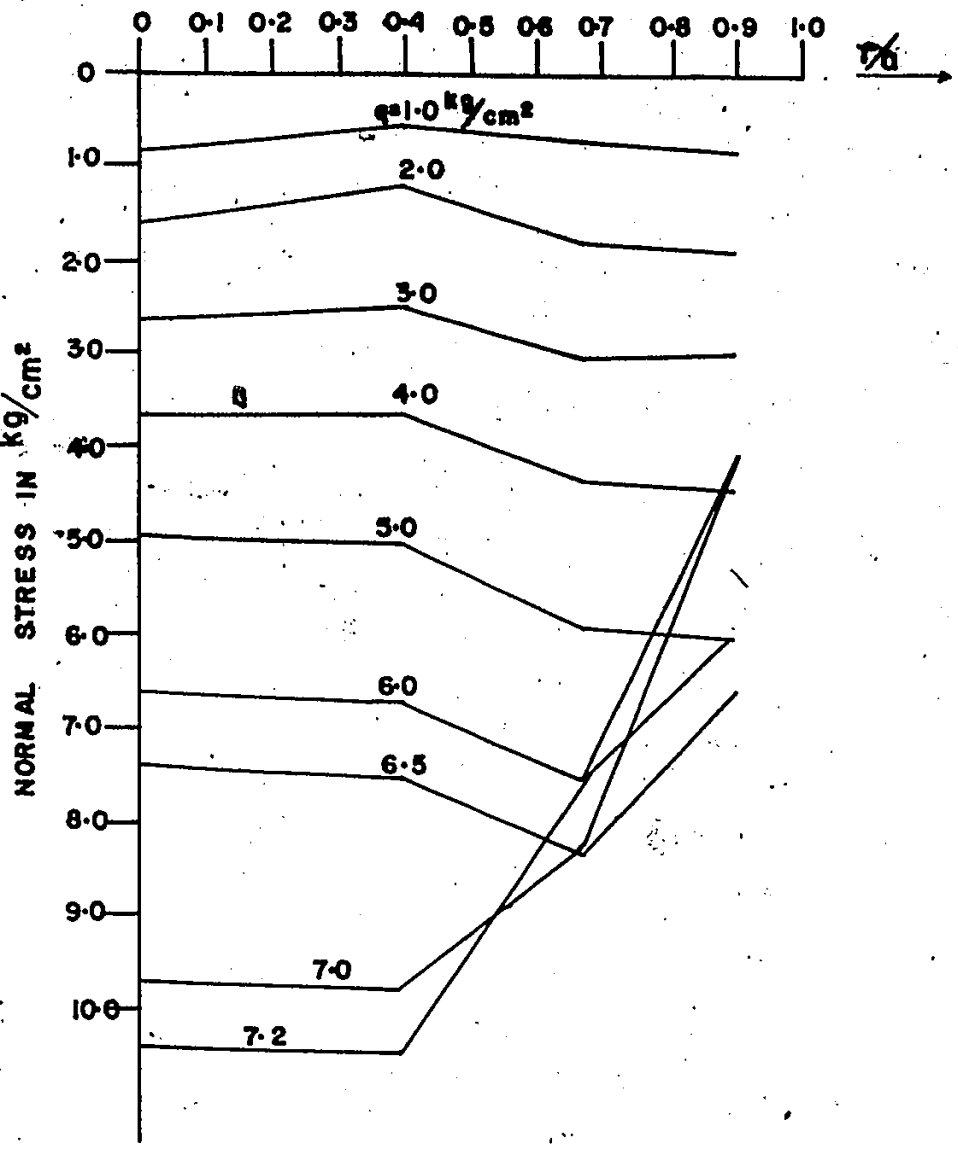

FIGURE 2.3.1 DISTRIBUTION OF NORMAL STRESS AFTER AKAI AND OTSUKI (1974)

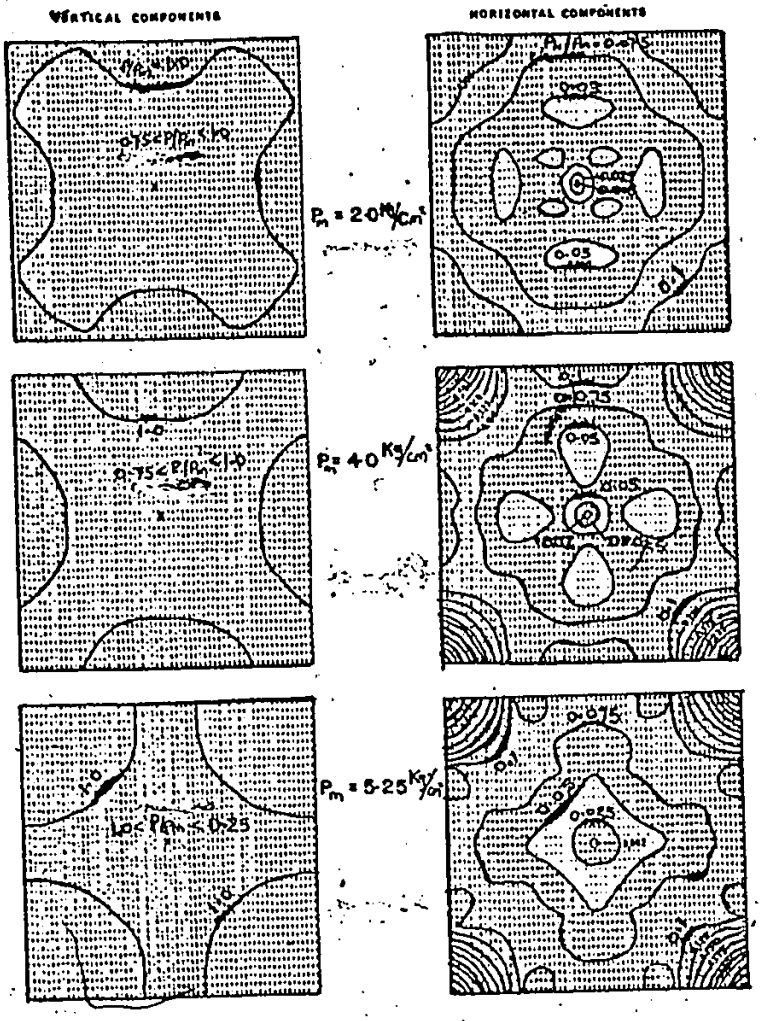

P = NORMAL STRESS

P_h = HORIZONTAL STRESS

P_m = MEAN NORMAL STRESS

FIGURE 2·1·4 CONTACT STRESSES AFTER HARTIKAINEN(1972) FOR SURFACE TESTS.

loads, the shear stress was equally well distributed both at virgin loading and reloading conditions.

Some of his results are shown in Figure 2.1.4.

(B) Full Scale Tests

Burger (1932) made measurements on a bridge pier founded on gravelly sand at a depth of 9.3 m. The pier had eight pneumatic pressure cells. He obtained a concave normal stress distribution. However, the applied load was relatively small in comparison to the ultimate load of the soil. His results are shown in Figure 2.1.5.

Siemonsen (1942) measured the contact stresses on a 3.5 m x 3.5 m square footing provided with Maihak pressure cells. He found that the normal stress at the edges of the diagonal increased with load. The highest load was in a range that could produce elastic deformation of the soil. The footing was at a depth of 8 m and 0 m very dense sand with the ground water table above the foundation level.

Siedek (1948) investigated the normal stress distribution under a 3.5 m x 3.5 m footing having thirteen Maihak pressure cells, on fine sand below the ground water table. He obtained a concave distribution within the load range in which he operated. The normal stress distribution is shown in Figure 2.1.6.

Muller-Hande (1967) measured the normal stress distribution under the foundation slab of a Berlin railway track on coarse sand. Readings were taken at each stage of construction and the authors concluded that:

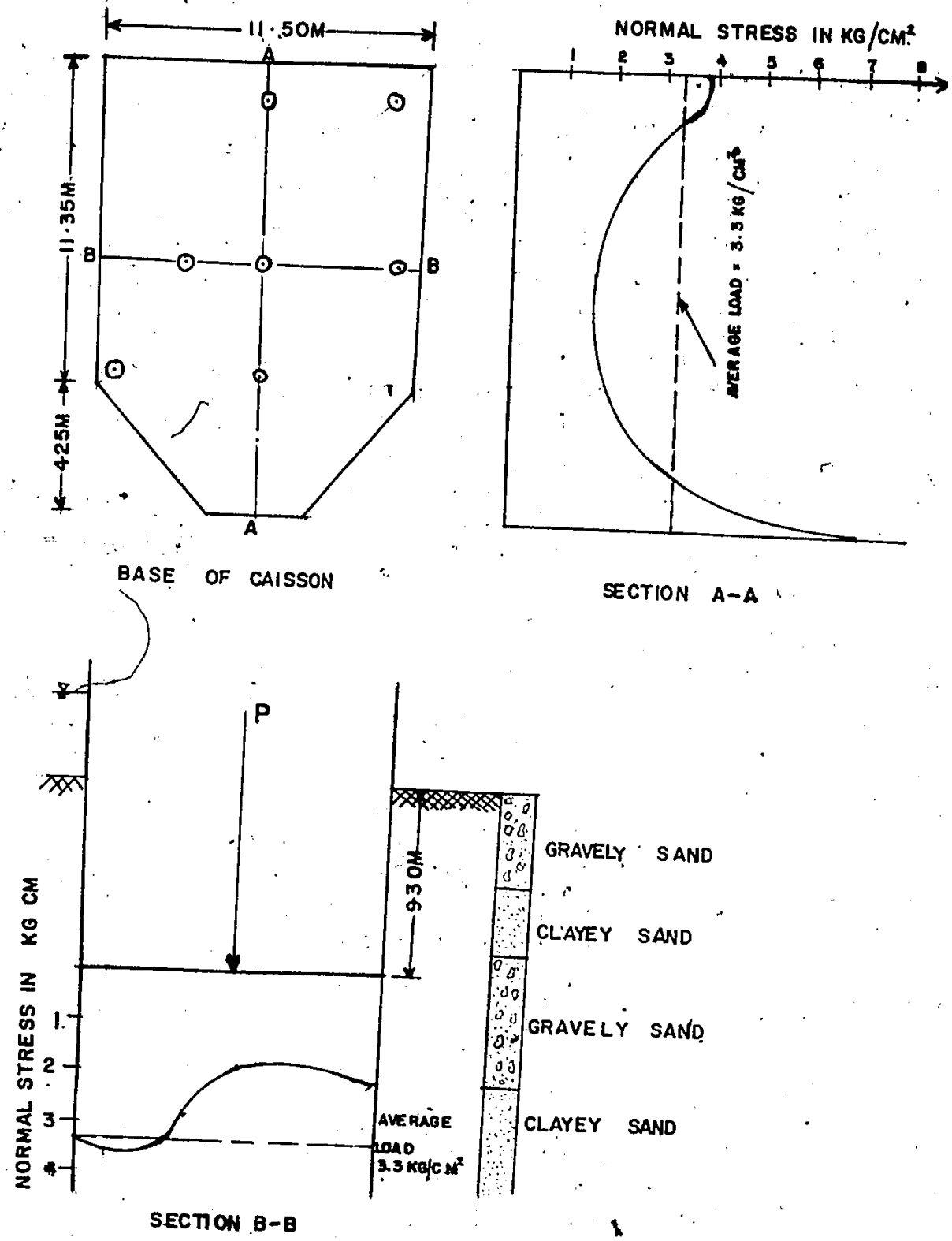

FIGURE 2·1·5 NORMAL STRESS DISTRIBUTION UNDER A CAISSON AFTER BURGER (1932).

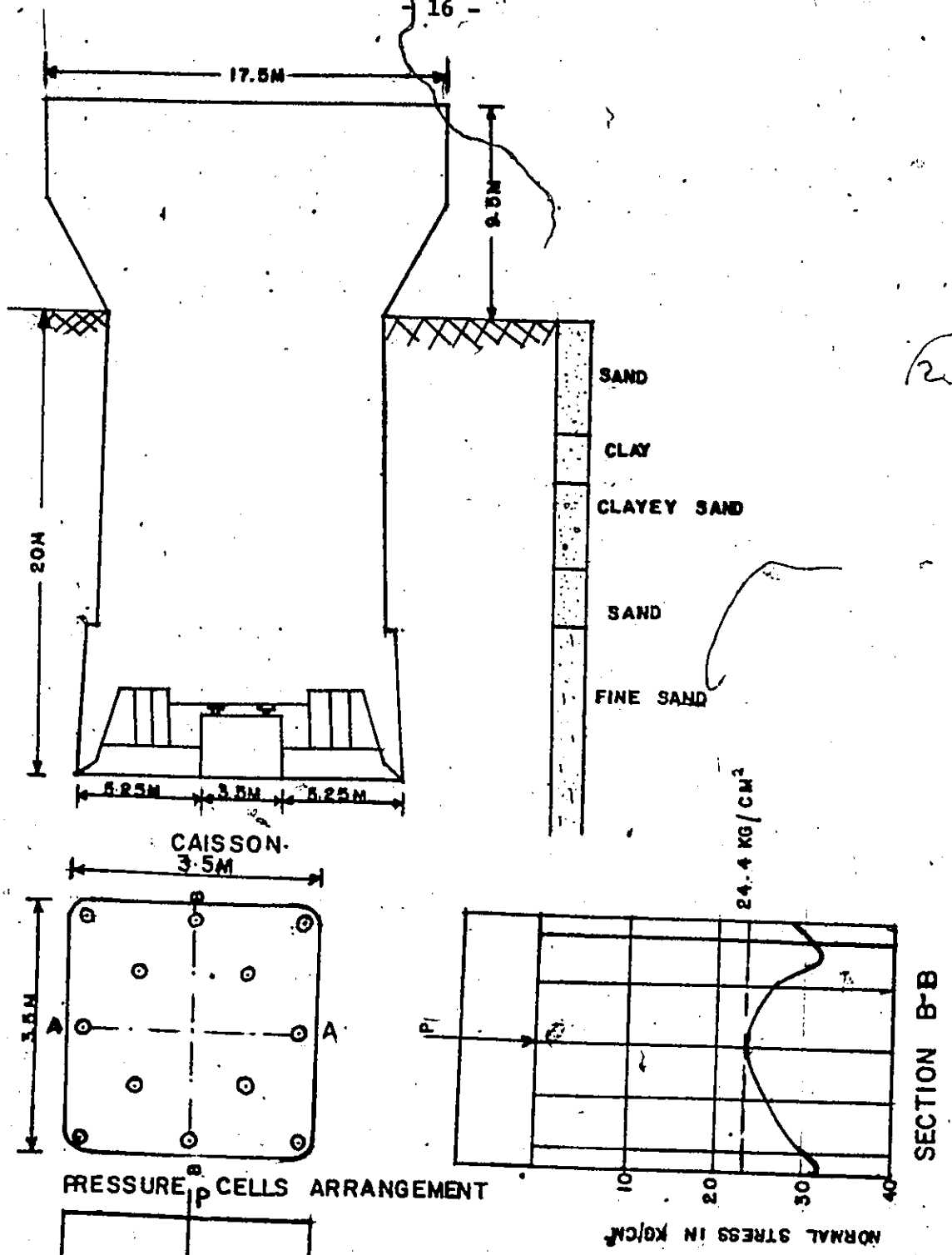

FIGURE 2·1·6 NORMAL STRESS DISTRBUTION UNDER A CAISSON AFTER SIEDEK (1948).

(1) The actions between the deformation of the structure and the foundation soil cannot be estimated by calculation.

(2) The nature of the transition member base had a notable role to play on the stress distribution.

(3) The normal stress distribution was concave in the transverse direction and convex in the longitudinal direction.

Muhs (1961) obtained a convex normal stress distribution under a 1 m x 1 m footing, provided with six pressure cells, on sand. The shape of the distribution might be attributed to the high initial load of 4.0 kp/cm^2 which might have caused plastification of the sand grains.

Bub (1963) investigated the normal and shear stresses under a 0.8 m x 2 m footing, that had twelve Maihak pressure cells and four cells capable of shear stress measurement installed in it, in dry sandy soil. Tests were carried out at the surface and at various depths. He obtained a concave parabola which decreased in the central part with depth and soil density for the normal stress distribution.

The shear stress distribution increased towards the edges according to a convex parabola. In the measurements made, the cells for the normal and shear stresses had to be fitted side by side, thus the normal and shear stresses were measured at different points.

Muhs and Elmiger (1969) showed that with their footing in sand, the shear stress had a concave distribution which increased towards the edges and the edge stresses increased with applied load.

They also found out that the edge shear stress decreased as the edge normal stress decreased.

Muhs and Bub (1965) used a 0.6 m x 1.2 m footing, with four pressure cells that could measure stresses in three dimensions embedded in it, in loose, medium and dense sand. Tests were performed at the surface and at various depths. The water level was also at the soil surface. Their results showed that a concave normal stress distribution was obtained under loads that caused elastic deformation, while an unsymmetrical convex parabola was obtained for failure loads. The shear stress was found to increase towards the edges. Their results are shown in Figure 2.1.7.

Leussink, Blinde and Abedlmade (1966) made normal stress distribution measurements under four footings A_1, A_2, B_1 and B_2. The footings A_1 and A_2 were 1 m x 2 m each while footings B_1 and B_2 were 1.5 m x 1.5 m. They were all provided with glotzl pressure cells. The tests were made in uniform sand at the surface and at different depths and the loads were applied in steps up to failure. They found out that with the soil in the elastic state a concave distribution prevailed while a convex distribution was obtained for the plastic state.

2.2 Model Experiment

An account has been given by Borodachev and Tarikov (1972) on the use of an electrical model in the solution of contact stress problems. However, inherent in their mode of solutions were the

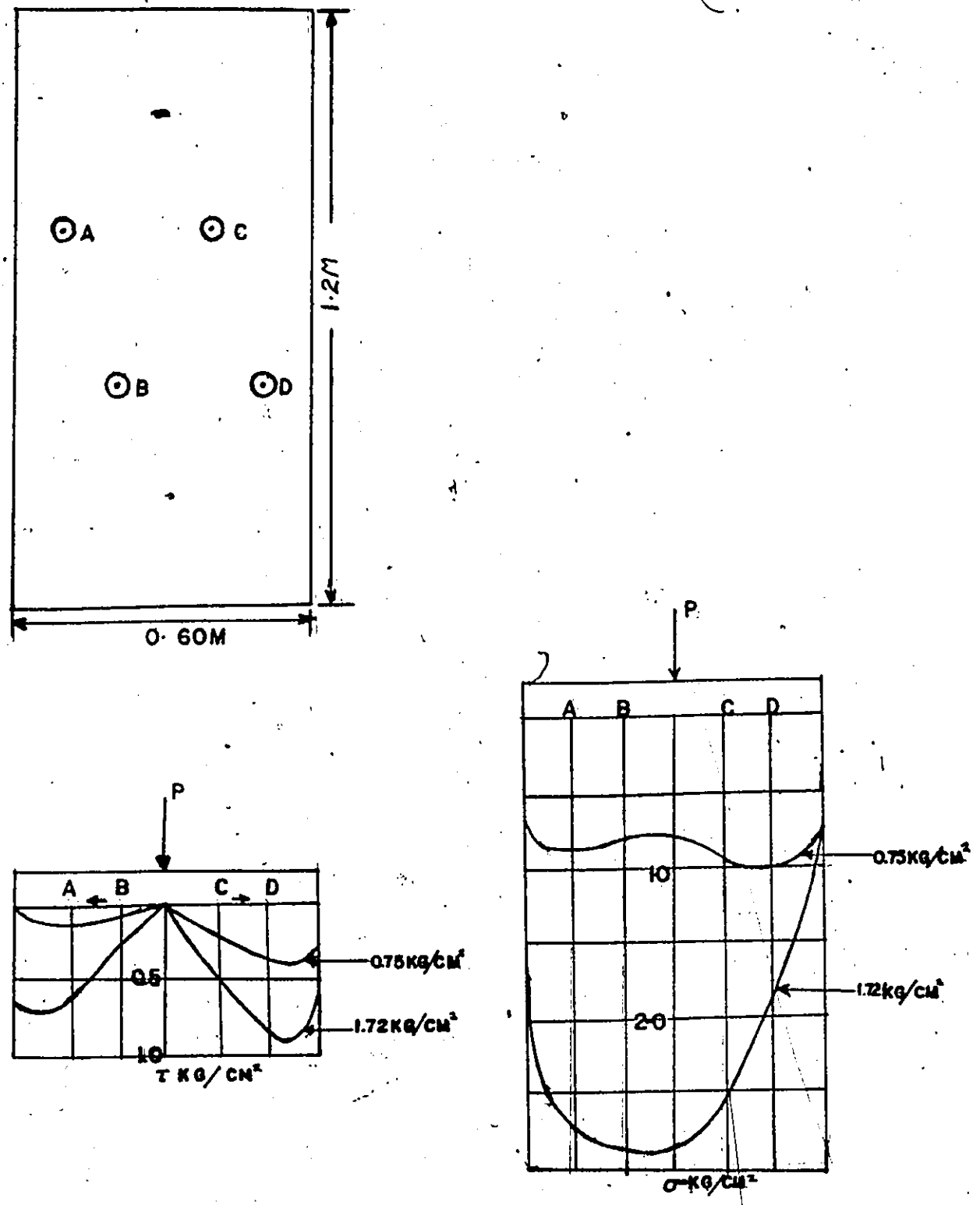

FIGURE 2.1.7 NORMAL AND SHEAR STRESS DISTRIBUTION AFTER MUHS AND BUB (1965)

following assumptions:

(1) No frictional forces at the base of the footing.

(2) No loading outside the footing.

(3) The soil is semi-infinite and elastic.

The procedure involves the application of a voltage at a frequency that would create a quasi-stationary electric field in the conducting plate of the shape of the footing in the plan. Points of equal potential are then plotted by means of a probe. The charge at the probe point is given by the relationship

$$\sigma = \frac{\varepsilon E}{4\pi} \quad \text{and} \quad E = \frac{u_1 - u_2}{d} \qquad 2.1$$

where σ = surface charge density

ε = dielectric constant of the plate used in simulating the footing

E = electric field strength

u_1 = the plates potential

u_2 = the potential of the equipotential lines

d = distance between plate and the equipotential line of the electric field.

Subsequently, the normal stress at the point where the surface charge density was determined is then given by

$$P = \gamma_m \sigma \qquad 2.2$$

where γ_m is a scale factor obtained from equation 2.2 after an

experimental and theoretical comparison of solutions for a circular plate.

The authors have solved the problem for a square plate with notches as shown in Figure 2.2.1 and finally gave the normal stress distribution along AB and AK as

$$P_{(x,o)} = \frac{a_o + a_1 x_o^2 + a_2 x_o^4 + a_3 x_o^6}{\sqrt{1 - x_o^2}} \cdot \frac{P}{F} \qquad 2.3$$

and

$$P_{(y,o)} = \frac{b_o + b_1 y_o^2 + b_2 y_o^4 + b_3 y_o^6}{\sqrt{(1 - 2\gamma)^2 - y_o^2}} \cdot \frac{P}{F} \qquad 2.4$$

respectively, where

$\gamma = \frac{C}{2a}$

P = force on plate

F = contact area of plate

$x_o = \frac{x}{a}$

$y_o = \frac{y}{a}$

a = half width of the plate.

The coefficients a_o, a_1, a_2, a_3, b_o, b_1, b_2 and b_3 are obtained by the method of least squares.

It could be concluded from their testsresults that a concave normal stress distribution was obtained which agrees with their assumption of an elastic medium (assuming that the shape obtained from Boussinesq's theory is the ideal). They also stated that their results might be 5% in error.

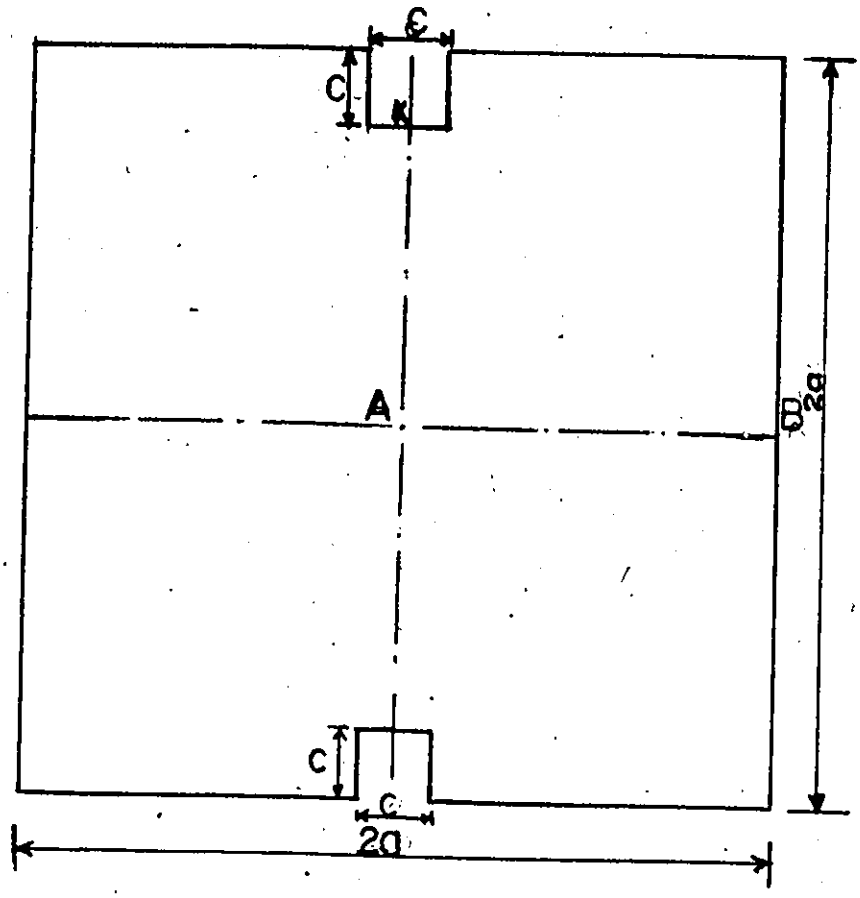

SHAPE OF PLATE

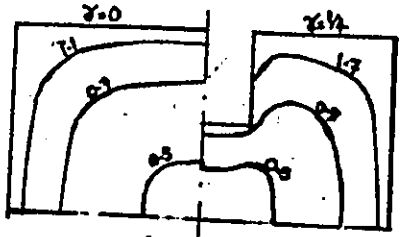

LINES OF EQUAL P/P_{0x}

FIGURE 2·2·1 AFTER BORODACHEV AND TARIKOV

2.3 Theoretical Analysis of Normal and Shear Stress Distribution

There are few cases of the analysis of contact stress distributions at the interface of a rigid footing and a granular medium in the literature. However, three cases will be cited in this thesis.

The first case is the method developed by Schultze (1961). He suggested that the normal stress distribution under a footing can be calculated by a judicious combination of the stress computed from Boussinesq's equation for the elastic state and Prandtl and Buisman's equation for the plastic state. This ultimately gives an equation for the elastic-plastic state. However, the problem has been considered in three steps, viz., elastic state, plastic state and elastic-plastic state.

Elastic-State: Boussinesq's equation, which gives a concave parabolic normal stress distribution under a rigid smooth footing loaded axially has been adopted.

Thus

$$P_s(x) = \frac{P}{\pi a} \cdot \frac{1}{\sqrt{1 - (x/a)^2}} \qquad 2.5$$

where

$P_s(x)$ = normal stress distribution

a = half width of the footing

P = axial load.

The above equation is independent of Youngs modulus of the soil and thus valid for surface loading. However, it gives infinite

edge stresses which invalidates the equation without modification.

Plastic-State: A full parabolic distribution is obtained at this stage when the soil fails upon the application of a certain maximum load. Under this circumstance the ultimate bearing capacity provides the normal stress distribution under the footing and is shown in Figure 2.3.1, the distribution curve has been divided into rectangles and triangles.

Thus,

$$P_s(x) = CN_c + \gamma_1 N_q D + 4a\gamma_2 N_\gamma (1 - x/a) \qquad 2.6$$

One easily realizes that the factors N are the bearing capacity factors which are dependent on the internal angle of friction of the soil, assumed frictions between the foundation and subsoil, the relative density of the soil and the shape of the sliding planes which indicate failure. Thus the normal stress is the sum of three components according to equation 2.6.

1) that due to the apparent cohesion which gives a rectangular distribution
2) that due to foundation depth which gives a rectangular distribution

and 3) that due to the footing width which gives a triangular (roof-shaped) distribution.

With equation 2.6 the normal stress distribution at failure load is now compatible with the strength of the soil. The above is

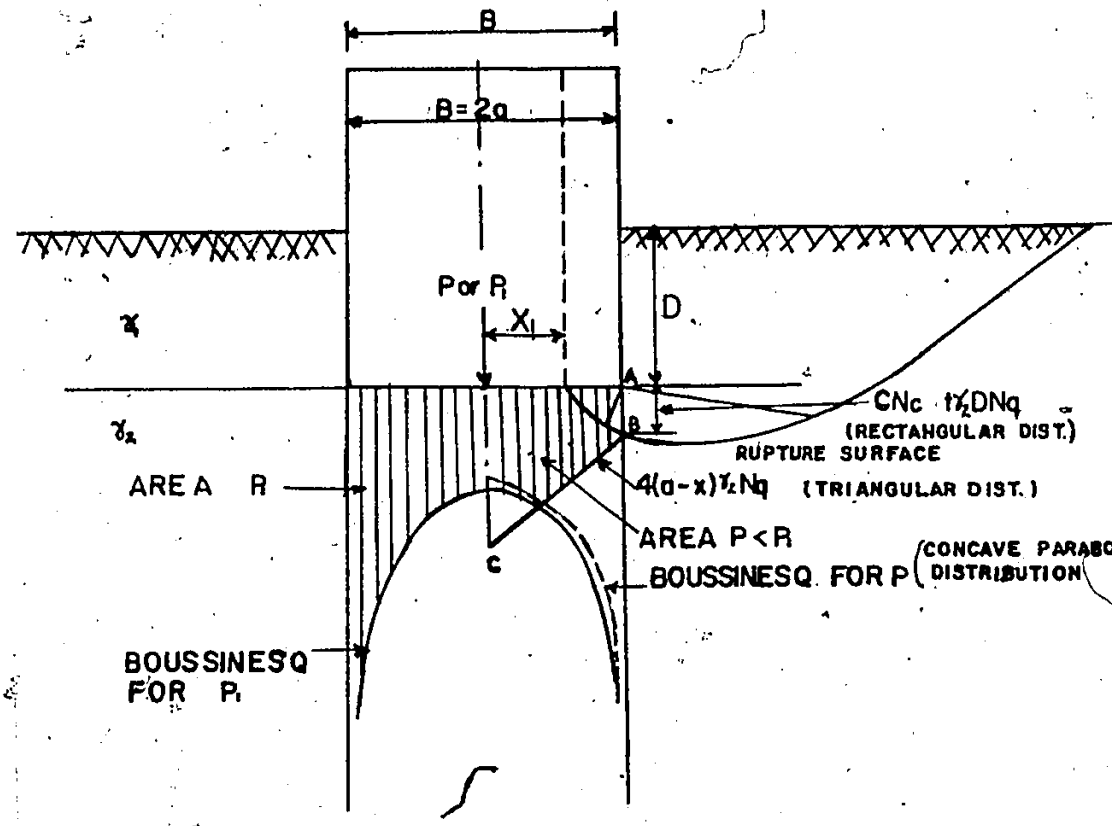

FIGURE 2·3·1 NORMAL STRESS DISTRIBUTION UNDER A RIGID FOUNDATION STRIP AFTER SCHULTZE(1961)

however, not valid for the elastic state or the elastic-plastic state which is often the situation under a footing.

Elastic-Plastic State: Reality is approached by combining the elastic state and plastic state equations. Under the middle region of a footing Boussinesq's distribution is assumed to be valid, but, the edge stresses cannot exceed the bearing capacity of the soil. Since for a given load the stress distribution area must be constant and the edge stresses not exceeding the bearing capacity of the soil, then the stress must be displaced towards the centre. Thus from Figure 2.3.1, if the distance x_1 from the centre of the footing is taken as the point of transition between the elastic and plastic states, then the stress at this point from Boussinesq's (equation 2.5) and Prandtl and Busiman (equation 2.6) must be the same.

From the above a load $P_1 > P$ must be supported at the centre of the footing. Then at the transition point

$$\frac{P_1}{\pi a} \cdot \frac{1}{\sqrt{1 - (x_1/a)^2}} = C N_c + \gamma_1 D N_q + 4a\gamma_2 N_\gamma (1 - x_1/a) \qquad 2.7$$

holds.

The shaded area in Figure 2.3.1 must be equal to P/2.

Thus

$$\frac{P}{2} = \frac{P_1}{\pi a} \int_0^{x_1} \frac{dx}{\sqrt{1-(x/a)^2}} + \int_{x_1}^{a} \{C N_c + \gamma_1 D N_q + 4\gamma_2 a N_\gamma (1-x/a)\, dx\} \qquad 2.8$$

$$= \frac{P_1}{\pi} \text{ arc Sin } \frac{x_1}{a} + a(CN_c + \gamma_1 DN_q)(1 - x_1/a) + \int_{x_1}^{a} 4a\gamma_2 N_\gamma (1-x/a)dx$$

$$= \frac{P_1}{\pi} \text{ arc Sin } \frac{x_1}{a} + a(CN_c + \gamma_1 DN_q)(1 - x_1/a)$$

$$+ 4a\gamma_2 N_\gamma (a - x_1) - 4a\gamma_2 N_\gamma (q/2 - x_1^2/2a)$$

$$= \frac{P_1}{\pi} \text{ arc Sin } \frac{x_1}{a} + a(CN_c + \gamma_1 DN_q)(1 - x_1/a)$$

$$+ 2a^2\gamma_2 N_\gamma - 4a\gamma_2 N_\gamma x_1 + 2\gamma_2 N_\gamma x_1^2$$

$$= \frac{P_1}{\pi} \text{ arc Sin } \frac{x_1}{a} + a(CN_c + \gamma_1 DN_q)(1 - x_1/a)$$

$$+ 2a^2\gamma_2 N_\gamma \{1 - \frac{2x_1}{a} + (x_1/a)^2\}$$

$$\frac{P}{2} = \frac{P_1}{\pi} \text{ arc Sin } \frac{x_1}{a} + a(CN_c + \gamma_1 DN_q)(1 - x_1/a) + 2a^2\gamma_2 N (1-x_1/a)^2 \qquad 2.9$$

Equations 2.7 and 2.9 can be solved to obtain P_1 and x_1 and then finally $P_s(x)$.

The solution of the above equations have been simplified by the introduction of constants such that

$$C_1 = a(CN_c + \gamma_1 DN_q)$$

$$C_2 = 2a^2\gamma_2 N_\gamma.$$

$$\xi_1 = x/a \quad \text{and} \quad \xi_1 = x_1/a$$

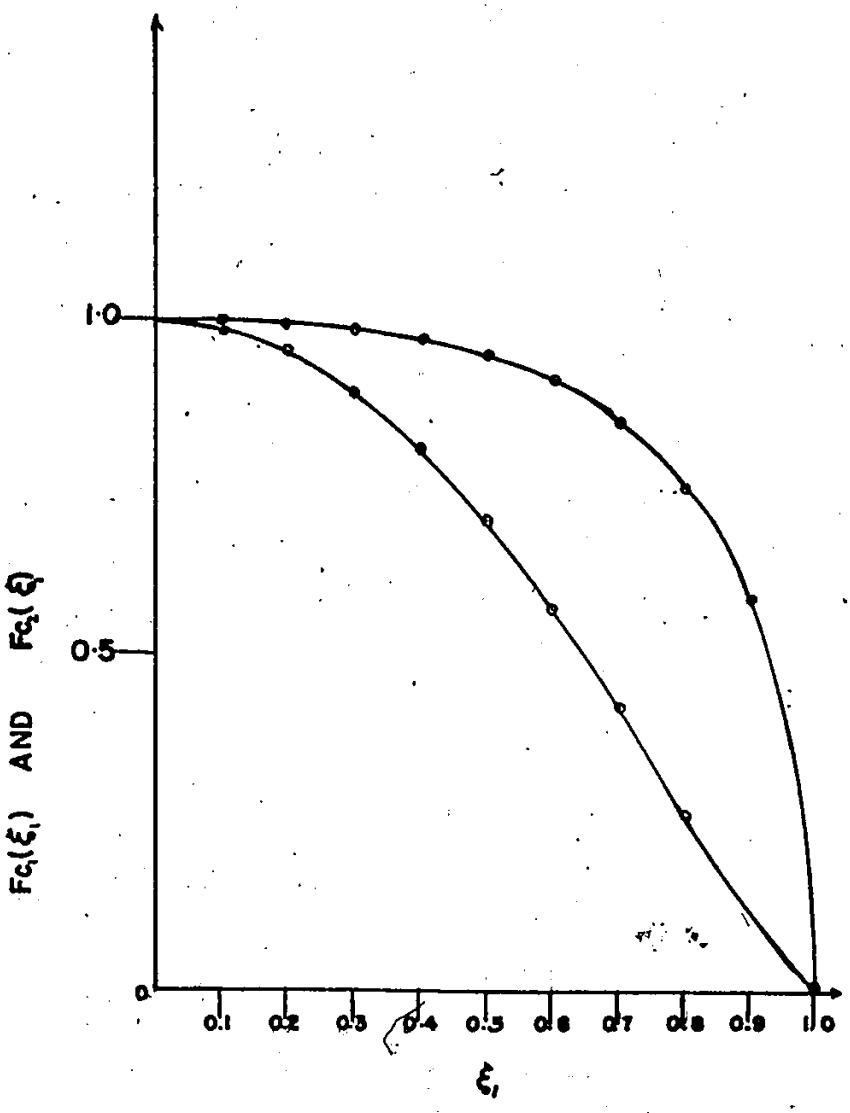

FIGURE 2·3·2 A PLOT OF $F_{c_1}(\xi_1)$ AND $F_{c_2}(\xi_1)$ VS ξ_1

Then equation 2.7 becomes

$$\frac{P_1}{\pi} = \sqrt{1 - \xi_1^2}\,[C_1 + 2C_2(1 - \xi)] \qquad 2.10$$

and equation 2.9 becomes

$$\frac{P}{2} = \frac{P_1}{\pi} \text{ arc Sin } \xi_1 + C_1(1 - \xi_1) + C_2(1 - \xi_1)^2 \qquad 2.11$$

Then putting for P_1 in equation 2.11 from equation 2.10 we have

$$\frac{P}{2} = C_1[\sqrt{1 - \xi_1^2} \text{ arc Sin } \xi_1 + (1 - \xi_1)]$$

$$+ C_2[2\sqrt{1 - \xi_1^2} \text{ arc Sin } \xi_1 (1 - \xi_1) + (1 - \xi_1)^2] \qquad 2.12$$

$$= C_1 \cdot f_{C_1}(\xi) + C_2 \cdot f_{C_2}(\xi_1) \qquad 2.13$$

where $f_{C_1}(\xi_1) = \sqrt{1 - \xi_1^2} \text{ arc Sin } \xi_1 + (1 - \xi_1)$

$$f_{C_2}(\xi_1) = 2\sqrt{1 - \xi_1^2} \text{ arc Sin } \xi_1 (1 - \xi_1) + (1 - \xi_1)^2.$$

A plot of ξ_1 vs $f_{C_1}(\xi_1)$ and $f_{C_2}(\xi_1)$ is given in Figure 2.3.2 whence equation 2.9 can be solved by trial and error for various values of ξ_1 in order to obtain P_1 and x_1 and then finally $P_{s(x)}$ from equations 2.5 and 2.6.

The second method was developed by Sedykh (1964) in which he proposed a solution in which the plastic zone has been sufficiently developed but an air hole, has not been formed in the soil surface,

that is a soil wedge has not been formed. The problem was solved for the following conditions and assumptions:

1) Centred load on the foundations,

2) rough foundation base,

3) constant vertical displacement and zero horizontal displacement at the base of the foundation for any particular load.

4) The displacement paths of the soil coincides with the slip lines for the plastic zone.

5) An elastic state exists directly under the foundation base at any load and investigations by Gorbunov-Posadov have shown that the plastic zones abut the edges of the foundations over a length not exceeding approximately 0.05 of the width of the foundation.

6) The boundary between the elastic and plastic zones have two sections (refer to Figure 2.3.3) OA which is not a slip line but is analogous to a rigid retaining wall with rupture induced by the passive yielding of the soil to the right along the second section ODC. ODC the extreme slip line of the plastic zone, that is, the logarithmic spiral OD and the straight section DC.

7) The three stress components along both sides of the boundary OA are mutually equal while the normal and tangential components of stress on both sides of the boundary ODC are mutually equal.

8) The slip lines are directed vertically upwards upon approaching the boundary OA.

The application of a centred load on a foundation will generally result in a symmetrical contact normal and shear stress distribution.

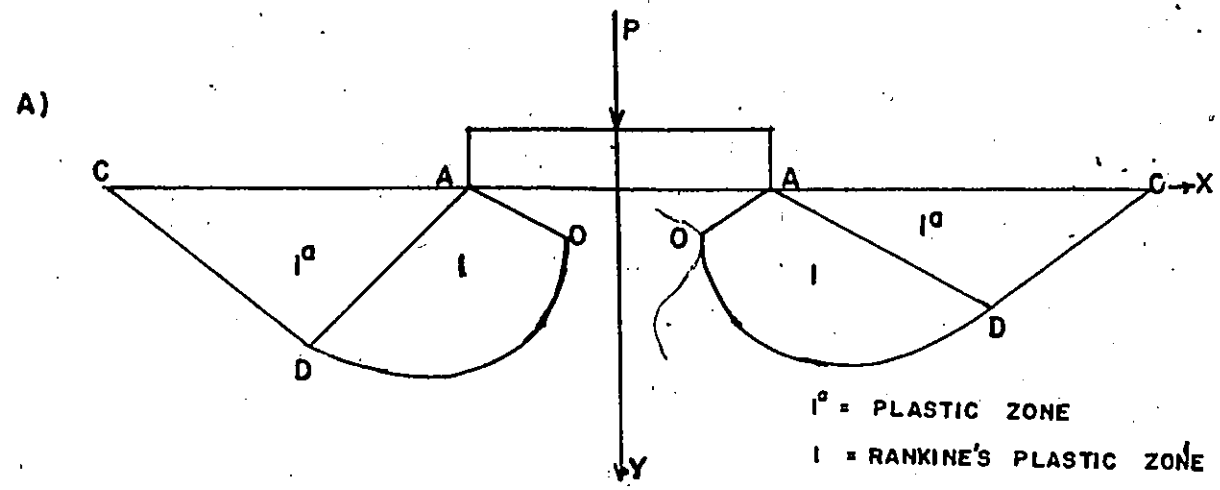

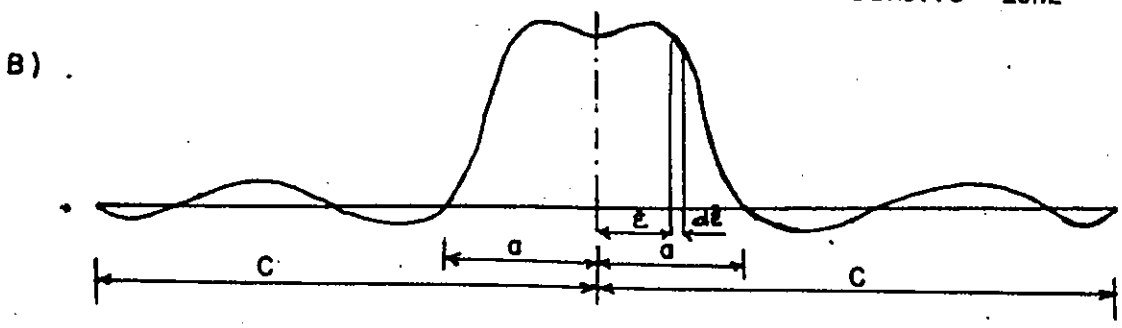

NORMAL STRESS AND VERTICAL COMPONENT OF FICTITIOUS LOAD

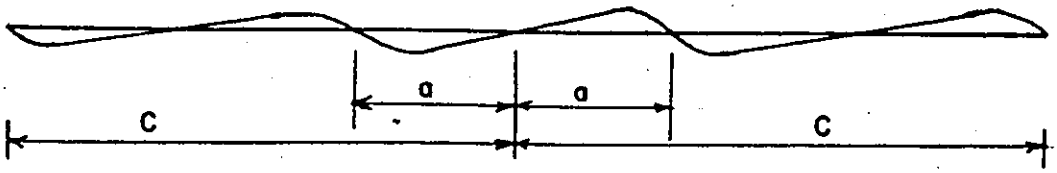

TANGENTIAL STRESS AND HORIZONTAL COMPONENT OF FICTITIOUS LOAD.

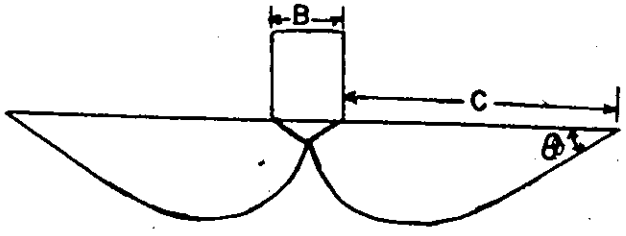

TERZAGHIS FAILUBE PATTERN

FIGURE 2·3·3 (A), (B) AND (C) AFTER SEDYKH (1964)

The normal stress can be represented by a polynomial of even numbers

$$P(\varepsilon) = a_o + a_2\varepsilon^2 + a_4\varepsilon^4 + \ldots\ldots\ldots a_{2n}\varepsilon^{2n} \qquad 2.14$$

where a_o, a_2, a_4 . . . . a_{2n} are numerical coefficients and ε, the abscissa of points lying on the contact surface AA'. Thesshear stress can similarly be expressed as a polynomial of odd powers

$$\varepsilon(\varepsilon) = a_1\varepsilon + a_3\varepsilon^3 + a_5\varepsilon^5 + \ldots\ldots\ldots a_{2n+1}\varepsilon^{2n+1} \qquad 2.15$$

where a_1, a_3, a_5 . . . . a_{2n+1} are numerical coefficients and ε, the abscissa of points lying on the surface AA'.

The effect of the plastic zone on the elastic zone can be fully simulated by replacing the plastic zone by a conditional elastic zone which can be achieved by placing fictitious self-balancing loads on the plastic zone surface (AC and A'C').

The vertical and horizontal components of these fictitious self-balancing loads are given by the following relationships:

$$q(\varepsilon) = b_o + b_2\varepsilon^2 + b_4\varepsilon^4 + \ldots b_{2n}\varepsilon^{2n} \qquad 2.16$$

$$q(\varepsilon) = b_1\varepsilon + b_3\varepsilon^3 + b_5\varepsilon^5 \ldots\ldots b_{2n+1}\varepsilon^{2n+1} \qquad 2.17$$

where b_o, b_1, b_2, b_3 . . . . b_{2n+1} are numerical coefficients a, ε the abscissa of points lying on AC or A'C'.

Since these fictitious loads are self-balancing, then

$$\int_{+1}^{+c} q(\varepsilon)\, d\varepsilon = 0 \qquad 2.18$$

$$\int_{+1}^{c} \eta(\varepsilon)\,d\varepsilon = 0 \qquad 2.19$$

From the relationship of stresses at any point within the elastic zone under a flexible strip developed by Kolosov, the two dimensional stresses are given by

$$\sigma_x = \frac{2}{\pi}\left\{ y\int_{-1}^{+1} \frac{(x-\varepsilon)^2 P(\varepsilon)\,d\varepsilon}{[(x-\varepsilon)^2+y^2]^2} + y\int_{-c}^{-1} \frac{(x-\varepsilon)^2 q(\varepsilon)\,d\varepsilon}{[(x-\varepsilon)^2+y^2]^2} \right.$$

$$+ y\int_{1}^{c} \frac{(x-\varepsilon)^2 q(\varepsilon)\,d\varepsilon}{[(x-\varepsilon)^2+y^2]^2} + \int_{-1}^{+1} \frac{(x-\varepsilon)^3 t(\varepsilon)}{[(x-\varepsilon)^2+y^2]^2}\,d\varepsilon$$

$$\left. + \int_{-c}^{-1} \frac{(x-\varepsilon)^3 \eta(\varepsilon)\,d\varepsilon}{[(x-\varepsilon)^2+y^2]^2} + \int_{1}^{c} \frac{(x-\varepsilon)^3 \eta(\varepsilon)}{[(x-\varepsilon)^2+y^2]^2}\,d\varepsilon \right\} \qquad 2.20$$

$$\sigma_y = \frac{2}{\pi}\left\{ y^3\int_{-1}^{+1} \frac{P(\varepsilon)}{[(x-\varepsilon)^2+y^2]^2}\,d\varepsilon + y^3\int_{-c}^{-1} \frac{q(\varepsilon)}{[(x-\varepsilon)^2+y^2]^2}\,d\varepsilon \right.$$

$$+ y^3\int_{-c}^{-1} \frac{q(\varepsilon)\,d\varepsilon}{[(x-\varepsilon)^2+y^2]^2} + y^2\int_{-1}^{+1} \frac{(x-\varepsilon)\eta(\varepsilon)}{[(x-\varepsilon)^2+y^2]^2}\,d\varepsilon$$

$$\left. + y^2\int_{-c}^{-1} \frac{(x-\varepsilon)\eta(\varepsilon)}{[(x-\varepsilon)^2+y^2]^2}\,d\varepsilon + y^2\int_{1}^{c} \frac{x(-\varepsilon)\eta(\varepsilon)}{[(x-\varepsilon)^2+y^2]^2}\,d\varepsilon \right\} \qquad 2.21$$

$$\tau_{xy} = \frac{2}{\pi}\{y^2 \int_{-1}^{+1} \frac{(x-\varepsilon)\,P(\varepsilon)}{[(x-\varepsilon)^2+y^2]^2}\,d\varepsilon + y^2 \int_{-c}^{-1} \frac{(x-\varepsilon)q(\varepsilon)}{[(x-\varepsilon)^2+y^2]^2}\,d\varepsilon$$

$$+ y^2 \int_{1}^{c} \frac{(x-\varepsilon)q(\varepsilon)}{[(x-\varepsilon)^2+y^2]^2}\,d\varepsilon + y^3 \int_{-1}^{+1} \frac{t(\varepsilon)}{[(x-\varepsilon)^2+y^2]^2}\,d\varepsilon$$

$$+ y^3 \int_{-c}^{-1} \frac{\eta(\varepsilon)\,d\varepsilon}{[(x-\varepsilon)^2+y^2]^2} + y^3 \int_{1}^{c} \frac{\eta(\varepsilon)\,d\varepsilon}{[(x-\varepsilon)^2+y^2]^2}\} \qquad 2.22$$

The above integration is to be performed with the limits obtained by using a footing half width of 1.

The integration of the above expressions with the weight of the soil borne in mind yields the following expressions:

$$\sigma_x = \frac{2}{\pi}\{a_o A_{01} + a_1 A_{11} + a_2 A_{12} + ... + b_o B_{01} + b_1 B_{11} + ...\} + K\gamma y \qquad 2.23$$

$$\sigma_y = \frac{2}{\pi}\{a_o A_{02} + a_1 A_{12} + a_2 A_{22} + ... + b_o B_{02} + b_1 B_{12} + ... + \gamma y\} \qquad 2.24$$

$$\tau_{xy} = \frac{2}{\pi}\{a_o A_{03} + a_1 A_{13} + ... + b_o B_{03} + b_1 B_{13} + b_2 B_{23}\} \qquad 2.25$$

where K is the coefficient of lateral pressure and γ, the bulk density of the soil,

and A_{iK} and B_{iK} are functions of the coordinates.

Investigations have shown that the normal and tangential stress components at the edges of the foundation are zero respectively.

Thus

$$a_o + a_2 + a_4 + a_6 + ... + a_{2n} = 0 \qquad 2.26$$

$$a_1 + a_3 + a_5 + ... + a_{2n+1} = 0 \qquad 2.27$$

Similarly, at the boundary between the elastic zone and the conditional elastic zone on the surface, that is, at A, C, A' and C' the fictitious load components are equal to zero.

Thus

$$b_o + b_2 + b_4 + ... + b_{2n} = 0 \qquad 2.28$$

$$b_1 + b_3 + b_5 + ... + b_{2n+1} = 0 \qquad 2.29$$

$$b_o + b_1 c^2 + b_4 c^4 + ... + b_{2n} + c^{2n} = 0 \qquad 2.30$$

$$b_1 c + b_3 c^3 + b_5 c^5 + ... + b_{2n+1} = 0 \qquad 2.31$$

The contact conditions at the base of the foundation will yield the following expressions

$$\int_{-1}^{+1} [P(\varepsilon)-q(\varepsilon)] \ln \frac{|x-\varepsilon|}{|\varepsilon|} d\varepsilon + \int_{-c}^{+c} q(\varepsilon) \ln \frac{|x-\varepsilon|}{|\varepsilon|} d\varepsilon - \frac{\pi}{2} \frac{(1-2\mu)}{1-\mu} \int_o^x \tau(\varepsilon) = 0 \qquad 2.32$$

and

$$\int_{-1}^{+1} [\tau(\varepsilon)-\eta(\varepsilon)] \ln \frac{|x-\varepsilon|}{|\varepsilon|} d\varepsilon + \int_{-c}^{+c} \eta(\varepsilon) \ln \frac{|x-\varepsilon|}{|\varepsilon|} d\varepsilon + \frac{\pi}{2} \frac{(1-2\mu)}{(1-\mu)} \int_o^x P(\varepsilon)\, d\varepsilon = 0 \qquad 2.33$$

where μ is Poissons ratio.

Thus the determination of the contact stress distribution requires the determination of the numerical coefficients a_i and b_i. The procedure for their determination for a chosen value of C is as follows:

(1) A certain number of points K are marked on the contact surface AA' and then the values of their abscissa are substituted in equations 2.32 and 2.33 to give 2K equations.

(2) Further, 8 equations are obtained from equations 2.18, 2.19 and 2.26 to 2.31 giving the boundary conditions of the problem and the condition of self-balancing of the assumed fictitious load on AC and A'C'.

(3) The boundary between the elastic and plastic zones is determined for the chosen value of C. On Section OA, T, points are marked and the values of their coordinates and stress components substituted in equations 2.23 to 2.25 to give 3T equations.

(4) M points are marked on the slip surface ODC and the values of their coordinates and stress components substituted in

$$\sigma_{nt} = \sigma_x \text{Cos}^2 x + \sigma_y \text{Sin}^2 \alpha + \tau_{xy} \text{Sin}^2 \alpha \qquad 2.34$$

and

$$\tau_{nt} = \frac{1}{2}(\sigma_y - \sigma_x) \text{ Sin } 2\alpha + \tau_{xy} \text{Cos } 2\alpha \qquad 2.35$$

to give 2m equations,

where σ_x, σ_y and τ_{xy} are obtained from equations 2.20 to 2.22 and is the angle between the x-axis and the tangent to the boundary slip line at the point in question.

The above procedure yields Z equations where

$$Z = 8 + 2K + 2m + 2T \qquad 2.36$$

This number of equations should be equal to the number of unknown numerical coefficients a_i and b_i.

A typical contact stress distribution by Sedykh (1964) using the failure pattern and boundary between the elastic and plastic zone proposed by Gorbunove-Posadou (1962) is shown in Figure 2.3.4.

The third is the method proposed by Schweickert (1964) which gives concave contact stress distributions.

The normal stress distribution in this case has finite edge values.

The expression for the normal stress and shear stress are as follows:

$$Ps(x) = \frac{Q(n+1)}{2b(n+1+\alpha)} [1 + \alpha \left(\frac{x}{b}\right)^n] \qquad 2.37$$

$$\tau_s(x) = \frac{5Q}{2b} \frac{(1+\alpha)}{(5+\alpha)} \tan \delta \left(\frac{x}{b}\right)^{n-1}$$

where $Ps(x)$ = normal stress at a distance x from the centre of the footing

Q = load per unit length of the footing

b = half width of the footing

n = order of the parabola

q_c = normal stress at the centre the footing: $\frac{Q(n+1)}{2b(n+1+\alpha)}$

q_E = stress at the edge of the footing = $\frac{Q(n+1)}{2b(n+1+\alpha)} [1+\alpha]$

α = ratio of q_c to q_E

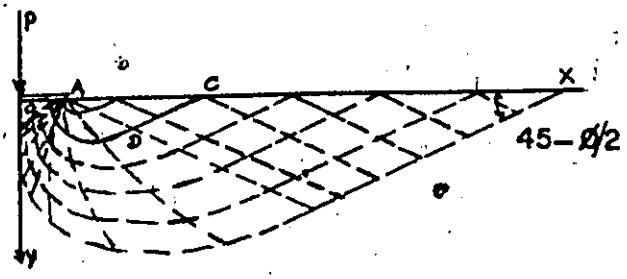

FAILURE PATTERN AFTER GORBUNOV POSSADOV.

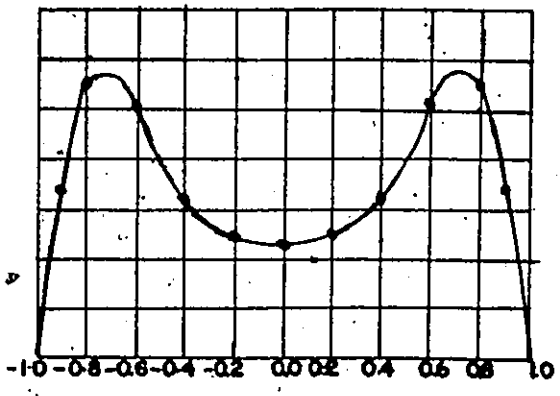

NORMAL STRESS DISTRIBUTION FOR C= 6, Ø= 40°

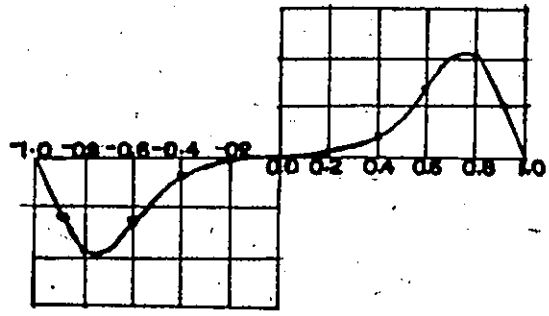

SHEAR STRESS DISTRIBUTION FOR C=6, Ø=40°

FIGURE 2·3·4 CONTACT STRESS DISTRIBUTION AFTER SEDYKH (1964).

$\tau_{\delta}(x)$ = shear stress at a distance x from the centre of the footing

δ = mobilized friction angles between soil and footing.

2.4 Discussion

An accurate experimental investigation into the contact stress distribution should entail a knowledge of the factors imposed during the experiment and the factors that were maintained constant. Similarly a correct theoretical of the contact stress distribution should also involve a consideration for these various factors on which they depend. Thus an account will be given here of the effects of some of the factors that have been investigated experimentally (rigid footings on sand).

1 Magnitude of load:

A. Virgin load: An increase in load causes the sand to move from the elastic state to the rupture state which consequently leads to an increase in the normal stress at the centre of the footing. Thus, a concave normal stress distribution prevails during the elastic state and a convex normal stress distribution during the plastic state (i.e. at and beyond the ultimate load of the soil).

The shear stress distribution has a shape which is not affected by the load levels, excepting that higher shear stresses are produced by higher loads.

B. Reloading: Under this condition the shape of the normal stress distribution under any load has been found to be convex. The

shear stress distribution under this condition increases with load and for a particular load, the shear stress under the reloading condition is greater than that at first loading (virgin loading)

2. Foundation depth:

This has a minimal effect on the contact stresses distribution when compared to other factors. However, its effect has been a reduction in the normal stress within the central region of a footing and consequently a smaller shear stress within the said region. At great depth plastification also occurs within a narrower edge zone.

3. Soil density:

An increase in the soil density has the effect of reducing the normal stress within the central region of the footing (Bub, 1963). The extent of yielding within the edge zone is also reduced, thus leading to higher edge contact stresses (Helenchund, 1966).

4. Moisture state of the soil:

It has been observed that higher loads are required for wet soils than dry soils to reach failure. Increment in the moisture content of sand has the effect of reducing the edge contact stresses owing to the loss of the apparent cohesion that might have existed in the sand and also a subsequent reduction of the effective unit weight of the soil. However, contrary results were obtained by Hartikainen (1972) from the tests performed at the surface and depths. At the surface the results obtained agreed with the above hypothesis while at depths the edge contact stresses were found to be higher in

wet sand than in dry sand. He, however, attributed this lack in conformity of results to the effect of foundation depth.

5. Roughness of foundation base:

This yields the shear stress which is related to the normal stress through the relationship

$$S = \mu N \qquad 2.39$$

where, S = shear stress

μ = tangent of the angle of friction between the soil mass and foundation base

N = the normal stress.

6. Rigidity of foundation:

This is an important factor in the nature and shape of the contact stress distribution.

Usually, the settlement of a soil mass subjected to uniform load is not uniform. Thus only a flexible footing which can conform to this settlement will yield a uniform contact stress distribution. On the other hand, a rigid foundation subjected to a uniform load or a centrally applied load will lead to a uniform settlement. Thus, there will be a redistribution of the contact stresses such that this uniform settlement is maintained. Consequently, a non-uniform stress distribution will prevail with higher stresses developed at the points of small settlements and smaller stresses at the points of larger settlements.

7. Distance to firm base:

This should be such that the slip surface or failure surface is enveloped within the sand mass. Thus the distance from the foundation base to the firm base should be at least twice the footing width (Schmertmann, 1970). Any distance less than this would normally lead to a redistribution of stress which cannot be quantitatively accounted for. As would normally be expected this would lead to high contact stresses.

Within the limits of the literature review done there seems to be no substantial experiments performed to clarify the effects of size and shape of footings, load application time and load application rate on the contact stresses distribution. However, from the theory proposed by Schultze (1961) the effects of the above factors within the edge zone are similar to their effects on the bearing capacity of the soil. Thus the edge contact stresses increases with the width of the foundation and for sand edge contact stress should be highest for rectangular foundations followed by square and circular footings respectively.

The method of electrical modelling gives an insight into the nature of the normal stress distribution that would be obtained under a foundation. However, the results obtained from the procedure would be true for a foundation resting on the surface of the soil and for the assumptions indicated. Thus, for a real soil and under normal loading conditions, a situation of elasto-plastic soil would arise, which cannot be accurately accounted for.

In Schultze's (1961) theory, consideration has been given to the effects of these factors from the transition points to the edges of the foundation (edge zones). It can also be deduced from his analysis that these factors also affect the distance of the transition points from the centre line of the foundation. However, the normal stresses within the edge zones has been given as a modified form of the bearing capacity equations. Thus the effects of these factors within the edge zones can be conveniently accommodated in their effects on the bearing capacity of the soil. Meyerhof (1963), has given expressions for the correction factors to be used in the bearing capacity equation to account for shape, depth of foundation and the angle of internal friction of the soil under plane conditions. However, the effect of these factors on the contact stress distribution within the transition points (elastic zone) in which Boussinesq's equation applies have not been considered. Thus further studies should be engaged to clarify this.

In Sedykh's theoretical analysis, he has represented the contact stresses by a set of polynomials of even and odd powers of the coordinates of points on the contact surface between the foundation and the soil mass. He has also made use of the coordinates and stresses of points lying on the boundary between the elastic and plastic zones. He has also imposed the condition of constant vertical displacement, which reduces the foundation to a rigid one, and zero horizontal displacement. In the solution of the problem it is envisaged that the boundary between the elastic and plastic zones given by Gorbunov-Posadov (1962) will be utilized.

A knowledge of the rupture surface under the foundation would involve the effects of the factors enumerated in Chapter 1. Thus with the above parameters known, the determination of the contact stresses, is then reduced to the solution of a set of equations. However, accuracy in the solution of the problem could be enhanced by taking as many points as possible along OA.

At this juncture the writer would like to suggest that for the determination of the contact stresses under the condition in which the rupture surface has been fully developed that the value of C should be B $\tan\theta$ Exp[$\pi/2 \tan \phi$], where θ is as indicated in Figure 2.3.3 and ϕ the angle of internal friction between the soil and the foundation.

CHAPTER 3

DESCRIPTION OF MODEL FOOTING

3.1 Cambridge Cells

3.1.1 General

For an accurate determination of the stress distribution on a soil/structure interface, it is necessary to know the normal stress, eccentricity of the normal stress and the shear stress.

Initially, cells were designed to measure normal stresses and shear stresses separately. These cells were placed side by side for stress measurements. However, this meant that the normal stress and shear stress were measured at different locations. Thus the relationship between the normal and shear stresses would be obtained by interpolation. This relationship would be invalidated if the soil was not homogeneous. This then led to the design of the following cells:

1. Agarwal and Venkatesan Cell. This cell measures both normal and shear stresses.
2. Telemetric Cell: This cell measures normal stress, eccentricity of the normal stress and shear stress.
3. Muhs Cell: This cell measures normal and shear stresses.
4. Cambridge Cell: This cell measures normal stress, eccentricity of normal stress and shear stress.

A careful consideration of the mode of operation and costs of the above cells led Hanna (1973) to conclude that the

Cambridge cell was the "ultimate for normal and shear stress measurements."

There are, however, three versions of the Cambridge cell in the literature and these will be briefly described.

(1) The original Cambridge cell (Figure 3.1.1):

This was designed by Arthur and Roscoe (1961) for the measurement of normal stress, eccentricity of the normal stress and shear stress. It was made out of a high grade aluminum alloy (BS 14477:1951 HP 15). It had two main components, viz., the active face and the interior block. The interior contained the normal and shear webs machined perpendicular and parallel to the active face. The normal force on the active face was measured by strain gauges glued on both sides of the four normal vertical thin webs. The shear force on the active face was transmitted through a shear pillar to the horizontal shear webs on which strain gauges, which indicated the shear forces, were glued.

There were twenty strain gauges in the cell which formed three four active arm bridge circuits through which the strains were monitored and registered as output voltages.

The eccentricity was computed from the proportion of the normal load carried by each vertical web. The cell was fitted with a rough face plate to simulate field conditions, before testing was carried out.

The sensitivity of the cell was determined by the web thickness and the surface area of the top plate.

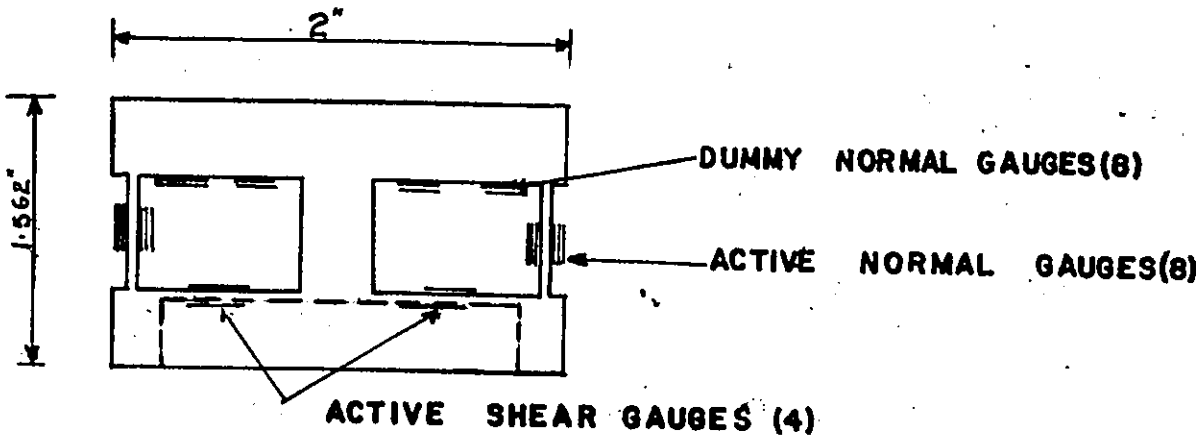

FIGURE 3·1·1 STRAIN GAUGES ON ARTHUR AND ROSCOES CAMBRIDGE CELL

(2) Bozozuk's Cambridge Cell (Figure 3.1.2):

This cell was developed by Bozozuk (1972) for stress measurements under an embankment. This cell is similar to that developed by Arthur and Roscoe in that the normal and shear forces are determined by aluminum temperature compensated strain gauges glued on the shear and normal webs.

However, there are 8 vertical normal webs on which strain gauges are attached to form the two normal bridge circuits. Each set of normal webs A C E G (Figure 3.1.2) consists of two tension webs and two compression webs. This helped in doubling the output voltages from each of the normal bridge circuit.

The horizontal shear webs to which 4 strain gauges X W Y Z (Figure 3.1.2) are glued on, were machined close to the active face. This was done by machining the shear pillar as part of the interior block, thus reducing the amount of load transmitted to the normal webs when a shear load is applied to the active face.

There were twelve strain gauges in the arrangment which formed the three bridge circuits, viz., the positive normal bridge circuit, the negative normal bridge circuit and shear bridge circuit, from which the normal stress, eccentricity of the normal stress and shear stress could be determined respectively.

3.1.2 Design Considerations for the Modified Cambridge Cell

A cell for the measurement of contact stress should possess the following basic properties:

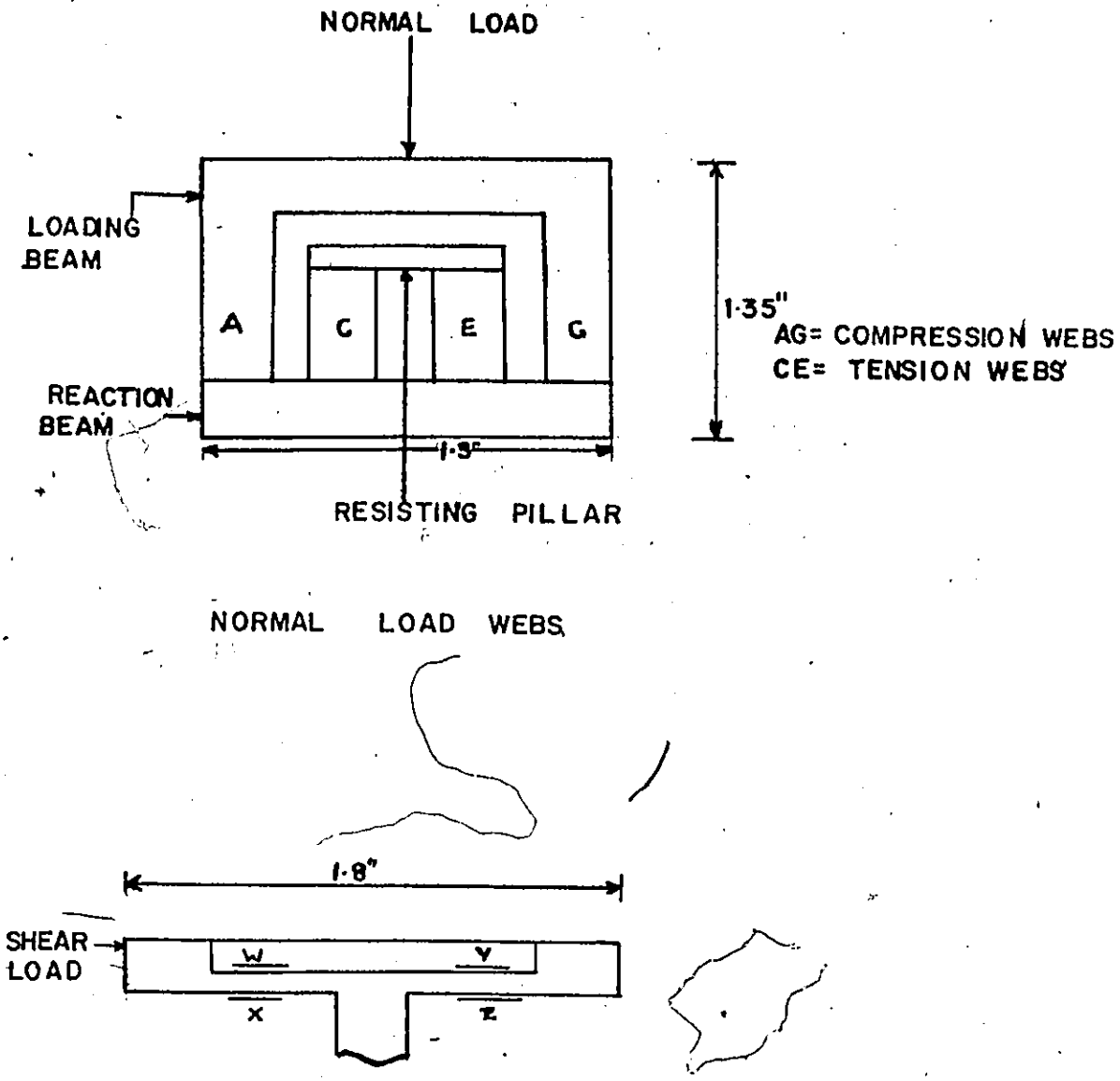

FIGURE 3·1·2 BOZOZUK'S MODIFIED CAMBRIDGE CELL.

(1) Simple principle of design and operation,

(2) reliable reproducibility of readings,

(3) sensitive to load changes,

(4) stable for both long and short term measurements,

(5) high degree of accuracy,

(6) easy to calibrate and recalibrate,

(7) simple installation procedures, and

(8) a minimum over all cost.

The modified Cambridge cell meets the above requirements more when compared to other pressure cells that could measure normal stress, eccentricity of normal stress and shear stress.

The range and sensitivity of the cell is governed primarily by the dimensions of the webs. Thus a careful analysis of this has been carried out by Doohan (1975) for the detemination of the thickness of the normal and shear webs that will be suitable for the load range for which the load cells will be used. The load cells were, however, designed for a maximum normal and shear stress of 10 tons/ft^2 (958 KPa). Thus, for a face plate of 3 in^2 (19.3559 cm), this corresponds to a load of 416 lbs (1.85 KN), for the four shear webs or 104 lbs (0.463 KN) for each shear web. In the case of the normal webs it was decided by Doohan (1975) that a maximum of 75% of the normal load 416 lbs (1.85 KN), might act on a pair of normal webs at any one time. This gives 156 lbs (0.694 KN) per normal web. Thus in the hookup to the read-out device, a sensitivity was chosen such that its range of 2000 micro strains was not exceeded

by the load induced strains that will subsequently be recorded. In the course of the experiments a sensitivity of 5 has been used.

The aluminum temperature compensated strain gauges have resistances of 120 ohms and gauge factors of 2.10 and a maximum allowable current of 50 milliamperes. Thus the maximum allowable voltage that could be applied to the bridge circuit as indicated in Figure 3.1.6 is 12 volts.

The application of the above maximum voltage to the bridge circuit depends on the limits within which the recording device could be balanced and also the safety of the strain gauges. Thus a voltage of 9 volts was applied. However, this supply voltage shown on the recording device is not the bridge circuit voltage since it depends on the position of the span control knob.

For the tests, a 6' x 1' (1.83 m x 0.305 m) long footing in sections of 2' x 1' (60.9 cm x 30.48 cm) footing has been envisaged in the sandbox. The two end footings adjacent to the walls of the sandbox are used as dummy footings with the central footing instrumented for contact stress measurements. The total length of the footings is the same as the width of the sandbox, thus guaranteeing a plane strain condition.

The effects of wall friction on the centre footing will be eliminated by the use of the dummy footings. The wall friction could be reduced by coating the inside of the box, especially around the perifery of the footing with paraffin, teflon, etc.

The size of the cell (1.6/16" x 1.3/16") (3.5 cm x 4.6 cm) and face plate (1.5" x 2")(3.81 cm x 5.08 cm) were chosen by Doohan (1975). He arrived at a compromise between having narrow load cells and large face plates. The former will limit the effects of the wall of the sandbox while the latter will prevent the relative movement of the edges of the plate with respect to the non-yielding boundary. In order to minimize the errors associated with edge effects a stiff pillar was decided on, coupled with limiting the deflection of the face plate to 0.001 inches (0.00254 cm).

3.1.3 The Modified Cambridge Cell (Figure 3.1.3)

This type of pressure cell was developed by Doohan (1975) at the University of Ottawa for the measurement of contact stresses between a model steel footing and a quartz sand bed.

The cell possesses some features similar to Arthur and Roscoe's cell and Bozozuk's cell in that the shear and normal forces applied to the active face produces strains in the normal and shear webs which are monitored through the three bridge circuits and could be registered either as output voltages or strains.

The modified Cambridge cell consists of three basic parts: (1) the face plate, (2) the active face and (3) the interior block. The face plate (Figure 3.1.3) is a high grade aluminum alloy plate which is screwed to the active face of the cell. The interior block of the cell is made from a high grade aluminum alloy (HS 15W) and it contains the four normal vertical webs, the four shear webs and the two shear pillars. The four normal vertical webs to which the

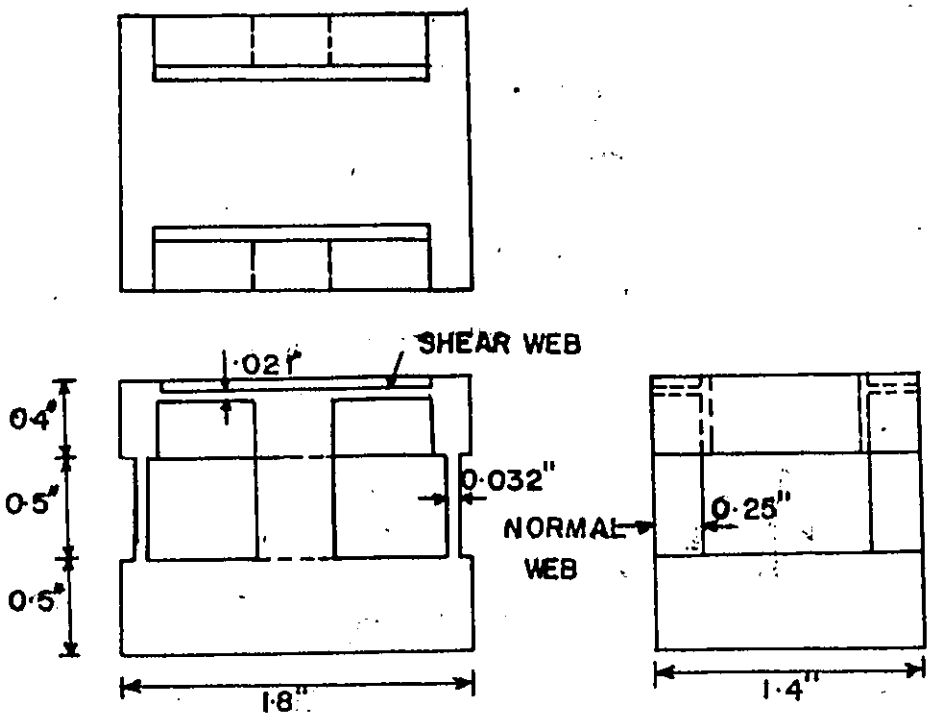

MODIFIED CAMBRIDGE CELL.

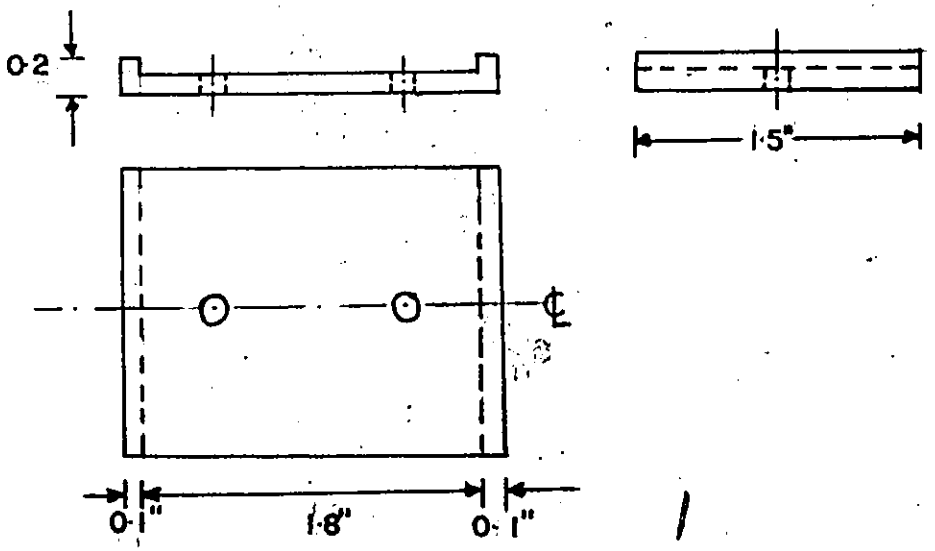

CELL FACE PLATE

FIGURE 3·1·3

aluminum temperature compensated strain gauges were glued on form the two normal bridge circuits, viz., the positive normal bridge circuit and the negative normal bridge circuit. Each normal bridge circuit is a full bridge circuit consisting of two active strain gauges and two dummy strain gauges.

The shear force is transmitted through two shear pillars to four horizontal webs which are machined very close to the active face. The shear bridge circuit consists of four actvie strain gauges which form the full bridge. The shear webs are closer to the active face than in the original Cambridge cellbbut of the same distance off the active face in Bozozuk's Cambridge cell.

The modified Cambridge cell makes use of twelve strain gauges in contrast to the twenty strain gauges used in either Arthur and Roscoe's Cambridge cell. Consequently, there is a relative saving in the cost of the load cell.

3.1.4 Gauging

Each load cell has twelve aluminum temperature compensated phenolic-glass foil strain gauges (SR 4). The strain gauges have a nominal resistance of 120 ohms, a gauge factor of 2.08 and a maximum current carrying capacity of 50 milliamperes.

The strain gauges were only attached to one face of the webs in contrast to the original Cambridge cell in which the strain gauges were on either face of the normal webs and on one face of the shear webs.

Leads were soldered to the terminals of the gauges to form the configuration shown in Figures 3.1.4 and 3.1.5. The gauges were connected in three separate bridge circuits, viz., the positive normal bridge circuit, the negative normal bridge circuit and shear bridge circuit. The two normal bridge circuits had two active strain gauges and two dummy strain gauges, while the shear bridge circuit had four active strain gauges with two in compression and two in tension.

For a hookup of the footing to the digital strain indicator, a modification to the number of leads from the terminals of the gauges was imperative. However, this was done externally at a junction box rather than soldering more wires to the existing configuration. This gives a bridge circuit configuration as shown in Figures 3.1.6 and 3.1.7. A typical cell connection is shown in Figure 3.1.8.

3.1.5 Princple of Operation

The modified Cambridge cell is capable of measuring the normal stress, eccentricity of the normal stress and shear stress.

As shown in Figure 3.1.9 an eccentric load applied at a distance x from the centre of the cell can be replaced by a central force N' and a moment N'x (M_1). The force N' is balanced by reactions from the four normal webs and two shear pillars. Thus, the central load produces strain readings in the three bridge circuits, viz., two normal bridge circuits and shear bridge circuit of magnitude +e,

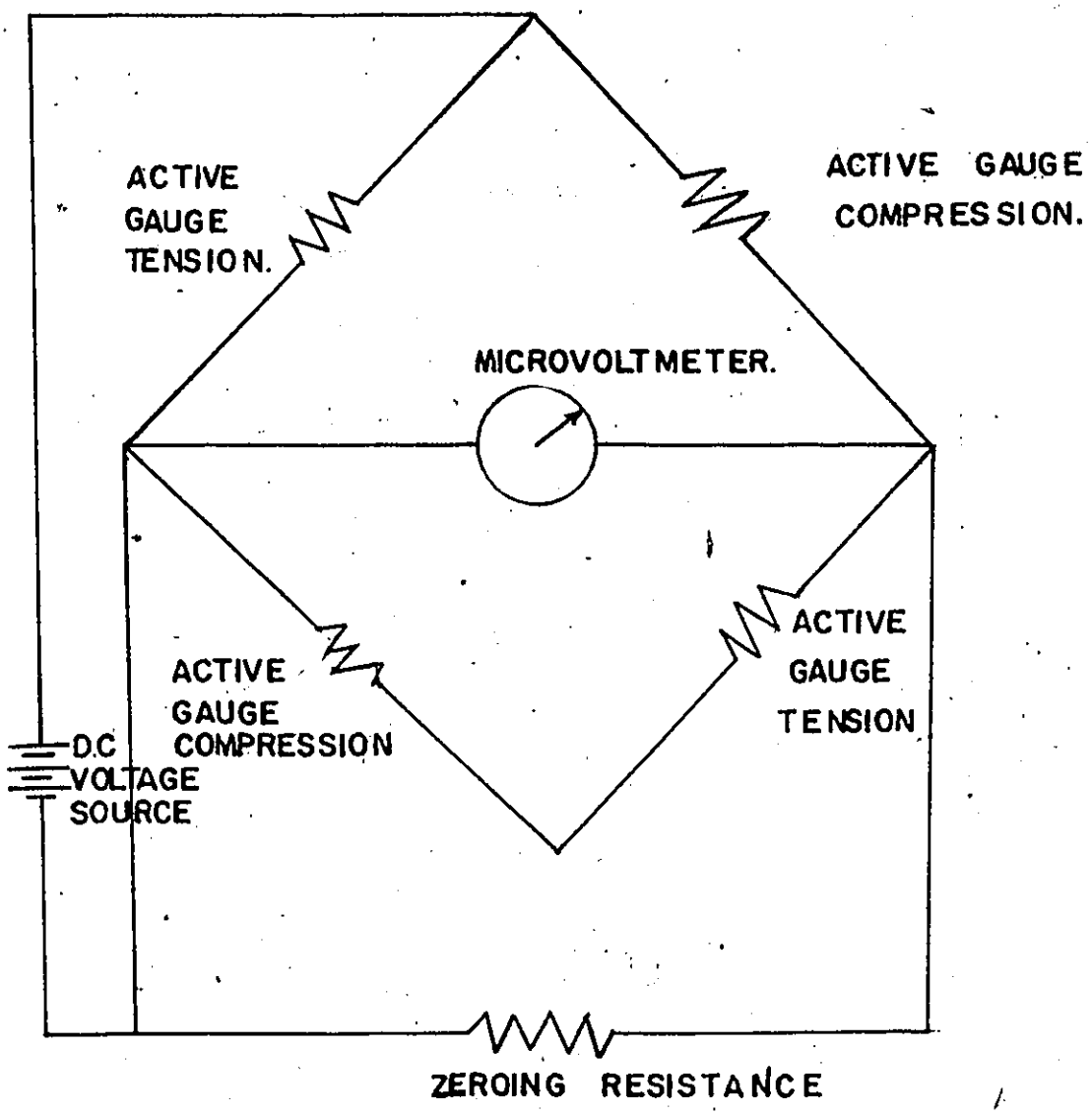

FIGURE 3·1·4 SHEAR BRIDGE CIRCUIT WIRING DIAGRAM (USING KIETHLEY INSTRUMENT MODEL 155).

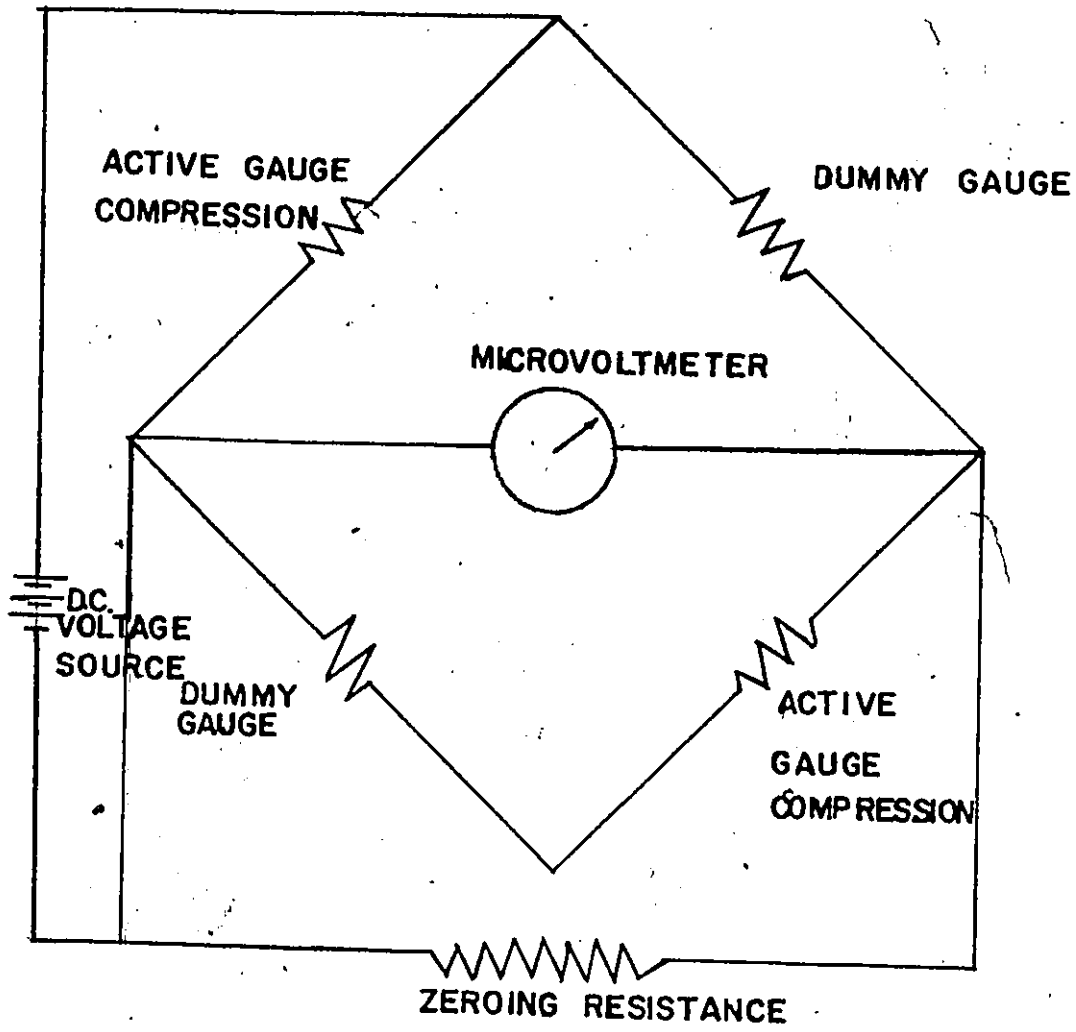

FIGURE 3.1.5 NORMAL BRIDGE CIRCUIT WIRING DIAGRAM (USING KIETHLEY INSTRUMENT MODEL 155).

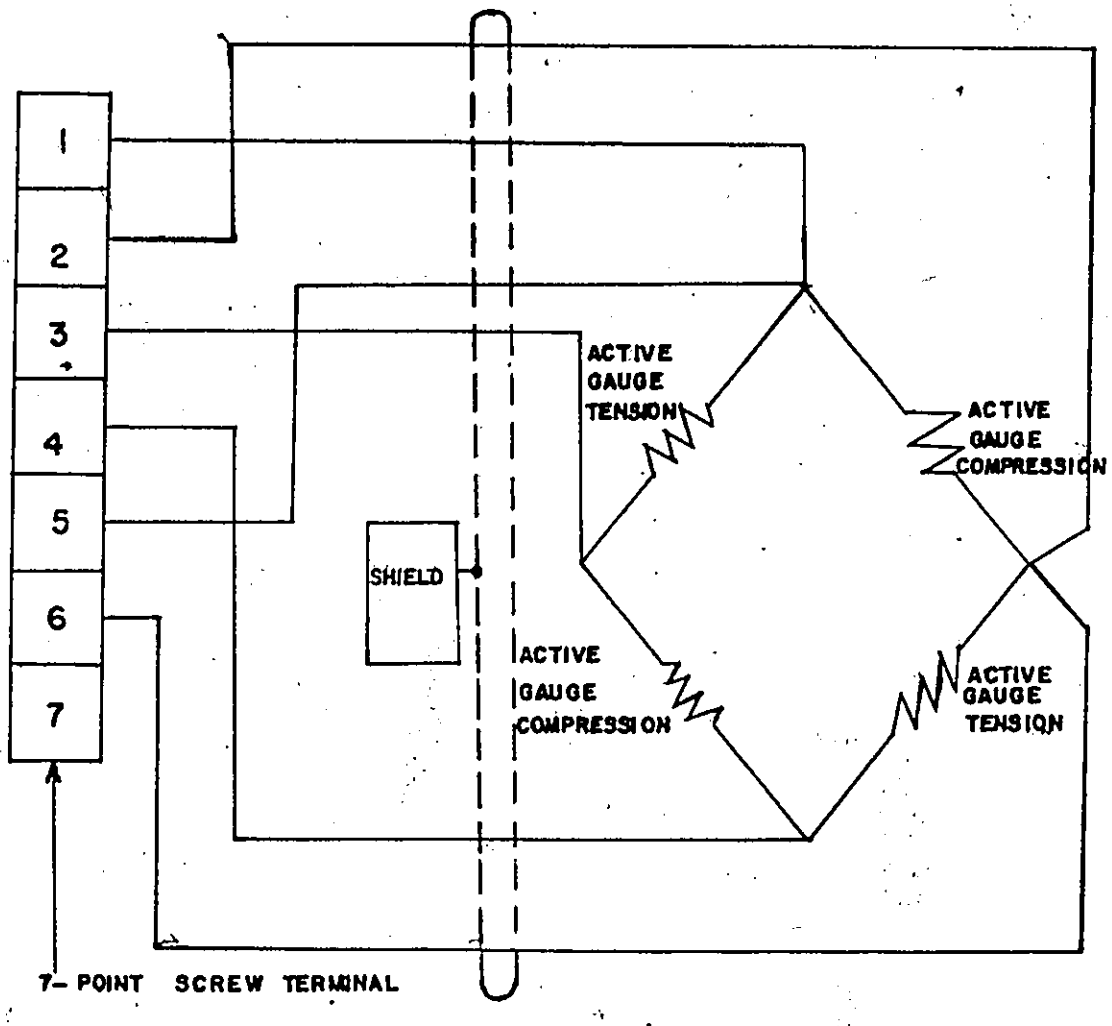

FIGURE 3.1.6 HOOK-UP OF THE SHEAR BRIDGE CIRCUIT TO THE 7-POINT SCREW TERMINALS OF THE JUNCTION BOX.

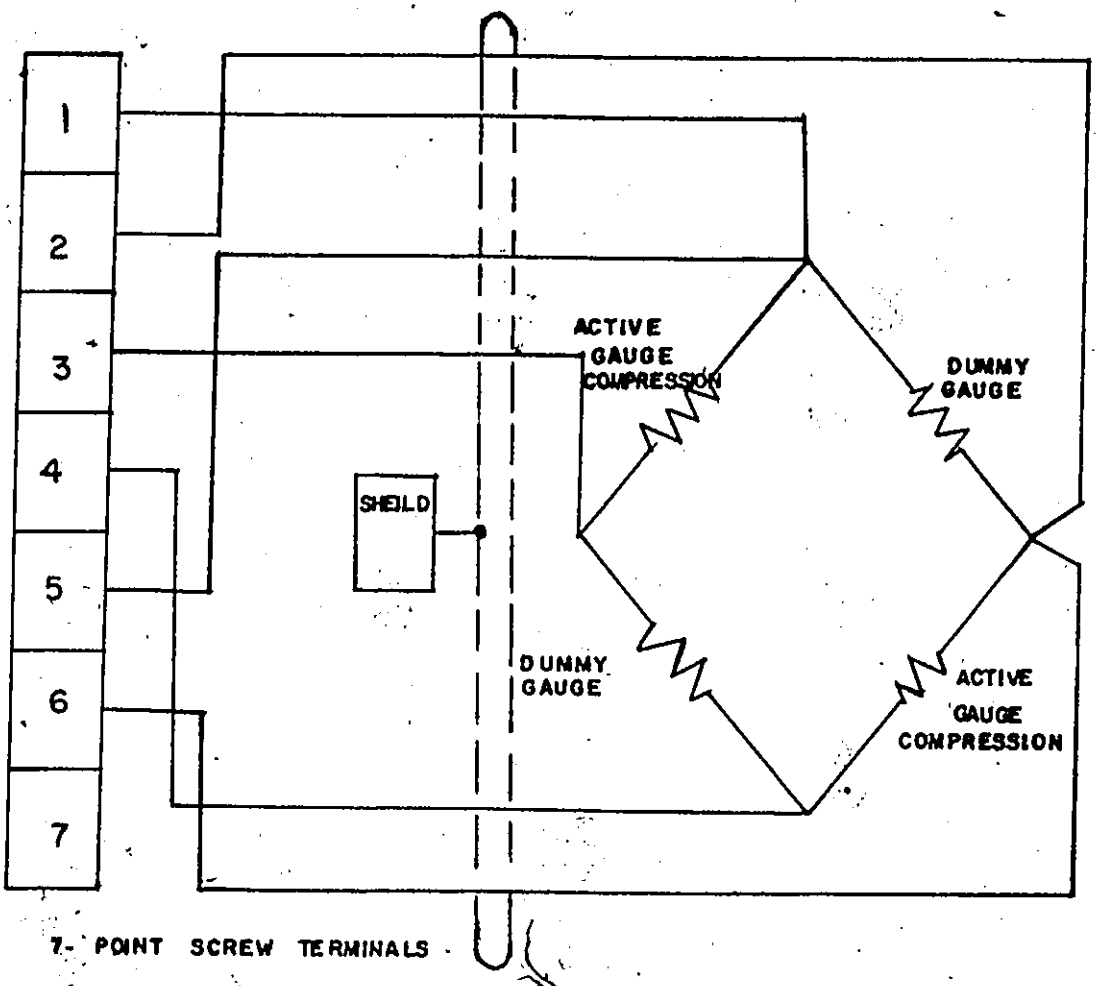

FIGURE 3.1.7 HOOK-UP OF THE NORMAL BRIDGE CIRCUIT TO THE 7-POINT SCREW TERMINALS OF THE JUNCTION BOX.

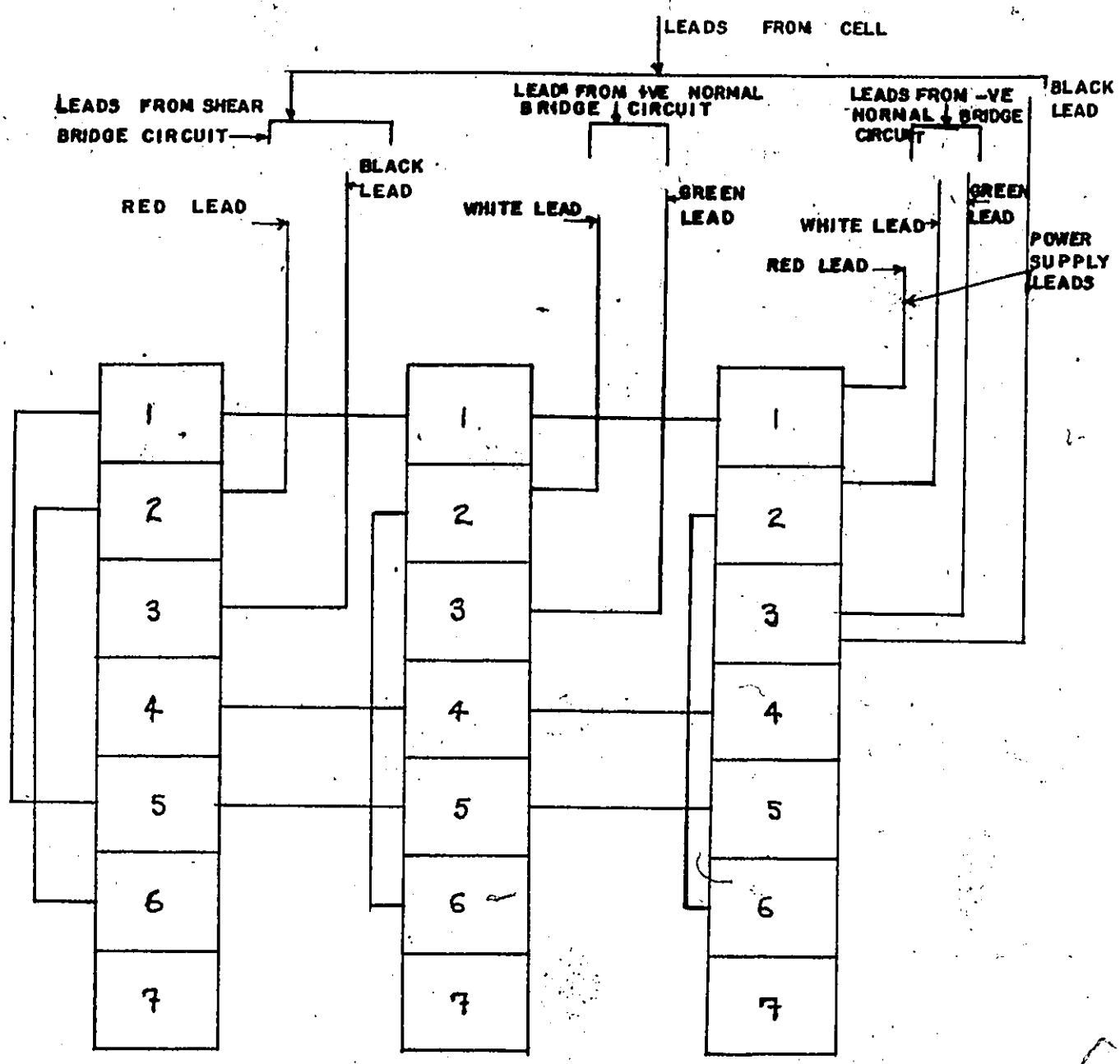

FIGURE 3.1.8 A TYPICAL CELL CONNECTION TO THE JUNCTION BOX

+e and Δs_1, respectively. The moment produces strain readings of $-\Delta e_1$, $+\Delta e_1$ and Δs_2. Simiarly, a shear force f can be replaced by a shear force f acting at the centre of the shear webs and a moment M_2 due to the fact that the actual shear force might be applied slightly above the position of the shear webs. The central shear force f on the shear webs produces reactions which gives strain readings of $S+\Delta s_3$ in the shear bridge circuit. The moment M_2 produces reactions which give strain readings of $-\Delta e_3$, $+\Delta e_3$ and $-\Delta s_3$ in the two normal bridge circuits and shear circuit respectively.

Thus in a general system of loading, the two normal bridge circuits and shear circuits will indicate strain readings of magnitude $(e_1 - \Delta e_1 - \Delta e_3)$, $(e_1 + \Delta e_1 + \Delta e_3)$ and $(s - \Delta s_1 - \Delta s_2)$, respectively. Thus there is a relationship between the output strains from the three bridge circuits and the applied loads which according to Bozouk is linear.

In this study, the three load components have been obtained from the multiplication of the inverse of the load cells calibration constant matrix and the output strain column matrix, from the three bridge circuits.

Thus,

$$\begin{bmatrix} N \\ S \\ Nx \end{bmatrix} = \begin{bmatrix} A^{-1} \end{bmatrix} \begin{bmatrix} \varepsilon^+ \\ \varepsilon^- \\ \varepsilon^s \end{bmatrix} \qquad 3.1$$

This gives three equations and once the calibration constants are

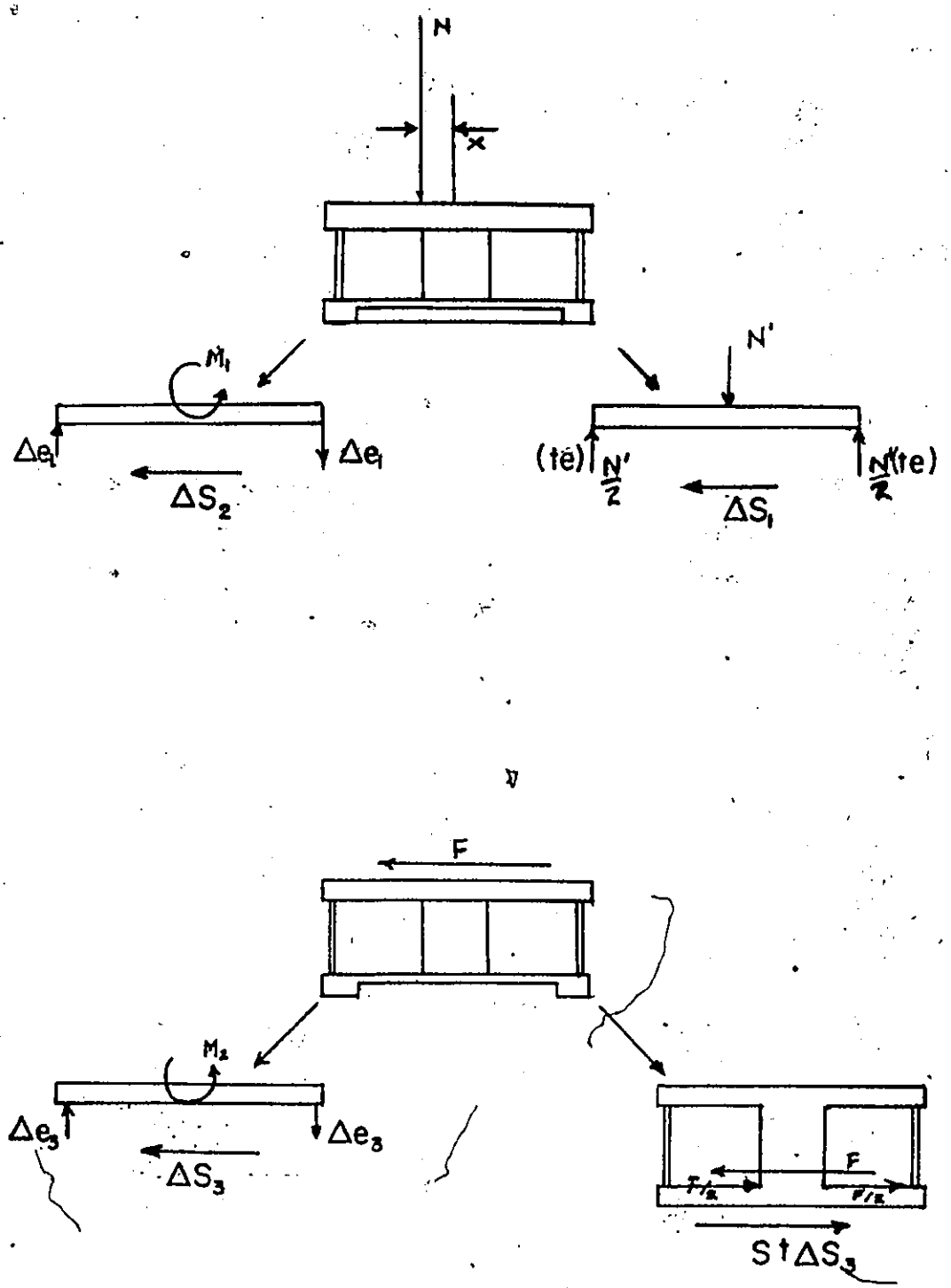

FIGURE 3·1·9 BEHAVIOUR OF THE MODIFIED CAMBRIDGE LOAD CELL UNDER NORMAL AND SHEAR LOADS.

known the operation could be carried out to yield the three load components and then finally, from N and Nx, the point of application of the normal stress.

3.2 Model Footing

3.2.1 Description

The rigid footing consists of three steel plates and an I beam with dimensions of 12" x 11.248" x 1-1/2", 12" x 11.248" x 1-1/2", 24" x 12" x 5/8" and 8" x 8", respectively. The cells were fixed to the 5/8" thick plate with a portion drilled out for the leads from the cells. The cells were located in between the 1-1/2" thick plates, thus at the centre of the footing. The steel plates were then bolted together by twnty-four bolts, each under a torque of 5 foot pounds (678.18 cm-KN), and then finally bolted to the I-beam. The load cells location on the footing and the clearance between cells, cell and steel plates are given in Figure 3.2.1.

The cells were mounted such that the direction of positive shear of the cells are towards the nearest edge of the footing. Consequently, an arrangement of the cells with numbers 2, 4, 6, 1, 3 and 5 as shown in Figure 3.2.2 was carried out, such that the even numbered cells had their direction of positive shear towards one edge of the footing while the odd numbered cells had their direction of positive shear towards the other edge. The direction of positive shear was determined during calibration such that it had a direction from negative normal webs to positive normal webs. The eccentricity was

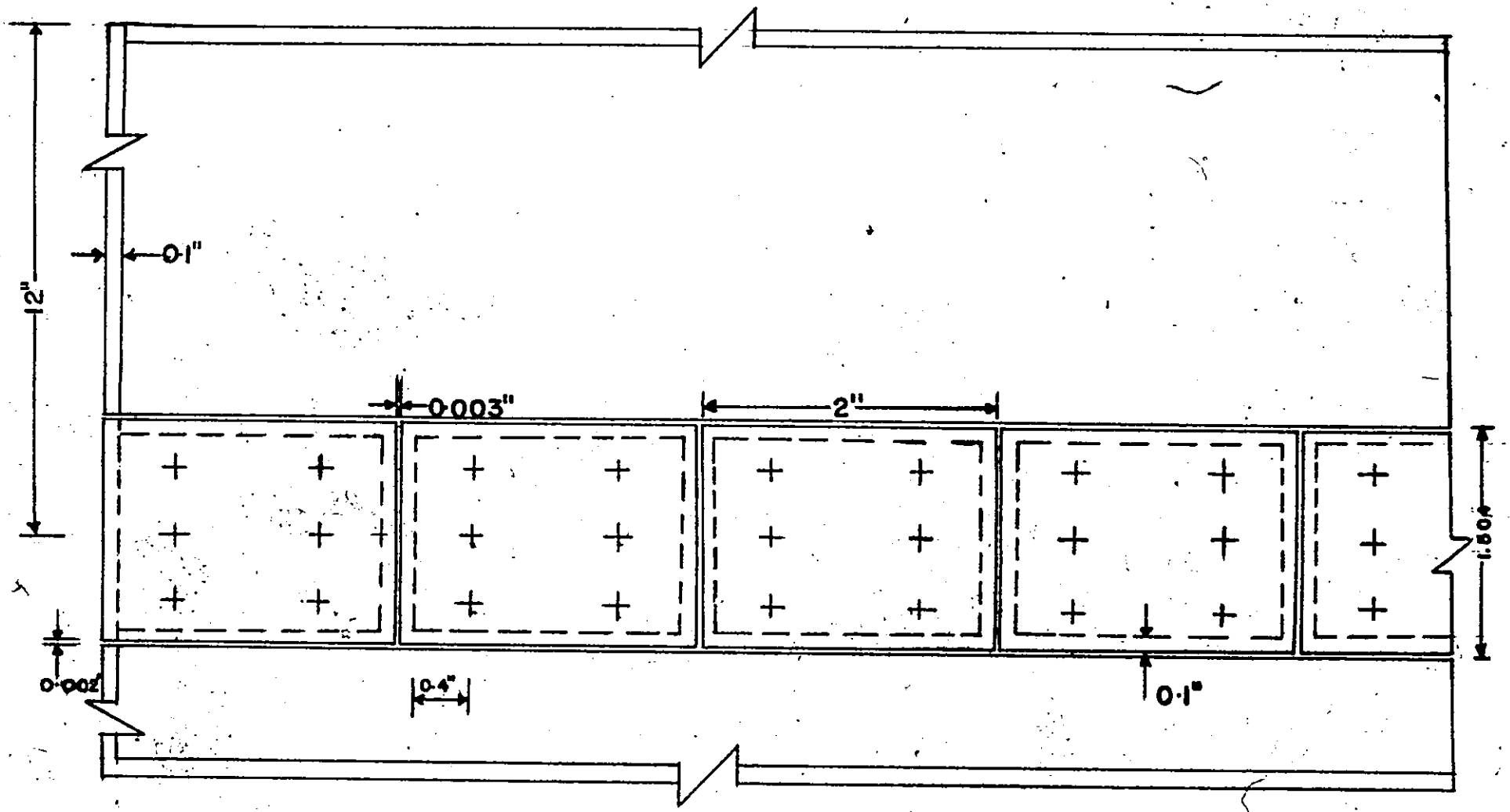

FIGURE 3·2·1 CAMBRIDGE CELLS LOCATION AT THE BOTTOM OF THE FOOTING

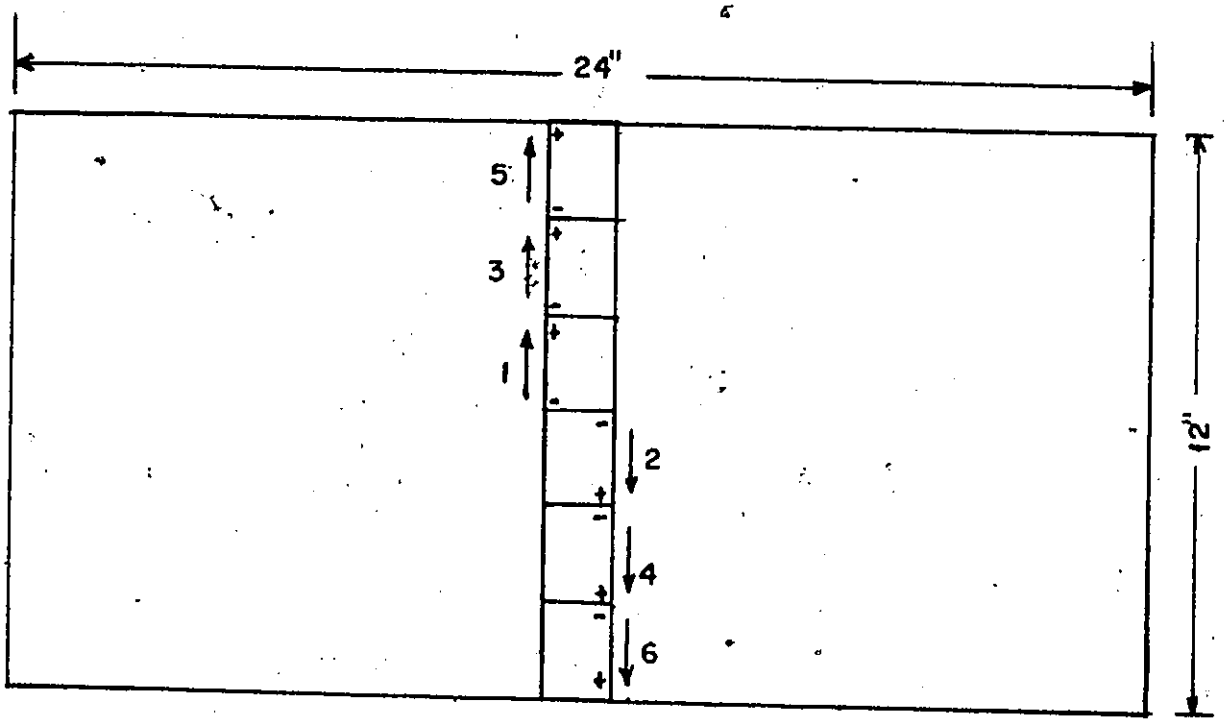

FIGURE 3·2·2 BASE OF FOOTING WITH CELL NUMBERS AND DIRECTION OF POSITIVE SHEAR STRESS.

such that it had a value of zero at the centre of the face plates and positive values towards the positive normal webs and negative values towards the negative normal webs.

The assembled rigid footing with an ultimate dimension of 1' x 2' (30.48 cm x 60.96 cm) weighed 228 lbs.

3.2.2 Footing Roughness

The surface of the footing consists of a central portion 12" x 1.504" (30.48 cm x 3.8 cm) housing the aluminum face plates of the cells, that have a clearance of 0.003" (.00762 cm) between adjacent face plates, and the surface of the 12" x 11.248" x 1-1/2" steel plates on either side of the said central portion.

The aluminum face plates (1.5" x 2"; 3.81 cm x 5.08 cm) were roughened with sand identical to that which will ultimately be used in the tests. This was however, accomplished by coating the surface of the face plates by E.Pox.E cement and filler and then pressing the sand into it to a level established by the point of application of the shear force during the calibration process. The face plates were later heat treated for about two hours.

The steel plates portion of the footing were treated in an identical manner.

Six aluminum plates were prepared as the face plates and tested in a shear box so as to determine the angle of friction between the sand mass and the roughened plate. The results are shown on Figure 3.2.3. The results indicate that the friction angle is highly dependent on the normal force.

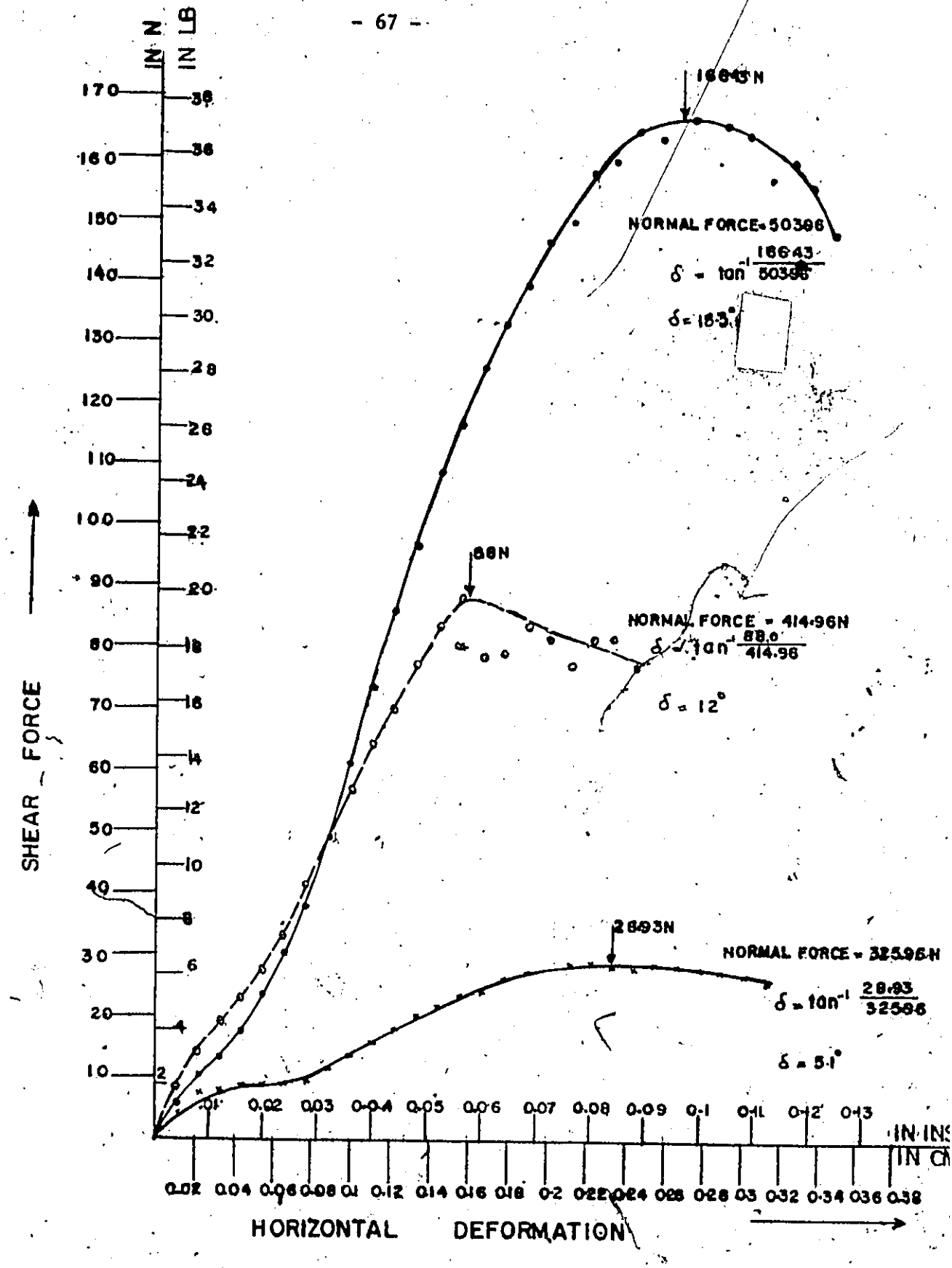

FIGURE 3·2·3 SHEAR FORCE VS HORIZONTAL DEFORMATION

3.2.3 Readout and Recording Equipment

The readout and recording device is an electronic multi-channel digital strain indicator (B and F Instruments, Model SY161-E30) designed for laboratory use. It has room for thirty channels with provisions made for expansion. Each channel was used for a bridge circuit.

Power supply of 117 volts and 60 Hz single phase from the main source was connected to the system by a three wire chord (including the ground wire).

The system can receive strain inputs with a maximum of 1000 micro inches per inch. Inputs greater than this can conveniently be accommodated by changes in the attenuator circuitry. However, in this study the maximum strain indicated above was sufficient as an upper limit for the test.

The scanning rate of the channels of the system is determined by the interaction of the Model P1237 programmer, the digital voltmeter and the printer. In this system the scanning rate is limited to 2 channels per second.

The readings can be noted as a print-out or mannually through the visual display provided on the voltmeter. The printer provides a paper tape copy of the data in the following format: 2DD-channel 1D, 1DD polarity, 4DD digitalized signal and 1D range.

The instrument can operate efficiently over a temperature range of 50°F to 105°F and a relative humidity of 90%.

3.2.4 Hook-up of the Footing to the Readout and Recording Equipment

The footing provided has six modified Cambridge load cells arranged across the footing. Each load cell has three four-arms bridge circuits, with eight lead terminals. The readings from the load cells were initially recorded by the Keithley instrument and since it was time consuming and cumbersome, a hook up of the load cells to the multichannel digital readout was performed. This, also, eliminated the time lag in reading the strains in the load cells by the Keithley instrument, thus offsetting the possible errors that might be induced by the load application time.

Each load cell has three 4-arm bridge circuits, viz., the positive normal bridge circuit, the negative normal bridge circuit and the shear bridge circuit. Each bridge circuit reading was recorded through a channel, thus, 18 channels were utilized during the study. For a proper connection of each bridge circuit to a channel, six wires, Figures 3.1.7 and 3.1.8, would be required. Thus, as a consequence of this hook-up some modifications in the number of wires from each load cell was necessary. However, these modifications were not performed by soldering new wires in the load cells but were made externally in the junction box provided with the recording instrument as shown in Figure 3.1.8.

A 120 ohm 1% resistor was used as the span limit resistor in order to prevent the excitation supply from being shorted when a particular bridge channel shorts. Similarly, a balance resistor of

10,000 ohm 1% resistor was used which was appropriate for the strain gauges installed in the load cells.

A calibration resistor of 40,000 ohm 0.5% resistor was used and by means of equation 3.2 the strain level simulated when it is shunted across a 120 ohm strain gauge with a gauge factor of 2.08 was computed.

The simulated strain (ε) is given by

$$\varepsilon = \frac{1}{nk} \left(\frac{R}{R + R_{cal}}\right) \qquad 3.2$$

n = number of arms

k = gauge factor

R = resistance of the shunted arm

R_{cal} = resistance of the calibration resistor

Thus, for the shear and normal bridge circuits with 4 arms each, the strain simulated:

$$\varepsilon = \frac{1}{4 \times 2.08} \left[\frac{120}{120 + 40,000}\right]$$

$$= \frac{1}{8.32} \left[\frac{120}{40.20}\right]$$

= 359 micro strains

After the completion of the connections at the junction box, the printed circuit connectors were fitted to the signal conditioning modules. The instrument was connected to the power source and thus set for use.

The power switches on the 15-1500 and PS 230 power supplies were turned on and the skip/record switch placed in the record position and the calibration switch placed in the off position. The instrument was left to warm up for 30 mins. The voltage adjustment control on the model 15-1500 power supply was adjusted until 9 volts was shown on the meter. This was the maximum voltage appropriate for the strain gauges and the system. This meter, however, shows power supply and not the bridge voltage which in the case of the 120 ohm strain gauges used varies between 0.1 and 0.5 times the power supply voltage depending on the setting of the span control knob. The input voltage through any bridge circuit should be constant throughout the test since any change in the voltage causes a similar error in the recorded values of strains.

The amplifier was zeroed and the balancing of the channels performed. The balance switches for the twenty channels was placed in the 0 position for each of the channels. The balance control knob was adjusted until the strain indicator displayed zero. If the strain read was too negative, the balance switch was switched to the positive position and balancing continued until the strain indicator displayed zero. If it was too positive, the balance switch was switched in the negative position, and balancing continued until the strain indicator displayed zero. This operation was performed for the 18 channels which were used.

The calibration switch was placed in the on position and the span control knob adjusted until the value of the strain simulated computed for equation 3.2 for the two normal and shear bridge circuits

were displayed on the strain indicator for their corresponding channels. This was performed for the eighteen channels. The calibration switch was placed in the off position and the balance control knob adjusted, for each of the eighteen channels, until zero was displayed on the strain indicator. The calibration switch was again placed in the on position and the span control know adjusted until the correct simulated strains were displayed on the strain indicator for each channel. These processes were repeated with the calibration switch in the off position and the correct simulated strain when the calibration switch was in the on position.

Thus, with the balancing completed, the footing was then ready for calibration and finally for use in the sandbox.

CHAPTER 4

CALIBRATION OF FOOTING

4.1 General

The calibration of the footing is synonymous with the calibration of the modified Cambridge load cells which are the stress indicators. Usually, the cells are calibrated individually but in this study, the six cells have been calibrated as an integral part of the footing. This has been done for the following reasons:

(1) The footing provided had the load cells already installed.

(2) This provided an opportunity for the calibration of the load cells in their true operating condition, thus offsetting any errors, if any, that might be induced in the determination of the contact stresses distribution, as a result of the individual calibration of the load cells prior to installation.

Owing to the first reason it was not possible to check if the behaviour of the load cells were hampered by their installation in the footing.

Subsequently, the calibration of the modified Cambridge load cells as an integral part of the footing led to the design of new calibration apparatus. At this juncture the writer thought it necessary to see if Arthur and Roscoes theory on the independence of the calibration constants on the method of loading was valid for the modified Cambridge cell, especially as an integral part of the footing.

Thus, an apparatus for line load, Figure 4.2.1, point load, Figure 4.3.1 and shear load were developed.

The apparatus required for the different loading conditions consisted of steel plates and a loading frame assembly. A steel plate has been utilized in place of the aluminum face plate so that it could withstand the calibration load of 400 lbs [1.669KN] that will be applied on the knife edge or ball bearing without cutting through it or denting it which would otherwise have produced projection on the underside of the aluminum plate that might lead to erroneous results.

The high bearing stress of the steel plate also prevents the wire on which the shear load is applied from tearing through it.

There are two methods developed for the determination of the calibration constants for the Cambridge load cells, one by Arthur and Roscoe (1961) and the other by Bozozuk (1972).

In Arthur and Roscoe's theoretical considerations of the action of a load cell under an eccentrically applied load, they declared that the sum of the outputs from the positive normal bridge circuit and the negative bridge circuit are directly proportional to the applied load and independent of the eccentricity and shear force. However, a slight inaccuracy is incorporated in the above theory since a difference in the stiffness of the webs and gauge factor of the strain gauges invalidates it. Practically, he proposes that the correct values of the normal stress, shear stress and eccentricity of the normal stress could be obtained by interpolation from graphs.

From the principle of operation of the modified Cambridge cell, it has been shown that the sum of the output from the two normal bridge circuits was not directly proportional to the applied load because of the portion of load taken up by the shear webs.

Bozozuk in his method, assumed a linear dependence between the output voltages from the three bridge circuits, viz., the positive normal bridge circuit, the negative bridge circuit and the shear bridge circuit and the applied loads, i.e., the normal load, the shear load, and the moment due to the eccentricity of the normal load. This then led to the following equations:

$$\begin{bmatrix} v^+ \\ v^- \\ v_s \end{bmatrix} = \begin{bmatrix} a_{+n} & a_{+s} & a_{+x} \\ a_{-n} & a_{-s} & a_{-x} \\ a_{sn} & a_{ss} & a_{sx} \end{bmatrix} \begin{bmatrix} N \\ S \\ Nx \end{bmatrix} \qquad 4.1$$

where

v^+ = output from the positive normal bridge circuit

v^- = output from the negative normal bridge circuit

v_s = output from the shear bridge circuit

N = normal load

S = shear load

Nx = moment due to eccentricity of normal load

x = distance from the centre of the face plate to the point of application of the normal load

a_y = calibration constants of the cell.

This method of determining the load cell constants seem to be in order with the mode of operation of the modified Cambridge cells for the load limits that the webs were designed for.

4.2 Line Load (Figure 4.2.1)

The line load apparatus consists of a steel plate and a loading frame assembly.

Steel Plate: As shown in Figure 4.2.1, it has a dimension of 1-1/2" x 2-3/4" and it is 1/4" thick for 2" of its length and 3/16" thick for the remaining 3/4". This allows the plate to be attached to a cell without resting on the adjacent load cell. The 1-1/2" x 3/4" x 3/16" portion allows a hole 7/8" Ø connected by 2 holes 1/16" Ø, equi-distant from the centre of the plate to be drilled for shear load application. The steel plates has grooves for a knife edge at the centre and at eccentricities of 0.25", 0.5" and 0.75" on either side of the centre of the plate.

Loading Frame Assembly: This consists of two steel bars A and B, two threaded rods and nuts.

Bar A has a dimension of 1" x 13/16" x 28" with a knife edge that is 1-1/2" long, 1/8" thick and 1/16" wide at the base, protruding from underneath the bar and with two hooks for supporting purposes.

Bar B has a dimension of 1" x 1" x 28" with a hook at the centre for the hanger.

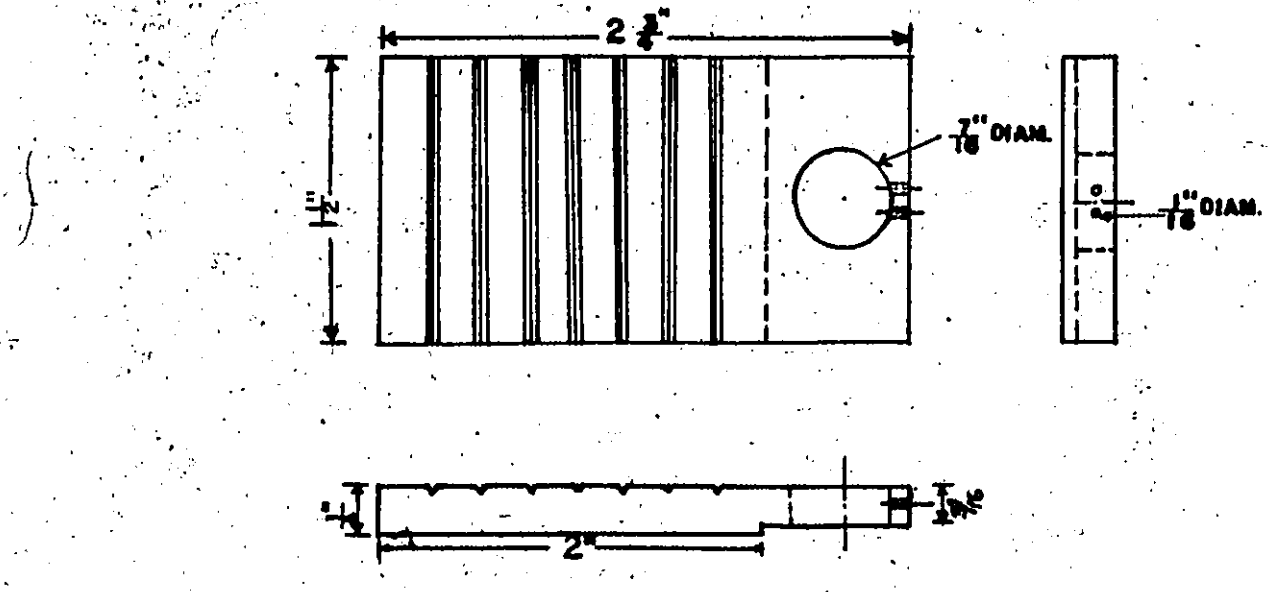

STEEL PLATE

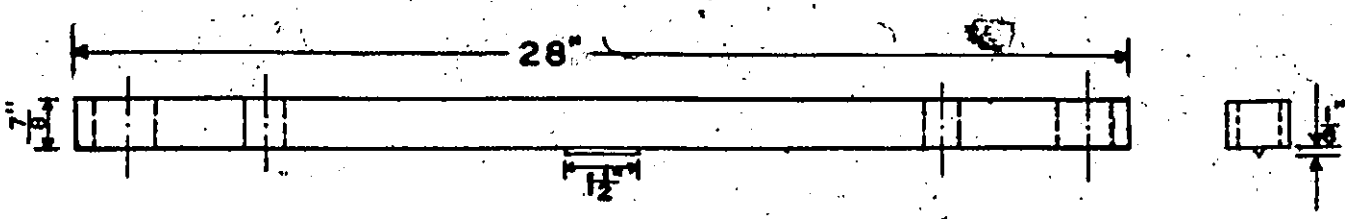

BAR A

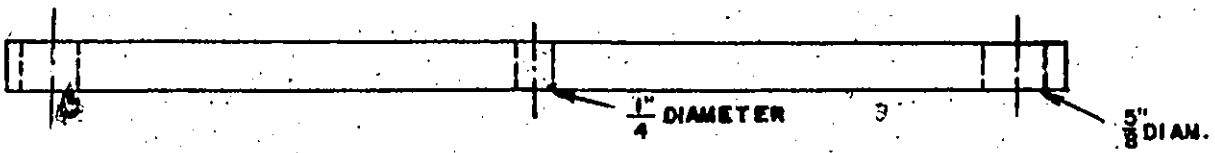

BAR B

FIGURE 4.2.1 APPARATUS FOR LINE LOAD.

The footing with its face upward was placed on a table. The aluminum face plates were removed and the steel plate attached to one of the load cells. The author had to make sure that during the screwing of the steel plate to the load cells that no strains were induced in the load cells. Bar A was then placed over the steel plate at a chosen eccentricity and connected to Bar B, under the table by threaded rods and nuts. The spirit level was then used to check if the bars were truly horizontal. The hanger was then placed through the hook in Bar B. The strain due to the weight of the loading frame assembly (18.66 lbs) was noted and then loading with dead weights was continued in steps of 20 lbs. This operation was carried out for the six modified Cambridge load cells. The results are shown graphically in Appendix A.

4.3 Point Load (Figure 4.3.1)

The point load apparatus consists of a steel plate and a loading frame assembly.

Steel Plate:

The steel plate is similar to that used for the line loading excepting that instead of the grooves for a knife edge there was dents which acted as seating for the steel ball bearing.

Loading Frame Assembly:

This consists of bars C and D, similar to bars A and B described for line loading excepting that in bar A the knife edge was replaced by a seat for a steel ball bearing to form bar C, while bar D remains the same as bar B.

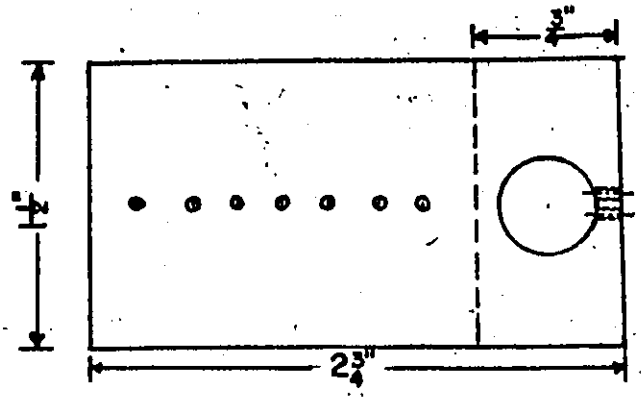

STELL PLATE

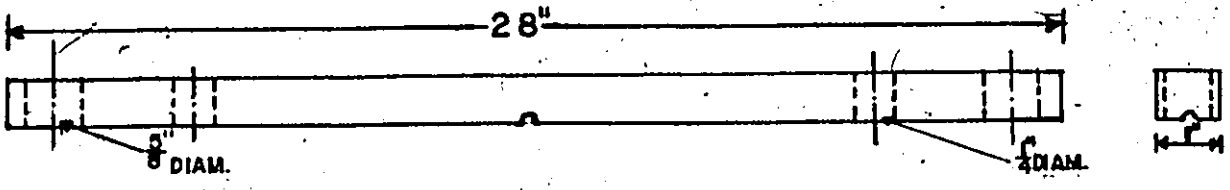

BAR C

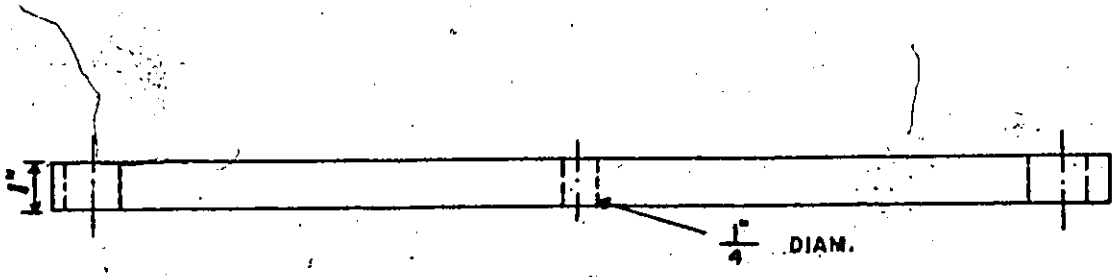

BAR D.

FIGURE 4·3·1 APPARATUS FOR POINT LOAD.

The calibration for the point load was then carried out with the steel plate attached to the active face of one of the load cells without any strains induced. A steel ball bearing was placed in one of the dents and Bar C placed over it. Bar C was then connected to Bar D by threaded rods and nuts. A hanger was then placed through the hook in Bar D and the strains caused by the weight of the loading frame assembly (9.6 lbs) was noted. Subsequent loading by dead weights were done in steps of 20 lbs. This was done for the six modified Cambridge load cells. The results for a typical Cell No. 5, is shown in Appendix B, pages

4.4 Shear Load

This apparatus consists of a steel plate and a loading frame assembly.

Steel Plate: This is one of the shear plates used for either the line loading or point loading. The centre of the 1/16" diameter holes was drilled such that its elevation would be at the sand surface on the aluminum face plate and the remainder of the footing.

Loading Frame Assembly: The load was applied by a piano wire that can withstand 400 lbs. This piece of wire was passed through the 1/16" diameter holes in the steel plate and tied together at its end by a bolt and nut arrangement.

The steel plate with the piano wire, bolt and nut arrangement was attached to the active face of one of the load cells. Precaution was taken in the attachment of the steel plate so that no

strains were induced. The footing was then turned over on its side making sure that its instrumented face was truly vertical. The hanger was placed on the bolt and nut arrangement. The strains induced by the weight of the loading medium was noted. Loading by means of dead weight was then carried out in steps of 20 lbs. This operation was repeated for the six load cells with the shear force being applied in the direction of positive shear force. The results are shown graphically in Appendix A.

4.5 Load Constants

In this study the method developed by Bozozuk has been simulated in the determination of the load cell constants. However, instead of the output voltages from the three bridge circuits, output strains have been employed. This has been possible because of the relationship that exists between output voltages and output strains. which is given as

$$V_{out} = V_{in} \times g.f \times \varepsilon$$

where

V_{out} = output voltage

V_{in} = input voltage

g.f = gauge factor

ε = strain (change in resistance of the strain gauges).

Thus since the gauges have the same gauge factors and the input voltages are the same then the strains should be directly proportional to the output voltages.

The following equations in matrix form was developed.

$$\begin{bmatrix} \varepsilon^{+} \\ \varepsilon^{-} \\ \varepsilon_s \end{bmatrix} = \begin{bmatrix} C_{+n} & C_{+s} & C_{+x} \\ C_{-n} & C_{-s} & C_{-x} \\ C_{sn} & C_{ss} & C_{sx} \end{bmatrix} \begin{bmatrix} N \\ S \\ N_x \end{bmatrix} \qquad 4.2$$

i.e. $\{\varepsilon\} = [C]\{F\}$ 4.3

where

ε^{+} = output strain from the positive normal bridge circuit

ε^{-} = output strain from the negative normal bridge circuit

ε_s = output strain from the shear bridge circuit

N = normal load

S = shear load

x = distance from the centre of the active face to the point of application of the normal force

N_x = moment due to the eccentricity of the normal force.

C_{ij} = calibration constants of the modified Cambridge load cell.

A matrix multiplication operation on equation 4.2 gives the following expression

$$\varepsilon^{+} = NC_{+n} + SC_{+s} + NxC_{+x} \qquad 4.4$$

$$\varepsilon^{-} = NC_{-n} + SC_{-s} + NxC_{-x} \qquad 4.5$$

$$\varepsilon_s = NC_{sn} + SC_{ss} + NxC_{sx} \qquad 4.6$$

Thus on differentiating the equation 4.4 with respect to N with the shear load kept constant (which was in fact zero during the calibration test) then

$$\left(\frac{d\varepsilon^+}{dN}\right)_{s=o} = C_{+n} + xC_{+x} \qquad 4.7$$

The above equation implies that if $\frac{d\varepsilon^+}{dN}$ is plotted against the eccentricity x then the intercept on the $\frac{d\varepsilon^+}{dN}$ axis gives the cell constant C_{+n} and the slope gives the cell constant C_{+x}.

On differentiating the equation 4.4 with respect to S and N and x kept constant which were in fact zero during the calibration tests then

$$\left(\frac{d\varepsilon^+}{dS}\right)_{N,x=o} = C_{+s}$$

The slope of the plot of ε^+ vs S gives the cell constants C_{+s}.

A similar manipulation of equations 4.5 and 4.6 yields the cell constants C_{-n}, C_{-x}, C_{-s}, C_{sn}, C_{ss} and C_{sn}.

The determination of the above load cell constants culminated in a calibration test.

Procedure for the calibration tests:

(1) Keep S = 0, X = 0 and vary N from 0 to 400 lbs in 20 lbs increments and then return to zero. Plot the results as shown in Appendix A, pages 202, 205 and 206 for cell number 1.

(2) Repeat the above procedure for X equals -0.25, -0.5, -0.75,

0.25, 0.50 and 0.75. Plot the results as shown in Appendix A pages 202 to 207 for Cell Number 1.

(3) Keep N = 0 and X = 0 and vary S from 0 to 400 lbs in 20 lbs increment and then return to zero. The results are given in Appendix A in graphical form, pages 208 to 210, for Cell Number 1.

(4) Plot the slope of ε^+ vs N, ε^- vs N and ε_s vs N against eccentricity (x). These give intercepts and slopes of C_{+n} and C_{+x}, C_{-n} and C_{-x} and C_{sn} and C_{sx}, respectively, for Cell Number 1. These are shown graphically in Appendix A, pages 211 to 213.

(5) The slope of the plot of ε^+ vs S, ε^- vs S and ε_s vs S gives the values for C_{+x}, C_{-s} and C_{ss}, respectively, for Cell Number 1. They are presented graphically in Appendix A, pages 208 to 210.

The above processes were repeated for the remaining five modified Cambridge cells. The results are shown graphically from pages 214 to 270 in Appendix A. The load cell constants for the six cells determined as outlined above were subsequently substituted in equation 4.2 and are as follows:

Cell Number 1:

$$\begin{bmatrix} \varepsilon^+ \\ \varepsilon^- \\ \varepsilon_s \end{bmatrix} = \begin{bmatrix} -1.44 & +0.0857 & -1.765 \\ -1.5 & -0.3875 & +1.875 \\ +0.024 & -4.231 & -0.1364 \end{bmatrix} \begin{bmatrix} N \\ S \\ N_x \end{bmatrix}$$

Cell Number 2

$$\begin{bmatrix} \varepsilon^+ \\ \varepsilon^- \\ \varepsilon_s \end{bmatrix} = \begin{bmatrix} -1.43 & +0.394 & -1.818 \\ -1.55 & -0.318 & +1.90 \\ -0.022 & -4.583 & -0.096 \end{bmatrix} \begin{bmatrix} N \\ S \\ N_x \end{bmatrix}$$

Cell Number 3:

$$\begin{bmatrix} \varepsilon^{+} \\ \varepsilon^{-} \\ \varepsilon_{s} \end{bmatrix} = \begin{bmatrix} -1.45 & +0.234 & -1.818 \\ -1.61 & -0.0455 & +1.852 \\ +0.058 & -3.75 & -0.143 \end{bmatrix} \begin{bmatrix} N \\ S \\ N_x \end{bmatrix}$$

Cell Number 4:

$$\begin{bmatrix} \varepsilon^{+} \\ \varepsilon^{-} \\ \varepsilon_{s} \end{bmatrix} = \begin{bmatrix} +1.43 & -0.304 & +1.818 \\ -1.52 & -0.1667 & +1.8 \\ -0.05 & -3.684 & -0.178 \end{bmatrix} \begin{bmatrix} N \\ S \\ N_x \end{bmatrix}$$

Cell Number 5:

$$\begin{bmatrix} \varepsilon^{+} \\ \varepsilon^{-} \\ \varepsilon_{s} \end{bmatrix} = \begin{bmatrix} +1.42 & -0.2826 & +1.765 \\ -1.58 & -0.2857 & +1.923 \\ -0.013 & -3.5294 & -0.182 \end{bmatrix} \begin{bmatrix} N \\ S \\ N_x \end{bmatrix}$$

Cell Number 6:

$$\begin{bmatrix} \varepsilon^{+} \\ \varepsilon^{-} \\ \varepsilon_{s} \end{bmatrix} = \begin{bmatrix} -1.43 & +0.064 & -1.785 \\ -1.50 & -0.0154 & +1.818 \\ -0.052 & -3.636 & -0.143 \end{bmatrix} \begin{bmatrix} N \\ S \\ N_x \end{bmatrix}$$

4.6 Factors Affecting Calibration

Within the scope of the calibration tests performed, three factors, viz., load (normal and shear loads), eccentricity of the normal load and temperature have been considered as the principal factors that might affect the calibration and footing test results.

Thus the cells have been calibrated with respect to load and eccentricity. Temperature calibration of the cells have not been undertaken since the calibration room had an identical temperature with the testing room.

4.6.1 Load

The load applied at a particular eccentricity has a linear relationship with the output strains from the three bridge circuits (the positive normal bridge circuit, the negative normal bridge circuit and the shear bridge circuit). For loads not exceeding the maximum design loads for the webs (104 lbs for each shear web and 156 lbs for each of the normal webs).

4.6.2 Eccentricity

An eccentrically applied load can conveniently be replaced by a central load and a moment. As described in the mode of operation of the cells, page 55, they induce strains in all the three bridge circuits. A plot of the strain output from the three bridge circuits vs eccentricity indicates a linear relationship between both variables for web loads not exceeding their design values (Figure 4.6.1).

As would be expected, as the eccentricity of the applied load increases towards a pair of particular normal webs (either positive or negative normal webs) a greater portion of the compressive load is carried through those webs leading to a greater value in strain output from the bridge circuit that contains that pair of normal webs.

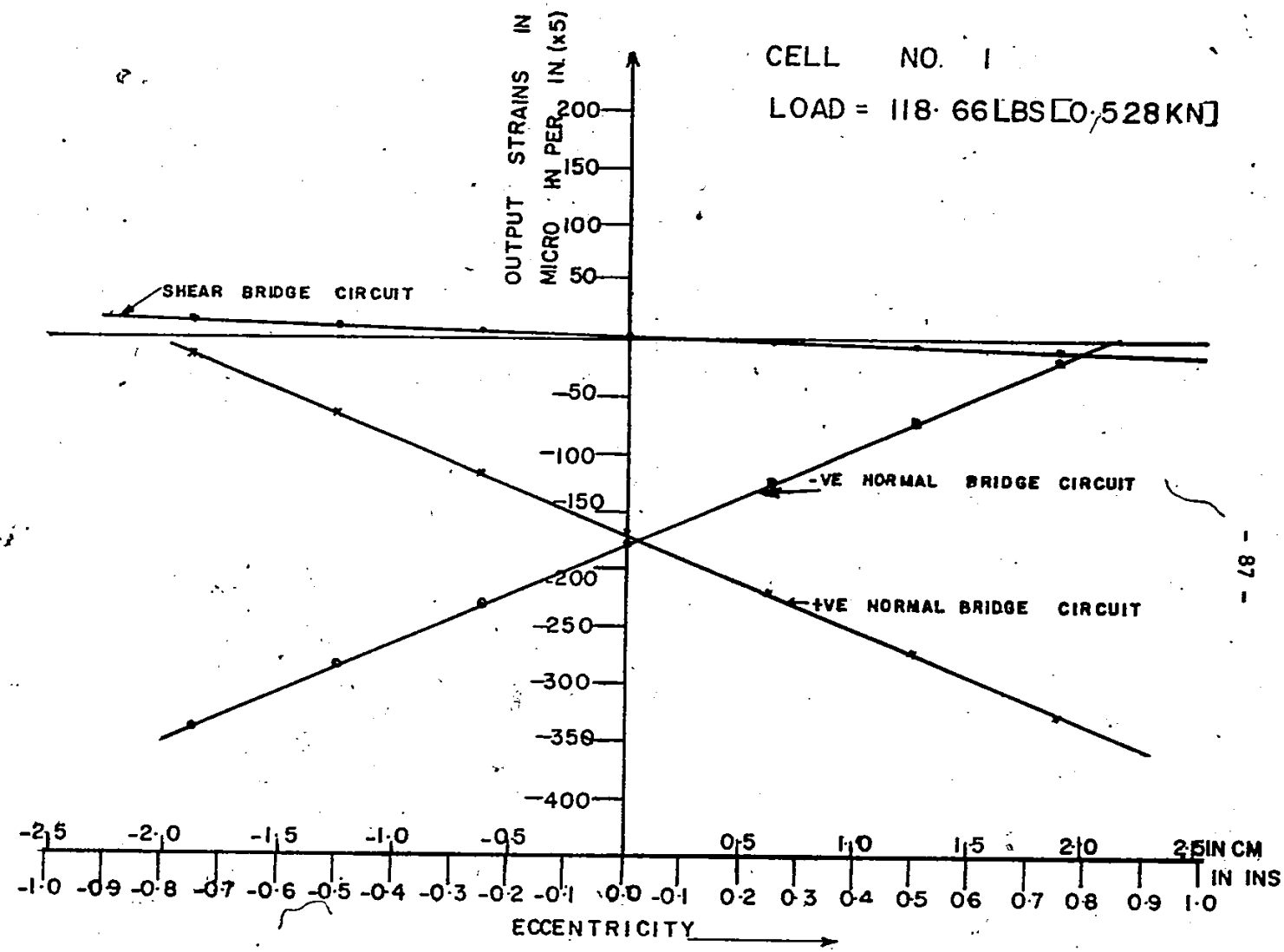

FIGURE 4·6·1 OUTPUT STRAIN VS ECCENTRICITY.

4.6.3 Temperature Effects

(A) Gauges attached to the Load Cell

A quantitative consideration has been given to the temperature effect on themmodified Cambridge load cells. Thus, calibration of the load cells with respect to temperature has not been undertaken, since the calibration room temperature and testing room temperature were identical. However, two temperature tests were performed on the load cells in order to ascertain if temperature had any effect on gauges attached to the webs of the modified Cambridge load cells.

(1) Test at 0°C

The footing was turned with its face upwards and a wooden box with an internal dimension of 24" x 12" x 6" (60.96 cm x 30.4 cm x 15.24 cm) was constructed around it. A plastic bag was placed in the wooden box and filled with water and ice blocks mixture to the top of the box. The readings of the strains due to the weight of the water-ice mixture in the webs were immediately monitored by the multi channel strain indicator, and their values for the eighteen channels noted.

The box was covered with a rubber sofa to reduce as much as possible the effect of room temperature (22.5°C) on the ice. The above arrangement applied a temperature gradient through the footing, which is the most serious temperature condition that the footing can be subjected to. The water-ice mixture was left for twenty-four hours before the final readings were taken.

TABLE 4.6.1

Results of Temperature Effects on Load Cells

Cell No	Channel No	Strain Due To Time in Micro Strains	Strain Due To Water-Ice Mixture Weight at Start in Micro Strains	Strain Due To Water-Ice Mixture at 0°C After 24 hrs in Micro Strains	Strain Due To Temperature Gradient in Micro Strains
	0	3	2	9	4
3	1	2	1	3	0
	2	0	3	-4	-1
	3	0	2	2	0
4	4	0	0	-2	-2
	5	0	0	2	2
	6	0	1	5	4
5	7	-4	-2	7	13
	8	-2	-2	9	13
	9	-	-	-	-
	10	2	0	2	0
6	11	1	0	0	-1
	12	1	1	1	-1
	13	2	0	3	1
2	14	2	0	0	-2
	15	0	0	0	0
	16	1	0	2	1
1	17	-1	1	-1	-1
	18	1	-1	0	0
	19	-	-	-	-

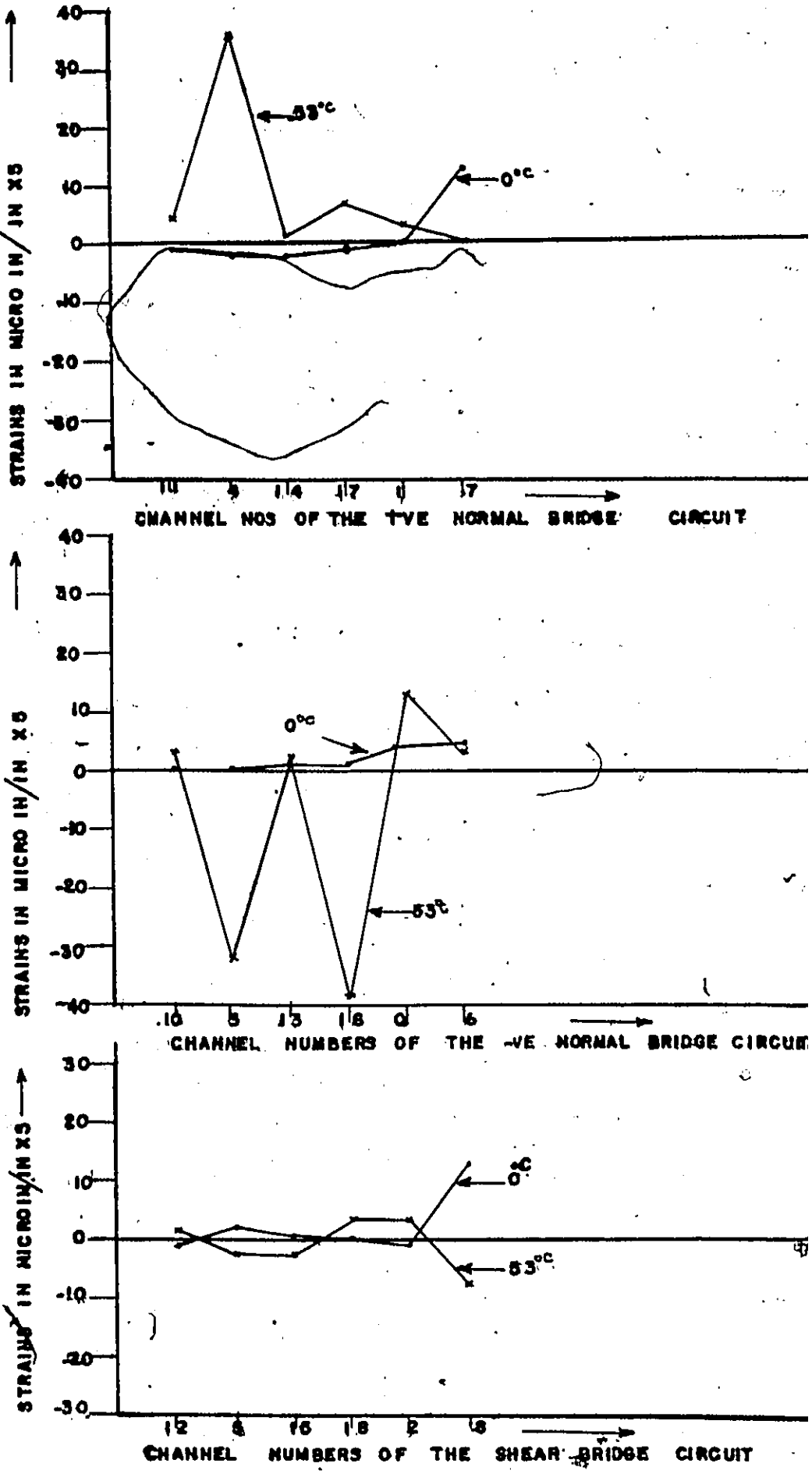

FIGURE 4.6.2 STRAIN INDUCED IN THE WEBS DUE TO TEMPERATURE

The results are given in Table 4.6.1 and has been presented graphically in Figure 4.6.2.

(2) Test at 53°C

Similar to the cold test, the box with the plastic bag was filled with hot water at a constant temperature of 53°C to a desired elevation. The strain readings for the eighteen channels in the multichannel strain indicator were immediately noted. The hot water was maintained at a constant height and temperature by the following process. The hot water in the plastic bag was sucked out by means of a siphon operation. The valve attached to the top was adjusted and the siphon operation continued until a system of equilibrium was maintained between the inflow of hot water and outflow. Thus maintaining a constant height and temperature (53°C). The hot water (53°C) was left for 1 hour before the final readings were taken.

The results are given in Table 4.6.2 and have been presented graphically in Figure 4.6.2.

(B) Recording Equipment

During the course of the calibration tests, it was observed that after balancing the channels and leaving the system to operate for hours that strains were induced in each of the bridge circuits. Thus after twenty-four hours the strain readings for the eighteen channels were noted. This is given in Table 4.6.1. During the calibration care was taken to see that all channels were balanced before each loading operation.

TABLE 4.6.2

Result of Temperature Effect on Load Cells

Cell No	Channel No	Strains Due To Hot Water At Time T=0 in Micro Strains	Strains Due To Water at 53°C After One Hour in Micro Strains	Strains Due To Temperature Gradient in Micro Strains
	0	-16	- 3	+13
3	1	-13	-10	+ 3
	2	- 5	2	+ 3
	3	- 9	-41	-32
4	4	+ 6	+42	+36
	5	1	- 2	- 3
	6	- 7	-10	+ 3
5	7	+ 6	+ 6	0
	8	- 6	-14	- 8
	9	-	-	-
	10	- 2	1	+ 3
6	11	0	+ 4	+ 4
	12	- 2	- 1	+ 1
	13	-14	- 2	+ 2
2	14	-18	-17	+ 1
	15	+14	+11	- 3
	16	- 7	-46	-39
1	17	- 7	0	+ 7
	18	6	+ 9	+ 3
	19	-	-	-

The recording equipment (SY161-E30) has been found by the manufacturers (B and F Instruments) to operate efficiently over a temperature range of 50°F and 105°F which meets the temperature conditions in the calibration and testing rooms.

CHAPTER 5

FOOTING TESTS IN THE SAND BOX

5.1 General

As indicated in Chapter 1, the density of the sand, which is a function of the void ratio and hence the porosity, is a factor which affects the distribution of the contact stresses under a footing.

In the field, variations in density along the horizontal and at different elevations exist. However, in a model footing test it is imperative to maintain a uniform density throughout the sand mass so that a quantitative deduction could be made on the effect of density changes on the contact stresses distribution. Uniform density was guaranteed by employing a sand raining device for spreading the sand into the sandbox.

Since a plane strain test was to be performed, the walls of the sandbox were made as rigid as possible so that no strains could be developed in the long direction of the footing. In order to satisfy the above testing condition, the transition member was made in three two-feet sections, thus simulating the long body, with the load applied normally to the three footings by three separate hydraulic jacks. Since friction was bound to affect the uniform downward motion of the three footings, displacement was chosen as a criterion for the loading of the footing, after which the valves to the jacks were opened so as to bring about equal settlement of the three sections of the footing.

Thus the footings were pushed into the sand mass through equal distances and the loads indicated by load transducers and by the gauges attached to the three jacks were noted.

5.2 Experimental Apparatus

5.2.1 Quartz Sand

In this study, the sand used was factory crushed quartz.

From an earlier study performed by Hasnain (1974) the following results were obtained:

1) The sand particles are sharp and angular with a uniformity coefficient of 2.1.

2) From the grain size distribution curve, Figure 5.2.1, it is apparent that the quartz sand can be classified as fine to medium sand.

3) The maximum and minimum densities determined under the ASTM procedure were 103.3 lb/ft^3 [16.24 KN/m^3] and 77.9 lb/ft^3 [12.25 KN/m^3], respectively.

4) The maximum and minimum void ratios were 1.13 and 0.61 and their corresponding porosities are 0.53 and 0.38, respectively.

5.2.2 Sand Box (Figure 5.2.2)

The box has a dimension of 48' x 6' x 7' [14.63 m x 1.83 m x 2.13 m] and has been divided into two equal compartments A and B by two bulkheads. Thus while one compartment was used as a testing box, the other acted as a storage bin for the sixty tons of quartz sand. The sand box is made of 1/2" (1.27 cm) thick steel plates held rigidly in place by 10WF sections which are 7' (2.134 m) long with a web

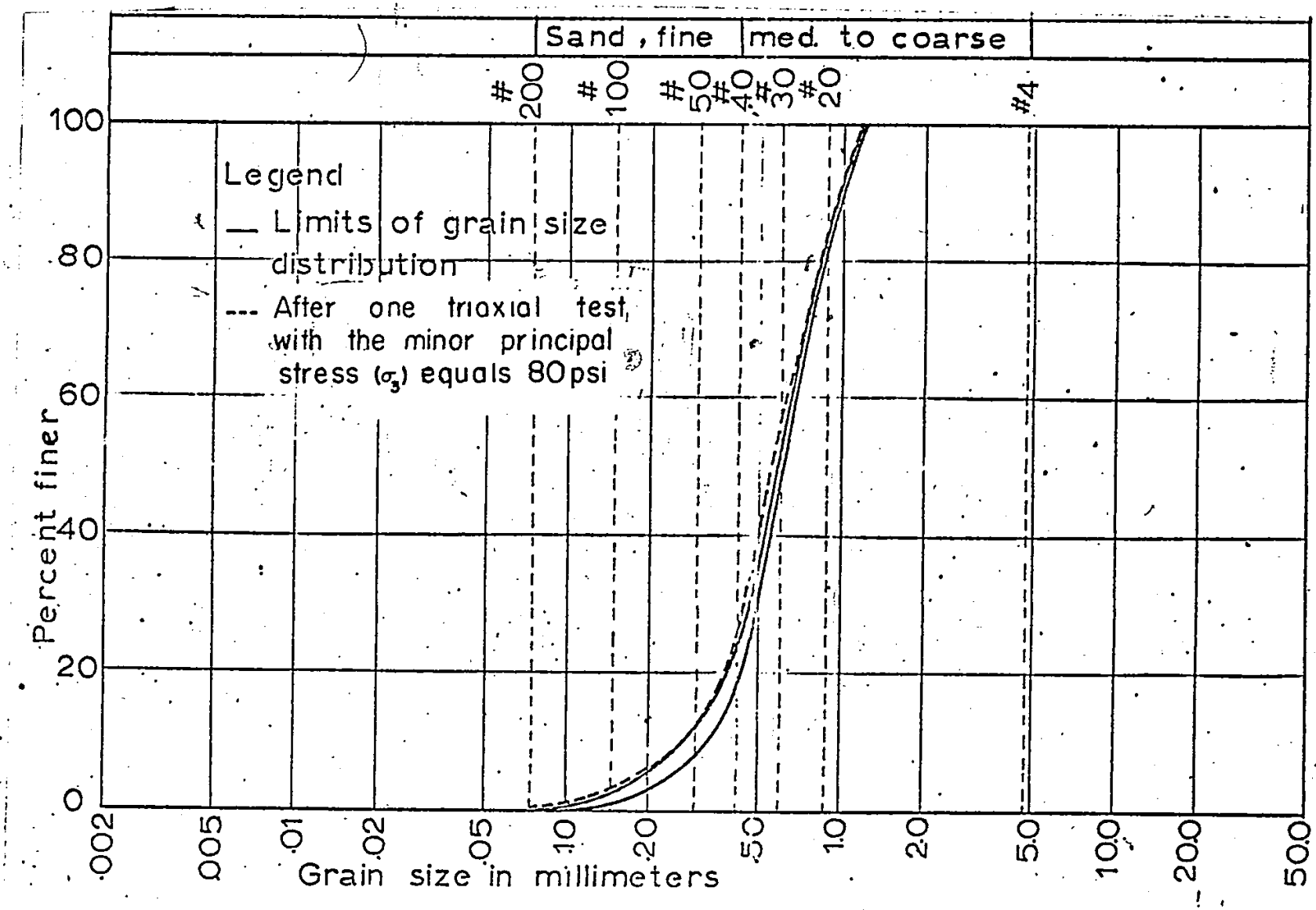
Sand, fine
med. to coarse
#200
#100
#50
#40
#30
#20
#4
Legend
— Limits of grain size distribution
--- After one triaxial test, with the minor principal stress (σ_3) equals 80psi
Percent finer
100
80
60
40
20
0
.002
.005
.01
.02
.05
.10
.20
.50
1.0
2.0
5.0
10.0
20.0
50.0
Grain size in millimeters

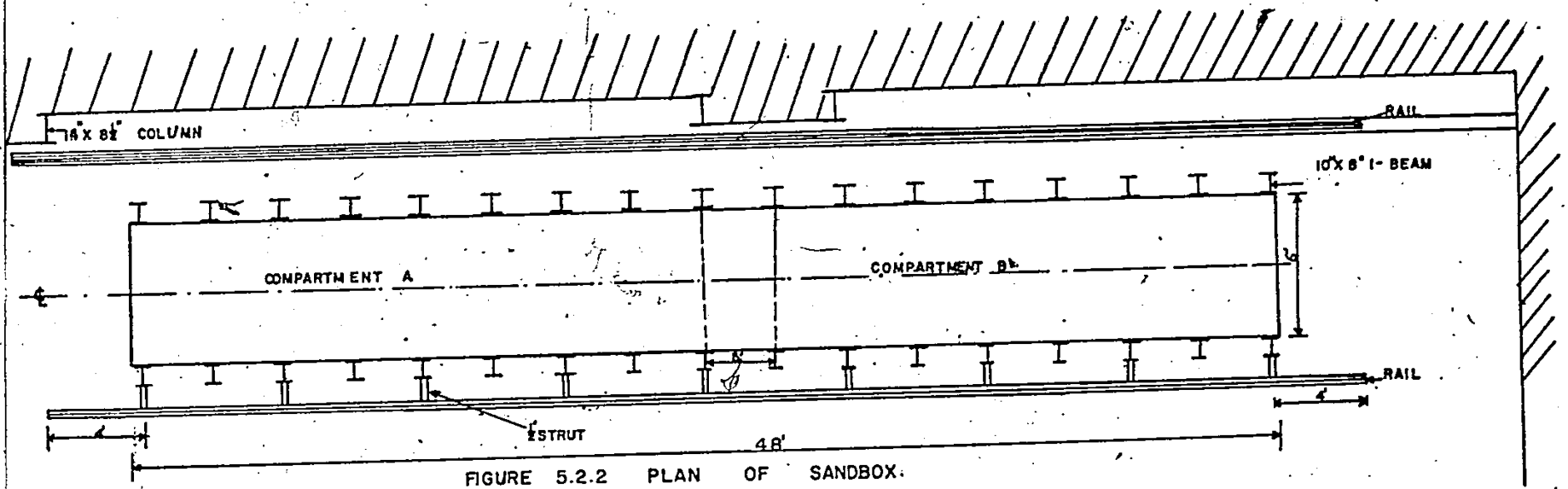

FIGURE 5.2.2 PLAN OF SANDBOX.

thickness of 1/4" (.635 cm) and a flange thickness of 1/2" (1.27 cm) spaced at 3' (0.9144 m) centres. The WF columns and steel plates were held rigidly in place by horizontal I-beams (10" x 8") [25.4 cm x 20.32 cm] spaced at 36" (0.9144 m) centres. These horizontal I-beams were subsequently connected to a 3 feet thick concrete reaction floor by 3" (1.18 cm) diameter steel anchors spaced at 36" (0.9144 m) centres. The space between the horizontal I-beams were filled with quartz sand and compacted by a vibrator to its maximum density and covered by 1" (2.54 cm) thick plywood thus providing an even floor for the sand box. The plywood floor was made rough by gluing sand on it. With the above procedure in the construction of the sand box, it was anticipated that no deflections would exist with the walls and floor of the sand box. Thus, obliterating any effect that might otherwise be introduced by the said deformation on the stresses within the sand mass during the lodding of the footing.

5.2.3 The Spreading Device

The sand was raised into the sand box from a hopper, Figure 5.2.3, of dimensions 107" x 47" x 57" (32.46 m x 14.33 m x 17.37 m) which is capable of travelling backwards and forwards over the sand box on rails which are independent of the sand box. Thus, preventing any further compaction of the sand during the process of spreading. The hopper is held in place at an elevation of one foot (30.48 cm) above the sand box by a rigid rectangular frame assembly, which consists of four WF-columns. These columns are attached to wheels which travel on the said rails. The rails are at a distance of 24" (60.9 cm) and 37"

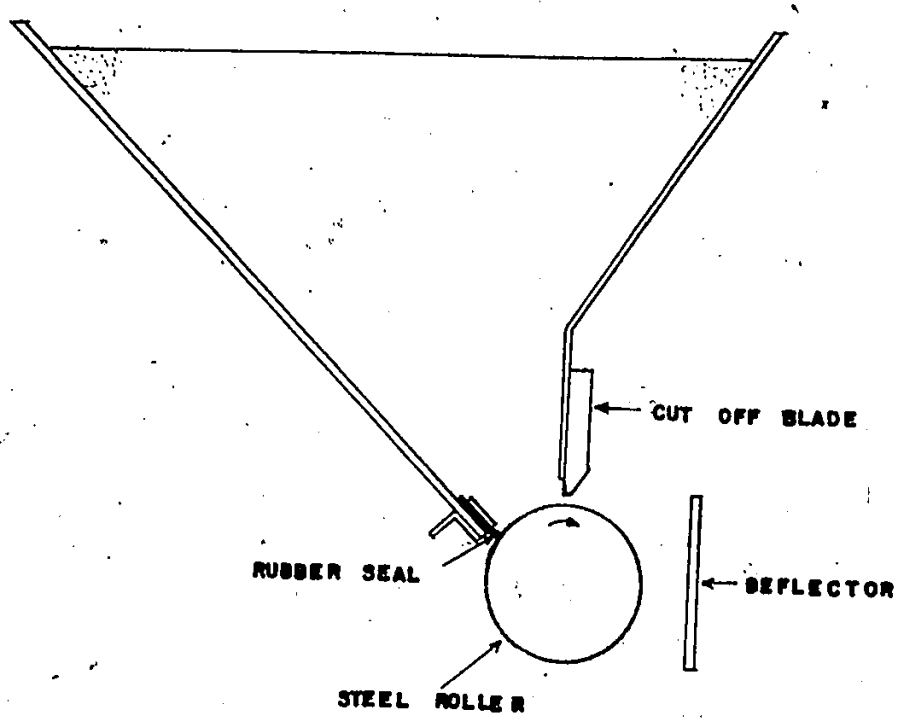

FIGURE 5.2.3 SCHEMATIC DIAGRAM OF THE HOPPER.

(93.98 cm) from the sand box and at elevations of 0" and 100" (2.54 m) respectively, with reference to the outside bottom of the sand box. The 10 HP motors required to drive the hopper and rigid rectangular framework and the 7" (17.78 cm) diameter steel roller were installed within the columns at an elevation of 0". The hopper within its framework is also capable of vertical motion for a distance of 6' (1.83 m) from its resting position of one foot (30.48 cm) above the sand box. Thus, giving a larger vertical distance through which the height of fall of the sand grains could be varied to produce the desired density.

The sloping sides of the hopper are closed by a 7" (17.78 cm) diameter steel roller with a (108" x 6" x 3/8") (274.36 cm x 15.24 cm x 0.95 cm) cut-off blade positioned vertically above the centre of the steel roller. The cut-off blade provides the gate opening for the sand and can be adjusted to give the desired aperture. The sand was prevented from escaping between the roller and sloping back plate by a rubber seal. Thus in the stationary position of the roller no sand grains could escape from the hopper. Once the hopper is set in motion, it imparts an initial horizontal velocity to the sand particles and a 108" x 8-1/4" x 7/8" (274.3 cm x 20.96 cm x 2.22 cm) plate in front of the roller deflects the sand into a vertical direction from where it finally gets to its destination - the sand box. The problem that subsequently calls to mind is how the hopper would be filled with sand.

5.2.4 Centrifugal Bucket Elevator (Figure 5.2.4)

This apparatus has buckets or digging boats (7" x 4" x 4-1/4") (17.78 cm x 10.16 cm x 10.8 cm) incorporated into the testing apparatus

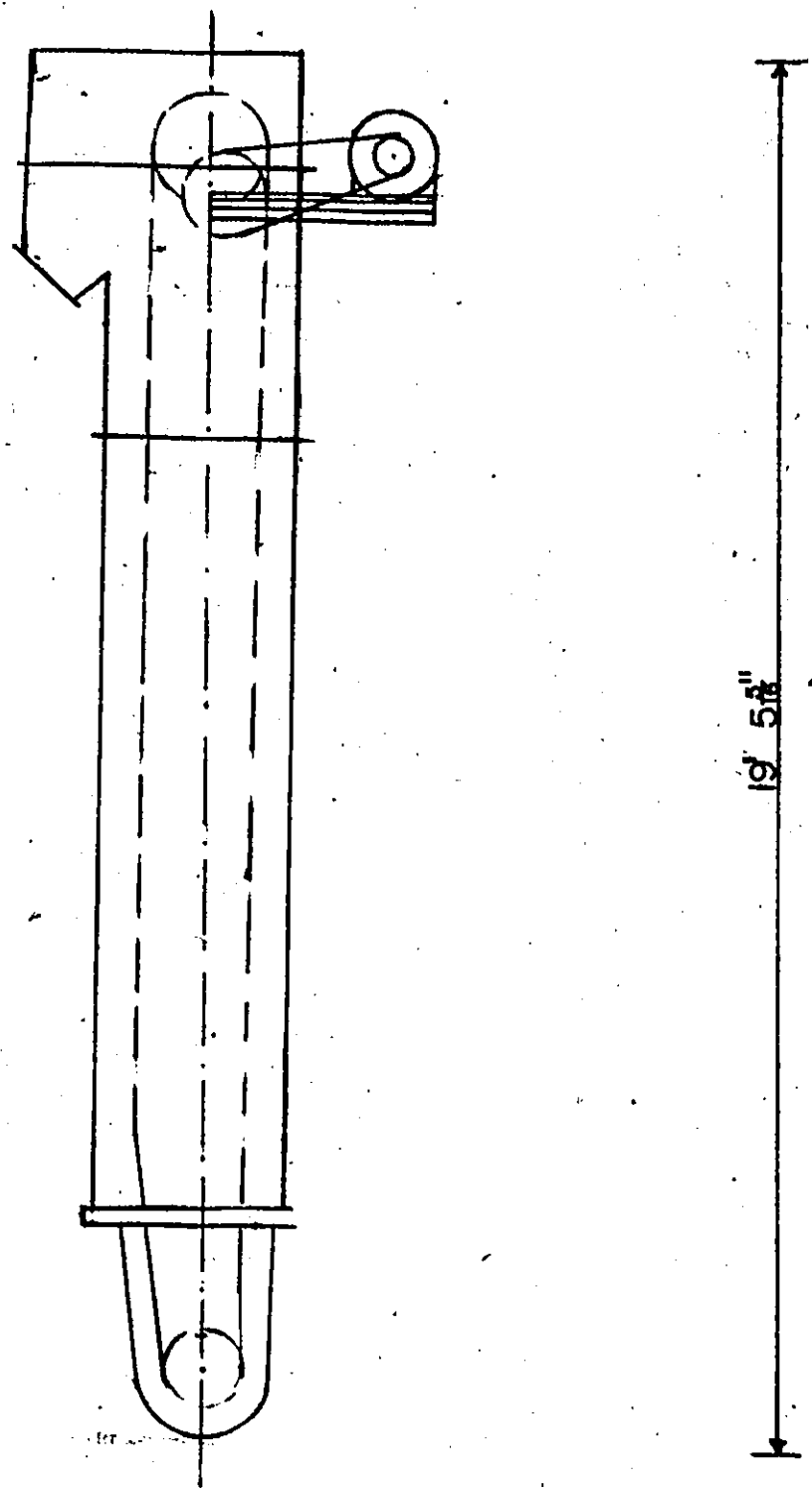

FIGURE 5.2.4 CENTRIFUGAL DISCHARGE BUCKET ELEVATOR

to fill the hopper with sand from the storage bin. The buckets are mounted on chains which revolve around a gear system and are spaced at 12" (30.48 cm) centres. As the name implies, the sand dug up by the buckets is discharged into a funnel by centrifugal action from where it is directed into the hopper by a hose attached to the funnel. The bucket elevator is held in place by a rigid rectangular frame structure which travels on rails built on the sand box. The elevator usually stays on the sand box compartment used as a storage bin.

5.2.5 Loading Frame

The loading frame is shown in Figure 5.2.5. It consists of a 20-1/4" x 6-1/4" (51.44 cm x 15.88 cm) I-beam with a web and flange thicknesses of 1/2" (1.27 cm) and of length 99" (2.515 m) with two sets of channels of length 95" (2.413 m) welded to each end of the I-beam. The I-beam was stiffened by 1/2" (1.27 cm) thick plates at points where the hydraulic jacks were installed. Six holes were drilled on either side of the centre line of the sand box's I-beam at the positions where the loading frame was to be installed. The first hole was at a distance of 9" (22.86 cm) from the top of the sand box. The holes were drilled at 3" (7.62 cm) centres. Compatible holes were also drilled in the channels of the loading frame, leaving the loading frame standing at a height of 68" (172.72 cm) above the sand box. The enormous height used was decided upon in order that, during the bearing capacity tests, that were to be performed at depths, additional I-beams could be installed between the existing reaction beam and the jacks, thus giving enough piston travel from the jacks.

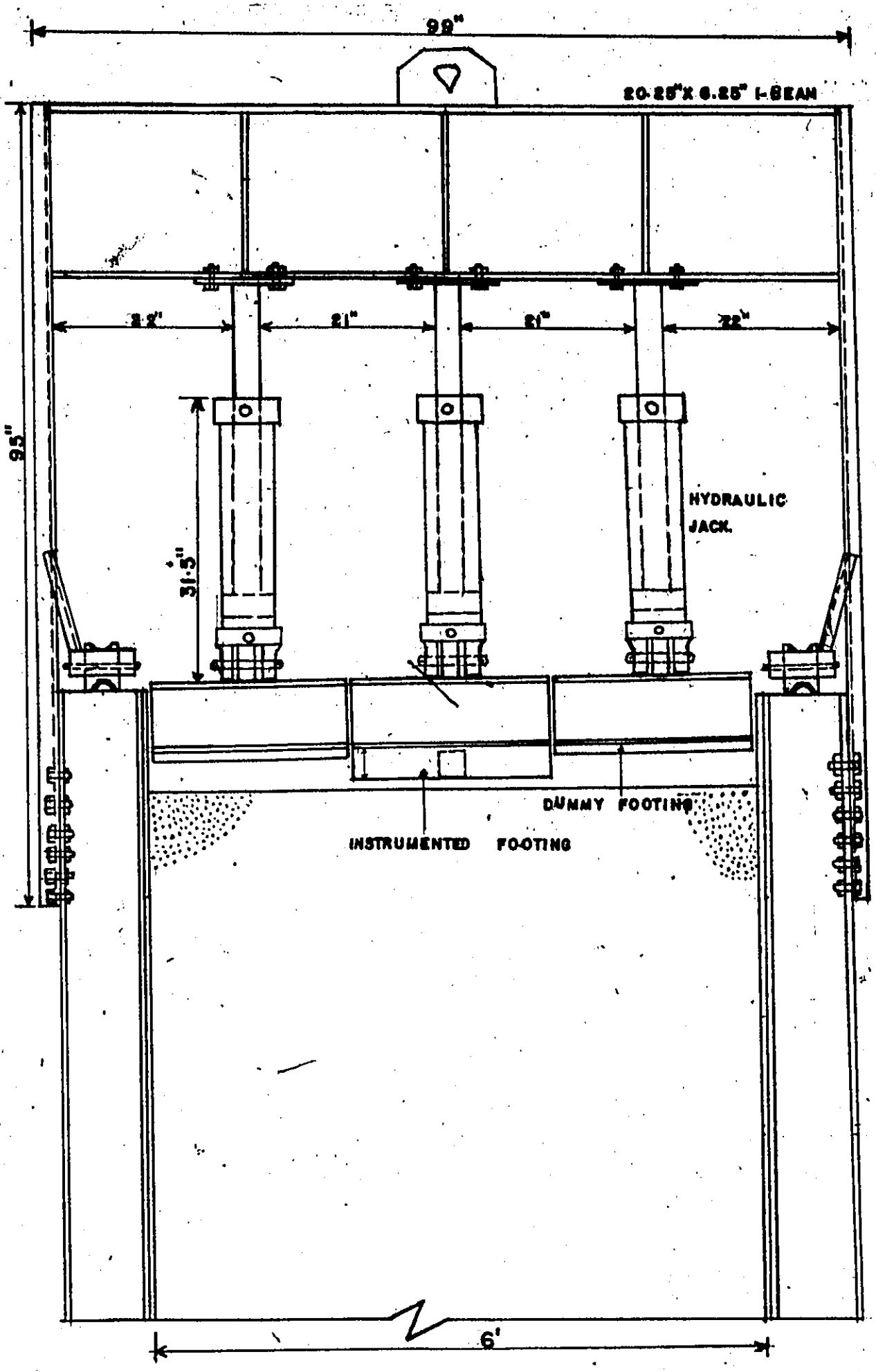

FIGURE 5.2.5 LOADING FRAME.

In order to enhance the installation of the loading frame and increase the stability of the structure, it was supported on four 6" (15.24 cm) diameter wheels which could travel on the rails built on the sand box.

Three aircraft hydraulic jacks were welded to 6" x 6" x 5/8" (15.24 cm x 15.24 cm x 1.59 cm) plates. These plates were subsequently bolted to the reaction beam at a distance of 235" (59.69 cm) from the end channels and at 24" (60.96 cm) centres. The cylinders of the jacks had an internal diameter of 5" (12.7 cm). The pressures exerted by these jacks were monitored by hydraulic gauges and electronic load transducers mounted between the jacks and reaction beam.

A three-sectional footing was used in the tests. Two of the sections were dummy footings used to nullify wall friction effects at the centre footing. The surface of the dummy footings were roughened by gluding sand on them. The central footing, which was instrumented for contact stress measurement was also roughened with sand from the sand box. The footings had wedges with circular holes welded to them. Similarly, the jacks had projections with holes of the same diameter (1", 2.54 cm) drilled in them. The dummy footings were installed on the outermost jacks and the instrumented footing in the central jack by pushing a pin through the compatible holes in the jacks and wedges. This gave the footings the freedom to rotate in the vertical plane about the horizontal pins. For later tests it was found necessary to fix the hinges and thus prevent rotation of the footings.

5.2.6 Pumping Configurations

The pump assembly is shown in Figure 5.2.6. The lines were filled with oil and bled to make sure that no air was trapped within the network, since this would lead to erroneous readings on the hydraulic gauges.

The oil was pumped into an oil regulator (A) from where it was directed to the lower ends of the jacks by opening the appropriate valves. The oil was returned to the pump from the top of the jacks through an oil regulator (C), from where it was directed to the reservoir. With this type of assembly, it was possible to obtain equal settlements of the footings by a single hand pump.

5.3 Settlement Measurements

The settlements of the footings were obtained from measuring tapes attached to the jacks. With these tapes, the distances moved by the pistons of jacks could be read off to an accuracy of 0.03125" (0.079 cm).

Accurate values for the settlement of the instrumented footing was obtained by two dial gauges with 8" (20.32 cm) and 6" (15.24 cm) travels. These dial gauges were attached to a rigid reference channel fixed to the sand box and placed on the instrumented footing. The gauges were placed on either ends of the width of the footing. With this arrangement it was envisaged that any tilting of the footing during the test could be observed.

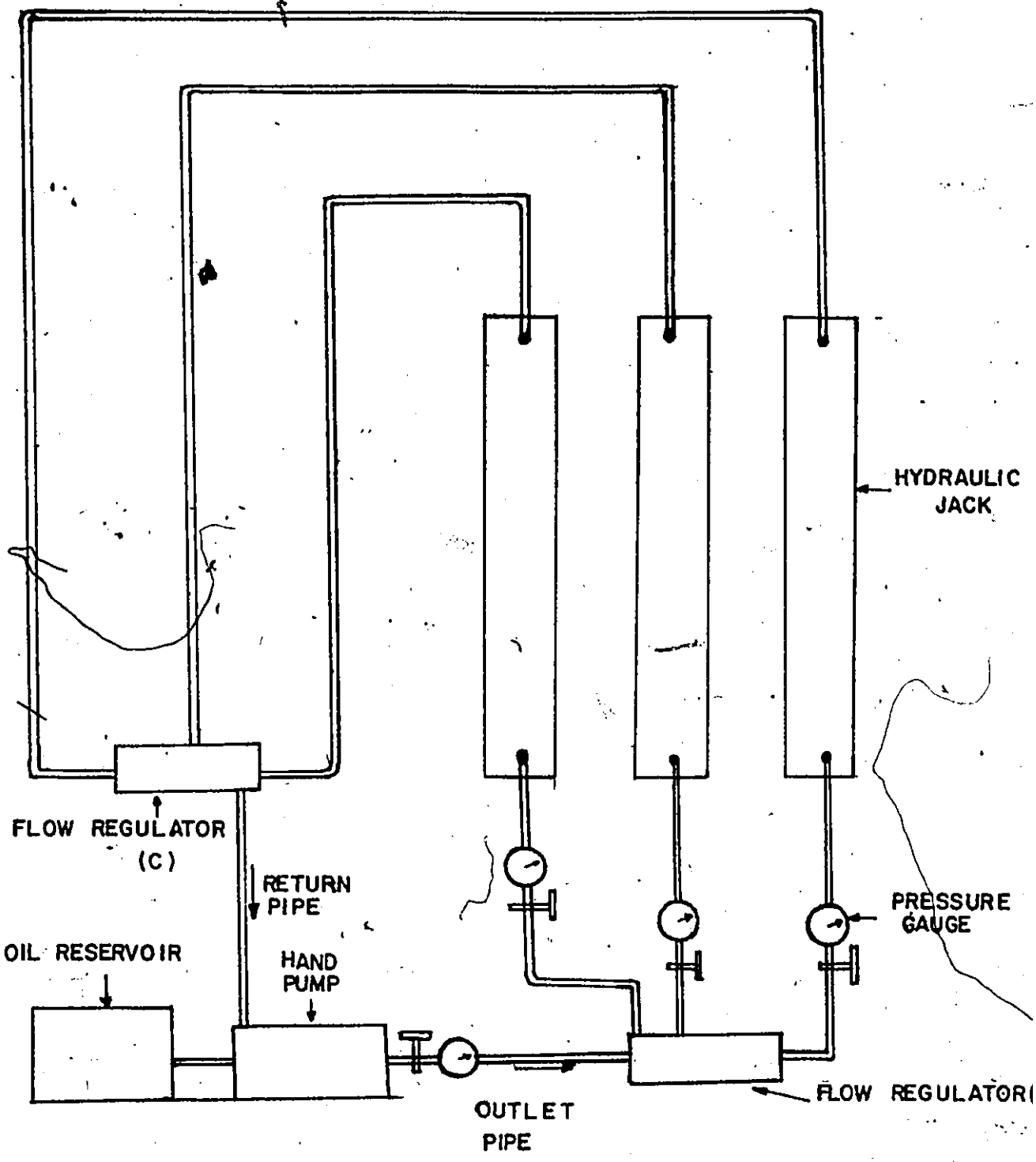

FIGURE 5·2·6 PUMPING CONFIGURATION.

5.4 Calibration Tests for Densities

The density of sand rained into the sand box by the spreading device depends on the intensity of the rain, the weight deposited per unit area per unit time and the height of fall of the sand particles.

The horizontal speed of the hopper also depends on the amount of sand in the hopper and varies in the forward and reverse directions. These problems were, however, eliminated.

Thus, tests were performed to ascertain the appropriate horizontal speed, volume of sand in the hopper, height of fall of the sand particles, drum speed and position of the cut-off blade above the steel roller required to produce the desired densities of 100 lb/ft^2 [15.725 KN/m^3] and 90 lb/ft^3 [14.46 KN/m^3] with corresponding relative densities of 89.9% and 54.7%, respectively.

For various position numbers on the valve, the drum speed was noted by a tachometer. The results are given in Table 5.4.1.

The horizontal speeds were determined by driving the hopper with different volumes of sand, forwards and backwards, between marked points on the rail and timed by a stop clock. The results are given in Table 5.4.2 and have been presented graphically in Figure 5.4.1. From Figure 5.4.1 it was found convenient to operate always at a capacity between 1/2 full to 3/4 full, which gives an average horizontal speed of 8.275 in/sec (21 cm/sec).

With the above in mind, tests were performed to determine the densities of the deposited quartz sand at various drum speeds and height of fall of the sand grains with the cut-off blade at 7/8" (2.2 cm) above the centre of steel roller. The results are given in Tables 5.4.3 to 5.4.8 and have been shown graphically in Figure 5.4.2.

TABLE 5.4.1

Variation of Drum Speed (rpm) with Position Numbers on Valve

Test Nos	1	2	3	4	5	6	Average
Position No							
4	4.0	4.0	4.0	4.0	4.0	4	4
5	16.2	16.2	16.2	16.2	16.0	16.0	16.13
6	23.0	23.0	22.6	22.6	23.0	23.6	22.8
7	30.0	30.0	30.0	30.0	30.0	30.0	30.0
8	33.3	33.3	32.5	32.5	32.5	32.5	32.8

TABLE 5.4.2

Horizontal Speed in Inches/Sec

Volume of Sand in Hopper	Direction of Travel	1	2	3	4	5	6	7
Empty	Forwards	9.2	9.2	9.2	9.2	9.2	9.2	9.2
	Reverse	8.7	8.9	8.9	8.9	8.7	8.8	8.8
1/4 Full	Forwards	9.2	9.4	9.1	9.2	9.1	9.2	9.2
	Reverse	8.6	8.6	8.9	8.9	8.7	8.8	8.8
1/2 Full	Forwards	8.6	8.6	8.1	8.6	8.6	8.6	8.6
	Reverse	8.3	8.3	8.1	8.3	8.3	8.3	8.3
3/4 Full	Forwards	8.3	8.4	8.4	8.4	8.4	8.4	8.4
	Reverse	8.0	8.1	7.7	7.7	7.7	7.9	7.9
Full	Forwards	8.0	8.1	8.3	8.0	8.0	8.0	8.067
	Reverse	7.5	8.0	8.0	7.7	7.8	7.8	7.9

TABLE 5.4.3

Drum Setting at No. 3, Drum Speed = 3.6 rpm

Height of Fall of Sand Grains	Pot Nos	Volume of of Pot in gm^3	Wt of Pot in gm	Wt of Pot in Sand in gms	Wt of Sand in gms	Density in lb/ft^3	Density in gm/cc	Average Density
6" (15.24 cm)	6	934.97	212	1669	1457	97.2	1.56	
	25	816.69	288	1576	1288	98.4	1.58	98 lb/ft^3
	1	932.36	213	1673	1460	97.7	1.57	
	26	876.20	268	1640	1372	97.7	1.57	(15.40 KN/m^3)
	9	817.46	283	1576	1293	98.7	1.58	
	23	801.01	280	1538	1258	98.0	1.57	
2' (60.96 cm)	5	936.63	212	1707	1495	99.6	1.596	100.1 lb/ft^3
	19	879.13	265	1604	1399	99.3	1.59	
	13	871.04	263	1669	1406	100.7	1.61	(15.70 KN/m^3)
	15	868.24	263	1655	1392	100.1	1.6	
	21	811.99	281	1583	1302	100.1	1.6	
	18	831.17	286	1626	1340	100.6	1.61	
4' (121.92 cm)	3	934.44	212	1714	1502	100.3	1.61	
	2	935.36	212	1706	1494	99.7	1.6	100.1 lb/ft^3
	7	938.15	212	1713	1501	99.8	1.6	
	17	874.38	260	1664	1407	100.2	1.61	(15.70 KN/m^3)
	11	826.11	291	1618	1327	100.2	1.61	
	14	833.45	257	1599	1342	100.5	1.61	
	22	871.56	264	1664	1400	100.2	1.61	
6' (182.88 cm)	8	813.85	193	1477	1284	98.5	1.58	
	10	823.35	283	1592	1309	99.2	1.59	
	4	933.89	212	1705	1493	99.8	1.6	99.6 lb/ft^3
	16	871.27	263	1665	1402	100.4	1.61	
	20	824.42	285	1605	1320	99.9	1.6	(15.70 KN/m^3)
	12	853.94	258	1612	1364	99.8	1.6	
	24	829.69	288	1607	1319	99.2	1.59	

TABLE 5.4.4

Drum Setting at No. 4, Drum Speed = 8 rpm

Height of Fall of Sand Grains	Pot Nos	Volume of of Pot in gm^3	Wt of Pot in gms	Wt of Pot in Sand in gms	Wt of Sand in gms	Density in lb/ft^3	Density in gm/cc	Average Density
6" (15.24 cm)	1	932.36	214	1582	1368	91.6	1.48	
	26	876.20	270	1591	1321	94.1	1.51	
	4	933.89	214	1592	1378	92.1	1.48	92.5 lb/ft^3
	20	824.42	286	1504	1218	92.2	1.48	
	21	811.99	282	1482	1200	92.2	1.48	(14.52 KN/m^3)
	5	936.40	214	1605	1391	92.7	1.49	
	14	833.45	259	1507	1248			
2' (60.96 cm)	7	938.15	214	1664	1450	96.5	1.55	
	13	871.04	264	1607	1343	96.2	1.54	
	25	816.69	290	1563	1273	97.3	1.56	
	6	934.92	214	1669	1455	97.1	1.56	96.8 lb/ft^3
	22	871.77	266	1675	1349	96.6	1.55	(15.21 KN/m^3)
	11	826.11	292	1578	1289	97.4	1.56	
	17	874.38	261	1610	1349	96.3	1.54	
4' (121.92 cm)	18	831.53	289	1602	13.3	98.5	1.58	
	2	935.36	214	1066	1452	96.9	1.55	
	23	800.70	282	1535	1250	97.4	1.56	97.6 lb/ft^3
	9	817.56	285	1567	1282	97.8	1.57	
	3	934.69	213	1674	1461	97.5	1.56	(15.30 KN/m^3)
6' (182.88 cm)	8	813.85	195	1449	1254	96.2	1.54	
	15	868.24	264	1595	1331	95.7	1.53	
	19	879.17	267	1633	1366	97.0	1.55	96.2 lb/ft^3
	10	823.35	285	1546	1261	95.6	1.53	
	12	853.94	261	1574	1313	96.0	1.54	(15.11 KN/m^3)
	24	829.64	290	1582	1292	97.2	1.56	

TABLE 5.4.5

Drum Setting at No. 5, Drum Speed = 12 rpm

Height of Fall of Sand Grains	Pot Nos	Volume of of Pot in gm^3	Wt of Pot in gms	Wt of Pot in Sand in gms	Wt of Sand in gms	Density in lb/ft^3	Density in gm/cc	Average Density
6"	17	874.38	255	1475	1220	87.1	1.40	
(15.24	23	800.70	276	1401	1125	87.7	1.41	87.7 lb/ft^3
cm)	14	833.45	253	1432	1179	88.3	1.42	
	3	934.69	207	1518	1311	87.5	1.4	(13.83 KN/m^3)
	9	817.51	281	1427	1146	87.5	1.40	
	21	811.99	277	1414	1137	87.4	1.4	
	2	935.36	208	1528	1320	88.1	1.41	
2'	11	826.11	287	1522	1235	93.3	1.50	
(60.96	7	938.15	207.5	1603	1395.5	92.8	1.49	92.8 lb/ft^3
cm)	26	876.20	264	1563	1299	92.5	1.48	
	22	871.77	259.5	1563	1303.5	93.3	1.50	(14.62 KN/m^3)
	5	936.4	207	1589	1382	92.1	1,48	
	4	933.89	208	1606	1398	93.4	1.50	
	13	871.04	257.5	1549	1291.5	92.5	1.48	
4'	16	871.29	258	1578	1320	94.5	1.51	
(121.92	19	879.17	260	1590.5	1330.5	94.4	1.51	94.1 lb/ft^3
cm)	24	829.64	284	1542	1258	94.6	1.52	
	8	813.55	188	1432	1244	95.4	1.53	(14.81 KN/m^3)
	18	931.53	282	1545	1263	94.8	1.52	
	6	934.97	207	1628	1421	94.8	1.52	
6'	15	868.24	258	1557	1299	93.4	1.50	
(182.88	20	824.42	280	1526	1246	94.3	1.51	93.9 lb/ft^3
cm)	1	932.36	208	1598	1390	93.0	1.49	
	25	816.69	284	1516	1232	94.1	1.51	(14.72 KN/m^3)
	12	853.94	254	1541	1287	94.1	1.51	
	10	823.35	279	1525	1246	94.4	1.51	

TABLE 5.4.6

Drum Setting at No. 6, Drum Speed = 23 rpm

Height of Fall of Sand Grains	Pot Nos	Volume of of Pot in gm^3	Wt of Pot in gms	Wt of Pot in Sand in gms	Wt of Sand in gms	Density in lb/ft^3	Density in gm/cc	Average Density
2" (15.24 cm)	22	871.77	259	1460	1201	86.0	1.38	
	4	933.89	208	1498	1290	86.2	1.38	
	9	817.51	279	1408	1129	86.2	1.38	
	21	811.99	277	1398	1121	86.2	1.38	86.1 lb/ft^3
	17	874.38	256	1460	1204	85.9	1.38	(13.54 KN/m^3)
	2	935.36	208	1496	1288	85.9	1.38	
2' (60.96 cm)	11	826.11	287	1480	1193	90.1	1.44	
	24	829.64	284	1474	1190	89.5	1.43	
	7	938.15	208	1554	1346	89.5	1.43	89.6 lb/ft^3
	26	876.20	264	1520	1256	89.5	1.43	
	19	879.17	262	1519	1257	89.2	1.43	(14.32 KN/m^3)
	13	871.04	258	1512	1254	89.8	1.44	
	10	823.35	279	1458	1179	89.4	1.43	
4' (121.92 cm)	5	936.4	208	1576	1368	91.2	1.46	
	8	813.85	189	1386	1197	91.7	1.47	91.9 lb/ft^3
	6	934.97	208	1588	1380	92.1	1.48	
	16	871.27	259	1547	1288	92.2	1.48	(14.42 KN/m^3)
	18	831.53	282	1518	1236	92.8	1.49	
	15	868.24	258	1527	1269	91.2	1.46	
6' (182.88 cm)	1	932.36	208	1626	1418	94.9	1.52	
	23	800.70	276	1474	1198	93.4	1.50	
	12	853.94	254	1542	1288	94.1	1.51	94.1 lb/ft^3
	3	934.69	207	1608	1401	93.5	1.50	
	14	833.45	253	1520	1267	94.8	1.52	(14.81 KN/m^3)
	25	816.69	284	1517	1233	94.2	1.51	
	20	824.42	280	1518	1238	93.7	1.50	

TABLE 5.4.7

Drum Setting at No. 7, Drum Speed = 30 rpm

Height of Fall of Sand Grains	Pot Nos	Volume of of Pot in gm^3	Wt of Pot in gms	Wt of Pot in Sand in gms	Wt of Sand in gms	Density in lb/ft^3	Density in gm/cc	Average Density
6" (15.24 cm)	21	811.99	277	1420	1143	87.8	1.41	86.5 lb/ft^3 ($13.64\ KN/m^3$)
	9	817.51	279	1397	1118	85.3	1.32	
	8	813.85	188	1340	1152	88.3	1.42	
	6	934.97	207	1493	1286	85.5	1.38	
	18	831.53	2882	1458	1176	88.2	1.41	
	15	868.24	258	1428	1170	84.1	1.35	
	10	823.35	279	1411	1132	85.8	1.38	
2' (60.96 cm)	14	833.45	253	1433	1180	88.3	1.42	88.2 lb/ft^3 ($13.83\ KN/m^3$)
	24	829.64	284	1459	1175	88.4	1.42	
	1	932.36	208	1520	1312	87.8	1.41	
	13	871.04	258	1478	1220	87.4	1.40	
	16	871.27	259	1493	1234	88.4	1.42	
	3	934.69	207	1526	1319	88.1	1.41	
	5	936.40	208	1539	1331	88.7	1.42	
4' (121.92 cm)	23	800.70	276	1435	1159	90.3	1.45	90.2 lb/ft^3 ($14.22\ KN/m^3$)
	20	824.42	280	1471	1191	90.2	1.45	
	25	816.69	284	1475	1191	90.9	1.46	
	12	853.94	254	1479	1225	89.5	1.43	
	22	871.77	260	1516	1256	89.9	1.44	
	4	933.89	208	1563	1355	90.5	1.45	
6' (182.88 cm)	2	935.36	208	1589	1381	92.1	1.48	91.9 lb/ft^3 ($14.42\ KN/m^3$)
	19	879.17	261	1579	1318	93.6	1.50	
	26	876.20	264	1536	1272	90.6	1.45	
	11	826.11	287	1507	1220	92.2	1.48	
	7	938.15	208	1603	1395	92.8	1.49	
	17	874.8	256	1526	1270	90.6	1.45	

TABLE 5.4.8

Drum Setting at No. 8, ~~Drum Speed~~ = 33 rpm

Height of Fall of Sand Grains	Pot Nos	Volume of of Pot in gm^3	Wt of Pot in gms	Wt of Pot in + Sand in gms	Wt of Sand in gms	Density in lb/ft^3	Density in gm/cc	Average Density
6'	18	831.53	281	1428	1147	86.1	1.38	
(15.24	6	934.97	207	1486	1279	85.4	1.37	85.9 lb/ft^3
cm)	5	936.40	207	1505	1298	86.5	1.39	(13.54 KN/m^3)
	24	829.64	283	1417	1134	85.3	1.37	
	15	868.24	253	1450	1192	85.7	1.37	
	1	932.36	208	1488	1280	85.7	1.37	
	9	817.51	279	1414	1135	86.6	1.39	
2'	10	823.35	278	1428	1150	87.2	1.4	
(60.96	17	874.38	255	1483	1228	87.6	1.4	
cm)	20	824.42	279	1442	1163	88.0	1.41	87.9 lb/ft^3
	26	876.20	264	1502	1238	88.2	1.41	(13.83 KN/m^3)
	4	933.89	208	1539	1331	88.9	1.43	
	11	826.11	28.6	1451	1165	88.0	1.41	
	19	879.17	260	1495	1235	87.7	1.41	
4'	21	811.99	277	1452	1175	90.3	1.45	
(121.92	2	935.36	208	1554	1346	89.8	1.44	
cm)	16	871.27	259	1507	1248	89.4	1.43	89.4 lb/ft^3
	25	816.69	284	1466	1182	90.3	1.45	
	13	871.04	258	1491	1233	88.3	1.42	(14.03 KN/m^3)
	3	934.69	208	1532	1324	88.4	1.42	
6'	7	938.15	207	1603	1396	92.8	1.49	
(182.88	12	853.94	254	1504	1250	91.4	1.46	91.7 lb/ft^3
cm)	8	813.85	188	1369	1281	90.5	1.45	
	14	833.45	253	1480	1227	91.8	1.47	(14.42 KN/m^3)
	22	871.77	260	1561	1291	92.4	1.48	
	23	800.70	276	1445	1169	91.1	1.46	

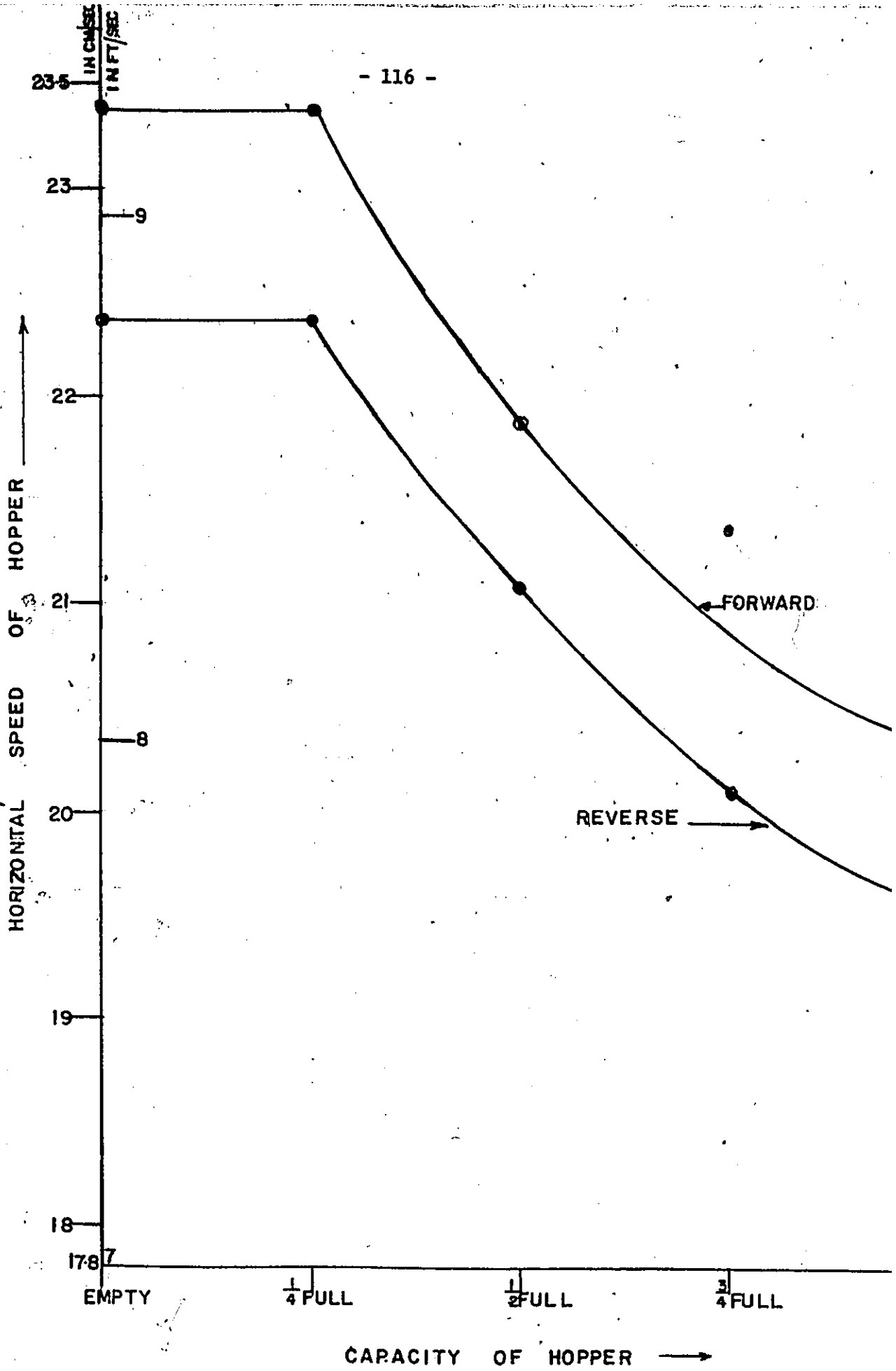

FIGURE 5·4·1 HORIZONTAL SPEED VS HOPPER'S CAPACIT

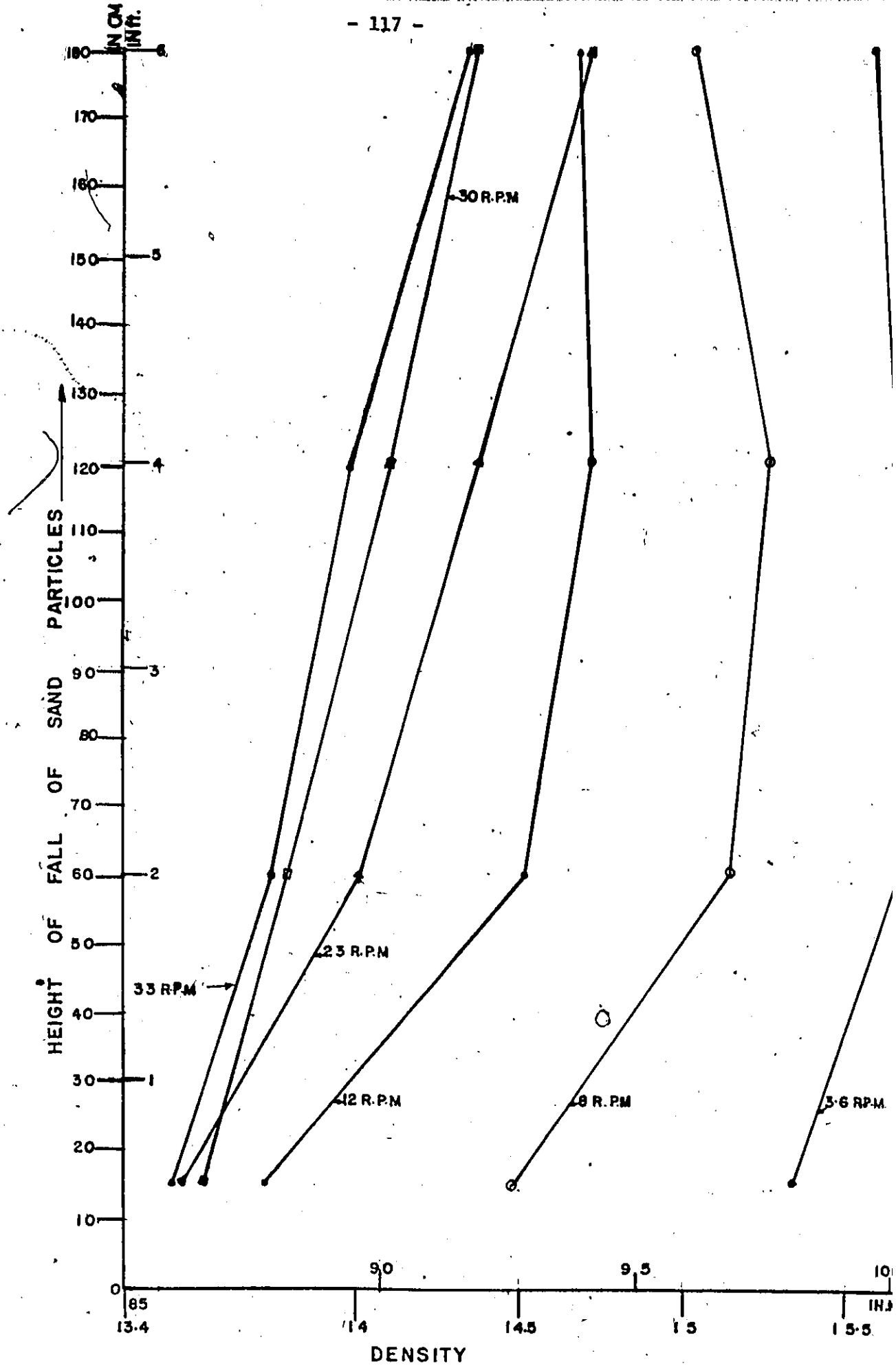

FIGURE 5·4·2 HEIGHT OF FALL VS DENSITY.

From the results of the above tests, it was concluded that the desired densities could be achieved by spreading the quartz sand under the following conditions.

A. For a density of 100 lb/ft^3 (15.725 KN/m^3) corresponding to a relative density of 89.9%, the following conditions had to be satisfied.

1) A hopper horizontal speed of 8.275 in/sec (21 cm/sec).
2) A drum speed of 3 rpm.
3) Height of fall of sand particles of 2' (60.96 cm).
4) A capacity of 1/2 to 3/4 full.
5) A gate opening of 7/8" (2.2 cm).

B. Similarly, for a density of 90 lb/ft^3 (KN/m^3) corresponding to a relative density of 54.7%, the following conditions were to be satisfied.

1) A hopper horizontal speed of 8.275 in/sec (21 cm/sec).
2) A gate opening of 7/8" (2.2 cm).
3) A capacity between 1/2 to 3/4 full.
4) For the first two feet of quartz sand in the sand box, a height of fall of the sand particles of 5' (1.524 m) and a drum speed of 30 rpm had to be satisfied.
5) For the next 3 feet, a height of fall of 3.5 feet and a drum speed of 23 to 25 rpm was to be maintained.
6) For the last foot, a height of fall of the sand particles of 2 feet (60.96 cm) and drum speed of 12 to 15 rpm had to be maintained.

5.5 Testing Procedure

5.5.1 General

The quartz sand was heaped up in one of the compartments of the sand box while the other was swept clean and ready to be used for testing. The sand was dug up by the centrifugal bucket elevator and deposited in the hopper. Once the hopper was filled, it was set in a horizontal motion at the desired speed with the cut-off blade at 7/8" (2.2 cm) vertically above the centre of the steel roller. The drum speed and height of fall of the sand particles were adjusted so as to give the desired densities.

The sand was rained into the testing compartment until the hopper was about half-full. The hopper was then loaded to the desired capacity and the sand raised into the testing compartment. These procedures of filling the hopper and spreading was continued until the sand box was filled to about 6" (15.24 cm) from the top. During the spreading circular containers and rectangular boxes were placed in the sand box in order to check the density of the sand in the sand box. During the spreading it was observed that more sand was deposited adjacent to the walls of the sand box. This has been attributed to the height of sand above the steel roller in the hopper. The height of sand decreases fastest over the central region of the hopper than at the end regions. This is due to the blockage of the ends of the hopper, which ultimately leads to a trapezoidal disposal of sand from the hopper. Most of the sand is thus lost in the central region leading to a reduced "overburden" pressure above the 7" (17.78 cm) diameter steel roller at the central region.

However, the effect of the above phenomenon has been minimal, since the difference in elevations of the sand surface adjacent to the walls of the sand box and the central region was limited to about 1/2" (1.27 cm). Once the spreading was completed, the sand surface was leveled and precaution was taken such that not more than 1/2" (1.27 cm) of the sand surface was disturbed.

The loading frame was then lifted off the floor of the heavy structures laboratory and placed over the sand box with its wheels on rails built on the sand box. It was then rolled to the point where the testing was to be performed. Compatible holes on the columns of the loading frame and I-beam of the sand box were aligned and bolts put through them and nuts placed on the ends of the bolts and tightened. All effort was made to see that the jacks were vertical. The instrumented footing was then hooked-up to the digital strain indicator instrument and zeroed by the balance knob and the simulated strain by the calibration resistor set to 359 microstrains.

Five tests were performed with the footings on a flat ground and at a distance of 2.5 feet (76.2 cm) from the top of a 2:1 slope and at two densities.

5.5.2 Description of Footing Tests

Test 1.

In this test, the footings were attached to the hydraulic jacks by pin connections such that the footings were free to rotate in a vertical plane about horizontal pins.

This test was performed in the middle of the 24' (7.315 m) long compartment with a flat ground being simulated. No heave measurements were made.

The values of the strains monitored by the bridge circuits in the Cambridge load cells for the load levels indicated in the load versus settlement diagram is given in Appendix C. The values of density measured by the boxes placed in the sand box during the spreading operation are as in Table 5.5.1.

5.5.3 Modifications to the Loading Frame

With the mode of connection employed in Test 1 (between footings and hydraulic jacks), it was observed that at high pressures from the jacks that the footings tilted prior to the attainment of failure load. Thus, for the subsequent five tests the footings were attached rigidly to the jacks such that it could move vertically downwards into the sand mass till failure was reached.

It was also observed that the pressure gauges were not as accurate as had been anticipated, thus a load cell was installed in between the central hydraulic jack and the reaction beam. The calibration chart for the load cell is shown in Figure 5.5.1

5.5.4 Test on Slopes

Test 2

In this test the footings were fixed to the jacks. A slope of 2:1 was made in the sand. The end of the width footings (with cell No. 6 of the instrumented footings) was 5' (1.524 m) from the edge of

TABLE 5.5.1

Volume of Box in cm^3	Wt of Box in gms	Wt of Box and Sand in cms	Wt of Sand in gms	Relative Density in %	Density in KN/m^3	Density in lb/ft^3
668.18	447	1516.5	1069.5	90	15.706	100.04
1110.495	648	24.3.5	1765.5	87.9	15.6	99.304

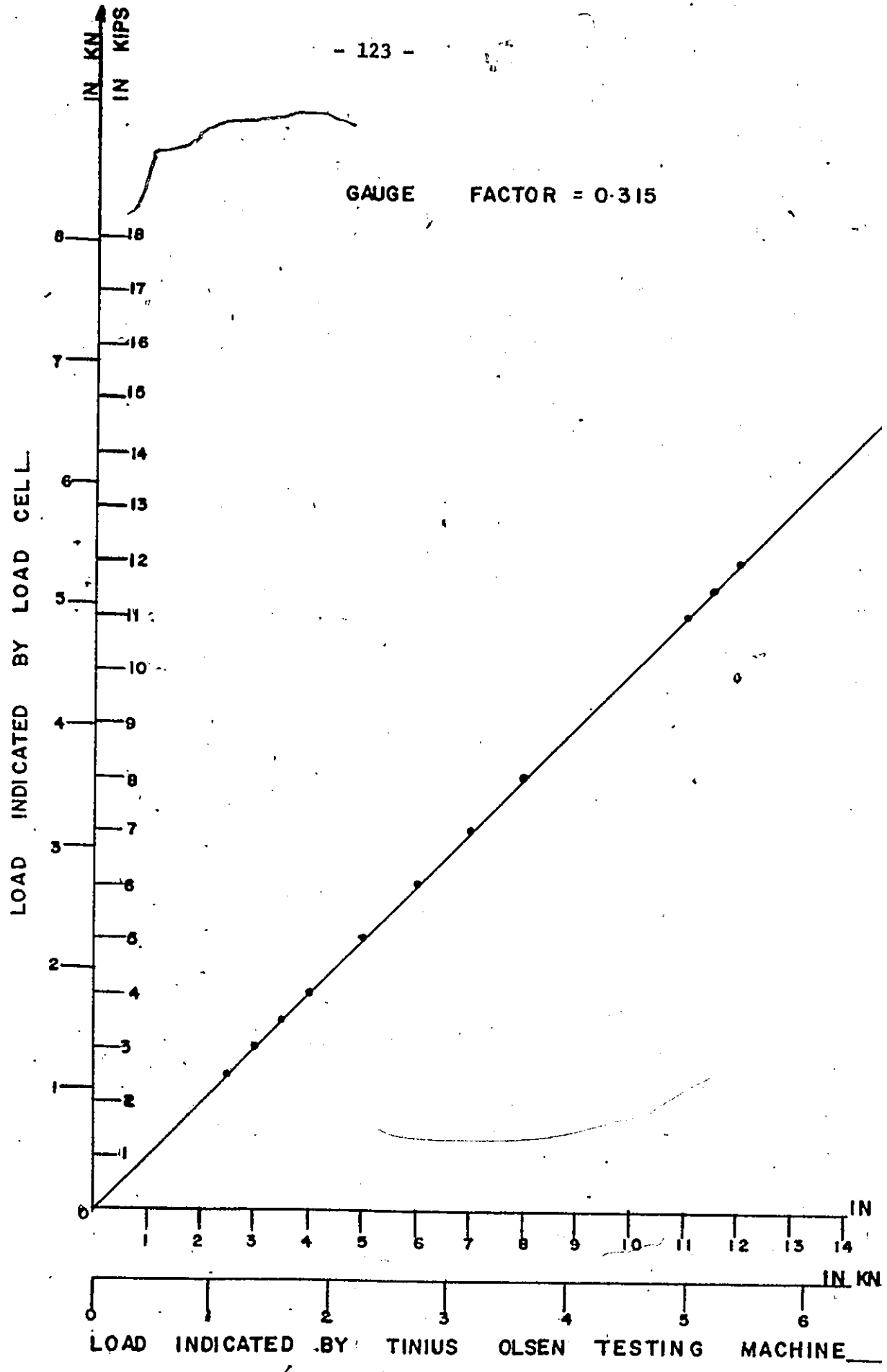

FIGURE 5·5·1 LOAD CELL CALIBRATION CHART.

the slope. The other end of the width of the footing was about 5' (1.524 m) from the end of the sand box. The settlement of the footing was monitored by dial gauges.

The strains monitored by the bridge circuits in theCCambridge load cells are given in Appendix C.

The density measured by boxes placed in the sand box during the spreading operation are shown in Table 5.5.2.

Test 3

Same as the preceding two tests, except that the footing edge was 2.5 feet (76.2 cm) from the edge of the 2:1 slope. The density of the sand was 100 lb/ft^3 (15.725 KN/m^3), corresponding to a relative density of 89.9%.

The strains monitored by the bridge circuits in the Cambridge load cells are given in Appendix C.

Test 4

This test was performed at a density of 90 lb/ft^3 (14.15 KN/m^3) corresponding to a relative density of 54.7% with the footing edge, 5' (1.524 m) from the top of the 2:1 slope.

Heave measurements were taken by a measuring stick from a rigid reference beam. The results of the densities measured by boxes placed in the sand box during the spreading operation is shown in Table 5.5.3.

The strains monitored by the bridge circuits in the pressure cells are given in Appendix C.

TABLE 5.5.2

Volume of Box in cm^3	Wt of Box in gms	Wt of Box and Sand in gms	Wt of Sand in gms	Relative Density in %	Density in KN/m^3	Density in lb/ft^3
670.56	444.0	1526.0	1082.0	92.5	15.83	100.85
1114.127	635.0	2429.0	1794.0	91.9	15.80	100.64

TABLE 5.5.3

Volume of Box in cm^3	Wt of Box in gms	Wt of Box and Sand in gms	Wt of Sand in gms	Relative Density in %	Density in KN/m^2	Density in lb/ft^3
670.56	440	1412.5	968.5	55.7	14.166	90.27
1114.127	635.0	2243.5	1608.5	55.6	14.163	90.23

Test 5

This test was performed at a density of 90 lb/ft^3 (14.15 KN/m^3) with the footings edge at a distance of 2.5' (76.2 cm) from the edge of the 2:1 slope.

The strains monitored by the bridge circuit is given in Appendix C.

The results of the density measured by boxes placed in the sand box during the spreading process is shown in Table 5.5.4.

TABLE 5.5.4

Volume of Box in cm^3	Wt of Box in gms	Wt of Box and Sand in gms.	Wt of Sand in gms	Relative Density in %	Density in KN/m^3	Density in lb/ft^3
891.078	556.5	1841.5	1285.0	55.2	14.146	90.129
1114.127	635	2243.5	1608.5	55.6	14.163	90.23

CHAPTER 6

EXPERIMENTAL RESULTS

6.1 General

In Section 4.4, the load cell constants were determined and the relationship between the output strains and force components (normal force, shear force and moment due to eccentricity of the normal force) was expressed in the form

$$\begin{bmatrix} \varepsilon^{+} \\ \varepsilon^{-} \\ \varepsilon_{s} \end{bmatrix} = \begin{bmatrix} C_{+n} & C_{+s} & C_{+x} \\ C_{-n} & C_{-s} & C_{-x} \\ C_{sn} & C_{ss} & C_{-sx} \end{bmatrix} \begin{bmatrix} N \\ S \\ N_{x} \end{bmatrix} \qquad 6.1$$

which can be written in the form

$$\{\varepsilon\} = [C]\ \{F\} \qquad 6.2$$

where $\{\varepsilon\}$ = 1x3 column matrix of the output strains from the three bridge circuits, viz., the positive normal, negative normal and shear bridge circuits, respectively.

$[C]$ = A 3x3 matrix of the load cell constants, that relates output strains to force components.

$\{F\}$ = 1x3 column matrix expressing the force components acting on the load cell.

The values of the load cell constants and output strains were obtained from calibration and footing tests respectively. The force components were obtained by solving equation 6.2 which gives

$$\{F\} = [C^{-1}]\ \{\varepsilon\} \qquad 6.3$$

The inverse of the cell constants for the six load cells are as follows

Cell 1

$$C_1^{-1} = \begin{bmatrix} -0.351318 & -0.329033 & 0.023019 \\ 0.007021 & -0.010504 & -0.235246 \\ -0.279603 & 0.267936 & -0.030203 \end{bmatrix}$$

Cell 2

$$C_2^{-1} = \begin{bmatrix} -0.343046 & -0.328579 & -0.006693 \\ 0.007483 & -0.003819 & -0.217289 \\ -0.278601 & 0.257625 & -0.041837 \end{bmatrix}$$

Cell 3

$$C_3^{-1} = \begin{bmatrix} -0.329621 & -0.324853 & -0.016627 \\ -0.005823 & -0.014832 & -0.266123 \\ -0.286406 & 0.257187 & -0.020992 \end{bmatrix}$$

Cell 4

$$C_4^{-1} = \begin{bmatrix} 0.336412 & -0.340996 & -0.012330 \\ -0.018210 & -0.008265 & -0.269567 \\ 0.282395 & -0.266838 & -0.035377 \end{bmatrix}$$

Cell 5

$$C_5^{-1} = \begin{bmatrix} 0.348297 & -0.319869 & -0.001995 \\ -0.015918 & -0.011993 & -0.281089 \\ 0.283807 & 0.255424 & -0.043401 \end{bmatrix}$$

Cell 6

$$C_6^{-1} = \begin{bmatrix} -0.344130 & -0.338436 & -0.004624 \\ 0.016083 & -0.005809 & -0.274720 \\ -0.283799 & 0.270768 & -0.006142 \end{bmatrix}$$

Considering the output strains from the three bridge circuits of Cell 1 under a load of 8541.2 lbs (38 KN); then from Appendix C, page 278, $\varepsilon^+ = -193$, $\varepsilon^- = -176$, and $\varepsilon_s = -36$ then the force components can be obtained from the relationship below

$$\begin{bmatrix} N \\ S \\ N_x \end{bmatrix} = \begin{bmatrix} -0.35138 & -0.329033 & 0.023019 \\ 0.007621 & -0.010504 & -0.23524 \\ -0.279603 & 0.267936 & -0.030203 \end{bmatrix} \begin{bmatrix} -193 \\ -176 \\ -36 \end{bmatrix}$$

$N = -0.35138 \times -193 + -0.329033 \times -176 + 0.023019 \times -36$

$S = 0.007021 \times -193 + -0.010504 \times -176 + 0.23523 \times -36$

$N_x = -0.279603 \times -193 + 0.267936 \times -176 + -0.030203 \times -36$

$N = 124.886$ lbs (555.74 N)

$S = 8.963$ lbs (39.88N)

$N_x = 7.894$ lb in (89.226 N-cm)

The eccentricity is given by

$$X = \frac{N_x}{N} = \frac{7.894}{124.886} = 0.0632 \text{ ms}$$

$$= 0.161 \text{ cm}$$

The normal and shear stresses were obtained by dividing the corresponding forces by the surface area of the Cambridge cell face place (3 sq.ins, 19.35 sq. cm).

Thus, Normal Stress

$$= \frac{124.886}{3} = 41.63 \text{ lb/in}^2$$

$$= 287.24 \times 10^3 \text{ pascals.}$$

Shear Stress

$$= \frac{8.963}{3} = 2.988 \text{ psi}$$

$$= 20.614 \times 10^3 \text{ pascals.}$$

The stress components for other load cells were computed in a similar manner. The procedure was also repeated for other load levels with the output strains as the variable for the various tests (Tables 6.1.1 to 6.1.5).

Five tests have been performed at two relative densities and at variable distances from the top of a 2.1 slope (as indicated in Chapter 5). For an explicit study to be made on the contact stress distribution under the footing, the contact stresses have been related to specific points on the load versus settlement curves. Thus an effective deduction can be made on the effect of the stress or strain state of the soil on the contact stress distribution.

6.2 Soil and Footing Movements

Owing to the tilting of the footing in Test 1, the footing could not be loaded to failure. However, the load versus settlement curve, Figure 6.2.1 for the load levels applied shows an initial elastic zone followed by a zone of local shear failure.

In Test 2 the load versus settlement curve, Figure 6.2.2, shows three zones, the elastic distortion zone, the local shear or

TABLE 6.1.1

Contact Stresses for Test One

Duration of Load Application in mins	Load	Cell Nos	Normal Stress in psi	Normal Stress in KPa	Shear Stress in psi	Shear Stress in KPa	Eccentricity of Normal Stress in inches	Eccentricity of Normal Stress in cms
5	805.03 lb [3.58 KN] [2.79 psi]	1	6.254	43.153	0.235	1.622	0.182	0.462
		2	6.188	42.697	1.054	7.273	0.504	1.280
		3	5.776	39.854	0.104	0.718	-0.0650	-0.165
		4	5.703	39.351	1.112	7.673	-0.0467	-0.119
		5	2.172	14.987	1.551	10.702	-0.429	-1.090
		6	2.156	14.876	0.282	1.946	-0.450	-1.143
5	3239.8 lb [14.42 KN] [11.25 psi]	1	22.671	156.423	1.804	12.448	0.079	0.201
		2	23.564	162.592	0.773	1.884	0.103	0.262
		3	19.862	137.082	0.772	5.327	-0.027	-0.069
		4	20.520	141.588	1.500	10.419	0.021	0.053
		5	9.736	67.198	2.756	19.016	-0.294	-0.767
		6	10.577	72.981	1.413	9.750	-0.231	-0.587
5	6185.0 lb [27.52 KN] [21.48 psi]	1	33.870	233.703	2.245	15.491	0.0684	0.174
		2	35.440	244.536	-0.246	-1.697	0.102	0.259
		3	31.344	216.274	1.390	9.591	-0.014	-0.0356
		4	32.142	221.781	11.237	8.535	0.030	0.0762
		5	17.470	120.543	3.525	24.323	-0.210	-0.533
		6	20.924	144.376	1.959	13.517	-0.182	-0.462
5	8541.2 lb [38.00KN] [29.66 psi]	1	42.674	294.451	3.068	21.169	0.0630	0.160
		2	43.721	301.675	-0.512	-3.533	0.0916	0.233
		3	39.359	271.577	2.404	16.588	-0.0118	-0.300
		4	41.527	286.536	1.445	9.971	0.036	0.0914
		5	22.747	156.954	4.692	32.375	-0.207	-0.526
		6	28.431	196.174	3.117	21.507	-0.199	-0.506
5	10465.43 lb [46.57 KN] [36.34 psi]	1	47.558	328.150	3.805	26.255	0.058	0.147
		2	46.373	319.981	-0.649	-4.428	0.064	0.103
		3	44.528	307.243	3.304	22.800	-0.0221	-0.056
		4	48.780	336.582	1.959	13.517	0.0395	0.100
		5	25.371	175.060	5.857	40.413	-0.217	-0.551
		6	33.443	230.76	4.383	30.243	-0.210	-0.533

TABLE 6.1.2

Contact Stresses for Test Two

Duration of Load Application in mins	Load	Cell Nos	Normal Stress in psi	Normal Stress in KPa	Shear Stress in psi	Shear Stress in KPa	Eccentricity of Normal Stress in Inches	Eccentricity of Normal Stress in cms
		1	8.221	56.725	0.449	3.098	-0.321	-0.815
		2	7.849	54.158	0.392	2.705	0.418	1.062
5	2770 lbs	3	5.902	40.724	0.368	2.539	-0.044	-0.112
	[12.33 KN]	4	4.798	33.106	1.116	7.700	-0.022	-0.152
	[9.62 psi]	5	4.630	31.942	1.340	9.246	-0.146	-0.371
		6	3.196	22.052	0.692	4.775	-0.034	-0.0864
		1	20.376	140.594	1.090	7.521	-0.044	-0.112
		2	17.712	122.213	1.070	7.383	0.0236	0.060
5	4853 lbs	3	16.858	116.320	1.323	9.129	0.007	0.018
	[21.60 KN]	4	11.972	82.607	2.355	16.250	0.027	0.069
	[16.85 psi]	5	13.685	94.427	4.003	27.621	-0.123	-0.312
		6	7.083	48.873	2.121	14.635	-0.078	-0.198
		1	53.401	368.467	3.895	26.876	-0.272	-0.691
		2	43.378	299.308	2.685	18.527	0.173	0.439
5	11275 lb	3	48.396	333.932	5.483	37.833	0.035	0.089
	[50.17 KN]	4	32.782	226.196	5.49	37.881	0.080	0.203
	[39.15 psi]	5	35.672	246.137	12.078	83.338	-0.168	-0.427
		6	19.985	137.897	6.619	45.671	-0.154	-0.391
		1	70.631	487.354	5.090	35.121	-0.018	-0.0457
		2	56.703	391.251	3.499	24.143	0.009	0.0229
5	14520 lbs	3	65.564	452.392	8.215	56.684	0.035	0.089
	[64.61 KN]	4	44.825	309.293	7.076	48.824	0.087	0.221
	[50.42 psi]	5	41.506	288.593	16.276	112.304	-0.218	-0.554
		6	27.632	190.661	9.237	63.735	-0.174	-0.442
		1	80.166	553.145	6.162	42.518	-0.0135	-0.0343
		2	64.092	442.235	3.977	27.441	0.005	0.013
5	16250 lbs	3	73.427	506.646	10.291	71.008	0.032	0.0813
	[72.31 KN]	4	50.756	350.216	8.329	57.470	0.0862	0.219
	[56.42 psi]	5	44.246	305.297	18.850	130.065	-0.220	-0.559
		6	30.836	212.768	10.56	72.864	-0.177	-0.450
		1	109.139	753.059	10.387	71.670	-0.0003	-0.0008
		2	81.720	563.868	6.658	45.940	0.003	-0.008
5	18510 lbs	3	92.268	636.773	17.912	123.593	-0.115	-0.292
	[82.37 KN]	4	68.027	469.386	13.397	92.439	0.130	0.330
	[64.27 psi]	5	53.436	368.708	26.773	184.734	-0.191	-0.485
		6	38.508	265.705	15.634	107.875	-0.214	-0.544

TABLE 6.1.3

Contact Stresses for Test Three

Duration of Load Application in mins	Load	Cell Nos	Normal Stress in psi	Normal Stress in KPa	Shear Stress in psi	Shear Stress in KPa	Eccentricity of Normal Stress in Inches	Eccentricity of Normal Stress in cms
		1	10.798	74.506	0.180	1.242	0.112	0.285
		2	9.498	65.536	-0.187	-1.290	-0.019	-0.0483
17	2000 lb	3	13.624	94.006	0.349	2.408	-0.0945	-0.240
	[8.90 KN]	4	8.263	57.015	0.197	1.359	-0.095	-0.241
	[6.94 psi]	5	7.388	50.977	2.37	16.353	-0.139	-0.353
		6	6.821	47.065	0.597	4.119	-0.196	-0.498
		1	18.360	126.684	0.753	5.196	0.102	0.259
		2	16.541	114.133	-0.441	-3.043	-0.005	-0.0127
16	4000 lb	3	23.170	159.87	1.589	10.964	-0.085	-0.216
	[17.8 KN]	4	15.858	109.42	0.728	5.023	-0.051	-0.130
	[13.89 psi]	5	13.807	95.268	4.841	33.403	-0.106	-0.269
		6	13.088	90.207	1.634	11.275	-0.155	-0.394
		1	24.342	167.960	1.240	8.556	0.102	0.259
		2	23.15	159.735	-0.555	-3.830	0.016	0.041
17	6000 lb	3	32.167	221.95	2.722	18.782	-0.074	-0.188
	[26.7 KN]	4	23.006	158.741	1.356	9.356	-0.036	-0.0914
	[20.83 psi]	5	20.01	138.069	6.819	47.051	-0.089	-0.226
		6	18.79	129.651	3.05	21.045	-0.149	-0.379
		1	36.527	252.036	2.002	13.814	0.0813	0.207
		2	36.147	249.414	-0.561	-3.871	0.0318	0.081
17	10,000 lb	3	47.626	328.619	4.398	30.346	-0.058	-0.147
	[44.5 KN]	4	36.968	255.079	2.774	19.141	-0.0102	-0.0259
	[34.72 psi]	5	32.518	224.374	10.122	69.842	-0.081	-0.206
		6	31.105	214.625	5.587	38.55	-0.134	-0.340
		1	48.666	335.754	3.163	21.825	0.068	0.173
		2	50.152	346.049	-0.127	-0.876	0.0318	0.081
17	13,000 lb	3	61.289	422.894	7.034	48.535	-0.558	-1.417
	[57.85 KN]	4	50.871	351.01	5.562	38.378	0.021	0.053
	[45.14 psi]	5	39.742	274.22	13.995	96.428	-0.116	-0.295
		6	39.558	272.95	8.936	61.658	-0.156	-0.396

TABLE 6.1.4

Contact Stresses for Test Four

Duration of Load Application in mins	Load	Cell Nos	Normal Stress in psi	Normal Stress in KPa	Shear Stress in psi	Shear Stress in PKa	Eccentricity of Normal Stress in Inches	Eccentricity of Normal Stress in c
		1	14.015	96.704	0.543	3.742	0.022	0.(
		2	12.749	87.968	0.978	6.748	-0.080	-0.2
15	3000 lb	3	13.558	93.55	0.725	5.003	0.034	0.(
	[13.35 KN]	4	9.427	65.046	1.179	8.135	0.110	0.2
	[10.42 psi]	5	11.276	77.804	3.034	20.935	-0.092	-0.2
		6	7.182	49.556	1.786	12.323	-0.194	-0.4
		1	19.170	132.273	1.051	7.252	0.005	0.(
		2	18.344	126.574	1.394	9.619	-0.071	-0.1
		3	17.424	120.226	1.696	11.702	-0.006	0.(
15	4000 lb	4	12.835	88.5615	1.579	10.895	0.091	0.2
	[17.8 KN]	5	13.144	90.694	4.180	28.842	-0.107	-0.2
	[13.89 psi]	6	10.605	73.175	2.961	20.431	0.210	-0.5
		1	22.095	152.456	1.302	8.984	0.008	0.(
		2	21.694	149.69	1.086	7.493	-0.057	-0.1
	5000 lb	3	21.048	145.231	2.199	15.173	-0.009	-0.(
	[22.25 KN]	4	16.352	112.829	1.891	13.048	0.074	0.1
	[17.36 psi]	5	14.330	98.877	4.777	32.961	-0.145	-0.3
		6	12.320	85.008	3.877	26.751	0.229	0.
		1	26.044	179.704	1.554	10.723	0.013	0.(
		2	25.611	176.716	1.139	7.859	-0.047	-0.
15	6500 lb	3	24.996	172.472	2.615	18.044	-0.007	0.(
	[28.93 KN]	4	19.648	135.571	2.234	15.415	0.035	0.(
	[22.57 psi]	5	18.453	127.326	4.467	30.822	-0.101	-0.
		6	14.936	103.058	4.024	27.766	0.191	0.
		1	28.626	197.519	1.733	11.958	0.005	0.(
		2	28.633	197.568	1.345	9.281	-0.046	-0.
15	7500 lb	3	27.416	189.170	3.010	20.769	-0.008	0.
	[33.38 KN]	4	22.034	152.035	2.554	17.623	0.040	0.
	[26.04 psi]	5	21.333	147.20	4.537	34.035	-0.095	-0.
		6	18.247	125.904	4.429	30.560	-0.148	-0.
		1	32.145	221.80	1.676	11.564	0.003	0.
		2	32.114	221.587	1.763	12.165	-0.038	-0.
15	9000 lb	3	30.685	211.727	3.069	21.176	-0.0139	-0.
	[40.05 KN]	4	24.637	169.995	2.682	18.506	0.050	0.
	[31.25 psi]	5	25.216	173.990	4.928	34.003	-0.084	-0.
		6	21.434	147.895	4.762	32.858	-0.140	-0.

TABLE 6.1.5

Contact Stresses for Test Five

Duration of Load Application in mins	Load	Cell Nos	Normal Stress in psi	Normal Stress in KPa	Shear Stress in psi	Shear Stress in KPa	Eccentricity of Normal Stress in Inches	Eccentricity of Normal Stress in cms
15	1000 lbs [4.45 KN] [3.47 psi]	1	3.379	23.315	0.253	1.746	0.026	0.066
		2	5.697	39.309	-0.17	-1.173	-0.021	-0.053
		3	4.483	30.933	0.242	1.670	0.028	0.0711
		4	4.856	33.506	-0.067	-0.462	0.005	0.0127
		5	3.541	24.433	0.850	5.865	-0.073	-0.185
		6	4.218	29.104	0.977	6.741	-0.173	-0.439
15	2000 lbs [8.9 KN] [6.94 psi]	1	7.682	53.04	0.342	2.394	0.046	0.117
		2	10.179	70.235	0.099	0.683	-0.010	-0.0254
		3	9.957	68.703	0.679	4.685	0.021	0.0533
		4	10.294	71.029	0.294	2.029	0.038	0.0965
		5	8.056	55.586	2.383	16.443	-0.124	-0.315
		6	8.209	56.642	2.147	14.814	-0.200	-0.508
15	3000 lbs [13.35 KN] [10.42 psi]	1	13.489	93.074	0.217	1.497	0.039	0.0991
		2	14.219	98.111	0.885	6.107	0.025	0.0635
		3	16.127	111.276	0.848	5.851	0.002	0.005
		4	13.938	96.172	0.0144	0.0994	0.094	0.239
		5	11.684	80.620	4.483	30.933	-0.145	-0.368
		6	13.794	95.179	2.899	20.003	-0.130	-0.330
15	4000 lbs [17.8 KN] [13.89 psi]	1	17.258	119.08	0.071	0.490	0.049	0.125
		2	16.286	115.823	0.876	6.044	-0.033	-0.084
		3	21.246	146.592	1.84	12.696	-0.001	-0.003
		4	15.711	108.406	0.269	1.856	0.080	0.203
		5	17.789	122.744	5.033	5.473	-0.101	-0.257
		6	17.876	123.344	1.427	9.846	-0.046	-0.117
15	4500 lbs [20.03 KN] [15.63 psi]	1	19.182	132.36	0.835	5.762	0.041	0.104
		2	18.685	128.93	0.647	4.464	0.023	0.058
		3	23.314	160.867	1.777	12.261	0.006	0.0152
		4	17.839	123.089	-0.126	-0.869	0.076	0.193
		5	20.889	144.134	4.939	34.079	-0.096	-0.244
		6	20.147	139.014	1.409	9.708	-0.057	-0.145

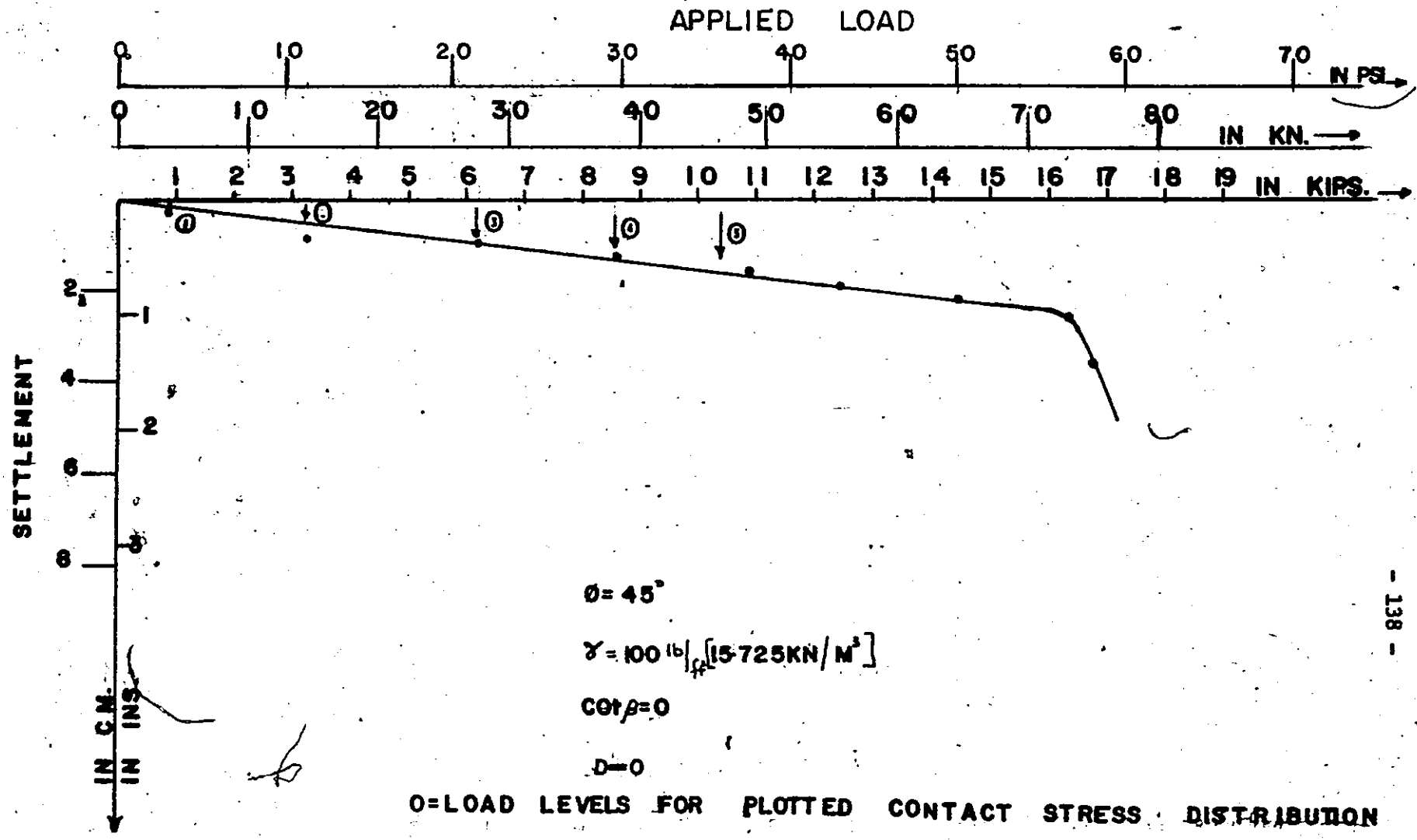

FIGURE 6.2.1 LOAD VS SETTLEMENT CURVE FOR TEST ONE.

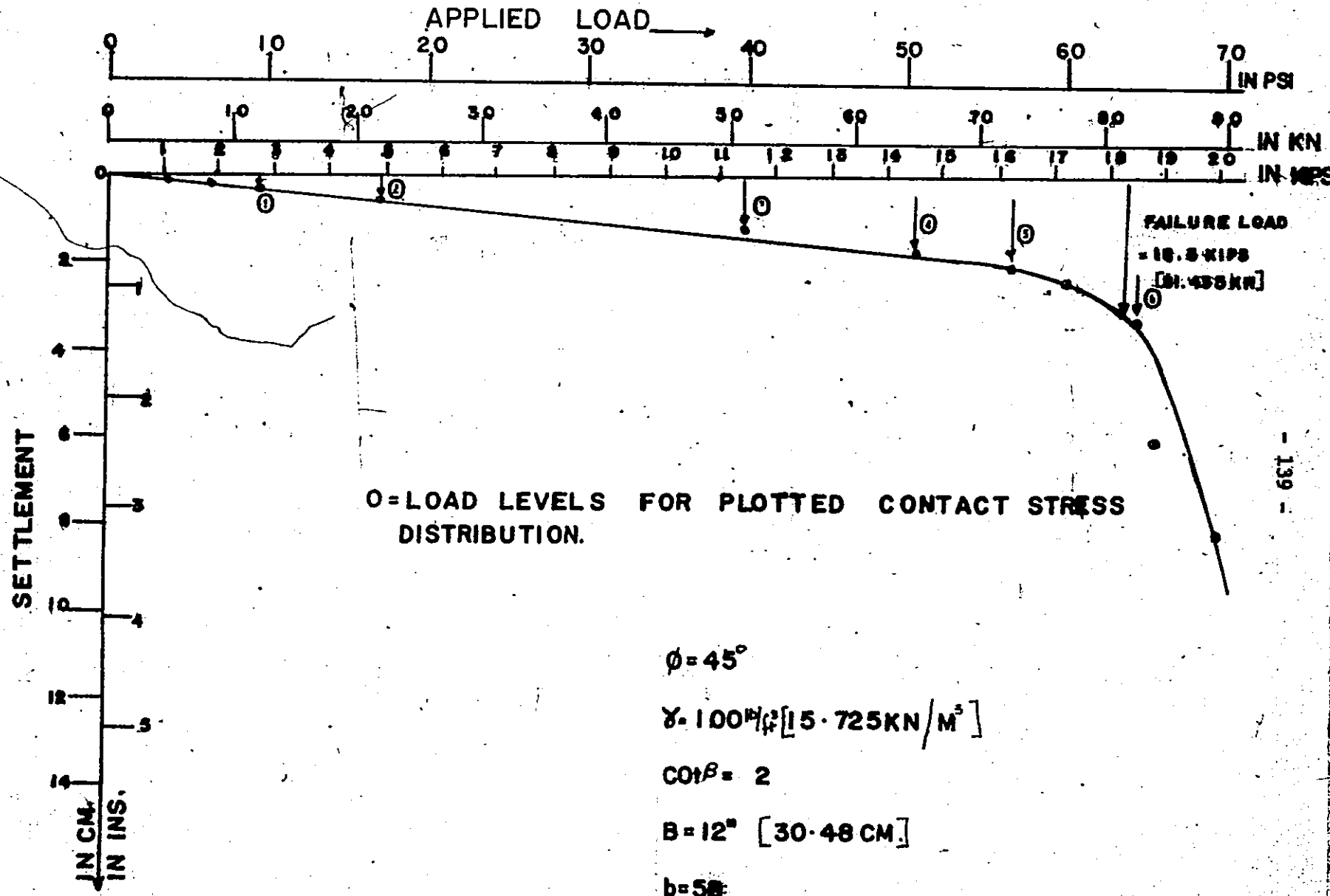

O = LOAD LEVELS FOR PLOTTED CONTACT STRESS DISTRIBUTION.

$\phi = 45°$

$\gamma = 100 lb/ft^3 [15.725 KN/M^3]$

$\cot\beta = 2$

B = 12" [30.48 CM.]

b = 5"

D = 0

FIGURE 6.2.2 LOAD VS SETTLEMENT CURVE FOR TEST TWO.

partial failure zone and the general shear failure zone. The elastic zone is as a result of the elastic distortion and compression of the soil. Within this region, the applied load was found to be proportional to the settlement of the footing. In the local shear and general shear failure zones, relatively large settlements were obtained for small increments in load.

The failure load was determined by the point of intersection of the tangents from the elastic branch and the steep branch. The value was found to be 18.3 kips (81.435 KN).

Test 3 was performed with the edges of the three footings located at a distance of 2.50 (2.5', 76.2 cm) from the top of the 2:1 slope. The load versus settlement curve is shown in Figure 6.2.3. The failure load was found to be 16 kips (71.2 KN). One would have anticipated a smaller failure load on account of the nearness of the footings to the 2:1 slope. However, a contrary result was obtained.

In Test 4, the edges of the footings were at 5B from the top edge of the 2:1 slope. The properties of the sand are as follows: a relative density of 55% which gives a density of 90 lb/cu.ft (14.146 KN/m^3) and an angle of shearing resistance of 38° under plane strain conditions. According to DeBeer (1970) this soil should exhibit a local shear failure which it actually did. The failure load of 5.4 kips (24.03 KN) is shown on the load versus settlement diagram, Figure 6.2.4 and was determined from the breaking point on the log of load versus log of settlement curve Figure 6.2.5. The heave beside one end of the width of the footing was measured and has been presented graphically, for the load levels indicated in Figure 6.2.6.

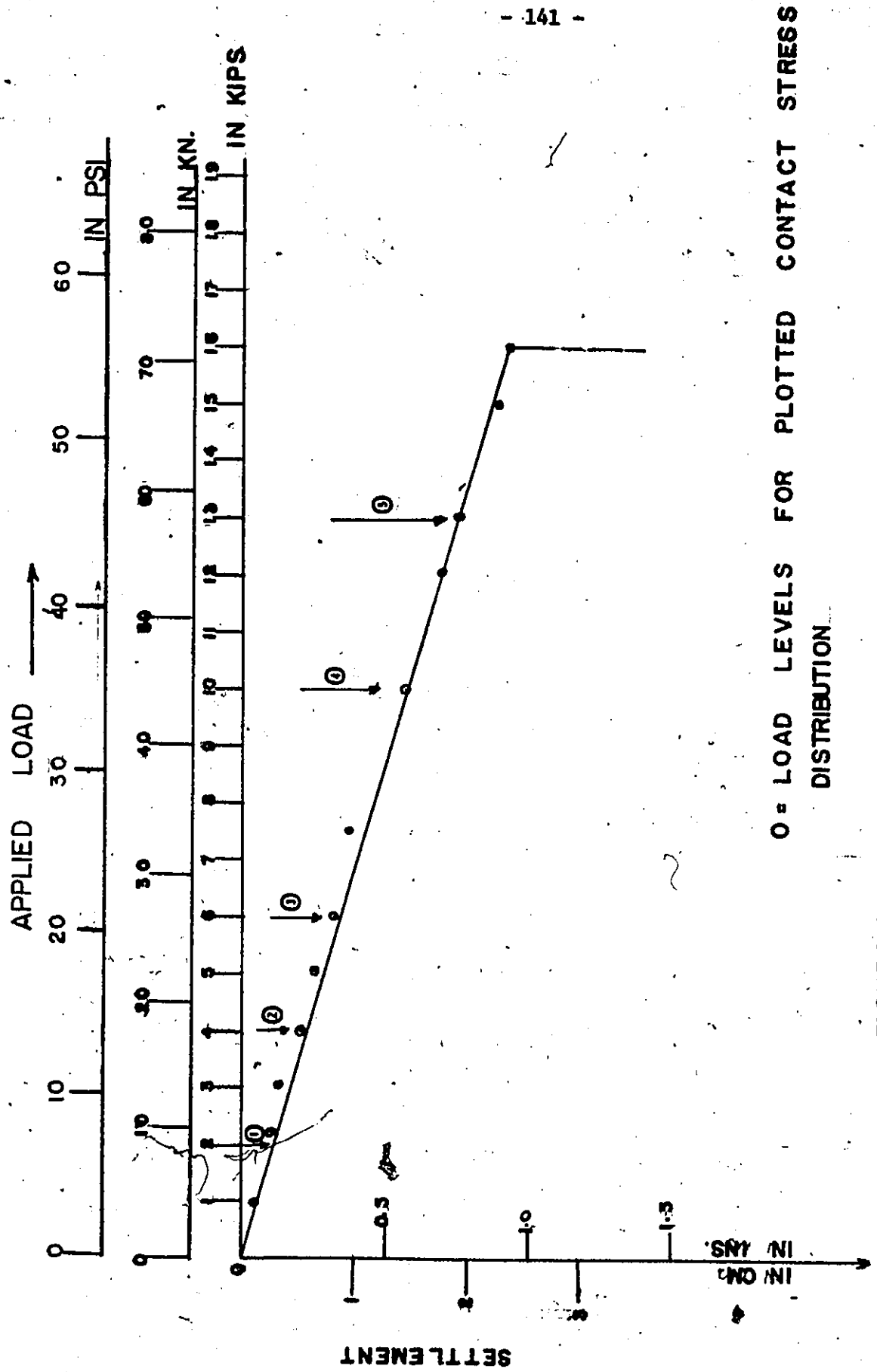

O = LOAD LEVELS FOR PLOTTED CONTACT STRESS DISTRIBUTION

FIGURE 6·2·3 LOAD VS SETTLEMENT CURVE FOR TEST THREE.

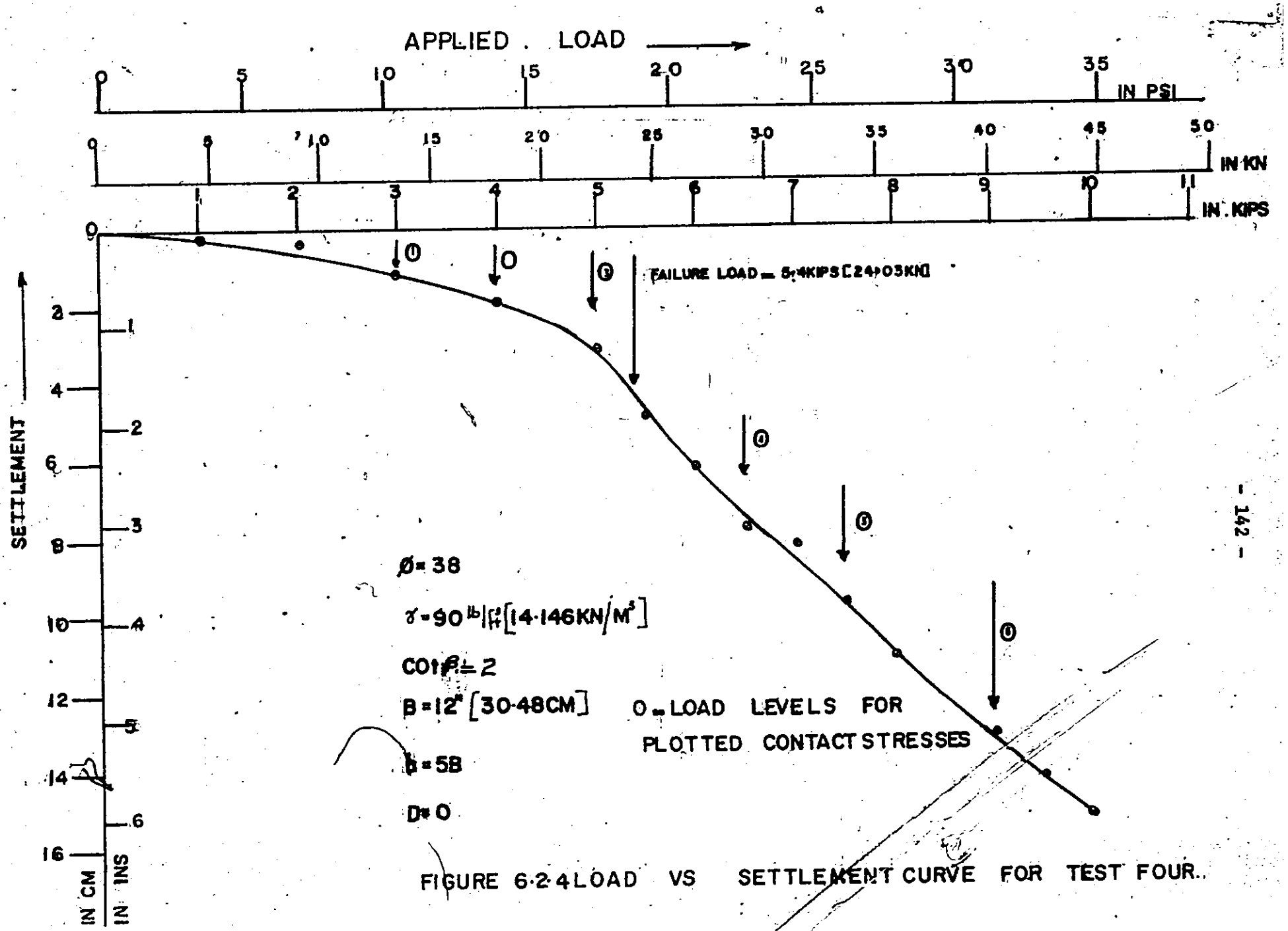

FIGURE 6.2.4 LOAD VS SETTLEMENT CURVE FOR TEST FOUR.

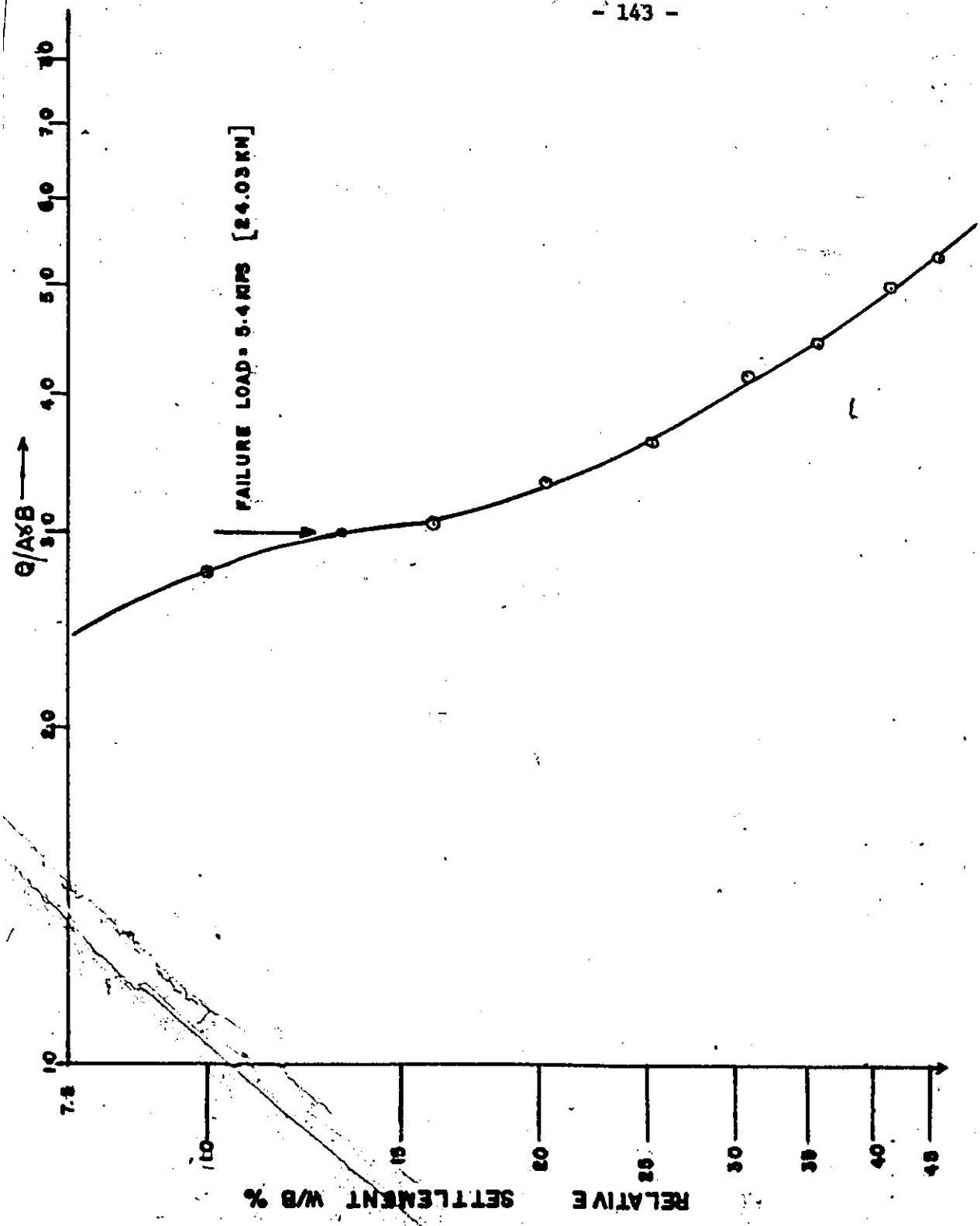

FIGURE 6.2.5 LOG SETTLEMENT VS LOG LOAD FOR TEST FOUR.

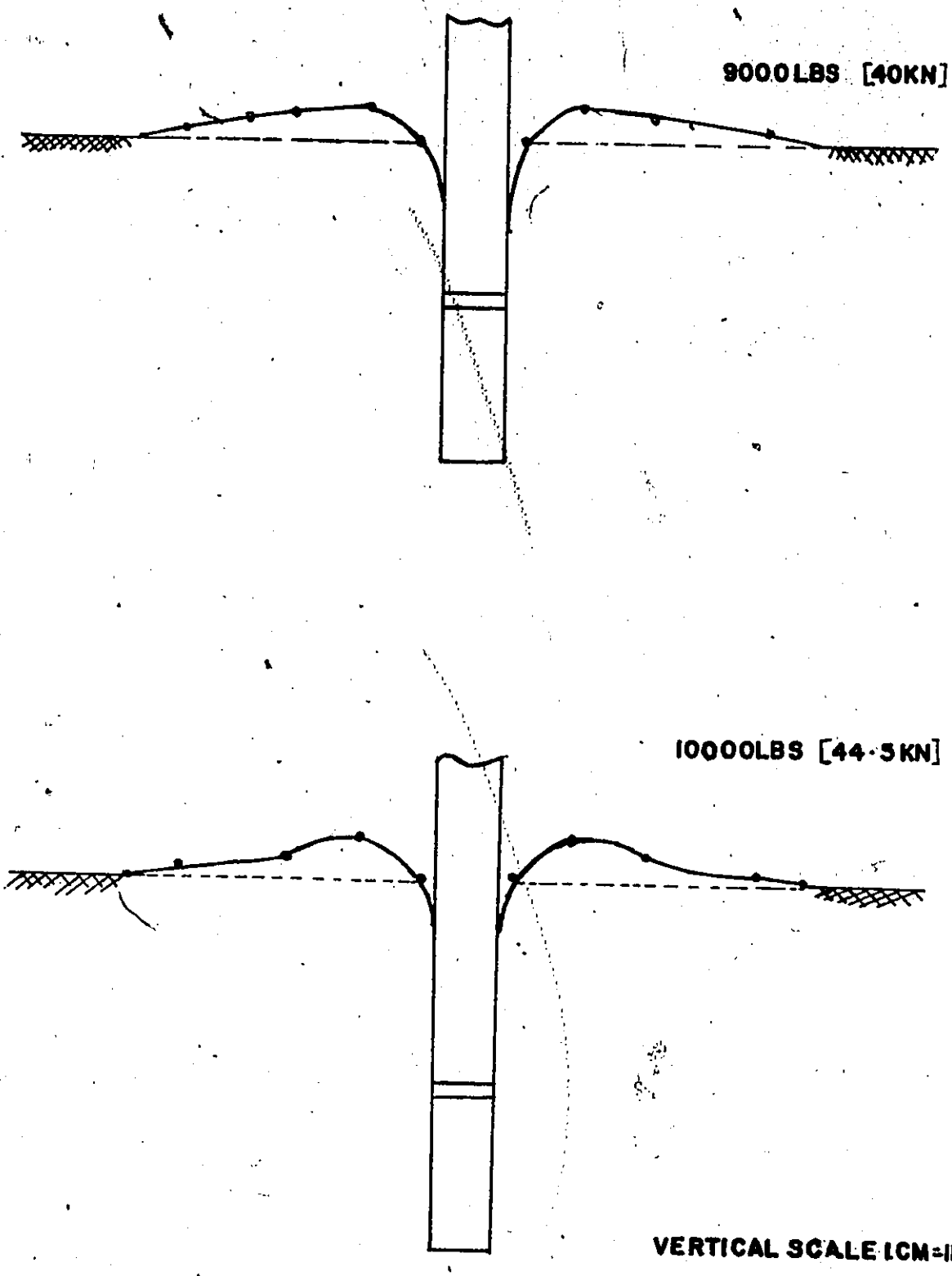

FIGURE 6. 2·6 HEAVE DIAGRAM.

Test 5 was performed with the edges of the footings at 2.5B from the top of the 2.1 slope with the properties of the sand the same as in Test.4. The failure load was determined as in Test 4, Figure 6.2.7. The oad versus settlement curve is shown in Figure 6.2.8.

The results for the load and their corresponding settlements are given in Appendix D.

6.3 Normal Stress

The experimental results of the normal stresses and their corresponding eccentricities for the five tests, are given in Tables 6.1.1 to 6.1.5.

Using the data from the above tables and assuming a linear normal stress distribution over each modified Cambridge load cell face plate, the normal stresses at the edges of each load cell have been computed, using the following expression

$$P_e = P_s(x)\ [1 \pm \frac{6x}{b}] \qquad 6.4$$

where

P_e = edge stresses at each load cell

$P_s(x)$ = normal stress at each load cell

x = eccentricity of the normal stress at each load cell

b = 2" (5.08 cm).

A typical distribution for test 4 is shown in Figure 6.3.4A.

The distribution of the normal stresses under the footing has been represented by curves owing to the continuity that must exist in the sand distribution.

The normal stress distribution has also been plotted for the load levels indicated on the load versus settlement curves so that an effective deduction can be made on the effects of the stress or strain state of the soil on the contact stress distribution.

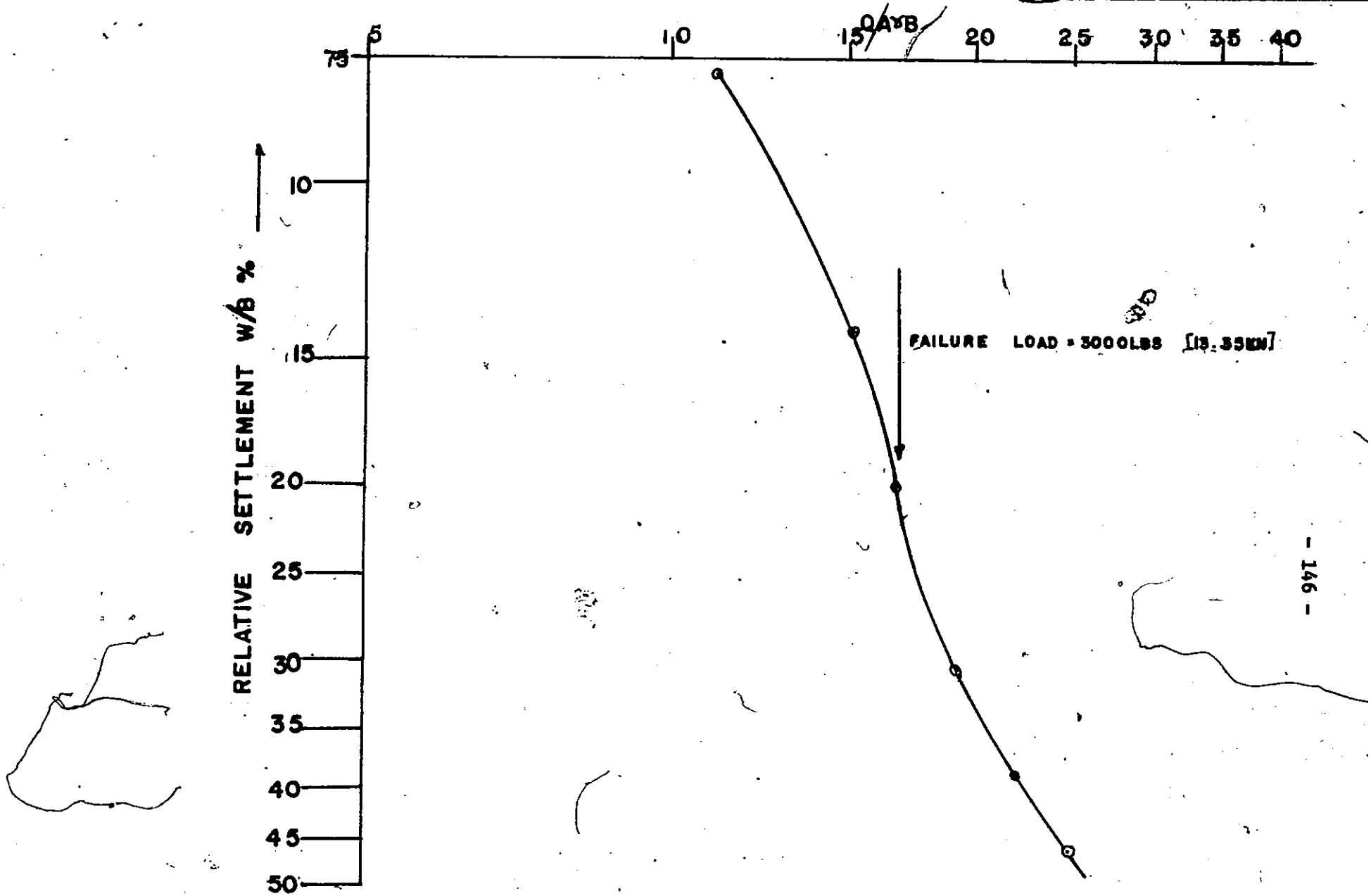

FIGURE 6·2·7 LOG SETTLEMENT VS LOG LOAD FOR TEST FIVE

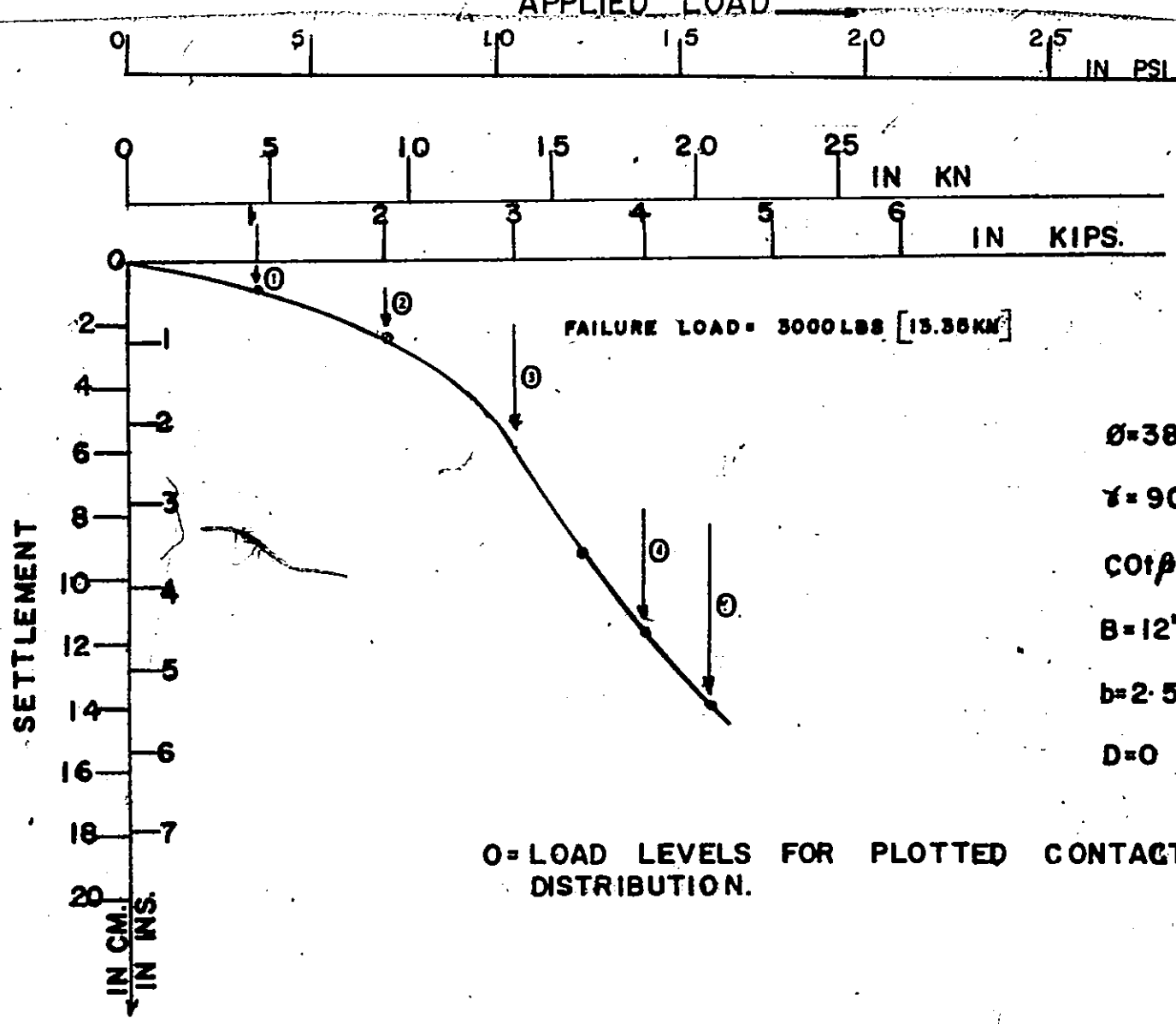

Ø=38

$\gamma = 90\ lb/ft^3$ [14.146KN/M³]

$\cot\beta = 2$

B=12" [30.48CM]

b=2.5B

D=0

O = LOAD LEVELS FOR PLOTTED CONTACT STRESS DISTRIBUTION.

FIGURE 6.2.8 LOAD VS SETTLEMENT CURVE FOR TEST FIVE.

The normal stress distribution for Test 1, Figure 6.3.1 gave a series of convex shaped curves which were symmetrical about the centre of the footing. The highest values of the normal stresses existed at the centre of the footing. The normal stress decreased from the centre of the footing towards the edges. As the load was increased, the normal stresses at the Cambridge load cell locations increased accordingly. Thus, there seems to be a linear relationship between the normal stress and the applied load. The convexity of the normal stress distribution also increased with load. Some normal stress existed at the edges of the footing and their values were smaller than those at the centre of the footing.

The calculated loads, Q, (computed from the normal stress distribution curve) were found to agree closely with the applied loads (Table 6.3.1). The discrepancy in the initial load levels can be attributed to: (1) the compression of the soil mass, (2) the poor response of the hydraulic gauges to the applied loads at small load levels which is obvious from the results obtained with a load cell installed between the central hydraulic jack and the reaction beam, and (3) a probable redistribution of stresses along the length of the footing.

Owing to the inability to attain failure with the footings hinged to the jacks, it was considered necessary and appropriate to fix the footings to the jacks. The subsequent four tests were performed under the above conditions.

The shape of the normal stress distribution for Test 2, Figure 6.3.2 gives a series of asymmetrical convex shapes curves. Thus it becomes apparent that: (1) an eccentricity or inclination of the jacks or both has been called into play during the loading process and (2) the sand surface was not properly levelled.

However, the applied load was found to be approximately equal to

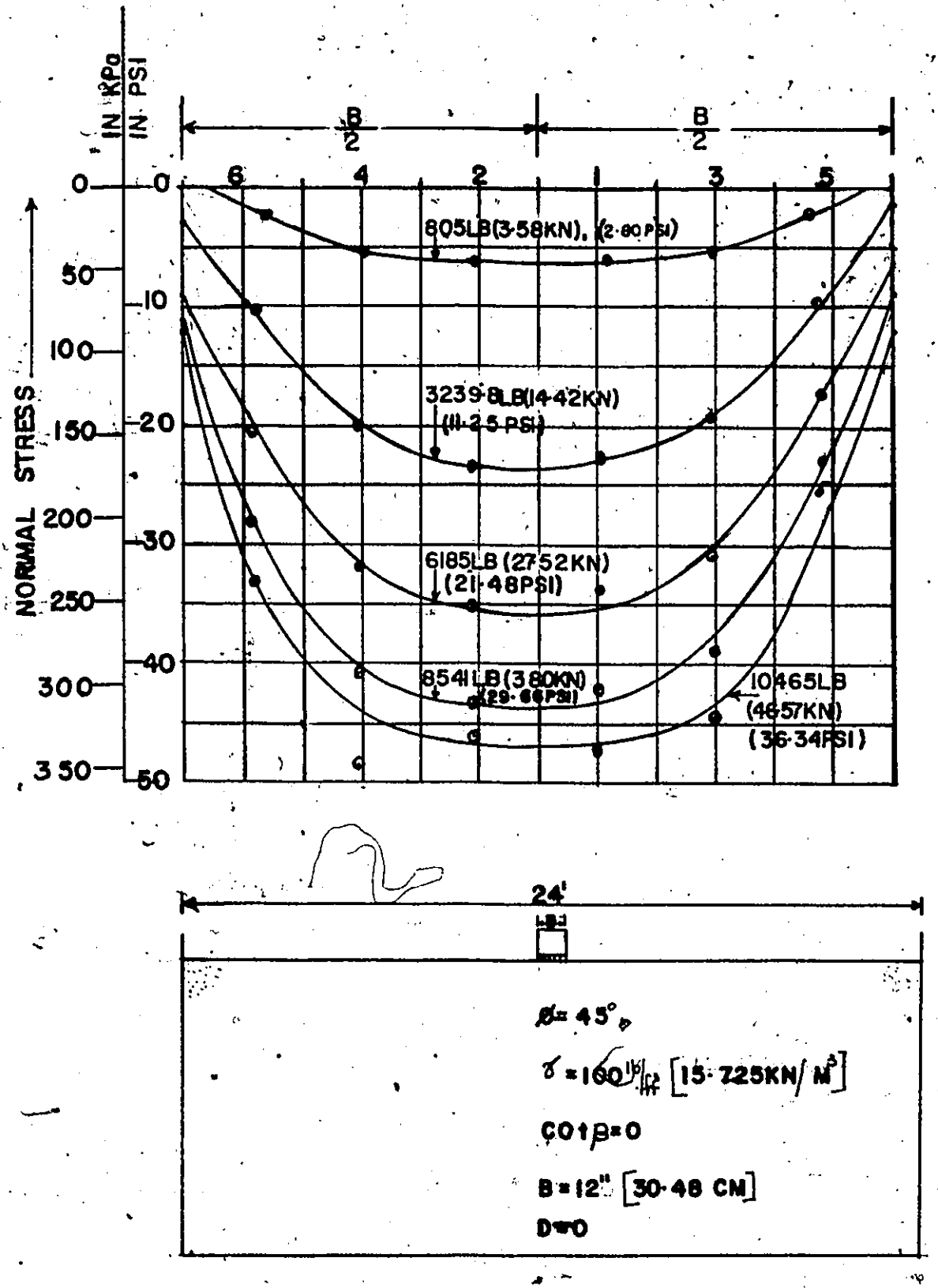

FIGURE 6·3·1 NORMAL STRESS DISTRIBUTION FOR TEST ONE·

TABLE 6.3.1

Comparison of Applied and Calculated Load

Test	Applied Load in lbs,	Calculated Load in lbs, Q	% of Calculated Loads Over Applied Load
1	805.03	1080	34
	3239.8	4920	52
	6185.0	8100	30
	8541.2	9960	16
	10465.43	10920	4
2	2770.	1752	-37
	4853	4200	-13
	11275	10857.6	-3.8
	14520	14400	-0.9
	16250	15960	-1.8
3	2000	2520	26
	4000	4440	11
	6000	6240	4
	10000	9978	-0.2
	13000	12912	-0.7
4	3000	3312	10
	4000	4440	11
	5000	5040	.8
	65000	6220	-4.4
	7500	7200	-4
	9000	8100	-9.3
5	1000	1200	20
	2000	2400	20
	3500	4320	23
	4000	5040	26
	4500	5760	28

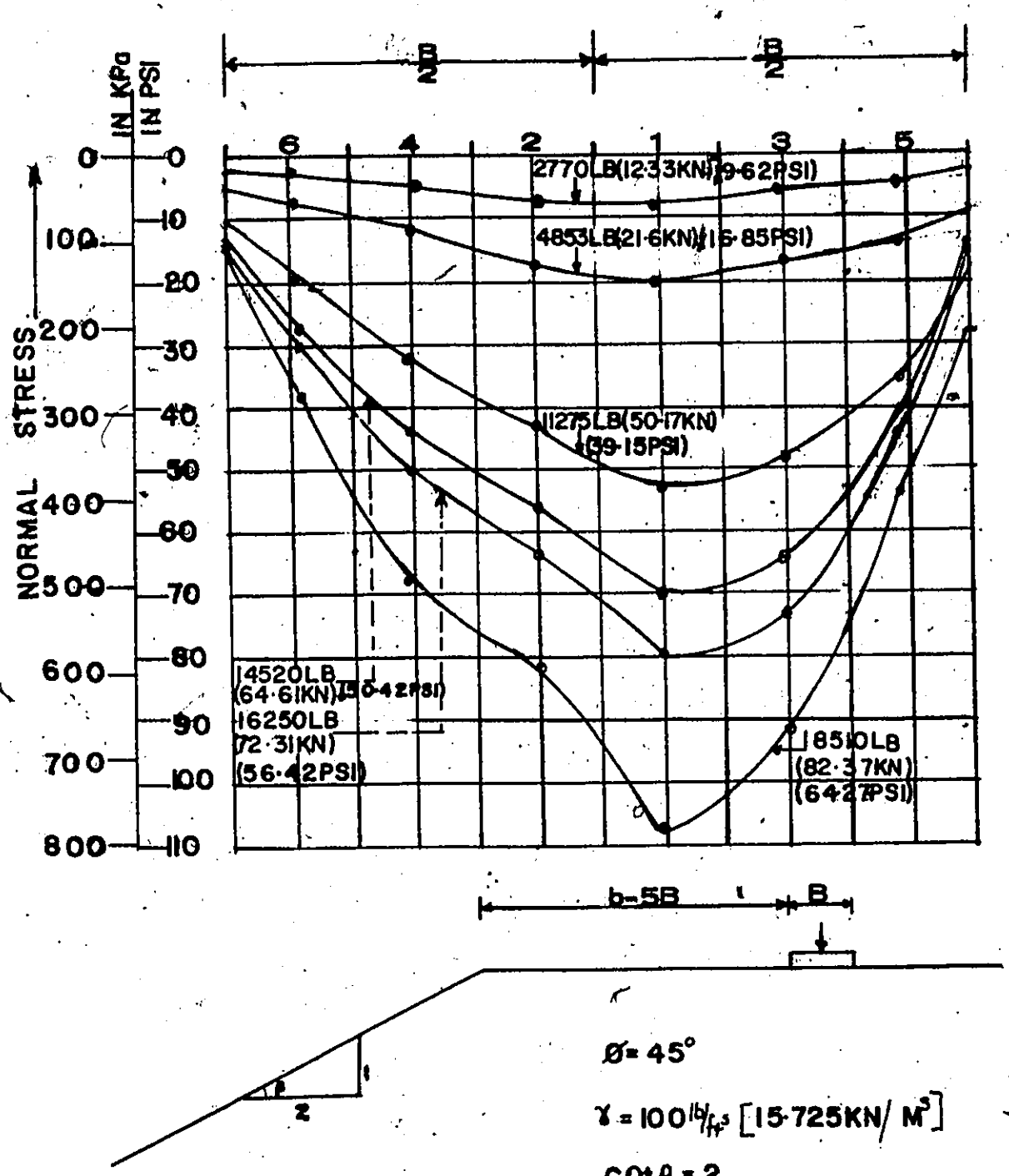

$\phi = 45°$

$\gamma = 100\ lb/ft^3\ [15.725\ KN/M^3]$

$\cot\beta = 2$

$B = 12"\ [30.48\ CM]$

$b = 5B$

$D = 0$

FIGURE 6·3·2 NORMAL STRESS DISTRIBUTION FOR TEST TWO.

the calculated load, with the applied load being 0.9% to 13% higher than the calculated load. This gives more faith in the second factor as the main source of the asymmetrical shaped curves obtained.

Test 3 (Figure 6.3.3) gave a series of convex shaped curves with the normal stresses lower on the footing half width close to the slope. At higher load levels, the convexity increased with the second load cells off the centre of the footing recording greater stresses than the load cells immediately off the footing centre.

However, the applied load was found to agree approximately with the calculated load (Table 6.3.1).

In Test 4 a series of convex shaped curves (Figure 6.3.4) were obtained with the highest normal stress being obtained at the centre of the footing. However, edge stresses were found to exist for all load levels. The convexity of the curves increased with increments in applied loads. The applied load was found to agree favourably with the load calculated from the normal stress distribution curves.

The discrepancy between the applied and calculated loads are shown in Table 6.3.1.

The 2:1 slope at 2.5B from the edge of the width of the footings in Test 5 affected the normal stress distribution. The results of the test have been plotted in Figure 6.3.5. It indicates a series of curves with the normal stresses being higher under the footing half width away from the slope.

The calculated loads (from the normal stress distribution curves) were higher than the applied load (Table 6.3.1) which might be attributed to a probable redistribution of stresses along the length of the footing.

6.4 Shear Stress

The results for the shear stresses are given in Tables 6.1.1 to 6.1.5.

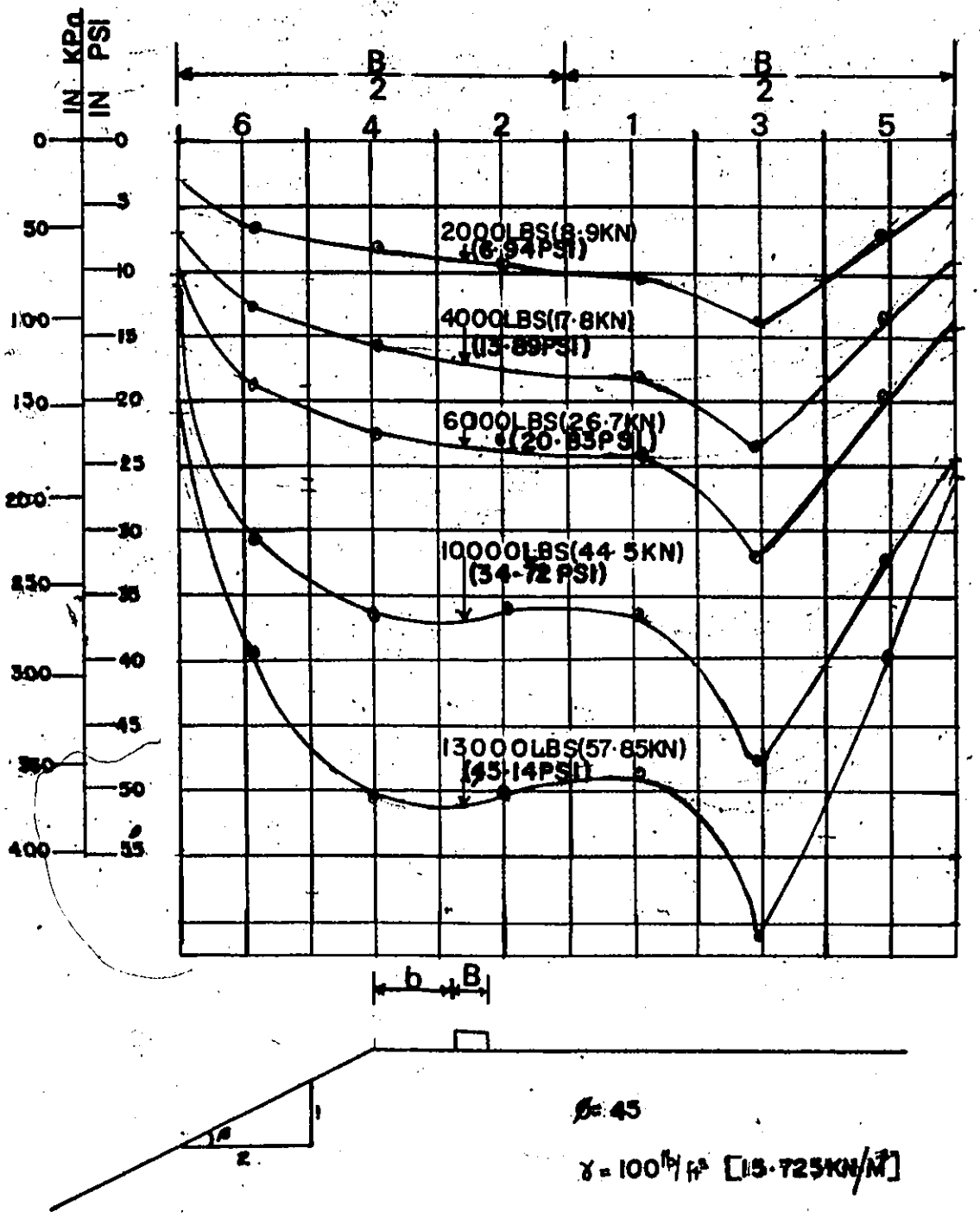

$\beta = 45$

$\gamma = 100^{lb}/ft^3$ [15·725KN/M³]

$\cot\beta = 2$

B = 12" [30·48CM]

b = 2.5B

D = 0

FIGURE 6·3·3 NORMAL STRESS DISTRIBUTION FOR TEST THREE

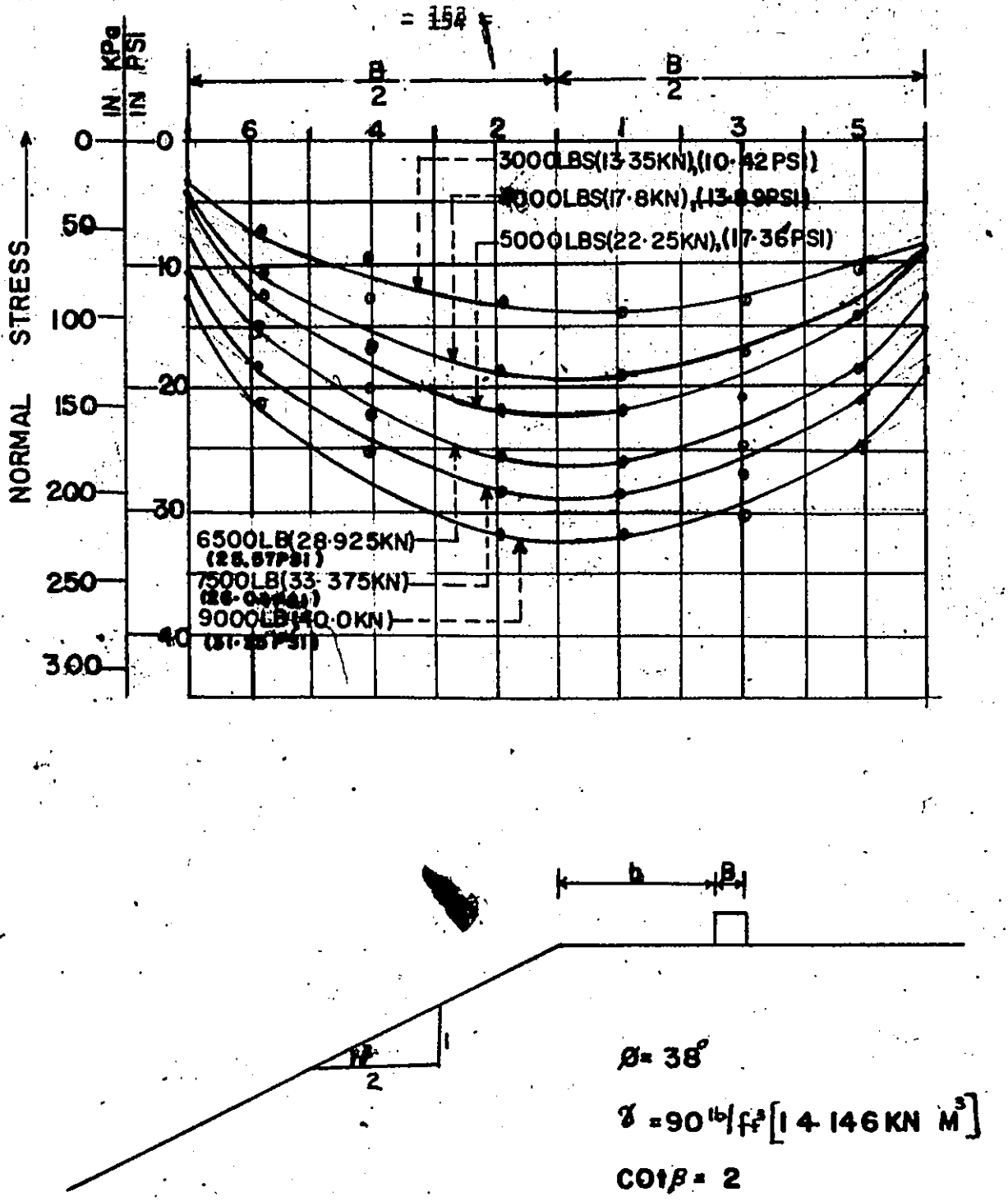

$\phi = 38^{\circ}$

$\gamma = 90\ lb/ft^3\ [14.146\ KN\ M^3]$

$Cot\beta = 2$

$B = 12''\ [30.48\ CM]$

$b = 5B$

$D = 0$

FIGURE 6·3·4 NORMAL STRESS DISTRIBUTION FOR TEST FOUR·

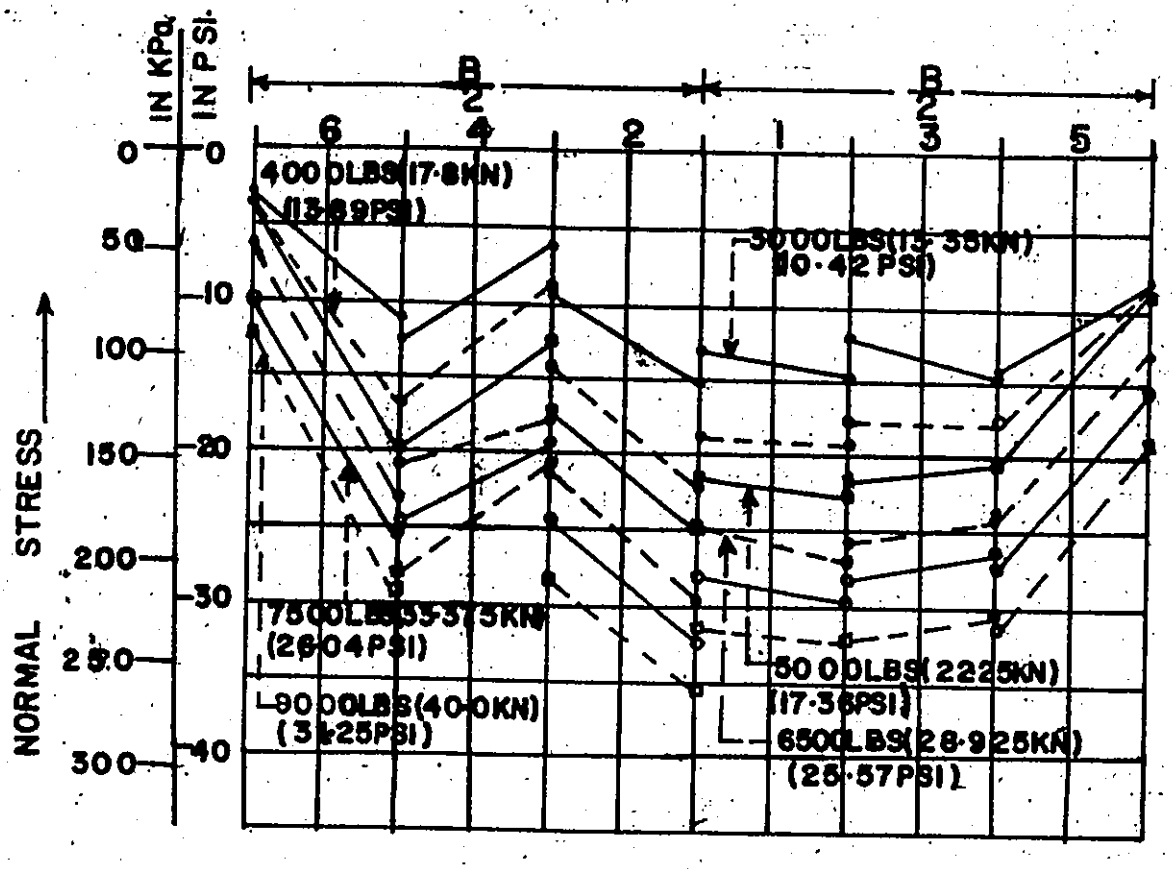

FIGURE 6·3·4 A NORMAL STRESS DISTRIBUTION FOR TEST FOUR, ASSUMING A LINEAR DISTRIBUTION OVER EACH LOAD CELL'S FACE PLATE.

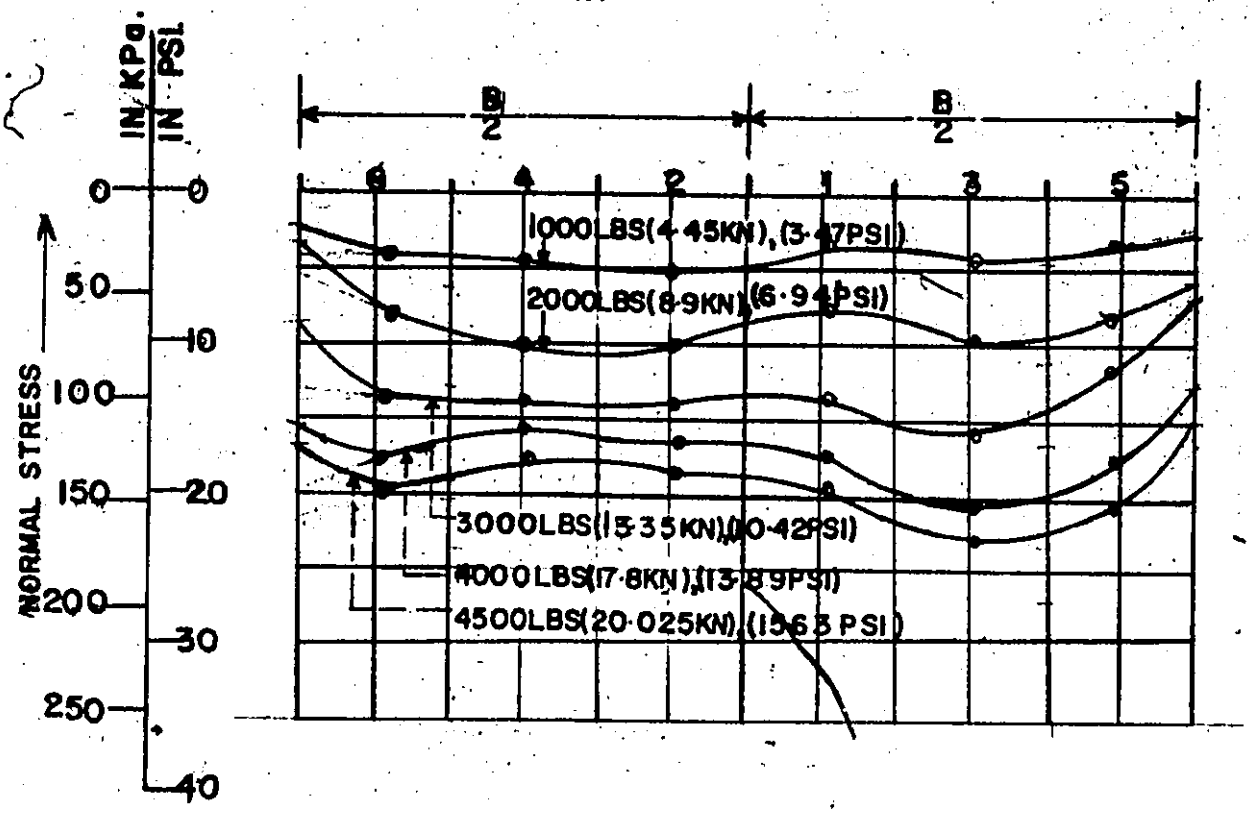

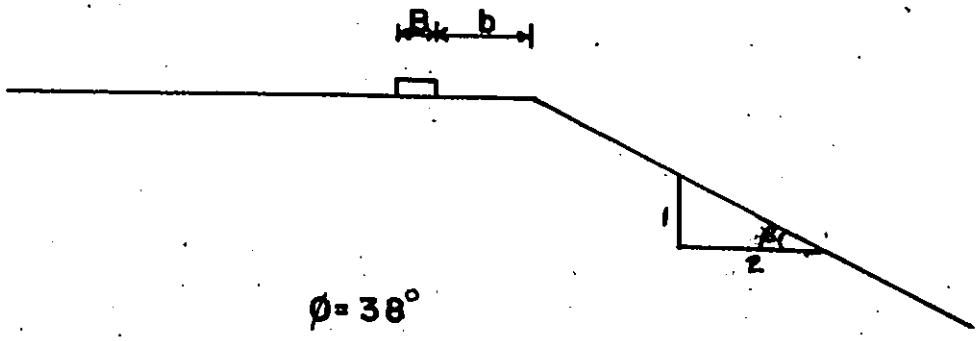

$\phi = 38^\circ$

$\gamma = 90\,lb/ft^3\ [14.146 KN/M^3]$

$\cot\beta = 2$

$B = 12"\ [30.48\ CM]$

$b = 2.58$

$D = 0$

FIGURE 6·3·5 NORMAL STRESS DISTRIBUTION FOR TEST FIVE

In Test 1 in which the footing tilted upwards at cell 5, the shear stresses (Figure 6.4.1), were found to be higher at the Cambridge load cell locations on that half of the footings width.

The shear stresses increased from Cell 1 to Cell 3 and then rapidly to Cell 5.

On the other half of the footings width, the shear stresses increased from Cell 2 to Cell 4 and then the rate of increase decreased to Cell 6. The above phenomenon has been attributed to the tilting which took place and has subsequently lead to the dissipation of the shearing strain necessary for the mobilization of the shear stress.

In Tests 2 and 3, Figures 6.4.2 and 6.4.3, respectively, the shear stresses were highest at the footing edges.

In Test 2, zero shear stresses were obtained at the footing centre from where it increased towards the edges.

In Test 3, the point of zero shear stresses shifted to points under the footings half width closest to the slope (2.5B test).

In Test 4, Figure 6.4.4, the shear stress distribution gave concave shape curves on both sides of the centre of the footing. The shear stresses at the edges of the footing were higher than within its central region. The shear stresses were zero at the centre of the footing for different magnitudes of applied loads.

Test 5, Figure 6.4.5, gave similar shaped curves as Test 4 for the shear stress distribution. However, as the load increased, the point of zero shear stressed moved to points under the footings half width closest to the slope (2.5B test). The shear stresses under the footing half width away from the slope were lower than those under the footing half width closest to the slope.

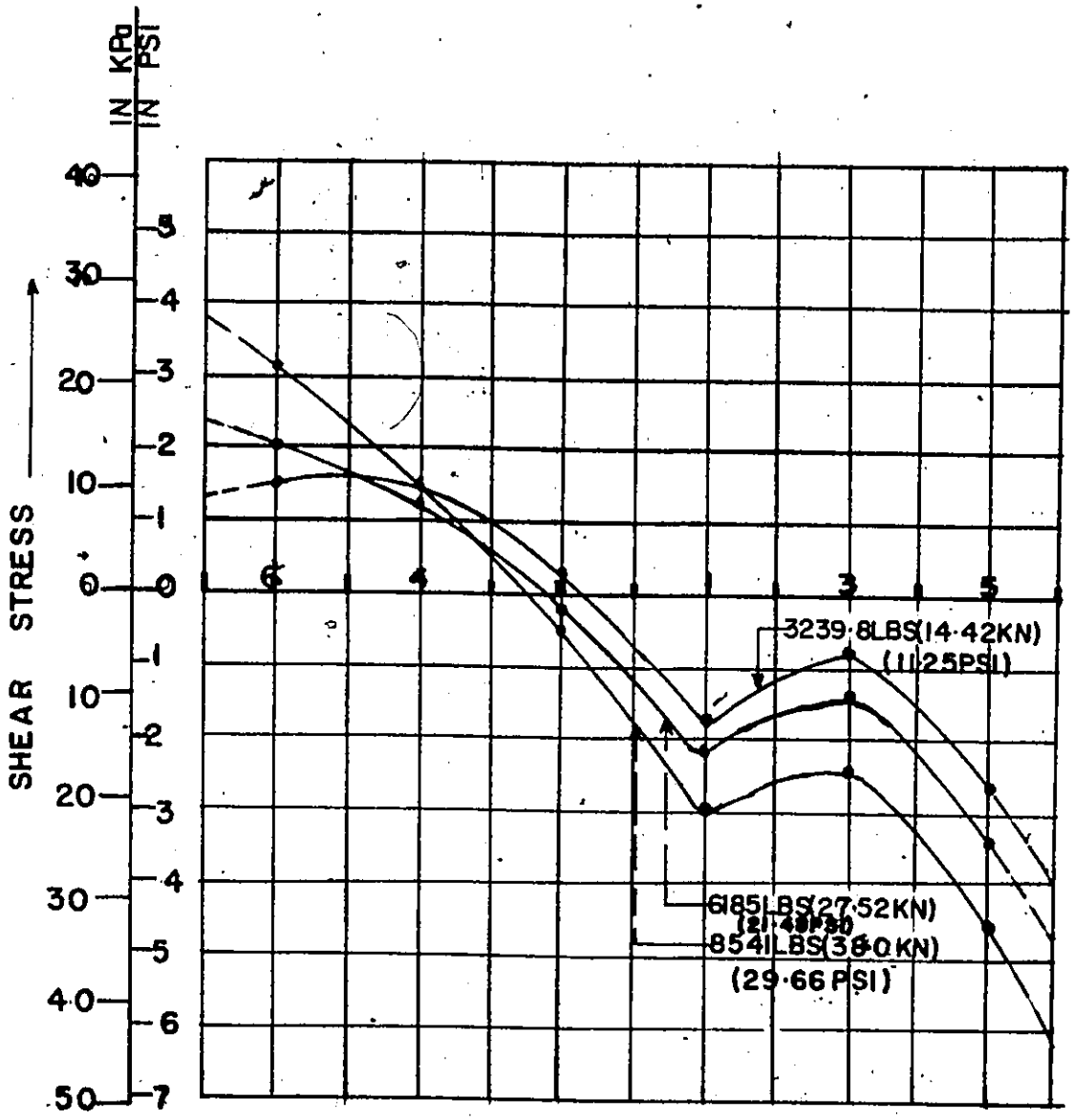

$\phi = 45°$

$\gamma = 100\ lb/ft^3\ [15.725\ KN/M^3]$

$Cot\beta = 0$

$B = 12"\ [30.48CM]$

$D = 0$

FIGURE 64-1 SHEAR STRESS DISTRIBUTION FOR TEST ONE.

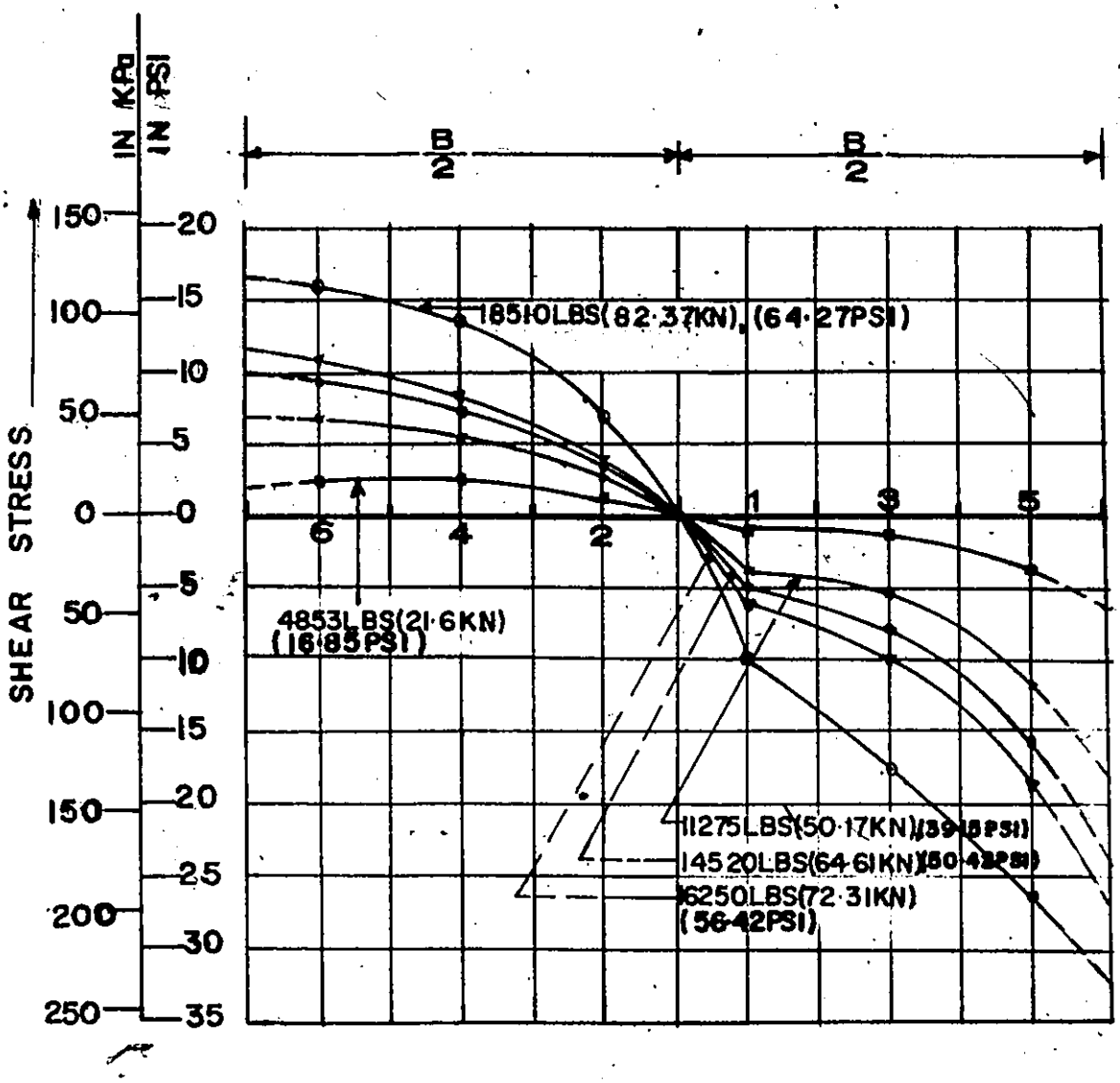

$\phi = 45^\circ$

$\gamma = 100\ lb/ft^3\ [15.725\ KN/M^3]$

$\cot\beta = 2$

$B = 12"\ [30.48\ CM]$

$b = 5B$

$D = 0$

FIGURE 6-4-2 SHEAR STRESS DISTRIBUTION FOR TEST TWO

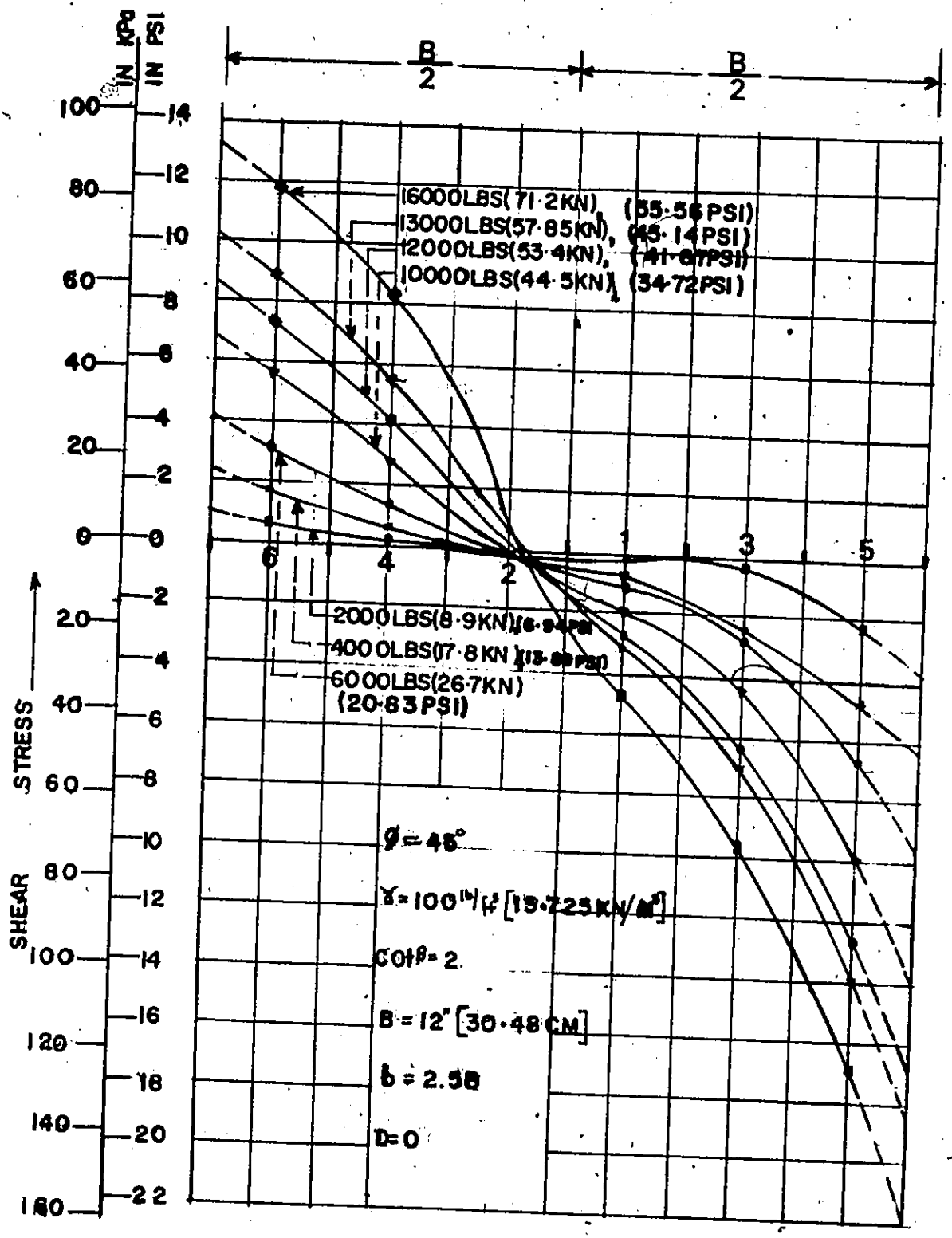

FIGURE 6.4·3 SHEAR STRESS DISTRIBUTION FOR TEST THREE.

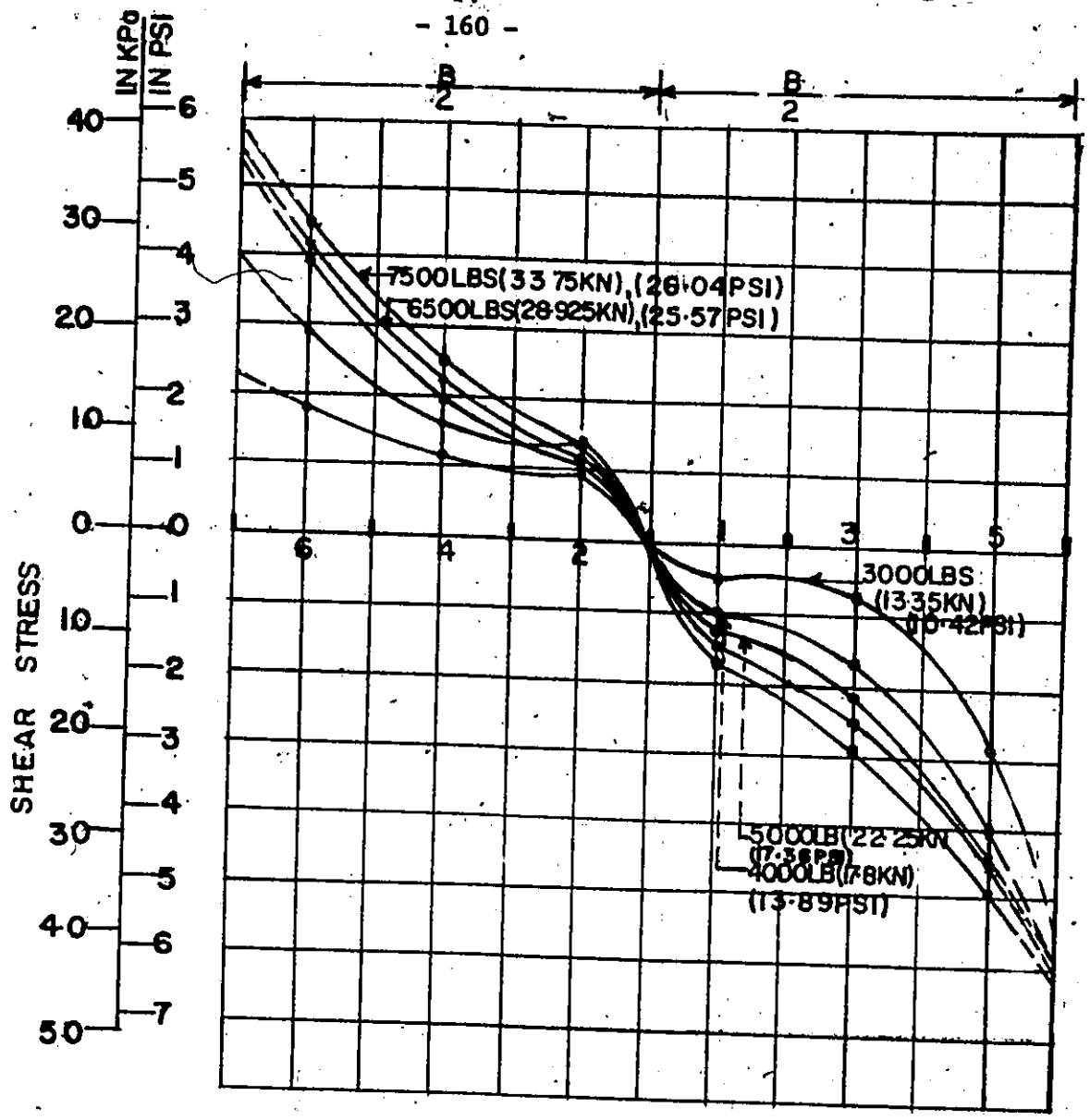

$\phi = 38°$

$\gamma = 90\ lb/ft^3\ [14.146 KN/M^3]$

$Cot\beta = 2$

$B = 12"\ [30.48 CM]$

$b = 5B$

$D = 0$

FIGURE 6.4.4 SHEAR STRESS DISTRIBUTION FOR TEST FOUR.

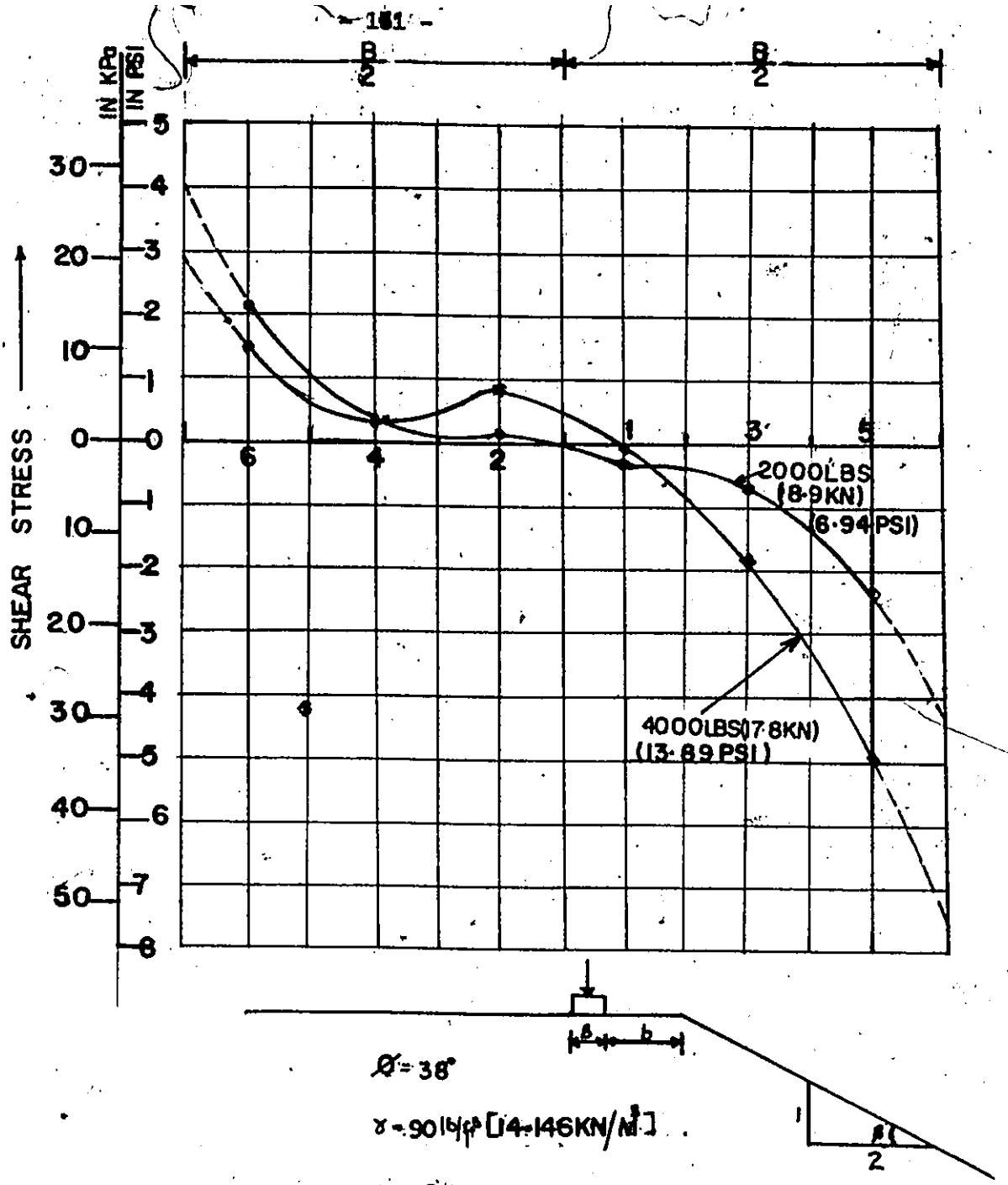

$\phi = 38°$

$\gamma = 90\,lb/ft^3$ [14·146KN/M^3]

$\cot\beta = 2$

B = 12" [30·48CM]

b = 2·5 B

D = 0

FIGURE 6·4·5 SHEAR STRESS DISTRIBUTION FOR TEST FIVE

Net shear stresses were noticed under the footing in each of the tests and have been shown in Table 6.4.1.

This has been attributed to: (1) the passive resistance offered by the sand adjacent to the footing edges; (2) the effect of the failure surface being developed on one half of the footing width, and (3) any eccentricity or inclination of the load resultant.

6.5 Eccentricity of the Normal Stress at the Modified Cambridge Load Cell Locations

The eccentricity of the normal stresses at the various modified Cambridge load cell locations under the different magnitudes of applied load for the five tests are given in Tables 6.1.1 to 6.1.5.

From the results of the tests the following can be deduced:

1. The eccentricity of the resultants of the normal stresses are highest at the load cell locations close to the edges of the footing (Cell Nos. 5 and 6). These resultants also act at eccentricities that are towards the centre of the footing. Thus negative, as indicated by the calibration process. The above have been attributed to the variation in the normal stress distribution at the above load cells location.

2. The magnitude of these eccentricities decreased to insignificant values at the load cell locations close to the centre of the footing (Cell Nos. 1 and 2), owing to the near uniform distribution of the normal stresses.

TABLE 6.4.1

Test	Applied Load in KN	Net Shear Stress in KPa	No. of Edge Cells to Which Net Shear Stress is Directed
1	14.42	14.74	5
	27.52	29.05	5
	38.0	42.19	5
	21.6	6.0	5
	50.17	45.97	5
	64.61	67.4	5
	72.31	84.33	5
	82.37	133.74	5
	8.9	15.8	5
	17.8	36.31	5
	26.7	47.82	5
	44.5	60.18	5
	53.4	73.34	5
	57.85	68.04	5
	71.2	76.73	5
	13.5	2.48	5
	17.8	6.85	5
	22.25	9.83	5
	28.925	8.55	5
	33.375	9.33	5
	8.9	6.0	5
	17.8	30.17	5

CHAPTER 7

ANALYSIS AND COMPARISON OF RESULTS

7.1 General

In this Chapter, comparison will be made for the tests on the flat and simulated flat grounds since all experimental and theoretical studies have been performed for the above case.

Tests 1, 2 and 4 indicate that the normal stress distributions under a rigid rough footing on the surface of sand at uniform density under a virgin loading and plane strain conditions are convex parabolae with the highest stresses at the centre of the footing. The normal stresses were also found to decrease towards the edges of the footing.

Studies performed by Faber (1937) (Figure 2.1.1) and Krivoroţov (1963), Figure 2.1.2 at the surface of a sandmass gave similar shaped normal stress distribution curves, with finite edge normal stresses.

However, other studies performed at depth seem to indicate contrary results. Their results seem to be compatible with the theory proposed by Schultze (1961), Chapter 2, Section 2.3. Burger (1932), Figure 2.1.5, obtained a skewed concave parabola in clayey sand. Siedek (1948), Figure 2.1.6, obtained a concave parabola in fine sand. In the above cases, the foundations were founded in saturated soils and at depths which might have given rise to the shape of the normal stress distribution obtained.

The shear stress distribution obtained in this study, using the results of test 4, in which there was a simultaneous development of slip surfaces under both halves of the width of the footing, gave a series of concave parabola, Figure 6.4.4. The shear stresses increased from zero values at the centre of the footing to maximum values at the edges of the footing.

The above result is similar to that obtained by Hartikainen (1972), Figure 2.1.4. Bub and Muhs (1963), Figure 2.1.7, reported a similar shear stress distribution, except that they obtained convex parabolae.

Three methods for the theoretical analysis of contact stresses under a rigid rough footing (Schultze 1961, Sedykh 1964, and Schweickert 1964) were given in Chapter 2, Section 2.3.

The theories proposed by Schultze (1961) and Sedykh (1964) for the normal stress distribution gave similar shaped curves (concave) within the central region of the footing, that is, with the transition points between the elastic and plastic zones. Within this zone their normal stress distributions are based mainly on the stress distributions in a soil mass as an elastic medium. The theory proposed by Sedykh (1964) indicates zero edge stresses which is contrary to the results obtained in this study even at zero embedment depth. The method proposed by Schultze (1962) gives edge stresses of magnitude γDN_q (for sand $C = 0$). Thus his theoretical analysis will be used for the computation of the normal stress distribution under the rigid rough footing.

The theory proposed by Schweickert (1964) yielded a concave parabolic normal stress distribution with finite edge stresses.

Sedykh's (1964) theory on the shear stress distribution indicates an increase from zero at the centre of the footing to a maximum value within the half width of the footing and then decreases to zero values at the edges of the footing. The above is however contrary to the result obtained in this study in which the shear stress increased from a zero value at the centre of the footing to maximum values at the edges of the footing.

The method proposed by Schweickert (1964) however gives results which are similar to that obtained in this study. Hence, his theory will be used for the computation of the shear stress distribution.

7.2 Normal Stress

The normal stress distribution will be computed by the theory proposed by Schultze (1961), given in Chapter 2, Section 2.3. Within the transition points, that is, in the elastic zone the following relationship holds:

$$P_s(x) = \frac{P}{\pi a} \cdot \frac{1}{\sqrt{1 - (\frac{x}{a})^2}} \qquad 2.5$$

where $P_x(x)$ = normal stress distribution

a = half width of footing

P = axial load per unit length of footing

In the plastic zones, the following relationship

$$P_s(x) = \gamma N_q D + 4a\gamma N_\gamma (1 - x/a) \qquad 7.1$$

where γ = soil density

D = depth of footing

q = footing half width

x = distance from centre of footing

N_q and N_γ = bearing capacity factors.

Equation 2.6 from Chapter 2, which includes the cohesion component, has been modified into Equation 7.1 since the soil used for the tests was sand and has no cohesion.

The computations will be carried out for some selected load levels [3000 lbs (13.35 KN), 5000 lbs (22.25 KN) and 7500 lbs (33.375 KN)] in test four.

Test 4 has been chosen because of the simultaneous formation of slip surfaces on both sides of the footing half width. The load levels have also been selected because of their strategic positions on the load vs settlement curve, viz., the elastic, local shear failure and general shear failure zones.

Thus for a load level of 5000 lbs (22.25 KN) in test 4 in which the soil mass had a density of 90 lb/ft^3 (14.15 KN/m^3) and an angle of shearing resistance of 38° (corrected for the plane strain condition), the settlement of the footing was 1.211 inches (3.08 cm).

The distance of the transition point from the centre of the footing is given by Equation 2.13 and has been repeated here for convenience. Then, using a factor of safety of unity

$$P/2 = C_1 f_{c_1}(\xi_1) + C_2 f_{c_2}(\xi_1) \qquad 2.13$$

where $C_1 = a\gamma DNq$

$C_2 = 2a^2\gamma N\gamma$

According to Meyerhof (1963), the bearing capacity factors are Nq = 46, and Nγ = 70.

Thus, $C_1 = 6 \times \frac{90}{1728} \times 1.211 \times 46 = 17.41$ lb/in (30.5 N/cm)

$C_2 = 2 \times 36 \times \frac{90}{1728} \times 70 = 262.5$ lb/in (459.89 N/cm)

$P/2 = \frac{5000}{24x2} = 104.2$ lb/in (182.56 N/cm)

from Figure 2.10 and using a value of $\xi_1 = 0.75$, this gives $f_{C_1}(\xi_1) = 0.810$ and $f_{C_2}(\xi_1) = 0.342$.

Then substituting for C_1, C_2, $f_{C_1}(\xi_1)$ and $f_{C_2}(\xi_1)$ in Equation 2.13 we have

$P/2 = 17.41 \times 0.81 + 262.5 \times 0.742$

$= 103.88$

$\simeq 104.0$ lb/in (182.2 N/cm).

Both P/2 values are approximately equal, thus the distance of the transition point x_1, from the centre of the footing is given by the expression

$\xi_1 = x_1/a = 0.75$

$x_1 = 6 \times 0.75 = 4.5$ inches

$= 11.4$ cm

The load P_1 assumed to be carried by the footing is given by

$$P_1 = \pi \sqrt{1-\xi_1^2}\ C_1 + 2C_2(1-\xi_1)] \qquad 2.10$$

$$= \pi \sqrt{1-0.75^2}\ 17.41 + 2 \times 262.5(1-0.75)$$

$$= 308.9 \text{ lb/in.}$$

The normal stress distribution within the elastic zone under the above assumed load P_1 is given by

$$P_s(x) = \frac{P_1}{\pi a} \cdot \frac{1}{\sqrt{1-(x/a)^2}} \qquad 2.5$$

The result of the computed normal stress distribution within the elastic zone is given in Table 7.2.1.

The stress at any point within the plastic zone is given by the expression

$$P_s(x)_{4.5" \text{ to } 6"} = \gamma D N_q + 4a\, N_\gamma (1 - x/a) \qquad 7.1$$

Substituting

$$\gamma = 90 \text{ lb/ft}^3 \ (14.15 \text{ KN/m}^3)$$

$$N_q = 46$$

$$N_\gamma = 70$$

we will get

$$P_s(x) = 2.9 + 87.5(1 - x/b) \text{psi}$$

The normal stresses within the plastic zone is given in Table 7.2.2.

TABLE 7.2.1

Normal Stress Distribution within the Elastic Zone

Distance From the Centre of the Footing (x)		Normal Stress	
inches	cm	psi	kPa
0	0	16.39	113.09
1	2.54	16.62	114.68
2	5.08	17.38	119.92
3	7.62	18.92	130.55
4	10.16	21.99	151.73
4.5	11.43	24.80	165.60

TABLE 7.2.2

Normal Stress Distribution within the Plastic Zone

Distance from the Centre of the Footing (x)		Normal Stress	
inches	cm	psi	kPa
4.5	11.43	24.80	165.60
5.0	12.7	17.48	120.01
5.5	13.97	10.19	70.31
6.0	15.24	2.90	20.01

The values in Tables 7.2.1 and 7.2.2 and the results obtained from the test for this load level have been plotted and are shown in Figure 7.2.1.

The above analysis has been repeated for 3000 lbs (13.35 KN) and 7500 lb (33.375 KN) and their corresponding normal stress distributions are given in Figures 7.2.2 and 7.2.3, respectively.

The results obtained from the theory proposed by Schultze (1961) for the three load levels (Figures 7.2.1, 7.2.2 and 7.2.3) gave concave normal stress distributions between their respective transition points and then decreased to finite edge stresses, giving w-shaped curves. The test results gave convex normal stress distribution for the load levels in question. Thus, between the transition points the theoretical and experimental normal stress distribution gave opposite curves.

The percentage of loads calculated from the experimental curves to the loads determined from Schultze's (1961) theoretical curves for the load levels 3000 lbs (13.35 KN), 5000 lbs (22.25 KN) and 7500 lbs (33.375 KN) are 110.4%, 100.8% and 96%, respectively. The discrepancies seem not to be very significant owing to the probable redistribution of stresses along the length of the footing.

However, under the presently used design load and from the comparisons shown in Figures 7.2.1, 7.2.2 and 7.2.3, a uniform average stress should give a satisfactory design normal stress distribution for a surface footing subjected to the conditions existing in this test.

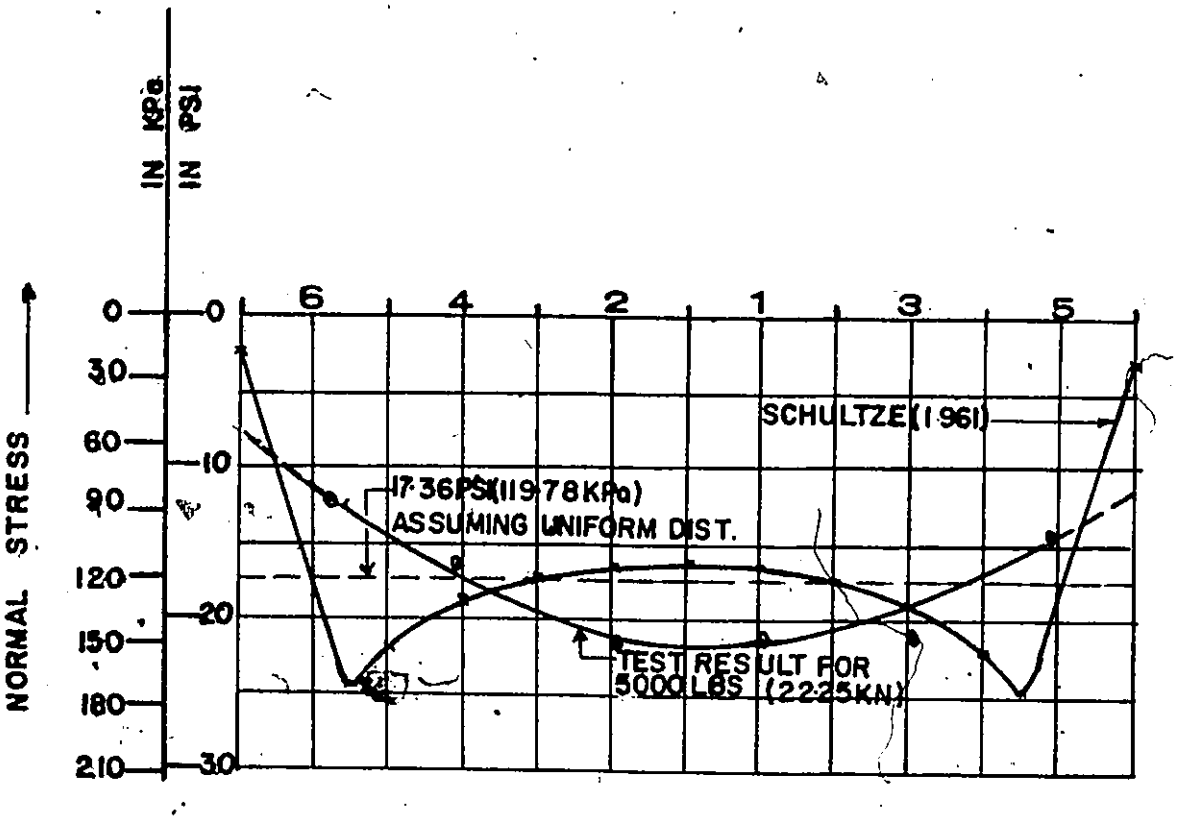

FIGURE 7.2.1 COMPUTED AND MEASURED NORMAL STRESS DISTRIBUTION UNDER THE FOOTING FOR AN APPLIED LOAD OF 5000LB [22.25KN]

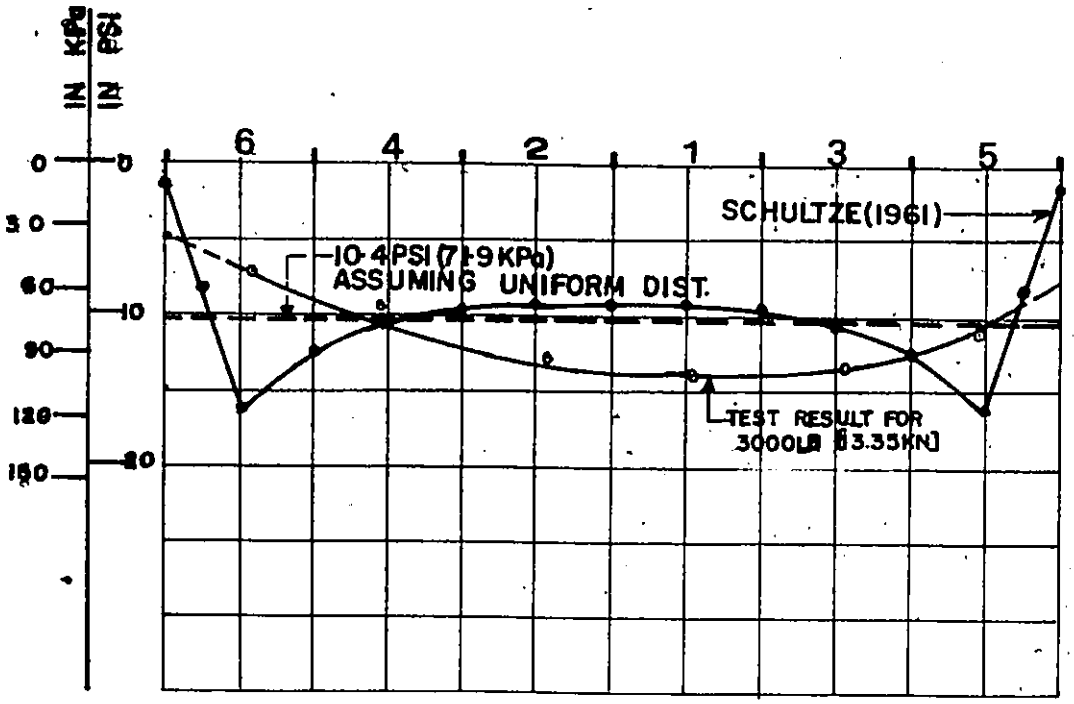

FIGURE 7.2.2 COMPUTED AND MEASURED NORMAL STRESS DISTRIBUTION UNDER THE FOOTING FOR AN APPLIED LOAD OF 3000LB [13.35KN]

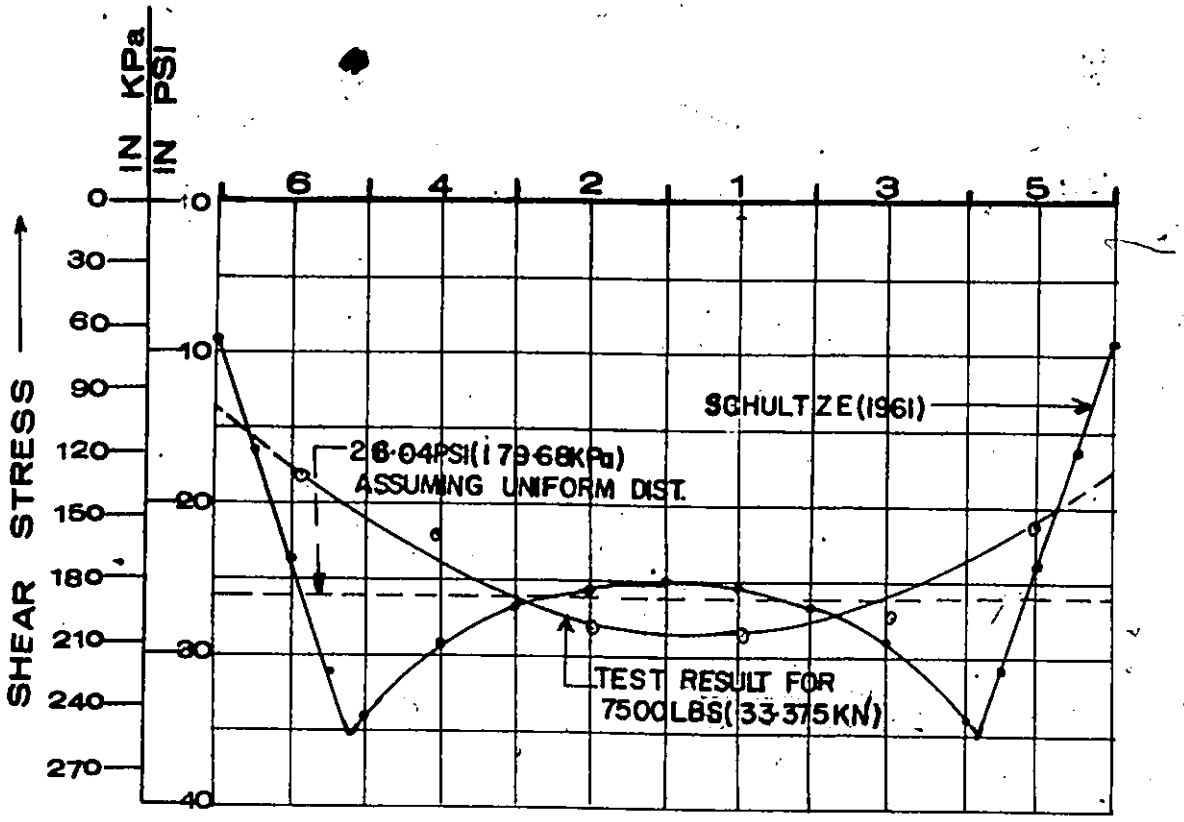

FIGURE 7.2.3 COMPUTED AND MEASURED NORMAL STESS DISTRIBUTION UNDER THE FOOTING FOR AN APPLIED LOAD OF 7500LB [33·375KN]

7.3 Shear Stress

The equation proposed by Schweickert (1964) will be utilized for the computation of the shear stress distribution under the footing for reasons discussed earlier.

The equation as stated in Chapter 2, Section 2.3 is as follows:

$$\tau_s(x) = \frac{5P}{2a}\,\frac{(1+\alpha)}{5+\alpha}\,\tan\delta\,(x/b)^{n-1} \qquad 2.35$$

where α - the ratio of the normal stress at the centre of the footing to the normal stress at the edge of the footing

P - load per unit length of the footing

a - footing half width

n - order of parabola

x - distance from the centre of the footing to the point where the shear stress is to be determined.

The computation will be performed for the following load levels, 3000 lbs (13.35 KN), 5000 lbs (22.25 KN) and 7500 lbs (33.38 KN) in test 4.

The above test has been chosen because of the simultaneous development of slip surfaces under both halves of the footings width. The load levels were also selected since they are representatives of the loads on the footing at the elastic, local shear failure and general shear failure zones of the load vs settlement curve (Figure 6.2.4).

From the results of test 4, (Table 7.4.1), the maximum friction angles, which occurred at the edges of the footing were between

one-third and two-thirds of the angle of shearing resistance of the sand.

Thus, for the computations in this section, a mobilized friction angle of one-third the angle of shearing resistance (38/3 = 12.67°) will be used. A value of four will be used for n, since this has been used extensively by Schweickert (1964).

Thus, for a load level of 3000 lbs (13.35 KN), P = 3000/24 = 125 lb/in = 218.996 N/cm, b = 6 ins (15.24 cm), α = 1.75, δ = 12.67° and n = 4.

$$\tau_s(x) = \frac{5 \times 125 \times 2.75}{12 \times 6.75} \tan 12.67 \left(\frac{x}{b}\right)^{4-1}$$

$$= 4.77 \left(\frac{x}{b}\right)^3 \text{ psi}$$

$$= 32.913 \left(\frac{x}{b}\right)^3 \text{ kPa}$$

The above expression was used in the computation of the shear stress distribution under the footing for various values of x (distance from the centre of the footing). The results are shown in Table 7.3.1. The results and the experimentally determined values are shown in Figure 7.3.1.

The above computations were repeated for 5000 lbs (22.25 KN) and 7500 lbs (33.375 KN). The calculated shear stresses and the experimentally determined values are shown in Figures 7.3.2 and 7.3.3.

The shear stress distribution derived from the theory proposed by Schweickert (1964) agrees closely with the experimentally determined distribution for the three load levels.

TABLE 7.3.1

Shear Stress Distribution under Footing Half Width

Distance From Centre of Footing		Shear Stress	
inches	cm	psi	kPa
1	2.54	0.022	0.152
3	7.62	0.596	4.112
5	12.7	2.76	19.044
6	15.24	4.77	32.913

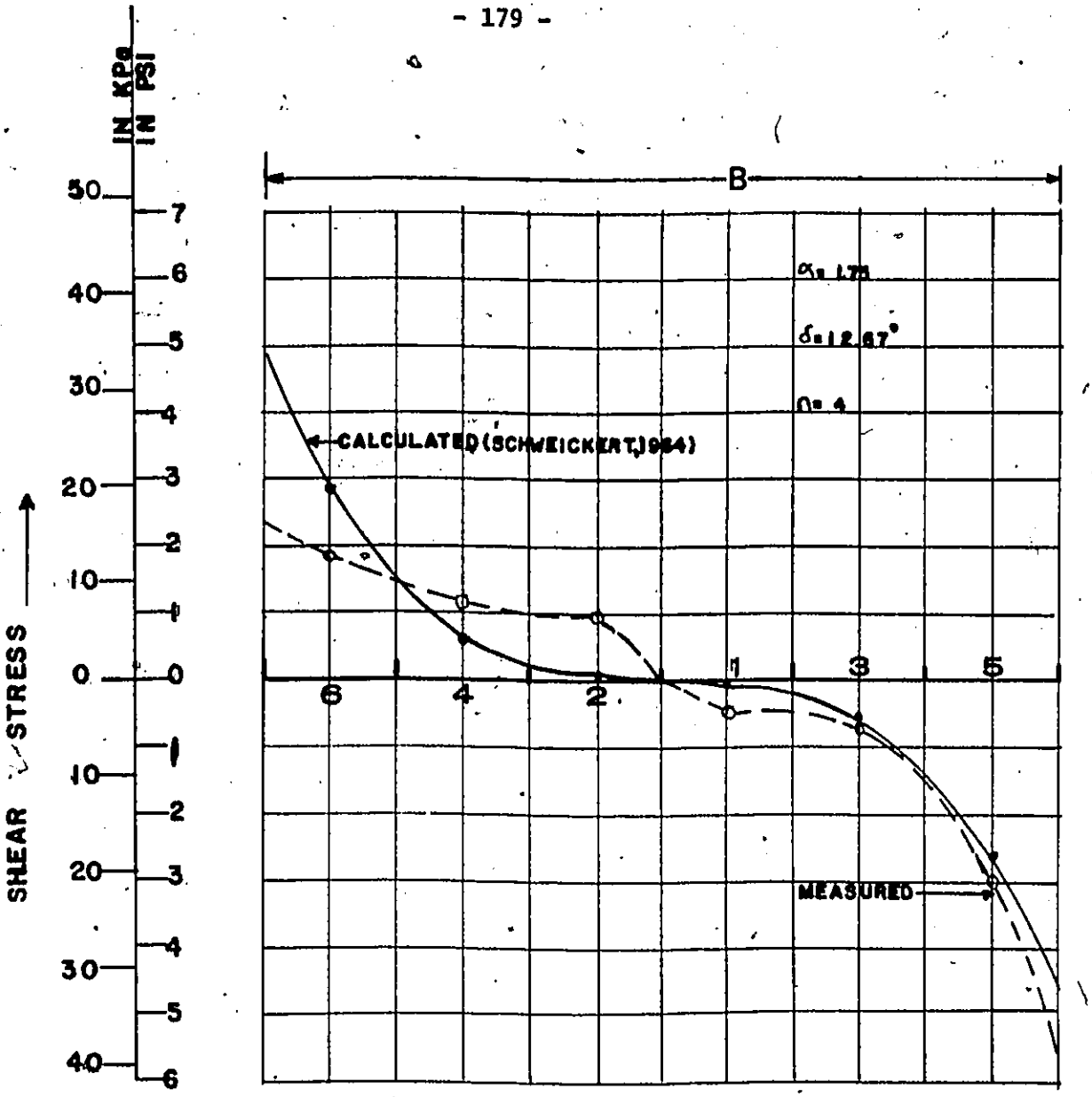

FIGURE 7·3·1 COMPUTED AND MEASURED SHEAR STRESS DISTRIBUTION UNDER THE FOOTING FOR AN APPLIED LOAD OF 3000 LBS [13.35 KN]

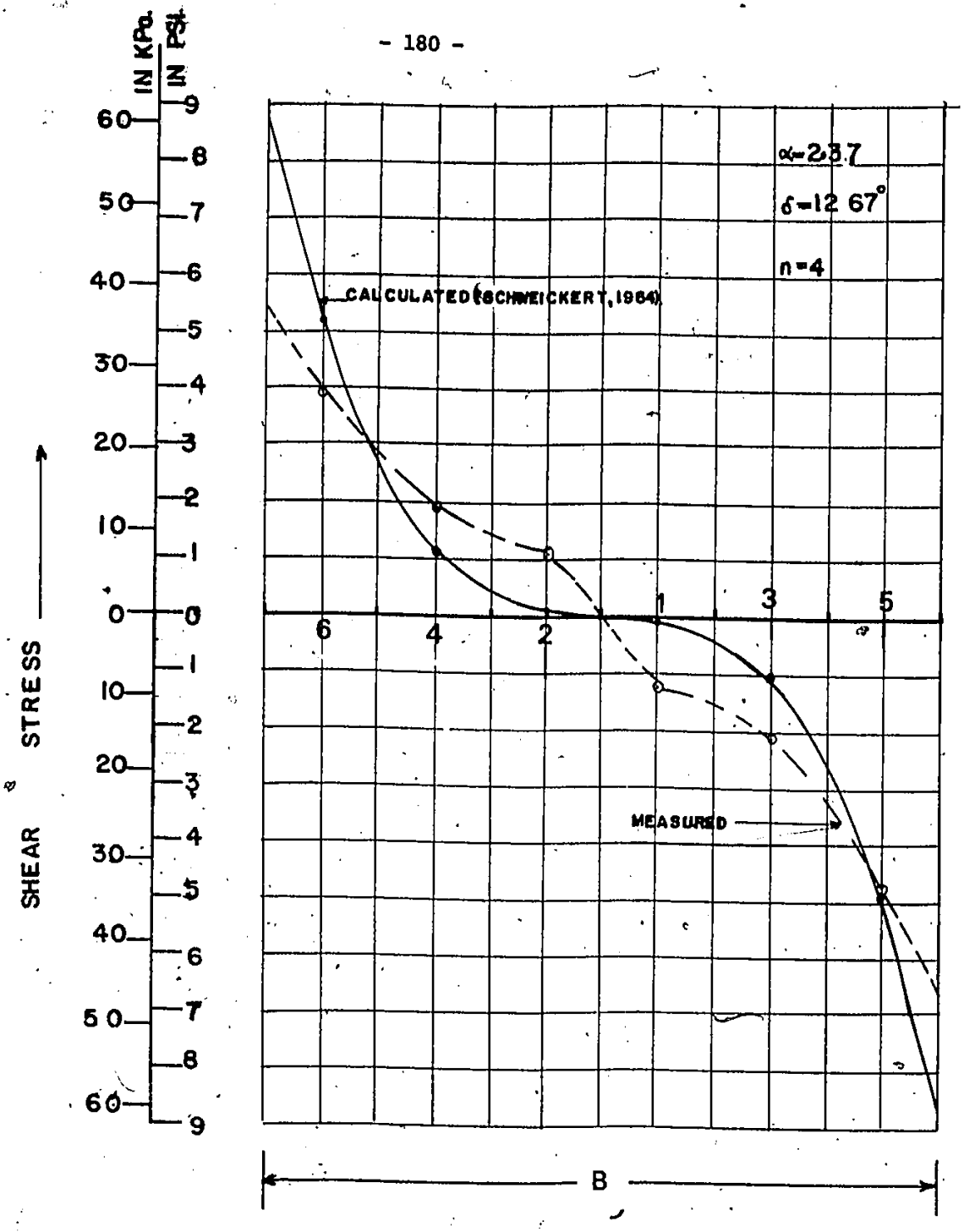

FIGURE 7·3·2 COMPUTED AND MEASURED SHEAR STR
DISTRIBUTION UNDER THE FOOTING
FOR AN APPLIED LOAD OF 5000LB
[22·25KN]

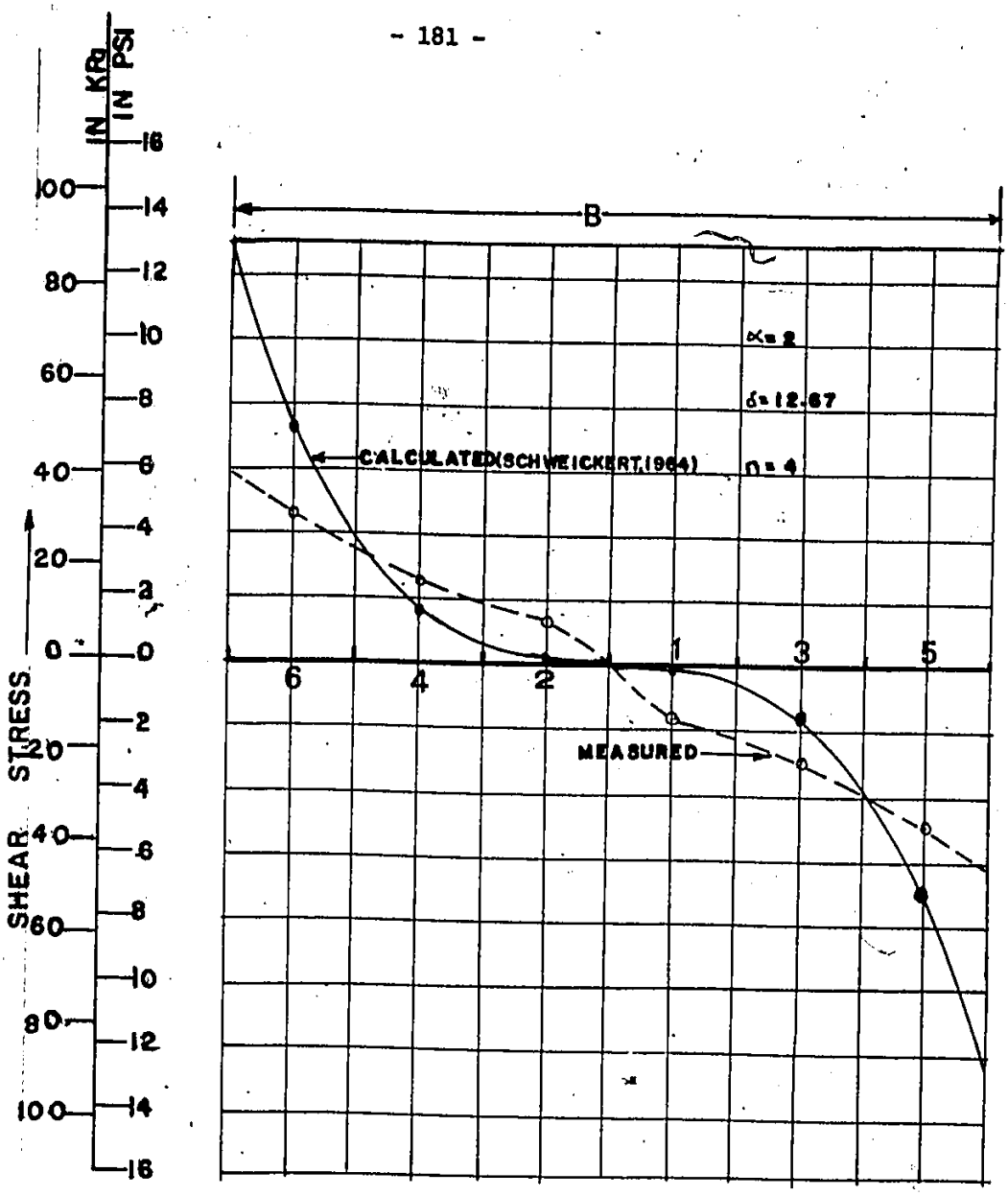

FIGURE 7·3·3 COMPUTED AND MEASURED SHEAR STRESS DISTRIBUTION UNDER THE FOOTING FOR AN APPLIED LOAD OF 7500LBS [33.375KN]

The shear stress distribution as given in Equation 2.38 depends on the following variables: α (the ratio of the normal stress at the centre of the footing to the normal stress at the edge of the footing) and n (order of the parabola), which cannot be easily determined. Thus some judgement has to be exercised in the choice of the values used for the said variables.

However, under the usually used design load a safe shear stress distribution should be obtained.

7.4 Relationship between Applied Load and the Contact Stresses

The results of test 4 in which the soil had an angle of shearing resistance of 38° (corrected from plane strain conditions as indicated by Meyerhof (1963)) and a density of 90 lb/ft^3 (14.5 KN/m^3) will be used for this analysis.

Figures 7.4.1 and 7.4.2 show the obtained relationship between the applied load and the normal stress developed under the rigid rough footing at the various modified Cambridge load cell locations. The normal stress at any particular load level is highest for the load cells nearest to the centre of the footing. Thus the normal stress decreases in magnitude from cells 1, 2 to cells 3,4 and then finally to cells 5,6. The figures also indicate an initially curved portion with the normal stress increasing with applied loads prior to the attainment of failure load of 5.4 kips (24.0 KN). After the failure load, a linear relationship prevailed between the normal stresses and the applied load. The initial curved portion can be attributed to the

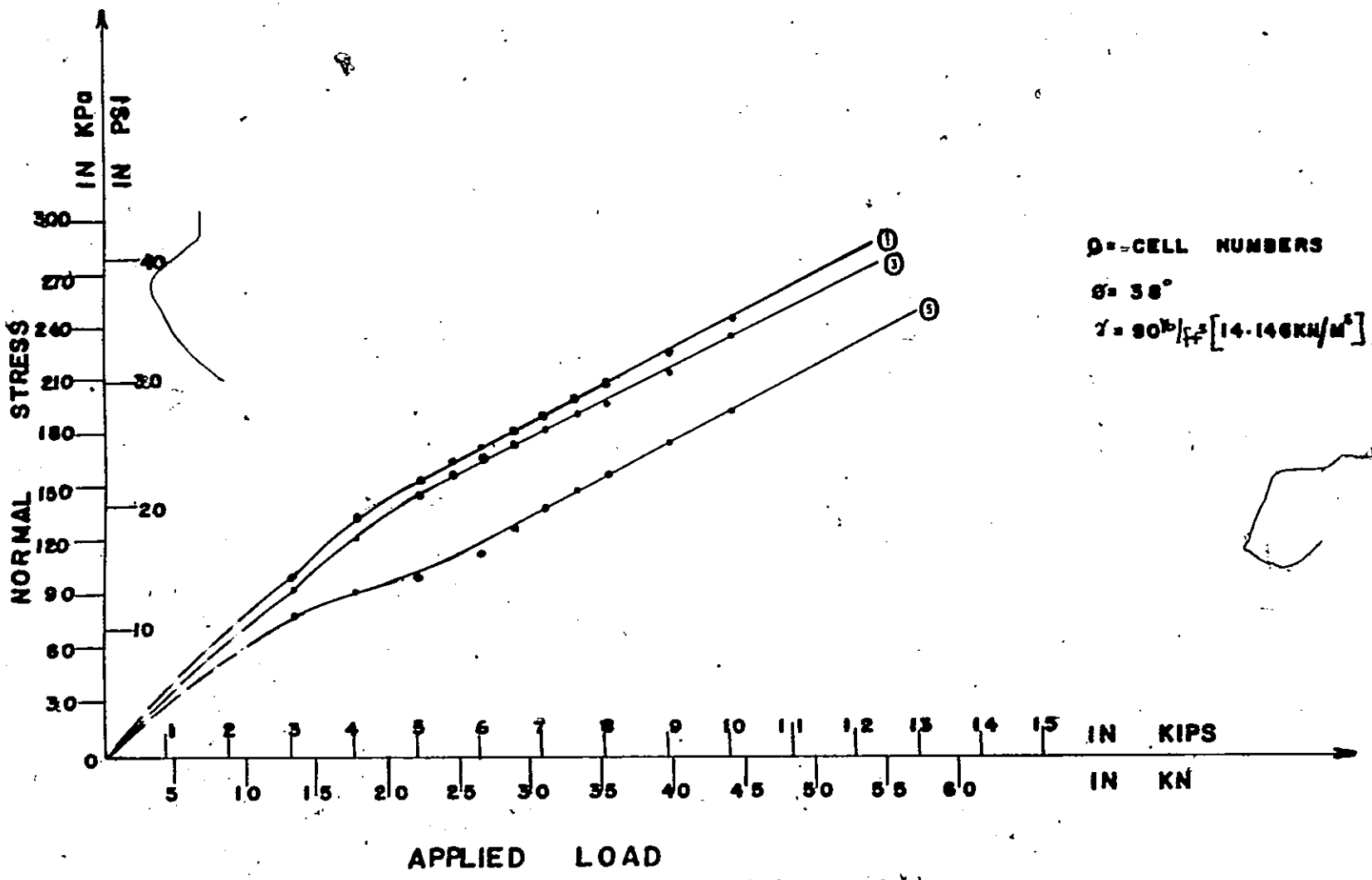

FIGURE 7·4:1 NORMAL STRESS VS APPLIED LOAD FOR TEST FOUR.

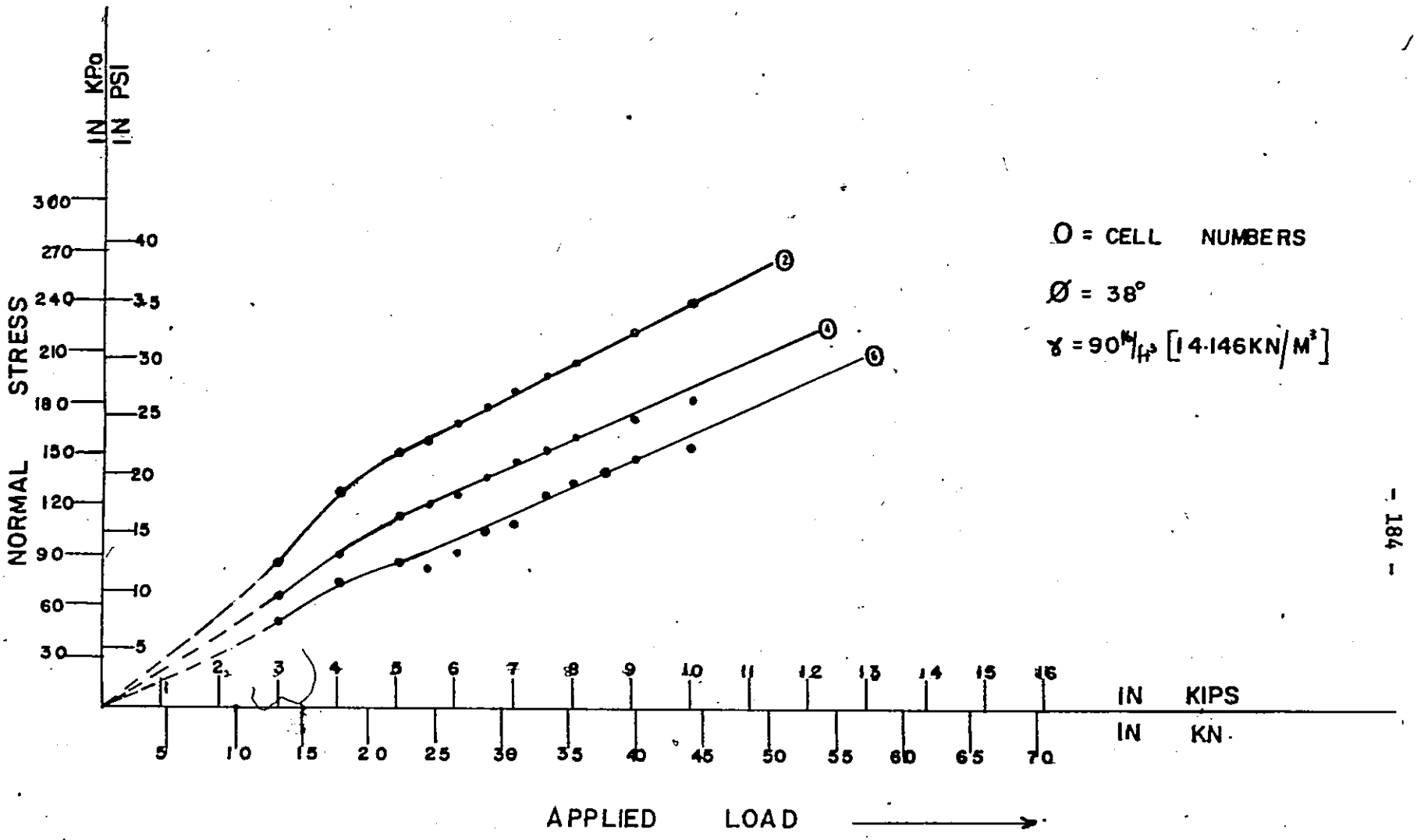

FIGURE 7-4-2 NORMAL STRESS VS APPLIED LOAD FOR TEST FOUR.

compression of the soil mass under the rigid rough footing into a denser state, thus reducing the air voids between the soil grains. This is then followed by a state in which equal increments in applied load produces equal increments in normal stress.

The relationship between the applied load and the shear stress developed under the rigid rough footing is given in Figure 7.4.3. It indicates an initially curved portion in which the shear stress increases with applied load at the different load cell locations. It also shows that the highest shear stresses were developed at the Cambridge load cell locations close to the edges of the footing. It is also important to note that the shear stress values seem to approach a limiting value at the load cell locations (load cells Nos. 1, 3 and 5).

Figures 7.4.4 and 7.4.5 gives the relationship between the normal stresses and the shear stresses developed under the footing. It indicates a non linear relationship between the shear stress and normal stress.

The different angles of friction mobilized under the rigid rough footing at the different load cell locations and for different applied loads are given in Table 7.4.1. These friction angles have been computed on the basis that

$$\delta = \mu N \qquad 2.39$$

where δ = shear force

μ = tangent of the friction angle

N = normal force at the location.

TABLE 7.4.1

Friction Angle Mobilized under the Footing for Test 4, $\phi = 38°$

Load Levels in lbs	Friction Angle Mobilized under the Modified Load Cells Location in Degrees					
Cells	1	2	3	4	5	6
3000	2.2	4.39	3.06	7.13	15.06	13.97
4000	3.14	4.35	5.56	7.01	12.64	15.6
5000	3.37	2.87	5.96	6.60	18.44	17.47
5500	2.01	3.85	5.82	7.12	22.2	17.62
6000	2.48	3.29	5.75	6.75	15.95	16.37
6500	3.42	2.50	5.97	6.49	13.01	15.08
7000	3.44	2.69	6.32	6.93	13.76	15.30
7500	3.46	2.69	6.27	6.61	13.03	13.64
8000	3.2	2.72	6.10	6.23	12.64	13.26
9000	2.99	3.14	5.72	6.21	11.06	12.53
10000	1.99	3.99	4.97	6.76	10.32	13.04

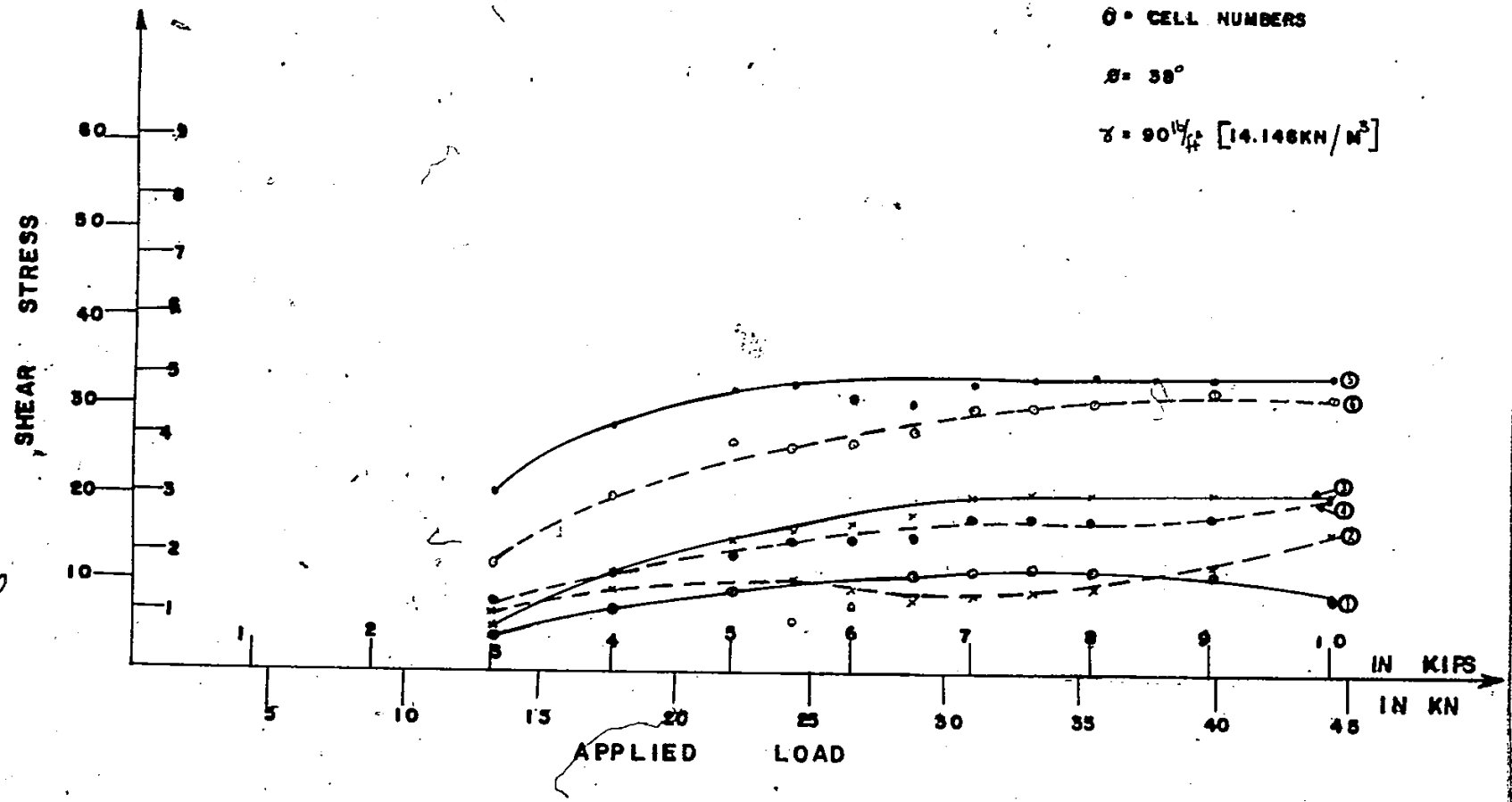

FIGURE 7-4 3 SHEAR STRESS VS APPLIED LOAD FOR TEST FOUR.

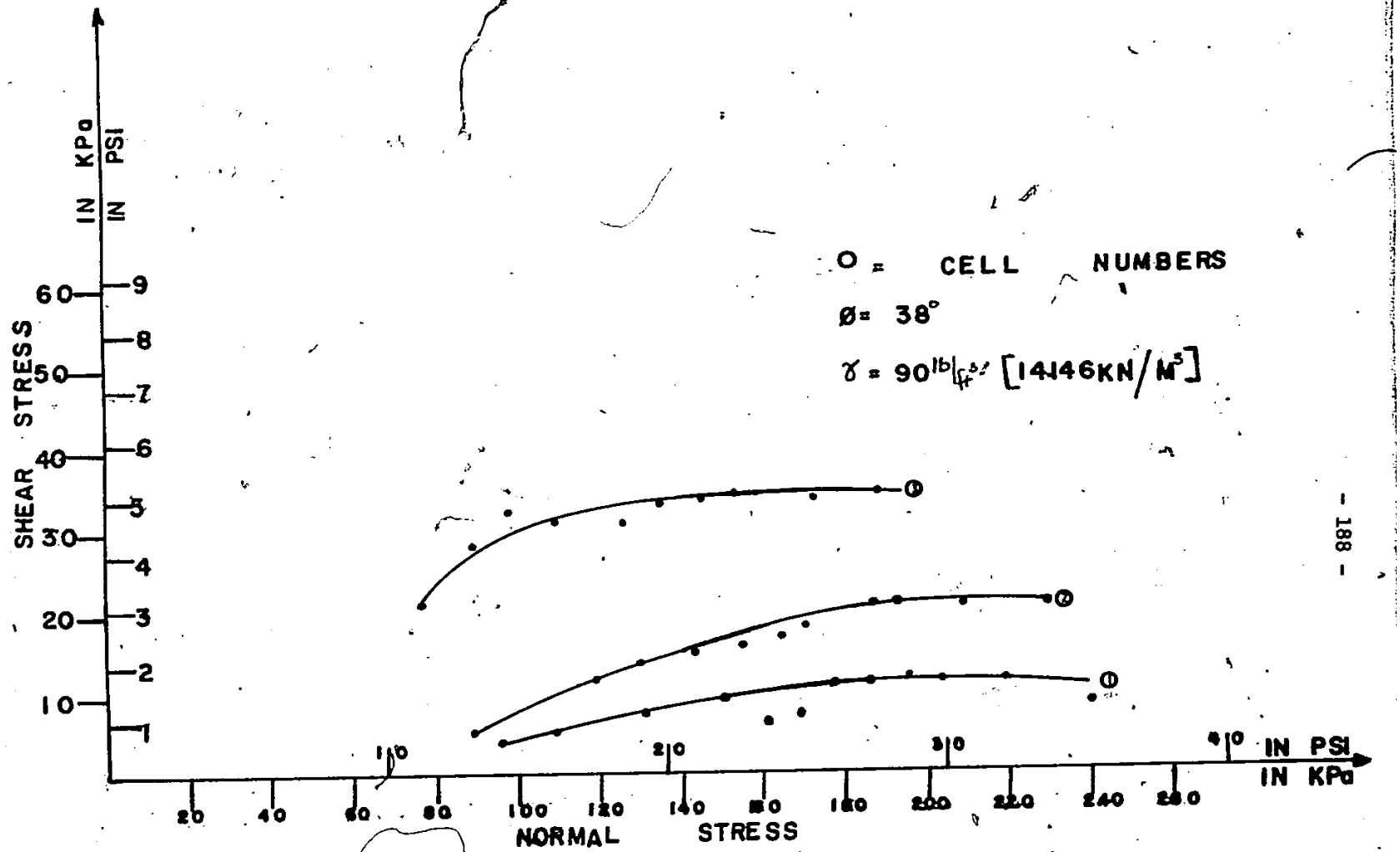

FIGURE 7·4·4 SHEAR STRESS VS NORMAL STRESS FOR TEST FOUR

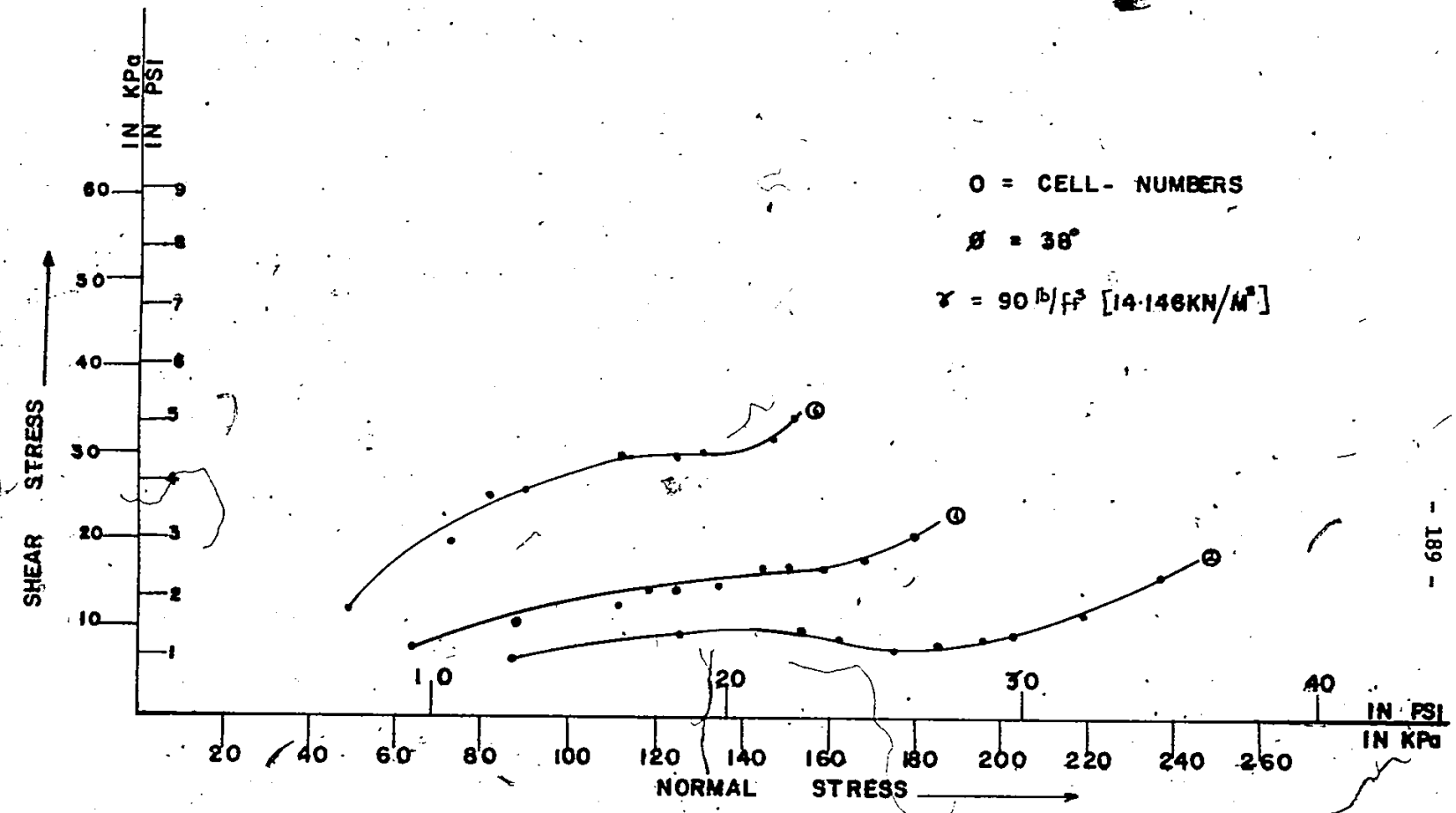

FIGURE 7·4·5 SHEAR STRESS VS NORMAL STRESS FOR TEST FOUR

one-third and two-thirds of the angle of shearing resistance of the sand.

Thus, for the computations in this section, a mobilized friction angle of one-third the angle of shearing resistance (38/3 = 12.67°) will be used. A value of four will be used for n, since this has been used extensively by Schweickert (1964).

Thus, for a load level of 3000 lbs (13.35 KN), P = 3000/24 = 125 lb/in = 218.996 N/cm, b = 6 ins (15.24 cm), α = 1.75, δ = 12.67° and n = 4.

$$\tau_s(x) = \frac{5 \times 125 \times 2.75}{12 \times 6.75} \tan 12.67 \left(\frac{x}{b}\right)^{4-1}$$

$$= 4.77 \left(\frac{x}{b}\right)^3 \text{ psi}$$

$$= 32.913 \left(\frac{x}{b}\right)^3 \text{ kPa}$$

The above expression was used in the computation of the shear stress distribution under the footing for various values of x (distance from the centre of the footing). The results are shown in Table 7.3.1. The results and the experimentally determined values are shown in Figure 7.3.1.

The above computations were repeated for 5000 lbs (22.25 KN) and 7500 lbs (33.375 KN). The calculated shear stresses and the experimentally determined values are shown in Figures 7.3.2 and 7.3.3.

The shear stress distribution derived from the theory proposed by Schweickert (1964) agrees closely with the experimentally determined distribution for the three load levels.

TABLE 7.3.1

Shear Stress Distribution under Footing Half Width

Distance From Centre of Footing		Shear Stress	
inches	cm	psi	kPa
1	2.54	0.022	0.152
3	7.62	0.596	4.112
5	12.7	2.76	19.044
6	15.24	4.77	32.913

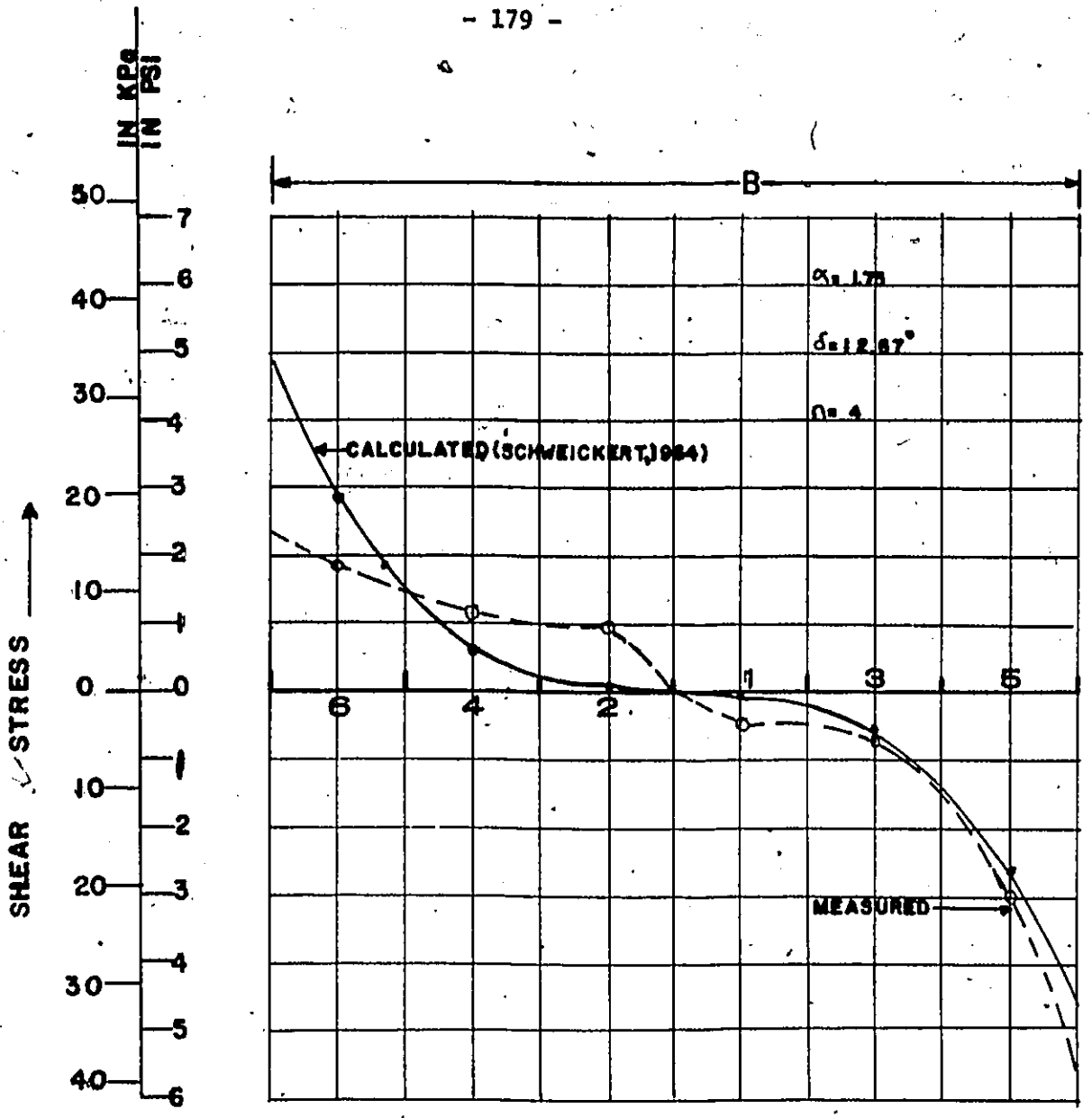

FIGURE 7·3·1 COMPUTED AND MEASURED SHEAR STRESS DISTRIBUTION UNDER THE FOOTING FOR AN APPLIED LOAD OF 3000 LBS [13.35KN]

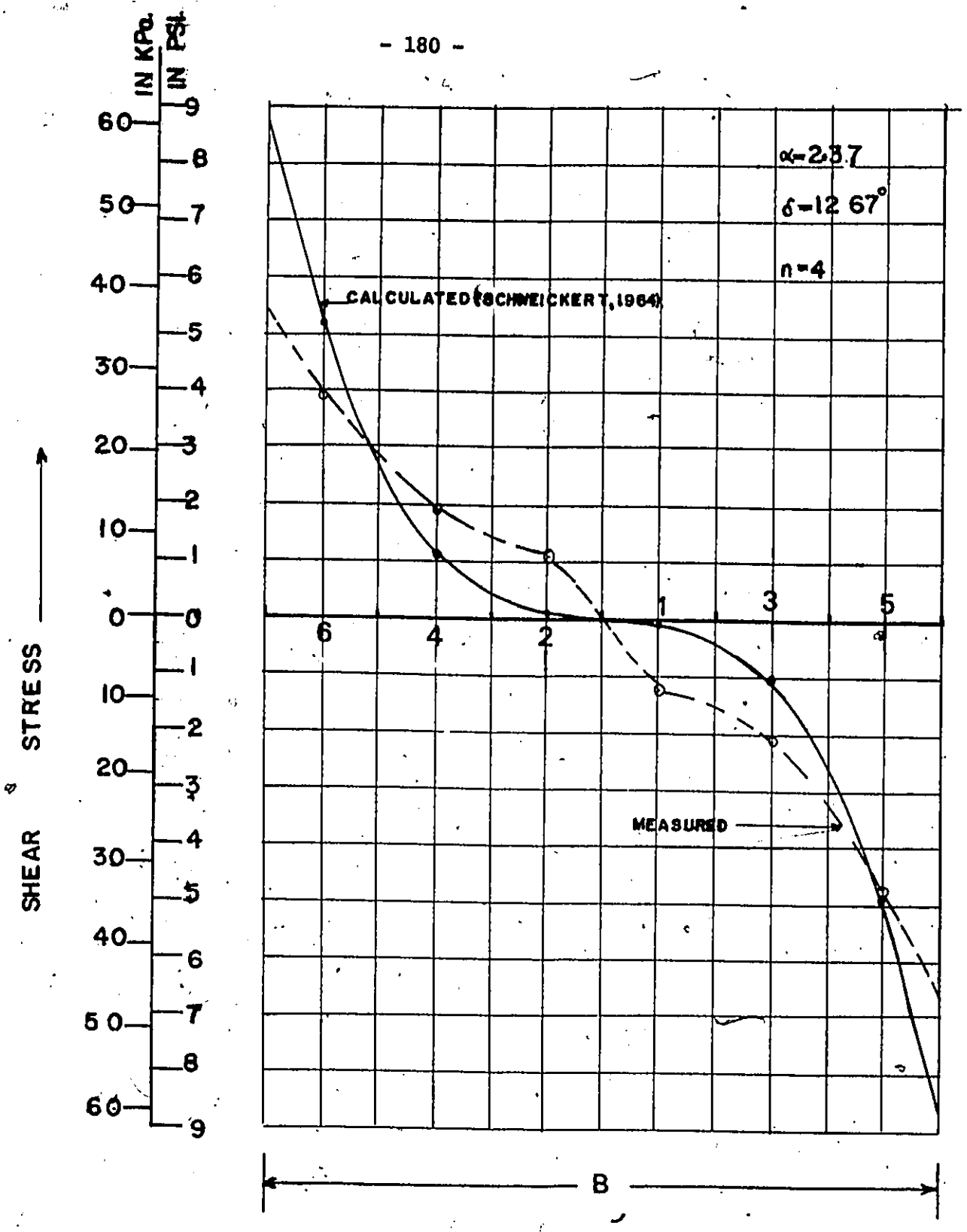

FIGURE 7·3·2 COMPUTED AND MEASURED SHEAR STRESS DISTRIBUTION UNDER THE FOOTING FOR AN APPLIED LOAD OF 5000LB [22·25KN]

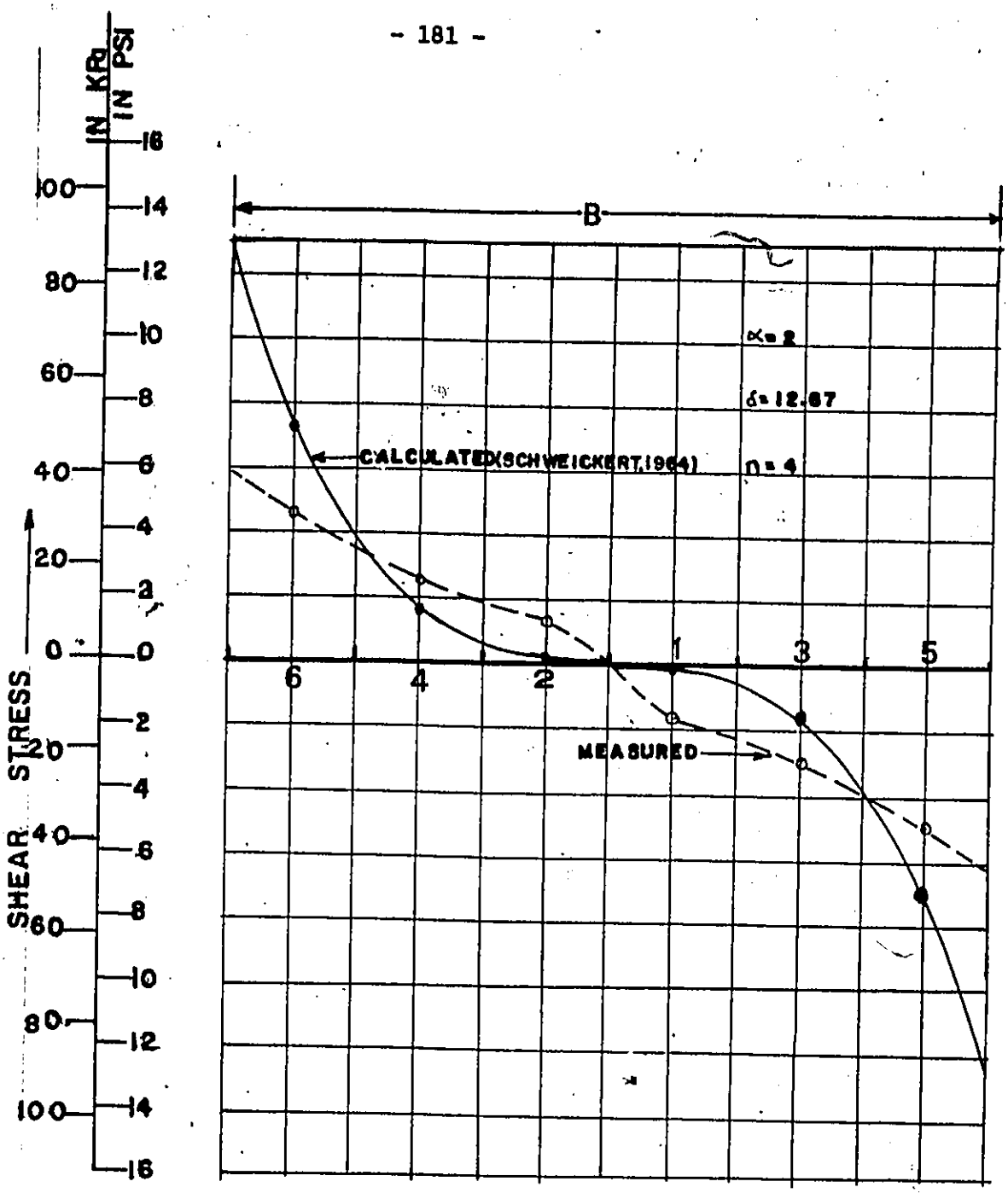

FIGURE 7·3·3 COMPUTED AND MEASURED -SHEAR STRESS DISTRIBUTION UNDER THE FOOTING FOR AN APPLIED LOAD OF 7500LBS [33.375KN]

The shear stress distribution as given in Equation 2.38 depends on the following variables: α (the ratio of the normal stress at the centre of the footing to the normal stress at the edge of the footing) and n (order of the parabola), which cannot be easily determined. Thus some judgement has to be exercised in the choice of the values used for the said variables.

However, under the usually used design load a safe shear stress distribution should be obtained.

7.4 Relationship between Applied Load and the Contact Stresses

The results of test 4 in which the soil had an angle of shearing resistance of 38° (corrected from plane strain conditions as indicated by Meyerhof (1963)) and a density of 90 lb/ft^3 (14.5 KN/m^3) will be used for this analysis.

Figures 7.4.1 and 7.4.2 show the obtained relationship between the applied load and the normal stress developed under the rigid rough footing at the various modified Cambridge load cell locations. The normal stress at any particular load level is highest for the load cells nearest to the centre of the footing. Thus the normal stress decreases in magnitude from cells 1, 2 to cells 3,4 and then finally to cells 5,6. The figures also indicate an initially curved portion with the normal stress increasing with applied loads prior to the attainment of failure load of 5.4 kips (24.0 KN). After the failure load, a linear relationship prevailed between the normal stresses and the applied load. The initial curved portion can be attributed to the

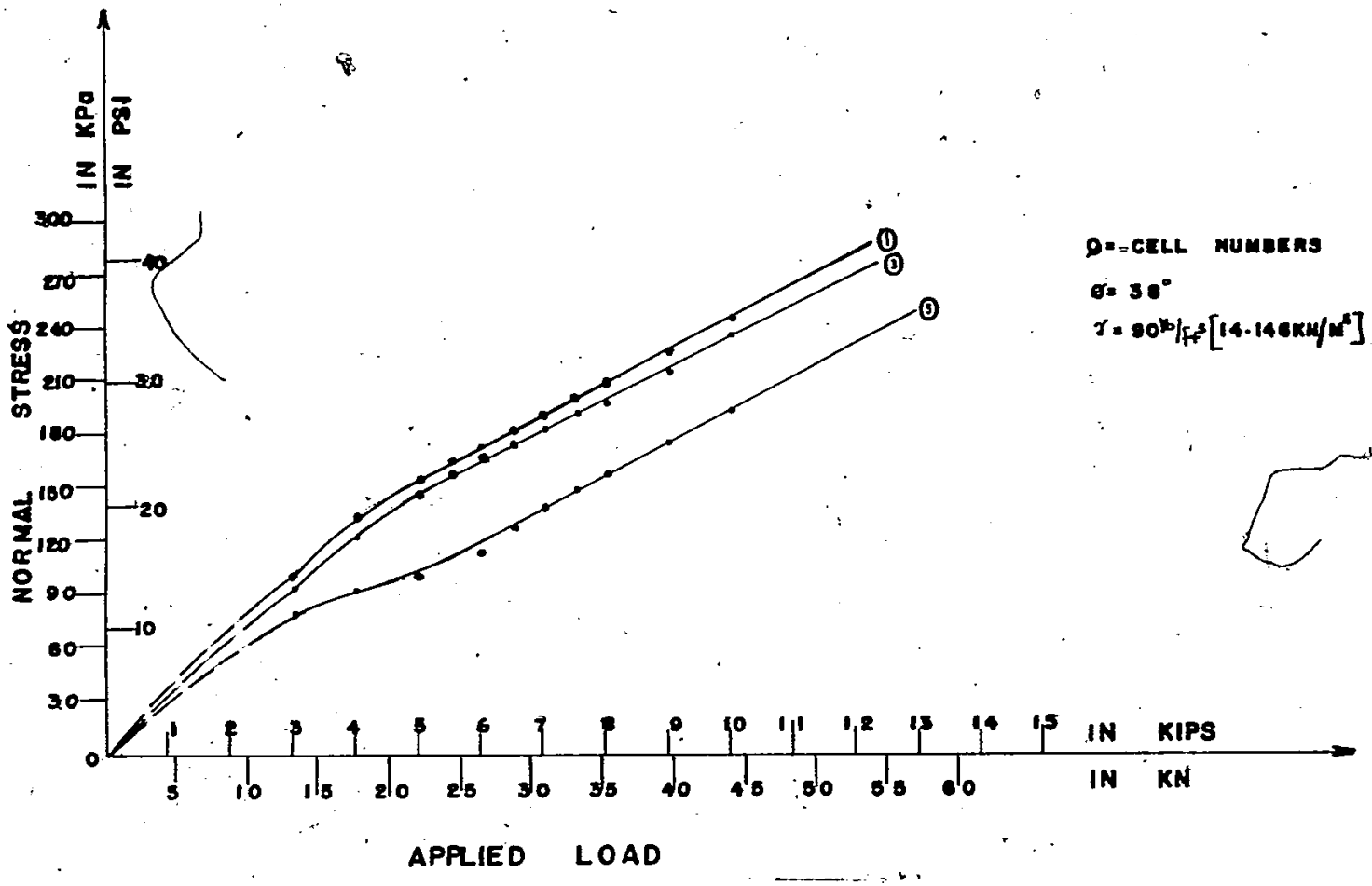

FIGURE 7·4:1 NORMAL STRESS VS APPLIED LOAD FOR TEST FOUR.

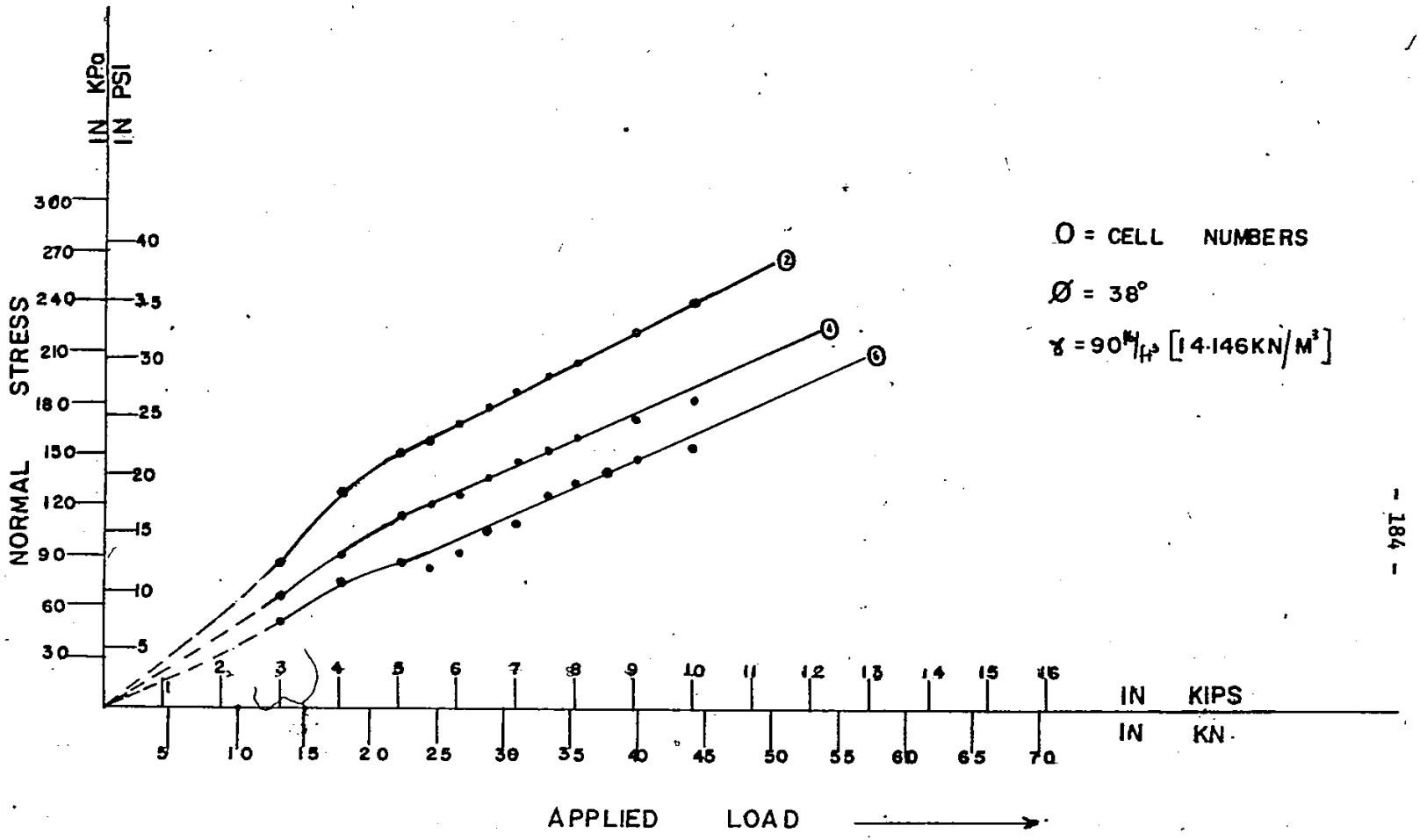

FIGURE 7-4-2 NORMAL STRESS VS APPLIED LOAD FOR TEST FOUR.

compression of the soil mass under the rigid rough footing into a denser state, thus reducing the air voids between the soil grains. This is then followed by a state in which equal increments in applied load produces equal increments in normal stress.

The relationship between the applied load and the shear stress developed under the rigid rough footing is given in Figure 7.4.3. It indicates an initially curved portion in which the shear stress increases with applied load at the different load cell locations. It also shows that the highest shear stresses were developed at the Cambridge load cell locations close to the edges of the footing. It is also important to note that the shear stress values seem to approach a limiting value at the load cell locations (load cells Nos. 1, 3 and 5).

Figures 7.4.4 and 7.4.5 gives the relationship between the normal stresses and the shear stresses developed under the footing. It indicates a non linear relationship between the shear stress and normal stress.

The different angles of friction mobilized under the rigid rough footing at the different load cell locations and for different applied loads are given in Table 7.4.1. These friction angles have been computed on the basis that

$$\delta = \mu N \qquad 2.39$$

where δ = shear force

μ = tangent of the friction angle

N = normal force at the location.

TABLE 7.4.1

Friction Angle Mobilized under the Footing for Test 4, $\phi = 38°$

Load Levels in lbs	Friction Angle Mobilized under the Modified Load Cells Location in Degrees					
Cells	1	2	3	4	5	6
3000	2.2	4.39	3.06	7.13	15.06	13.97
4000	3.14	4.35	5.56	7.01	12.64	15.6
5000	3.37	2.87	5.96	6.60	18.44	17.47
5500	2.01	3.85	5.82	7.12	22.2	17.62
6000	2.48	3.29	5.75	6.75	15.95	16.37
6500	3.42	2.50	5.97	6.49	13.01	15.08
7000	3.44	2.69	6.32	6.93	13.76	15.30
7500	3.46	2.69	6.27	6.61	13.03	13.64
8000	3.2	2.72	6.10	6.23	12.64	13.26
9000	2.99	3.14	5.72	6.21	11.06	12.53
10000	1.99	3.99	4.97	6.76	10.32	13.04

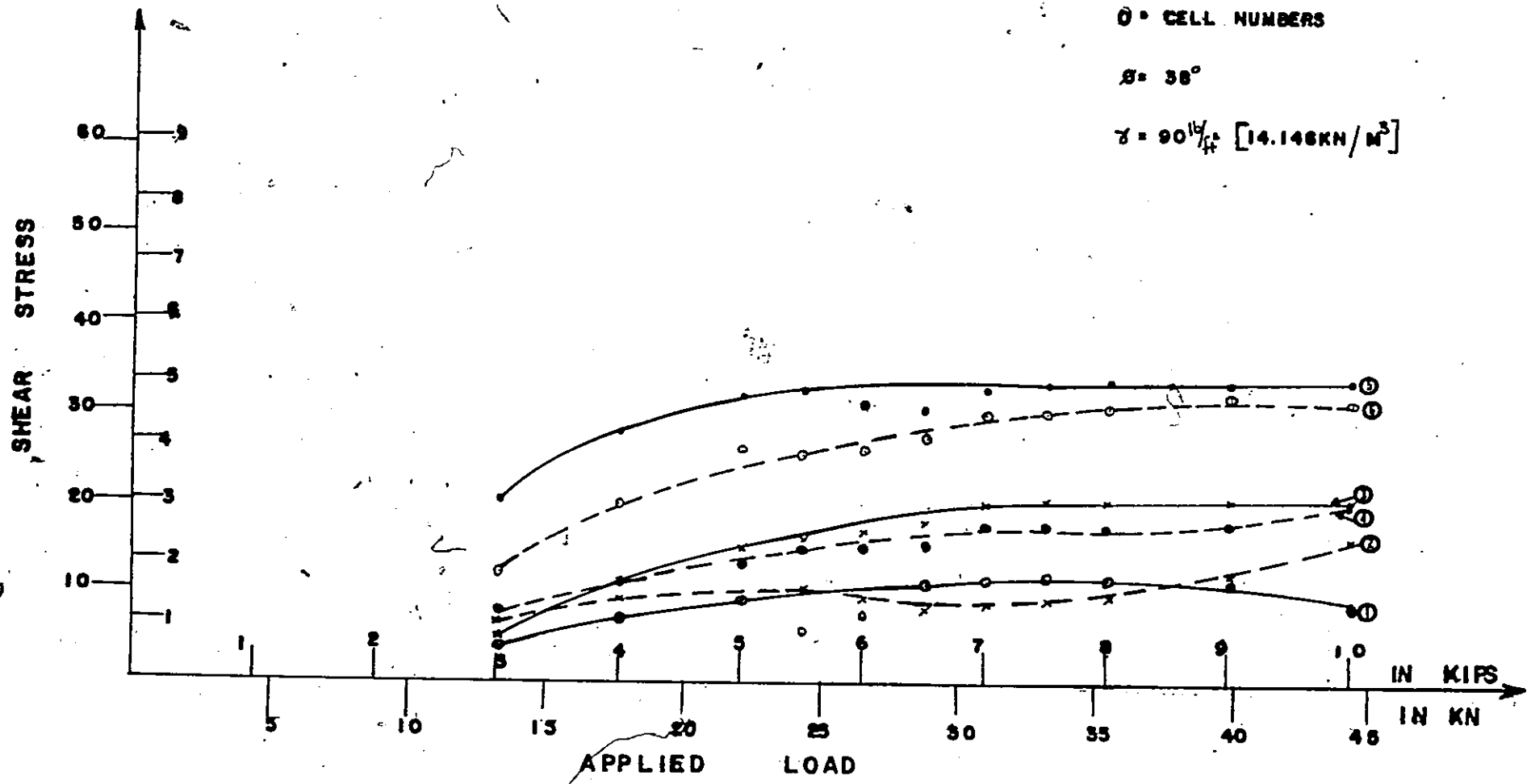

FIGURE 7-4 3 SHEAR STRESS VS APPLIED LOAD FOR TEST FOUR.

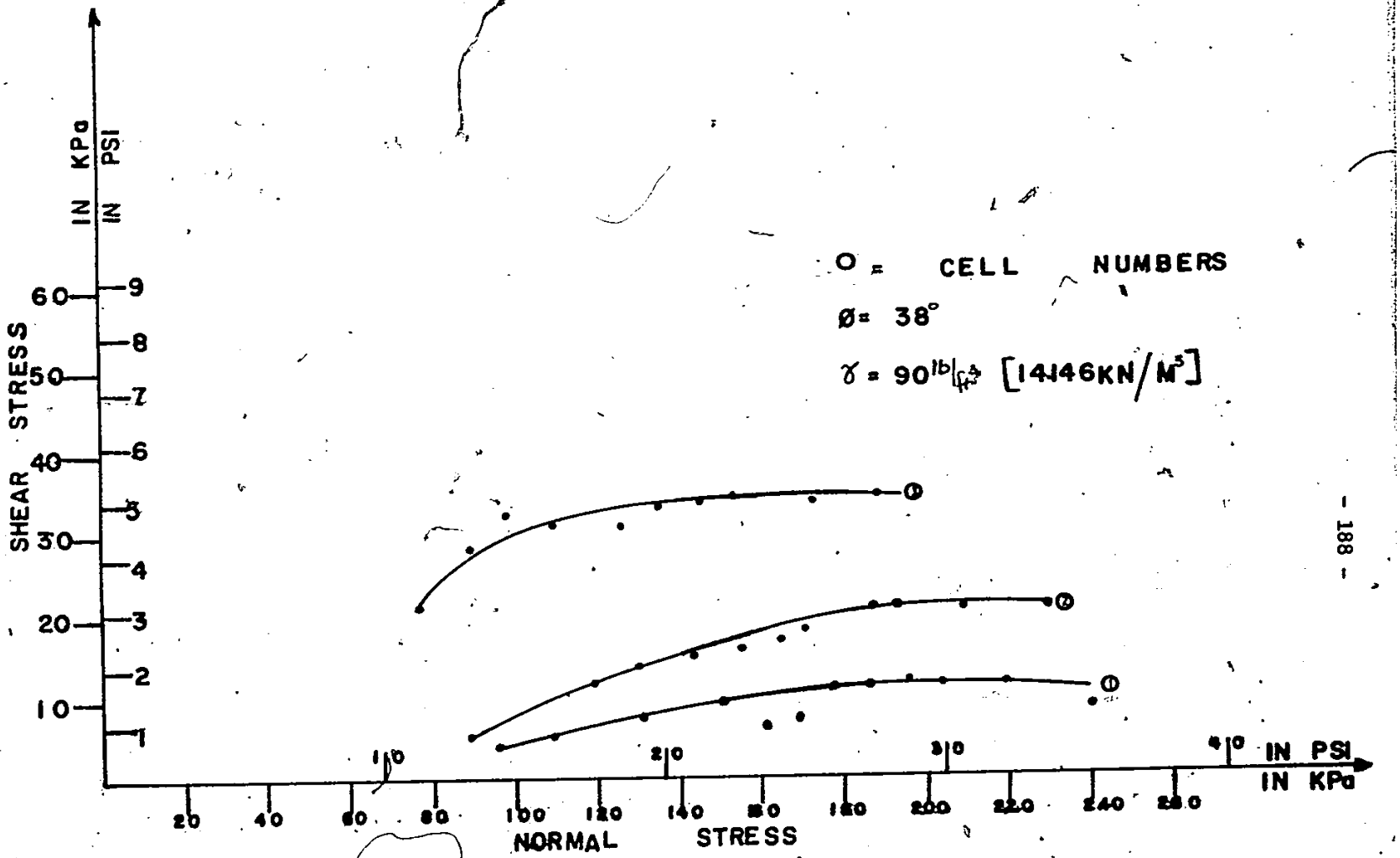

FIGURE 7·4·4 SHEAR STRESS VS NORMAL STRESS FOR TEST FOUR.

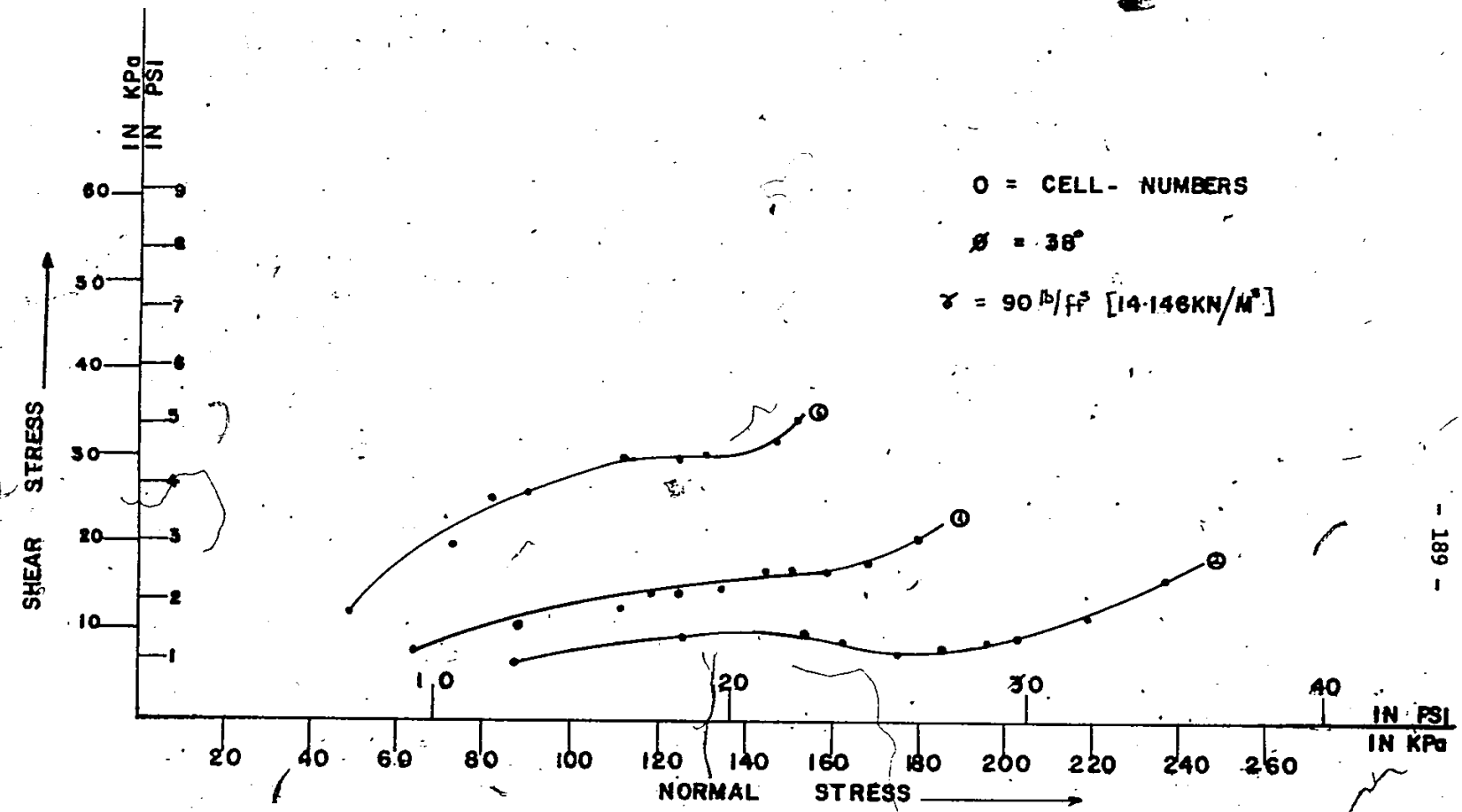

FIGURE 7-4-5 SHEAR STRESS VS NORMAL STRESS FOR TEST FOUR

From Table 7.4.1, it is obvious that the friction angle mobilized under the footing increases from a value of zero at the centre of the footing to maximum values, which varies between one-third (12.67°) to two-thirds (25.33°) of the angle of shearing resistance of the sand (38°) at the edges of the footing.

Also from Table 7.4.1 the maximum friction angles mobilized under the footing edges occurred at 5500 lbs (24.475 KN). This load level is approximately equal to the failure load of the soil mass. Thus, as far as this test is concerned, the maximum friction angles seem to be mobilized at approximately the failure load. It should be also noted that the friction angle mobilized under the footing edges increased with load levels until about the failure load after which it decreased. Beyond the failure load the mobilized friction angle decreases due to the fact that the rate of increase of the normal stress with applied load is greater than the rate of increase of shear stress with applied load.

The mean of the friction angles mobilized under the edges of the footing at 5500 lbs (24.475 KN), that is at Cell Nos. 5 (22.2°) and 6 (17.62°) is 19.91°. Fortunately, this ties in approximately with the results (Figure 3.2.3) obtained from the direct shear box test on aluminum plates coated with sand from the sandbox under a normal force of 113.25 lbs (503.96 N) in which the friction angles was 18.3°.

7.5 Factors Influencing Test Results

Test 1 was carried out with the footings hinged to the jacks. The footings could not be loaded to failure load of the soil before they tilted. However, a normal stress distribution in which the normal stresses were equal on either half of the width of the footing were obtained for load levels up to about 10,000 lbs (44.5 KN). The tilting of the footings must have led to the dissipation of the deformations necessary for the production of the desired shear stresses. However, some amount of shear stresses were monitored and have been plotted in Figure 6.4.1. There was also a discrepancy between the applied load and the corresponding value calculated from the curves describing the normal stress distribution. This has been attributed to the poor response of the hydraulic pressure gauges in the lower load range.

In Test 2, skewed convex shaped parabolae were obtained for the normal stress distribution. This has been attributed to the uneveness in the sand surface. This factor has been decided on, since the load calculated from the curve describing the normal stress distribution was found to be approximately equal to the applied load. This then offsets any other sources of errors such as eccentricity or the inclination of the jacks. It also provides satisfactory proof that the modified Cambridge cells are working properly.

The above factors were borne in mind during subsequent tests.

In test 2 and subsequent tests, loads were monitored by load transducers.

CHAPTER 8

SUMMARY AND CONCLUSIONS

8.1 Summary

The main purpose of this study was to calibrate the modified Cambridge load cells in their true operating condition, that is, with the load cells already installed in the footing. Calibrations have been undertaken for line loads and point loads at different eccentricities and for shear loads. Furthermore, the load cells had to be checked out if they would respond properly under actual loading conditions.

The modified Cambridge load cells have been hooked-up to the digital strain indicator. This has eventually reduced the time lag in reading or noting the values of the strains indicated by the bridge circuits in the six load cells employed. With this instrument the above said strains have been noted as print-outs from the printing unit attached to the digital strain indicator.

The effect of temperature on the load cells readings have been undertaken from the results obtained, the cells are affected under extreme temperature conditions and where temperature gradients also existed. Under normal working temperature conditions, the effects seemed insignificant since the temperature of the calibration room and testing room were identical. However, if the cells were used under adverse temperature conditions such as extreme cold or exposed to direct sunlight, a calibration for temperature effects should be undertaken.

Since density is one of the factors that affect the contact stress distribution, a spreading device has been used to rain the sand into the sandbox at the desired density.

After the spreading, the surface tests were performed. The normal and shear stress distribution under the rigid rough footing were determined. The tests were performed on simulated flat ground and at distances from the edge of the top of the 2:1 slope made in the quartz sand in the sandbox. The results obtained have been plotted on the transverse section of the footing.

The relationship existing between the applied load and contact stresses, the normal stress and shear stress, for a typical test have been presented graphically. The friction angle mobilized at the different load cell locations for this typical test has also been computed for various load levels.

Theoretical analysis using existing proposed mathematical relationships have been performed for the contact stresses distribution. The results have been compared with the experimentally determined values.

It has to be pointed out here that the analysis and comparison of results was intended to be only a minor part of this thesis.

8.2 Conclusion

The results obtained from this study and the preceding discussions will allow the following conclusions to be made.

1. The load cells were found to give reliable and reproducible results during the calibration process. Thus the load cells can be

said to have operated satisfactorily. However, tests under extreme temperature conditions will affect the cell readings to some extent. These effects were insignificant in this study, since the temperature of the calibration room and testing room were similar. The above subsequently leads to a confidence in the results obtained.

2. It has also been shown that the nature of loading did not affect the values of the modified Cambridge load cells calibration constants. This has been shown from the results obtained for the line loading (Appendix A) and point loading (Appendix B) tests. However, it is easier to perform the line loading tests since for the point loading, the hanger tends to rotate on the ball bearing.

3. The electronic digital readout and recording equipment has facilitated the reading of the strains indicated by the bridge circuits in the modified Cambridge load cells.

4. The shape of the normal stress distribution curves obtained for tests on the simulated flat ground (Tests 1, 2 and 4) were convex parabolae with the maximum ordinates at the centre of the footing. Edge stresses were also noted to exist in the three cases but of lower magnitude when compared to the stresses at the centre of the footing. The above has been attributed to the lateral flow of sand grains at the edges of the footing which culminated in a reduction of the normal edge stresses. The considerable confinement of the sand within the central region of the footing and the subsequent resistance to deformation has led to high central normal stresses. This can be deduced from the nature of shear distribution and angle of friction mobilized at the load cell locations.

5. The convexity of the normal stress distribution is increased by an increase in load, the angle of shearing resistance of the sand and hence the density of the sand.

6. The shape of the contact stress distribution is not affected significantly by the load level. This can be attributed to the fixation of the footings to the jacks which did not permit any tilting of the footings.

7. The eccentricity of the normal stress for each load cell increased from about zero for the cell located at the centre of the footing to maximum values at the edge load cells.

8. The distribution of the shear stress under the footing gave a series of concave parabolae for the case in which there was simultaneous development of failure surfaces (Test 4). The shear stress increases from a value of zero at the centre of the footing to maximum values at the edges of the footing. This fits with the displacement of the sand grains that takes place near the edges of the footing. Also, from the analysis performed for test 4, it can be said that the angle of friction mobilized under the footing increases from a zero value at the centre of the footing to a maximum value at the edges of the footing. Thus it could be inferred that the shearing strain under the footing is not constant but varies along the half width of the bottom of the footing.

9. The analysis performed indicates that the relationship between the applied load and the normal stress was initially curved and then becomes linear. In the case of the shear vs. applied load an initially curved relationship was obtained after which a limiting value seemed

to be approached at each load cell location.

10. The contact stress distribution under the footing at 2.5' (76.2 cm) from the edge of the top of the 2:1 slopes has been presented. Higher normal stresses were obtained at the load cells locations under the footing half width away from the slope.

The point of zero shear stress was also found to have been shifted away from the centre of the footing to locations under the footing half width close to the slope.

From the studies performed, it can be concluded that the present design assumptions of normal stress being equal to the design load divided by the surface area of the foundation yields conservative (safe) results for sand.

8.3 Suggestions for Further Research

It would be of great significance if a modified Cambridge load cell could be installed at the centre of the footing so as to obtain the true central contact stress.

Modified Cambridge load cells should also be installed along longitudinal sections of the footing. This would help to determine the distribution of contact stresses at the said sections and probably improve on the magnitude of the calculated loads from the stress distribution curves.

Some modifications should also be made to the pumping configuration such that a constant rate of penetration of the footings is achieved. This could be accomplished by the use of flow regulators.

Further studies should also be engaged to investigate, experimentally, the relationship between the applied load, contact stresses and distances along the footing width. The magnitude of the effect of density changes and depth of the footing should also be undertaken. This would help in elucidating the nature and shape of the contact stress distribution before any mathematical relationship can be safely proposed.

REFERENCES

Arthur, J.R.F. and Roscoe, K.H. 1961. An Earth Pressure Cell for the Measurement of Normal and Shear Stresses. Civil Engineering and Public Works Review, Vol. 56, No. 659, pp.765-770.

Borodacher, N.M. and Tarkov, G.P. 1972. Determination of the Reaction Pressure under a Foundation by Electrical Modelling Method. Osnosariya Fundamenty i Mekhanika Gruntov, No. 6, pp.33-34.

Bozozuk, M. 1972. The Gloucester Test Fill, Ph.D. Thesis, Perdue University, Department of Civil Engineering, Lafayette, Indiana, pp.49-60.

Bub, H. 1963. Flachgegrundete Streifenfundamente. Berlin. Berichte ans der Bauforschung, Heft 30.

Burger, R. 1932. Der Bau der neuer Rheinbrucke bei Ludwigshafen-Mannheim. Bautechnik 10, Vol. 45, pp.597-599.

Doohan, J.P. 1975. Earth Pressure Cells to Measure the Distribution of Shear and Normal Stresses on a Footing. M.A.Sc. Thesis, Department of Civil Engineering, University of Ottawa, Ottawa, Canada.

Faber, O. 1933. Pressure Distribution under Bases and Stability of Foundations. The Journal of the Institution of Structural Engineers, pp.116-125.

Gorbunov-Posadov, M.I. 1962. Stability of Foundations on a Sandbed. Gosstroiizdat.

Hanna, T.H. 1975. Foundation Instrumentation. Trans Teck Publications.

Hartikainen, J. 1972. The Distribution and Direction of Contact Pressure under a Rigid Foundation. Acta Polytechnica Scandinavica Civil Engineering and Building Construction. Series No. 74.

Hasnain, M. 1974. Shear Strength Characteristics of Crushed Quartz Sand. M.A.Sc. Thesis, Department of Civil Engineering, University of Ottawa, Ottawa, Canada.

Helenchund, K.V. 1966. Kitkaraalajien Kantasuusomina-arsuuksista. Helsinki. The State Institute for Technical Research Report, Series III, Building 97, pp.43-50.

Kogler, F. and Scheidig, A. 1972. Druckverteilung im Baugrund. Bautechnik 5, Vol. 29, pp.418-421 and 445-447.

Koichi, Akai and Hideo Otsuki. 1974. Model Studies on the Stress Distribution and the Bearing Capacity of Soil Ground. Proceedings, Japanese Society of Civil Engineers, No. 223, pp.99-107.

Krivorotov, A.P. 1963. Experimental Determination of Normal Load Distribution using a Plate on a Sandy Foundation. Osnovaniya, Fundamenty I Mekhanika Gruntov. Vol. 2, pp.8-12.

Leussink, K.H., Blinde, A., and Abedlmade, P.A. 1966. Versuche uber die Sohldruckvertechung unter Starsen Grundungskorpern auf Kohasionslosem Sand. Karlsruhe. Veroffentlichungen des Institues fur Bodenmechanik and Felsmechanik der Technischen Hochschule Fridericiana in Karlsruhe, Heft 22.

Meyerhof, A.A. 1963. Some Recent Research on the Bearing Capacity of Foundations, Canadian Geotechnical Journal, Vol. 1, No. 1.

Muhs, H. and Bub, H. 1965. On the Measurement of the Friction in the Base of Flat Footings Founded in Sand and First Test Results Gained by a New Gauge Developed for the Combined Measurement of Normal and Tangential Stresses. Diskussionsbertrag, 6th International Conference of Soil Mechanics and Foundation Engineering, Montreal.

Muhs, H. and Elmiger, R. 1969. Sohlspannung und Sohreibung in Sand unter Flachgegrundeten Einzelfundamenten Miheilung der Deutschen Forschungsgesellschaft fur Bodenmechanik (Degebo) an der Technischen Universitat, Berlin, Heft 24, pp.15-68.

Muller Hande, H.L. 1967. Ergebois der Sohldinck-Messurgen and dem Grossprogrammdes Berliner U-Bahnbanes. Bautechnik 44, Vol. 8.

Ohde, J. 1942. Berechung der Sohldruckverteilung unter Grundungskorpern. Bauingenieum 23, Vol. 14.

Salvaduri, A.P.S. 1975. The Response of a Rigid Plate Resting on an Idealized Elastic-Plastic Foundation Paper, Civil Engineering Department, Carleton University, Ottawa, Canada.

Schultze, E. 1961. Distribution of Stress Beneath a Rigid Foundation. Proceedings of the 5th International Conference of Soil Mechanics and Foundation Engineering. Paris, Vol. I, pp.807-813.

Schmertmann, J.H. 1970. Static Cone to Compute Static Settlement over Sand. Journal of the Soil Mechanics and Foundations Division. Proceedings A.S.C.E.

Schwickert, K. 1964. Uber den Einfluss von Reibungskraften in der Sohlfuge eines Starren Streifenfundamentes auf die Sohldruckverteilung. Karlsruhe (1964). Veroffentlichungen des Institutes fur Bodenmechanik und Grundban der Technischen Hochschule Fridericiana in Karlsruhe, Heft. 14.

Sedyich, E.K. 1964. On the Diagram of Reaction Pressures under the Base of a Rigid Foundation. Osnovaniya, Fundamenty i Mekhanika Gruntov, Vol. I, No. 3, pp. 8-11.

Siedek, P. 1948. Belastugsversuche in einem Senkkaster. Verlag Schmidt, Bielefeld.

Siemonsen, F. 1942. Die Lastanfrahmekrafte in Baugrund und die Dadurch Hersorgerufenen Spannungen.

APPENDIX A

CALIBRATION GRAPHS (LINE LOADS)

This section consists of the calibration graphs for the six modified Cambridge load cells under line loads. They were obtained as a result of the following operations:

1. A plot of the output strains from the positive normal bridge circuit, negative normal bridge circuit and shear bridge circuit at different eccentricities against the normal line loads.

2. A plot of the output strains from the aforementioned bridge circuits against the shear loads.

3. A plot of the slopes of the lines derived in (1) against the eccentricities of the normal line loads. The point of zero eccentricity was taken at theccentre of the load cells active faces.

The graphs have been arranged according to the following modified Cambridge load cellsnumbers: 1, 2, 3, 4, 5 and 6.

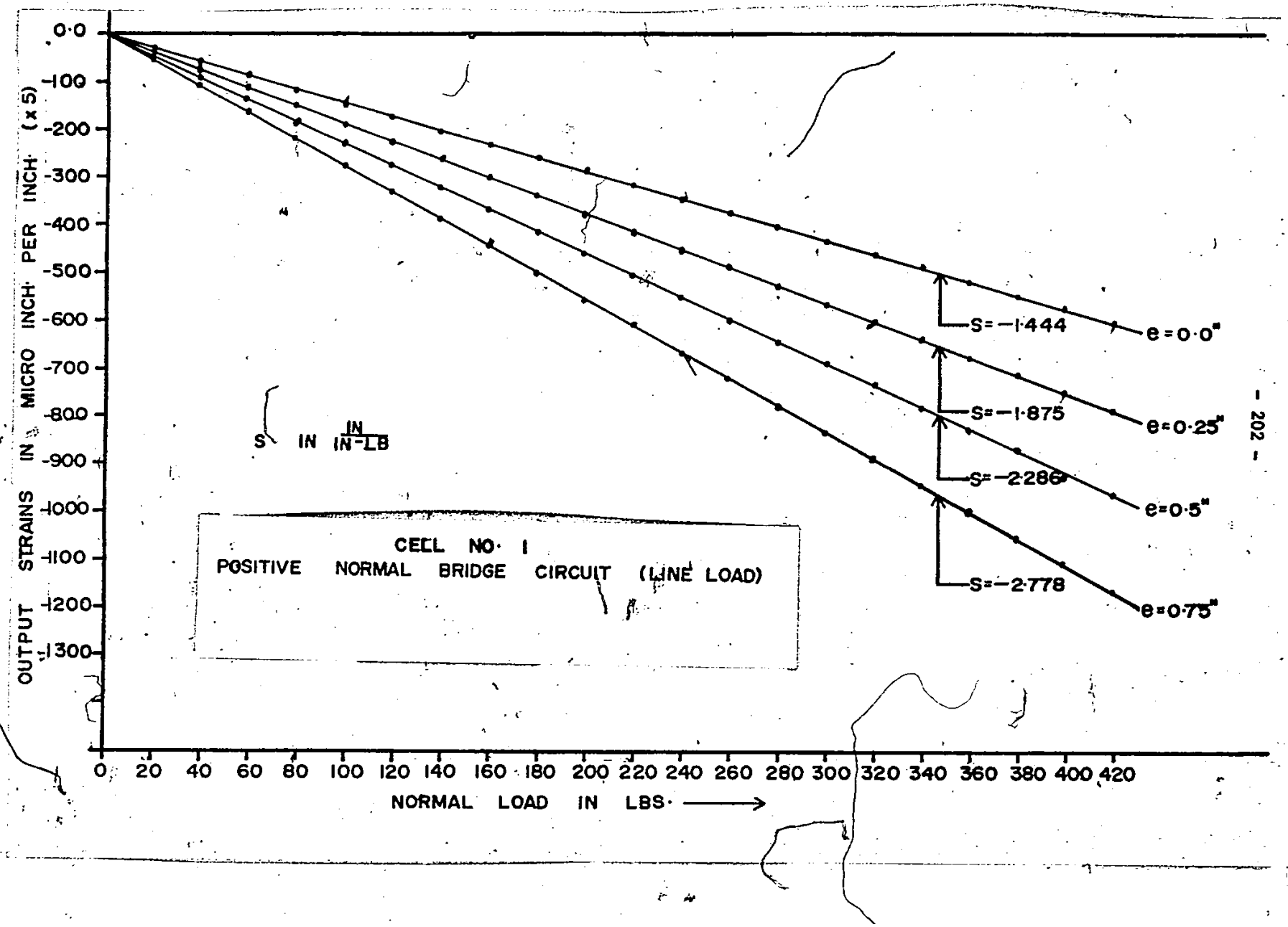
OUTPUT STRAINS IN MICRO INCH PER INCH (x 5)
0·0
-100
-200
-300
-400
-500
-600
-700
-800
-900
-1000
-1100
-1200
-1300
S IN IN/IN-LB
S=-1·444
S=-1·875
S=-2·286
S=-2·778
e=0·0"
e=0·25"
e=0·5"
e=0·75"
CELL NO· 1
POSITIVE NORMAL BRIDGE CIRCUIT (LINE LOAD)
0 20 40 60 80 100 120 140 160 180 200 220 240 260 280 300 320 340 360 380 400 420
NORMAL LOAD IN LBS·

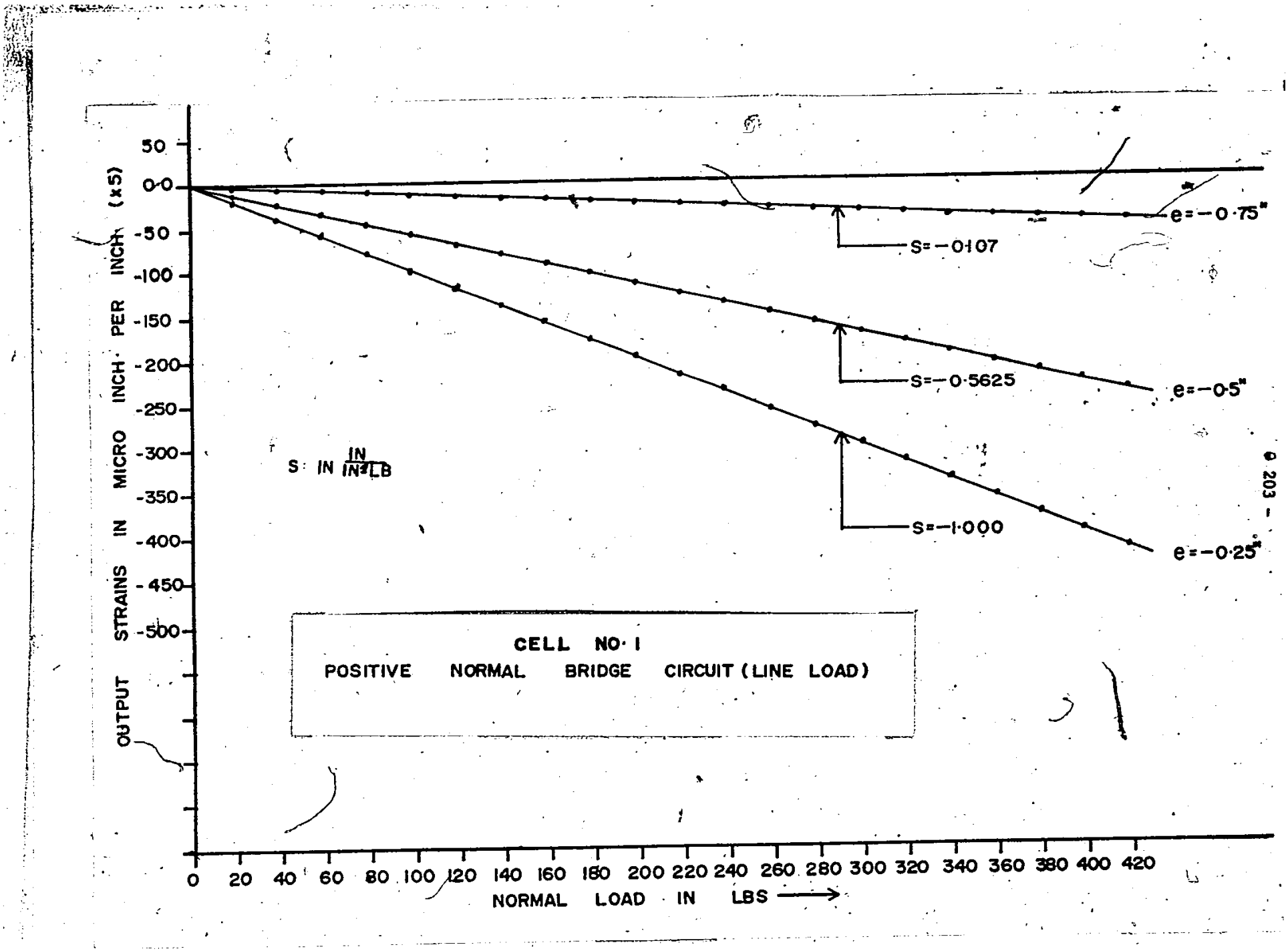
OUTPUT STRAINS IN MICRO INCH PER INCH (x5)
50
0·0
-50
-100
-150
-200
-250
-300
-350
-400
-450
-500
S: IN $\frac{IN}{IN^2 LB}$
e=−0·75"
S=−0107
S=−0·5625
e=−0·5"
S=−1·000
e=−0·25"
CELL NO· 1
POSITIVE NORMAL BRIDGE CIRCUIT (LINE LOAD)
0 20 40 60 80 100 120 140 160 180 200 220 240 260 280 300 320 340 360 380 400 420
NORMAL LOAD IN LBS ⟶
- 203 -

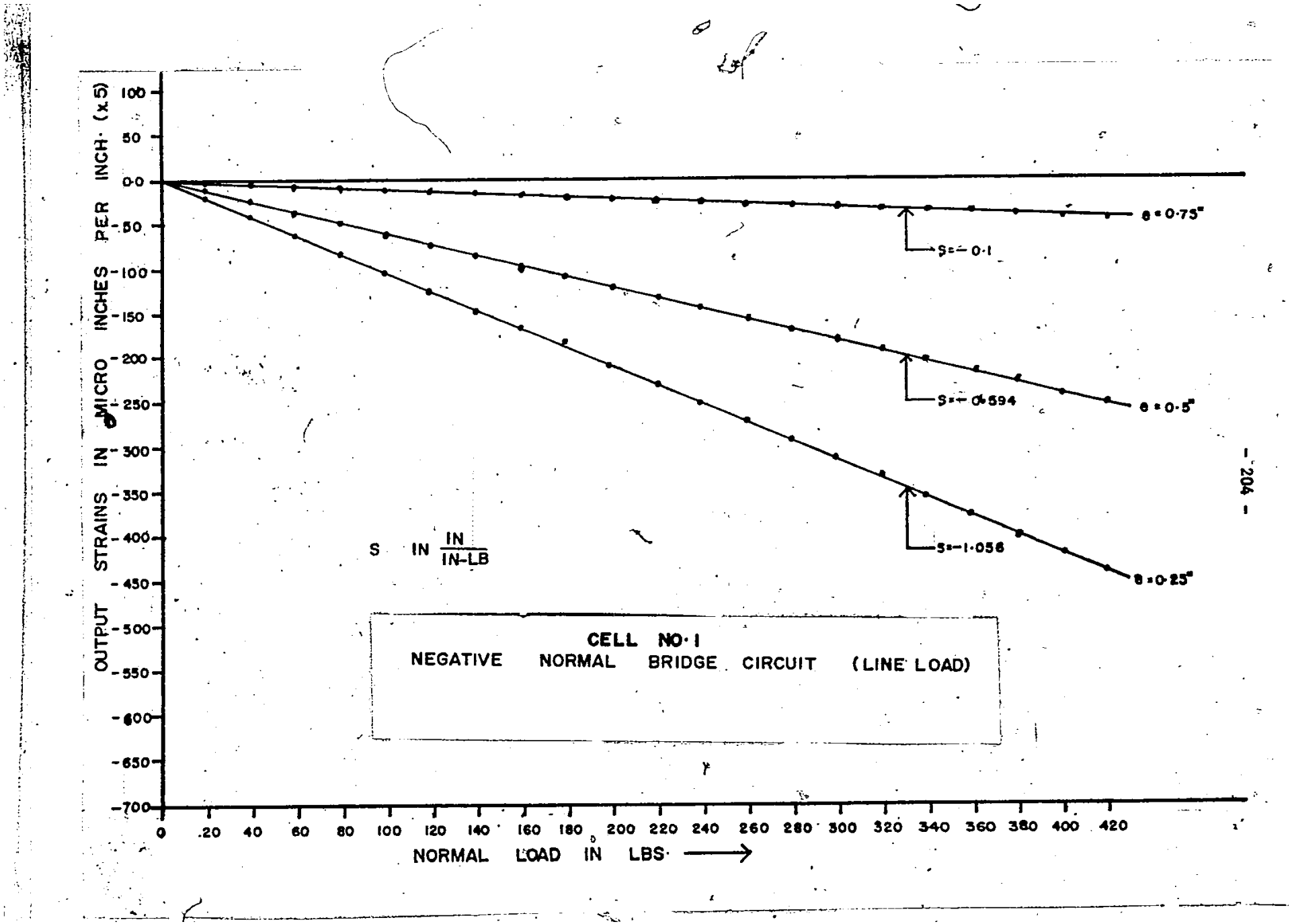
OUTPUT STRAINS IN MICRO INCHES PER INCH (x5)
100
50
0.0
-50
-100
-150
-200
-250
-300
-350
-400
-450
-500
-550
-600
-650
-700
0
20
40
60
80
100
120
140
160
180
200
220
240
260
280
300
320
340
360
380
400
420
NORMAL LOAD IN LBS.
S IN IN/IN-LB
S=-0.1
S=-0.594
S=-1.056
e=0.75"
e=0.5"
e=0.25"
CELL NO. 1
NEGATIVE NORMAL BRIDGE CIRCUIT (LINE LOAD)
- 204 -

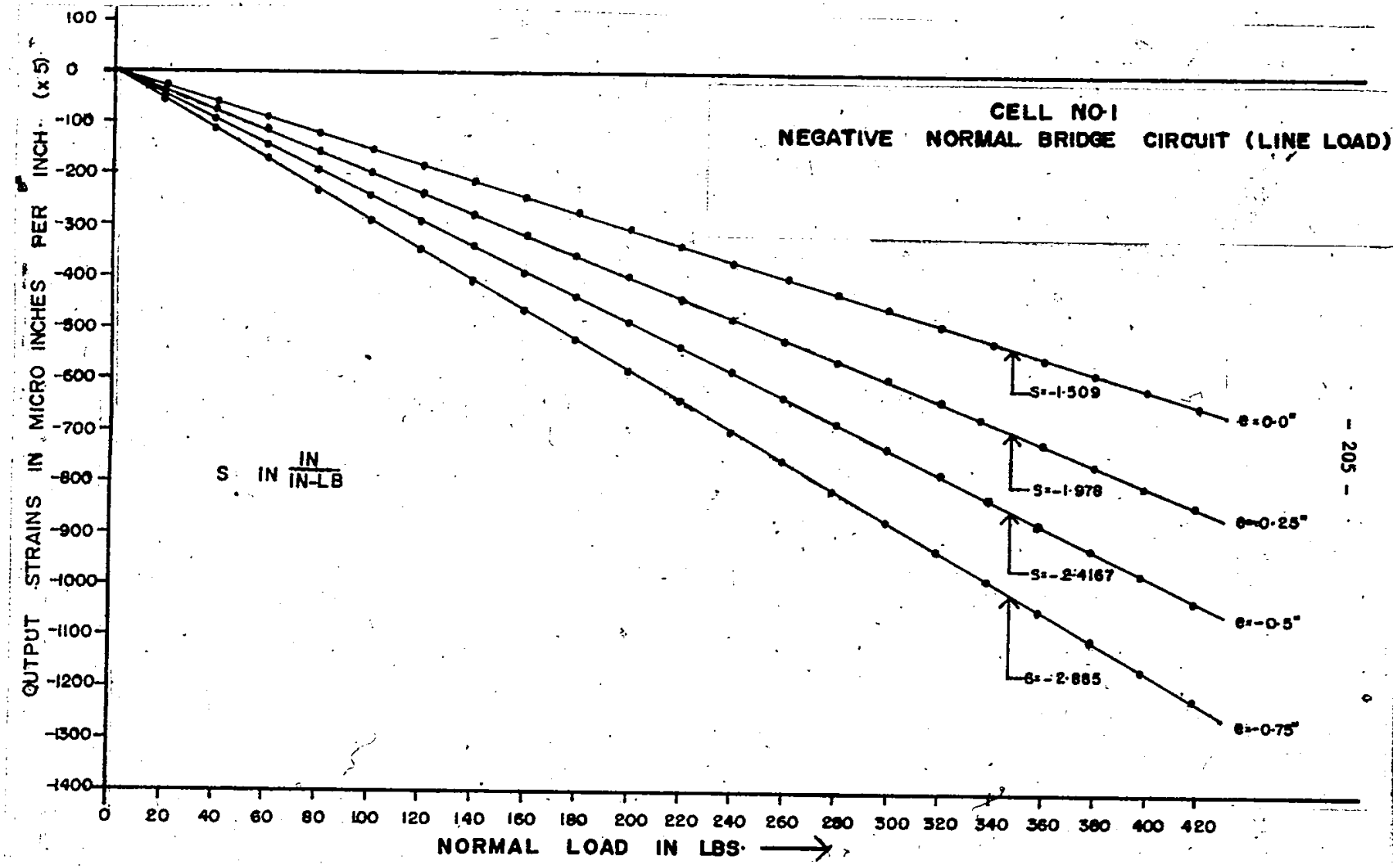
CELL NO-1
NEGATIVE NORMAL BRIDGE CIRCUIT (LINE LOAD)
OUTPUT STRAINS IN MICRO INCHES PER INCH (x 5)
100
0
-100
-200
-300
-400
-500
-600
-700
-800
-900
-1000
-1100
-1200
-1300
-1400
S IN IN/IN-LB
S=-1·509
S=-1·978
S=-2·4167
S=-2·885
e=0·0"
e=0·25"
e=0·5"
e=0·75"
0 20 40 60 80 100 120 140 160 180 200 220 240 260 280 300 320 340 360 380 400 420
NORMAL LOAD IN LBS.

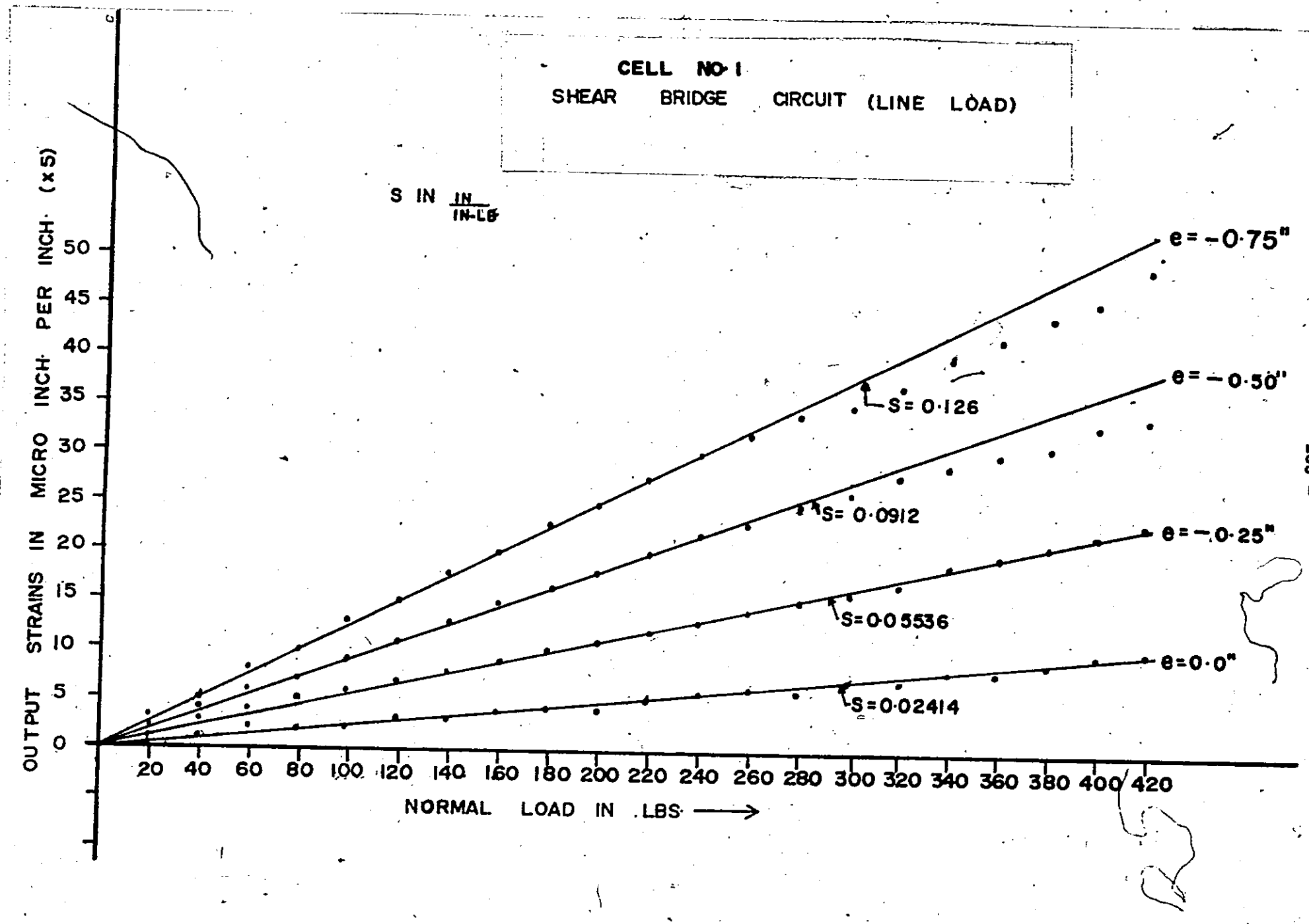
CELL NO. 1
SHEAR BRIDGE CIRCUIT (LINE LOAD)
S IN IN/IN-LB
OUTPUT STRAINS IN MICRO INCH PER INCH (x5)
0
5
10
15
20
25
30
35
40
45
50
20 40 60 80 100 120 140 160 180 200 220 240 260 280 300 320 340 360 380 400 420
NORMAL LOAD IN LBS
e = -0.75"
e = -0.50"
e = -0.25"
e = 0.0"
S= 0.126
S= 0.0912
S=0.05536
S=0.02414

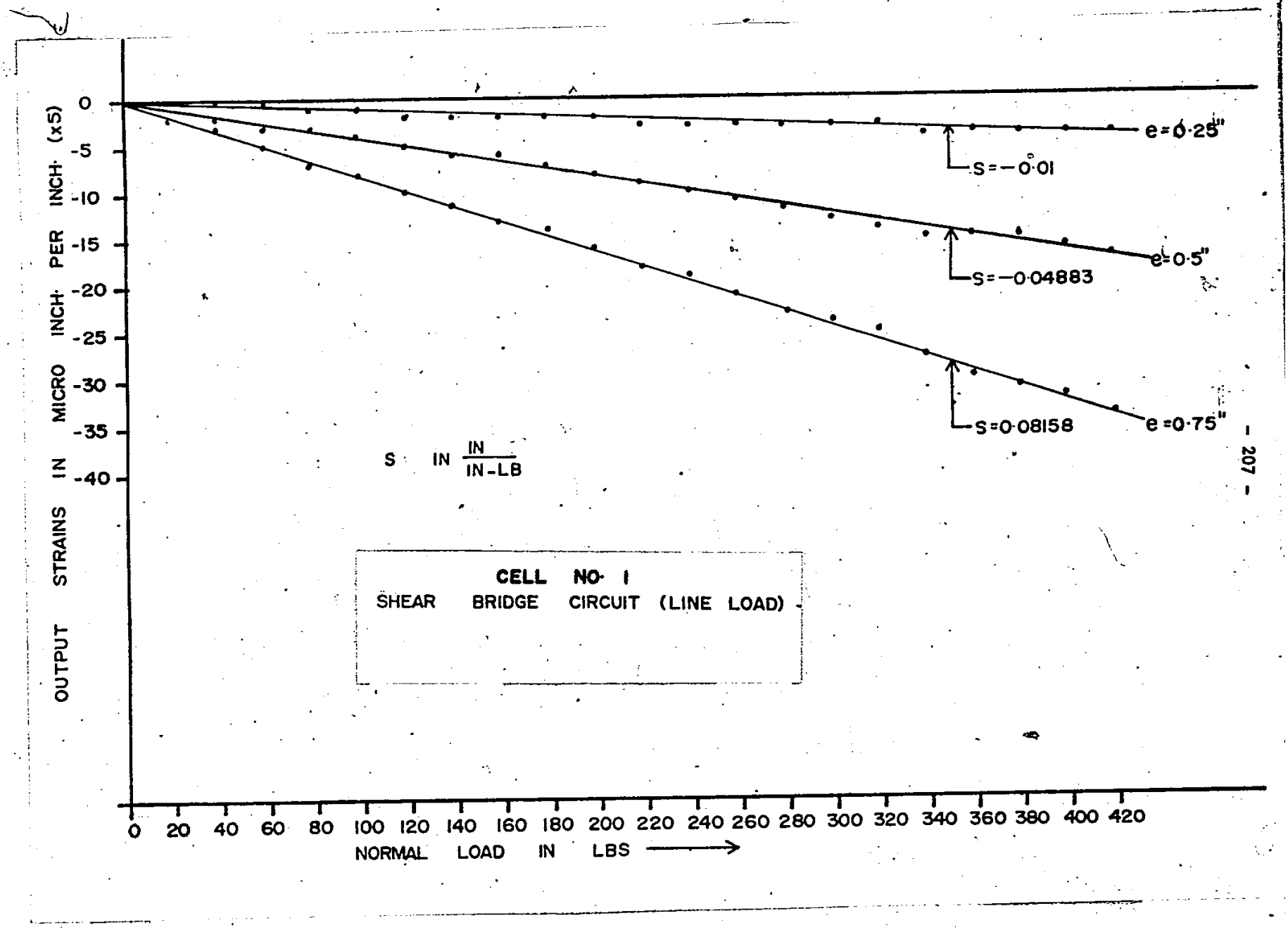
OUTPUT STRAINS IN MICRO INCH PER INCH (x5)
0
-5
-10
-15
-20
-25
-30
-35
-40
e=0·25"
S=−0·01
e=0·5"
S=−0·04883
e=0·75"
S=0·08158
S IN IN/IN-LB
CELL NO. 1
SHEAR BRIDGE CIRCUIT (LINE LOAD)
0 20 40 60 80 100 120 140 160 180 200 220 240 260 280 300 320 340 360 380 400 420
NORMAL LOAD IN LBS

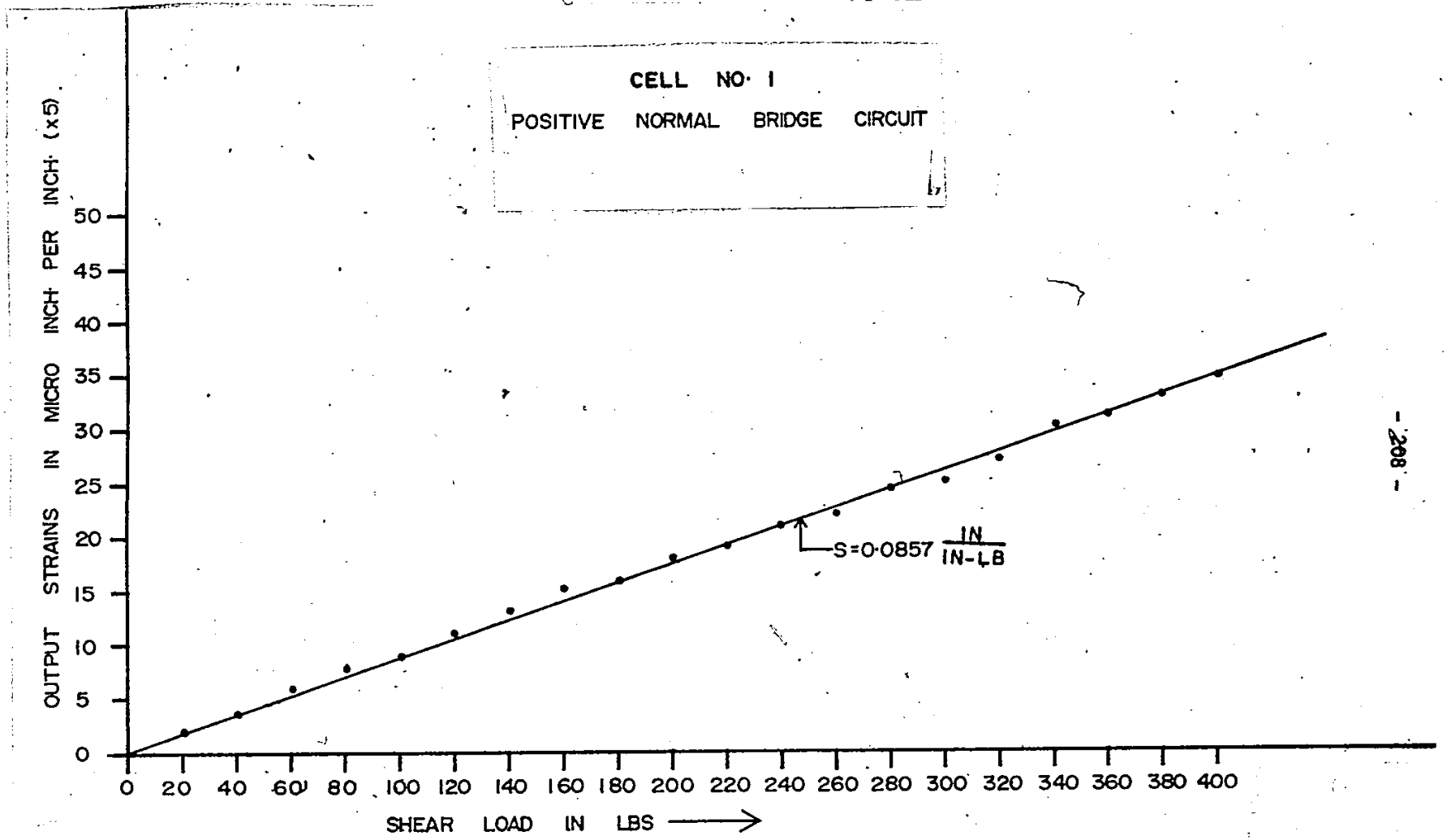
CELL NO. 1
POSITIVE NORMAL BRIDGE CIRCUIT
OUTPUT STRAINS IN MICRO INCH PER INCH (x5)
0
5
10
15
20
25
30
35
40
45
50
0 20 40 60 80 100 120 140 160 180 200 220 240 260 280 300 320 340 360 380 400
SHEAR LOAD IN LBS
S=0.0857 IN/IN-LB

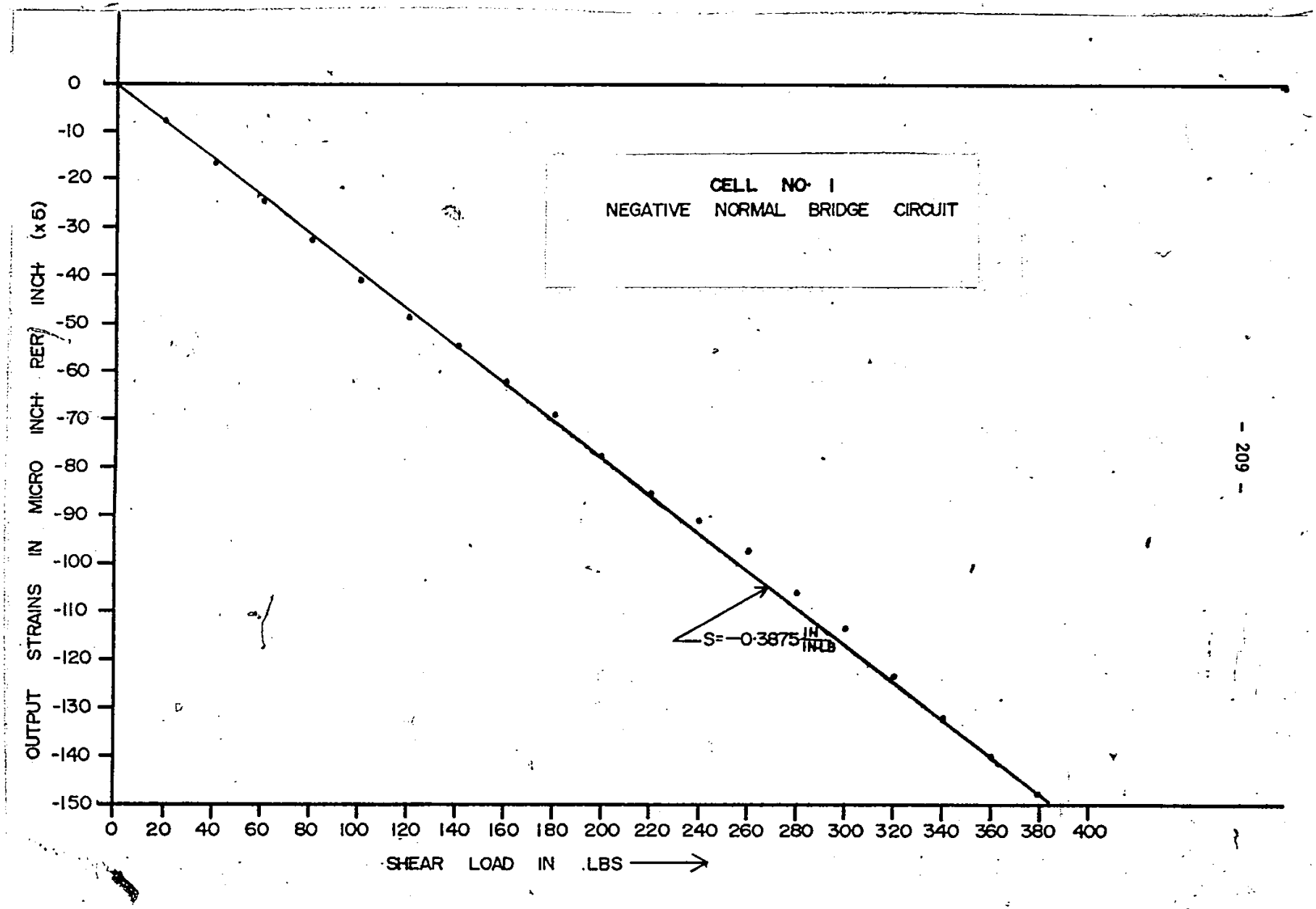
CELL NO. 1
NEGATIVE NORMAL BRIDGE CIRCUIT
OUTPUT STRAINS IN MICRO INCH PER INCH (x6)
0
-10
-20
-30
-40
-50
-60
-70
-80
-90
-100
-110
-120
-130
-140
-150
0 20 40 60 80 100 120 140 160 180 200 220 240 260 280 300 320 340 360 380 400
SHEAR LOAD IN LBS
S=-0·3875 IN/INLB

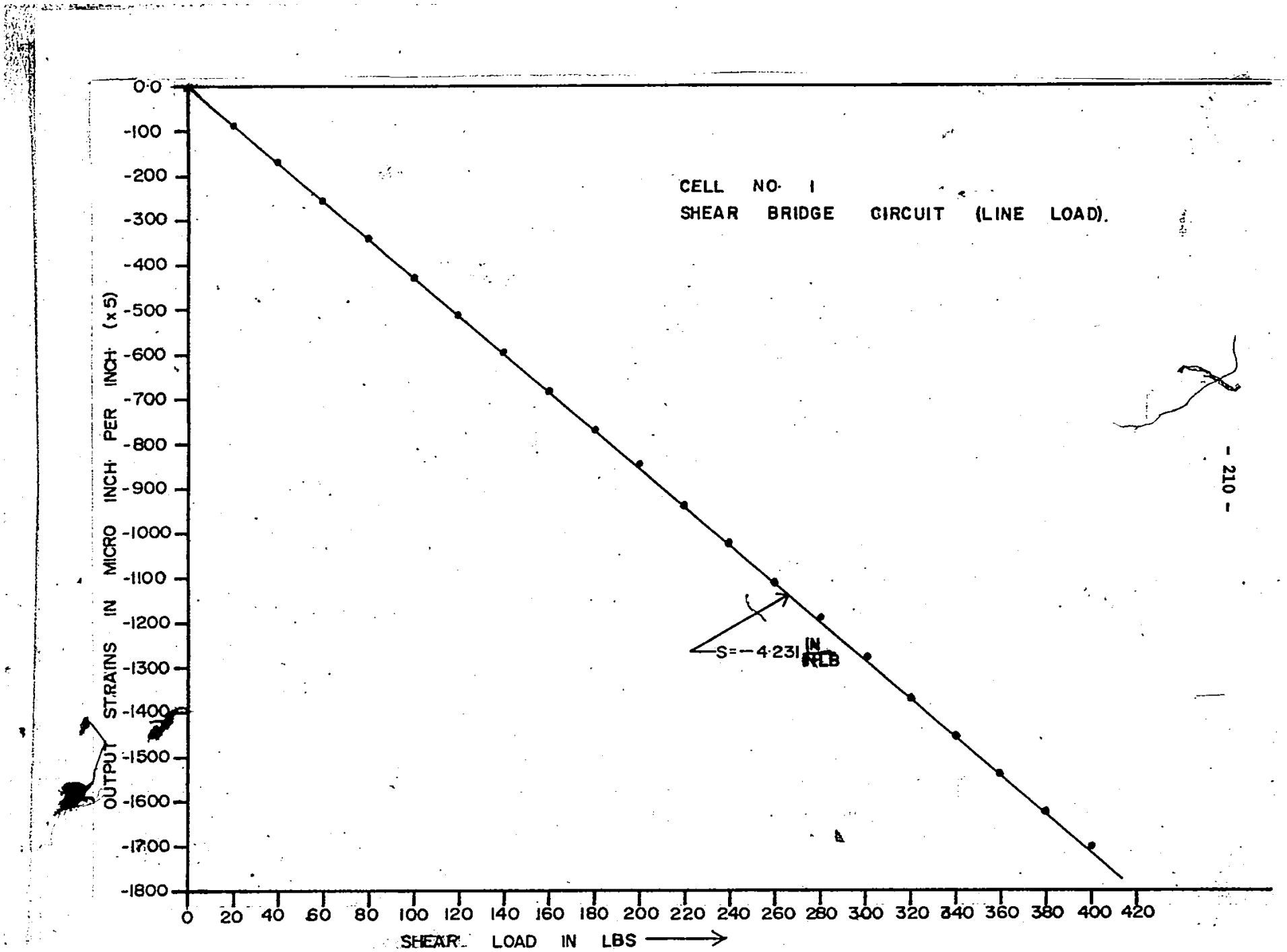
CELL NO. 1
SHEAR BRIDGE CIRCUIT (LINE LOAD).
S=-4.231 IN/LB
OUTPUT STRAINS IN MICRO INCH PER INCH (x5)
0·0
-100
-200
-300
-400
-500
-600
-700
-800
-900
-1000
-1100
-1200
-1300
-1400
-1500
-1600
-1700
-1800
0 20 40 60 80 100 120 140 160 180 200 220 240 260 280 300 320 340 360 380 400 420
SHEAR LOAD IN LBS

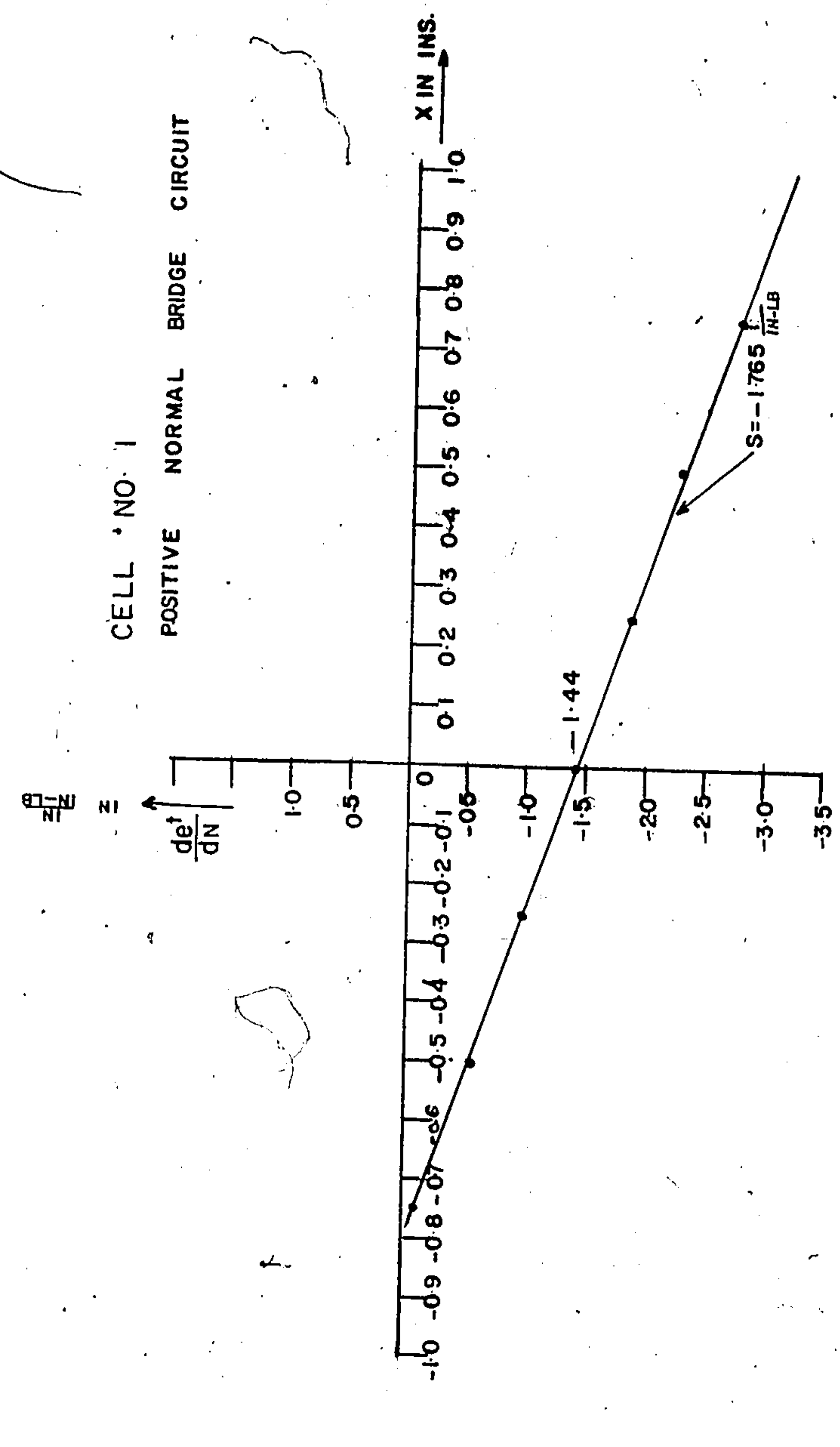
CELL NO 1
POSITIVE NORMAL BRIDGE CIRCUIT
X IN INS.
$\frac{de^{\prime}}{dN}$ IN $\frac{IN}{IN\text{-}LB}$
S=-1.765 $\frac{1}{IN\text{-}LB}$
-1.44

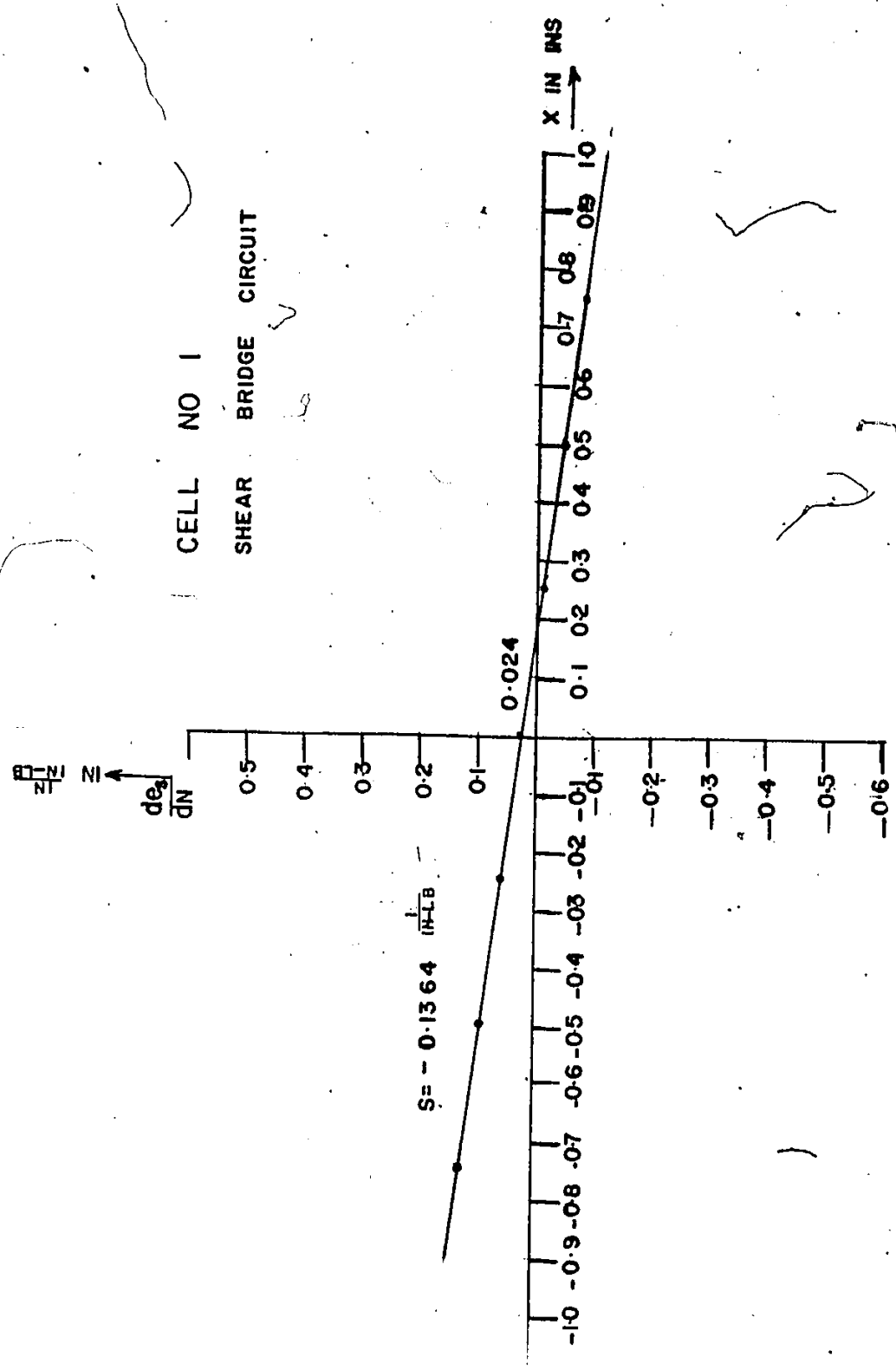
CELL NO 1
SHEAR BRIDGE CIRCUIT
X IN INS
0·024
S = - 0·1364 1/IN-LB
de_s/dN
0·5
0·4
0·3
0·2
0·1
-0·1
-0·2
-0·3
-0·4
-0·5
-0·6
0·1
0·2
0·3
0·4
0·5
0·6
0·7
0·8
0·9
1·0
-0·7
-0·8
-0·9
-1·0

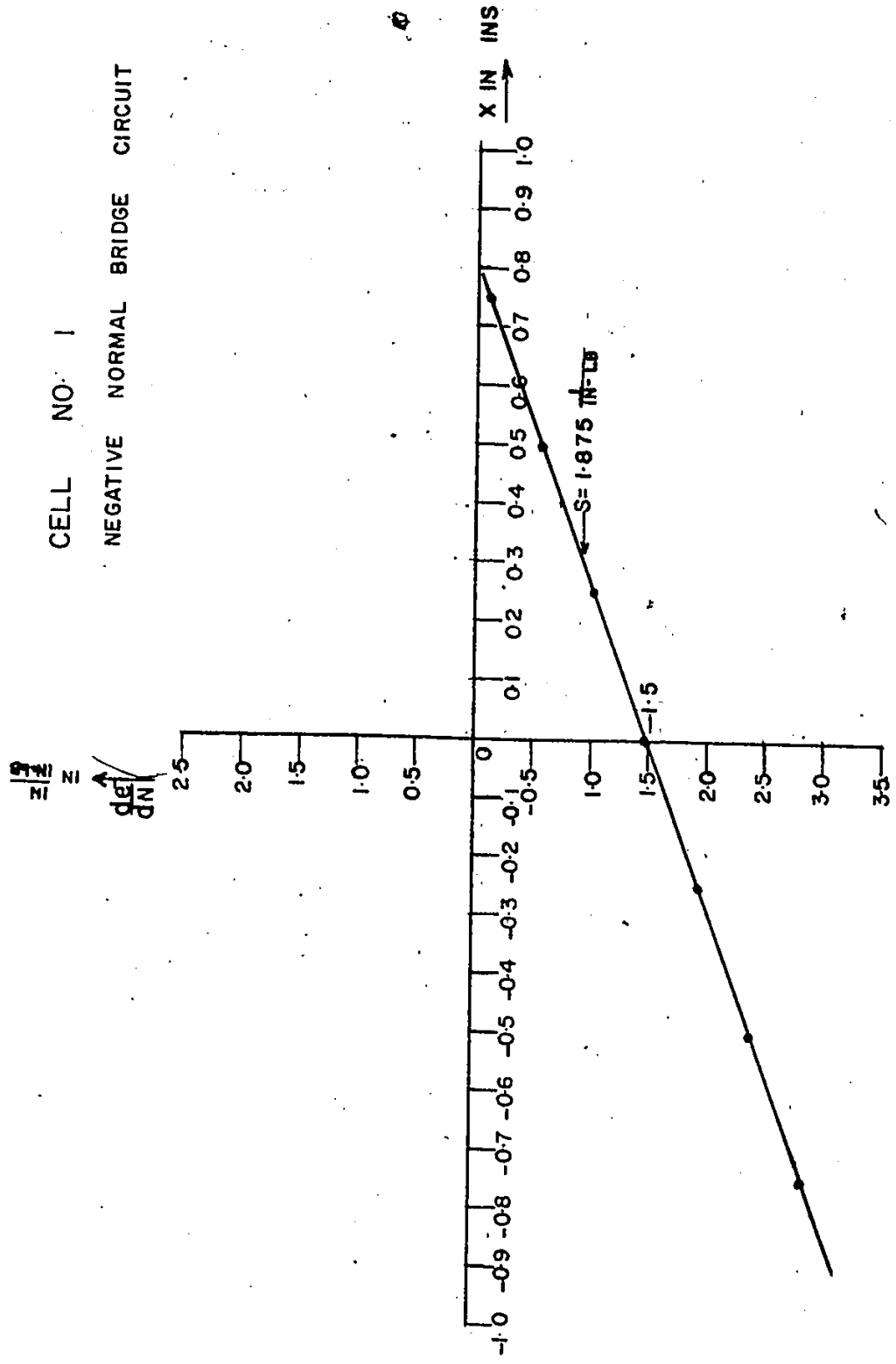
CELL NO. 1
NEGATIVE NORMAL BRIDGE CIRCUIT
X IN INS
S= 1·875 IN-LB
dE/dN

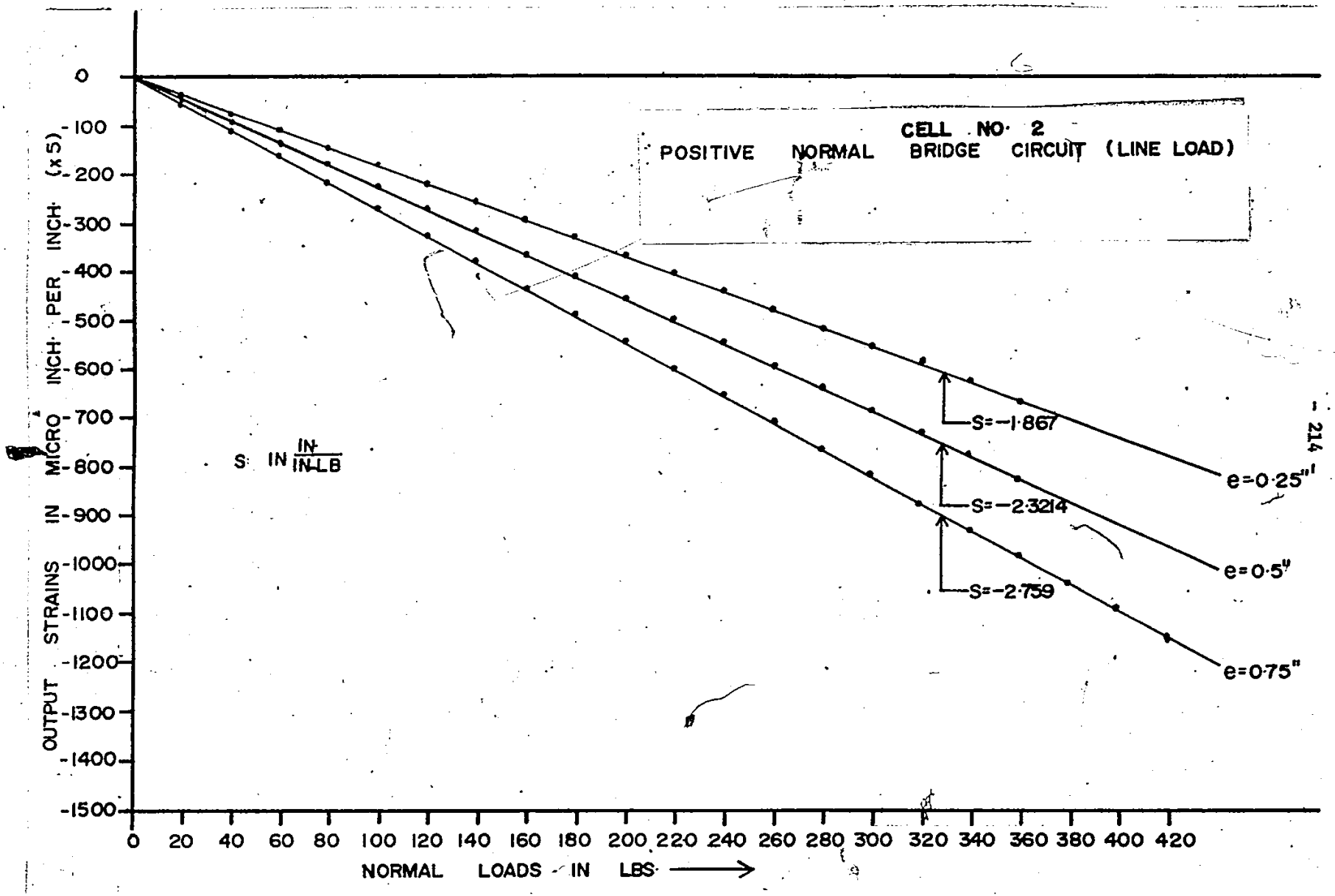
CELL NO. 2
POSITIVE NORMAL BRIDGE CIRCUIT (LINE LOAD)
OUTPUT STRAINS IN MICRO INCH PER INCH (x5)
0
-100
-200
-300
-400
-500
-600
-700
-800
-900
-1000
-1100
-1200
-1300
-1400
-1500
S IN IN/IN-LB
S=-1·867
S=-2·3214
S=-2·759
e=0·25"
e=0·5"
e=0·75"
0 20 40 60 80 100 120 140 160 180 200 220 240 260 280 300 320 340 360 380 400 420
NORMAL LOADS IN LBS

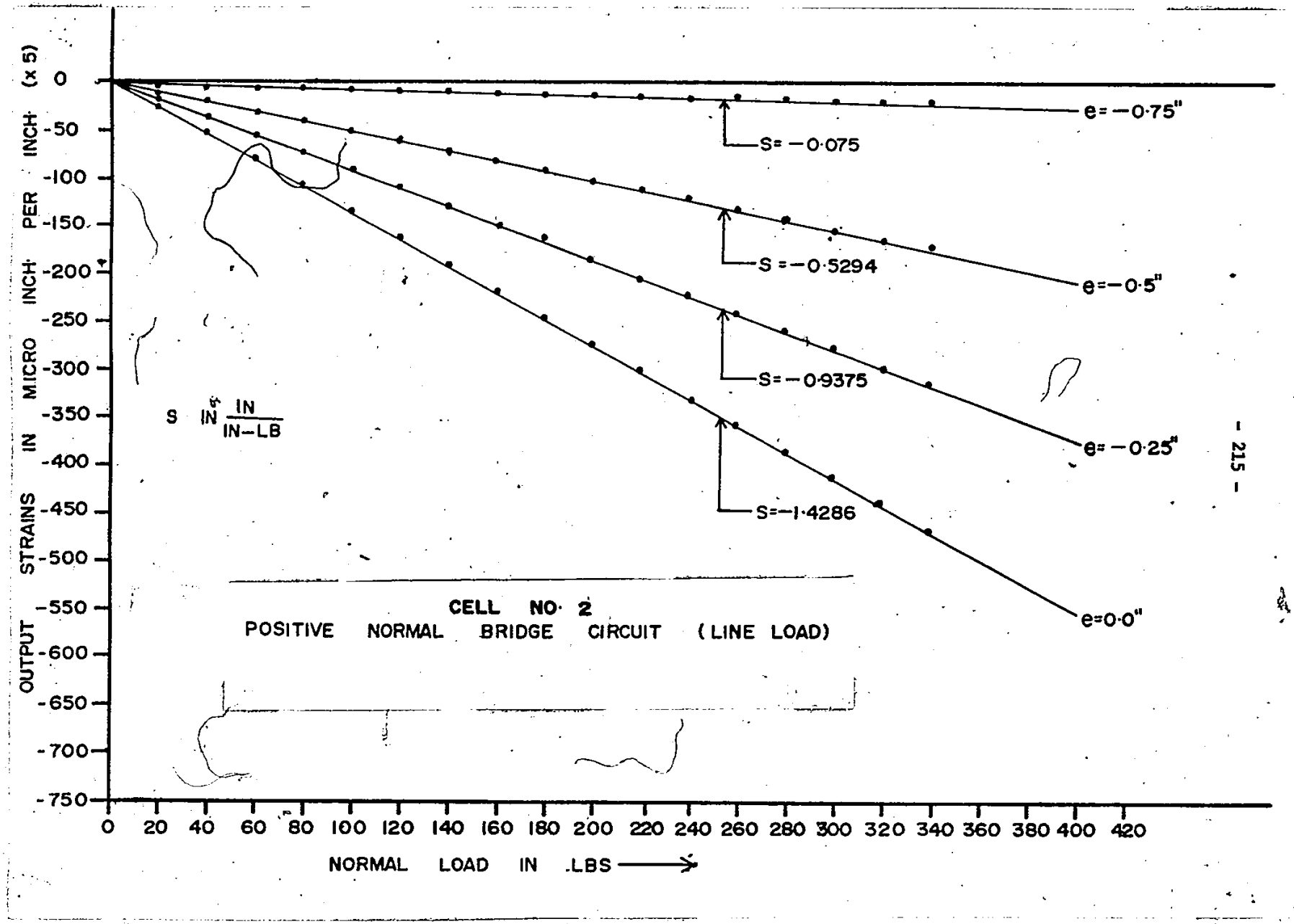
OUTPUT STRAINS IN MICRO INCH PER INCH (x 5)
0
-50
-100
-150
-200
-250
-300
-350
-400
-450
-500
-550
-600
-650
-700
-750
S IN IN/IN-LB
e=-0·75"
S=-0·075
S=-0·5294
e=-0·5"
S=-0·9375
e=-0·25"
S=-1·4286
e=0·0"
CELL NO· 2
POSITIVE NORMAL BRIDGE CIRCUIT (LINE LOAD)
0 20 40 60 80 100 120 140 160 180 200 220 240 260 280 300 320 340 360 380 400 420
NORMAL LOAD IN LBS

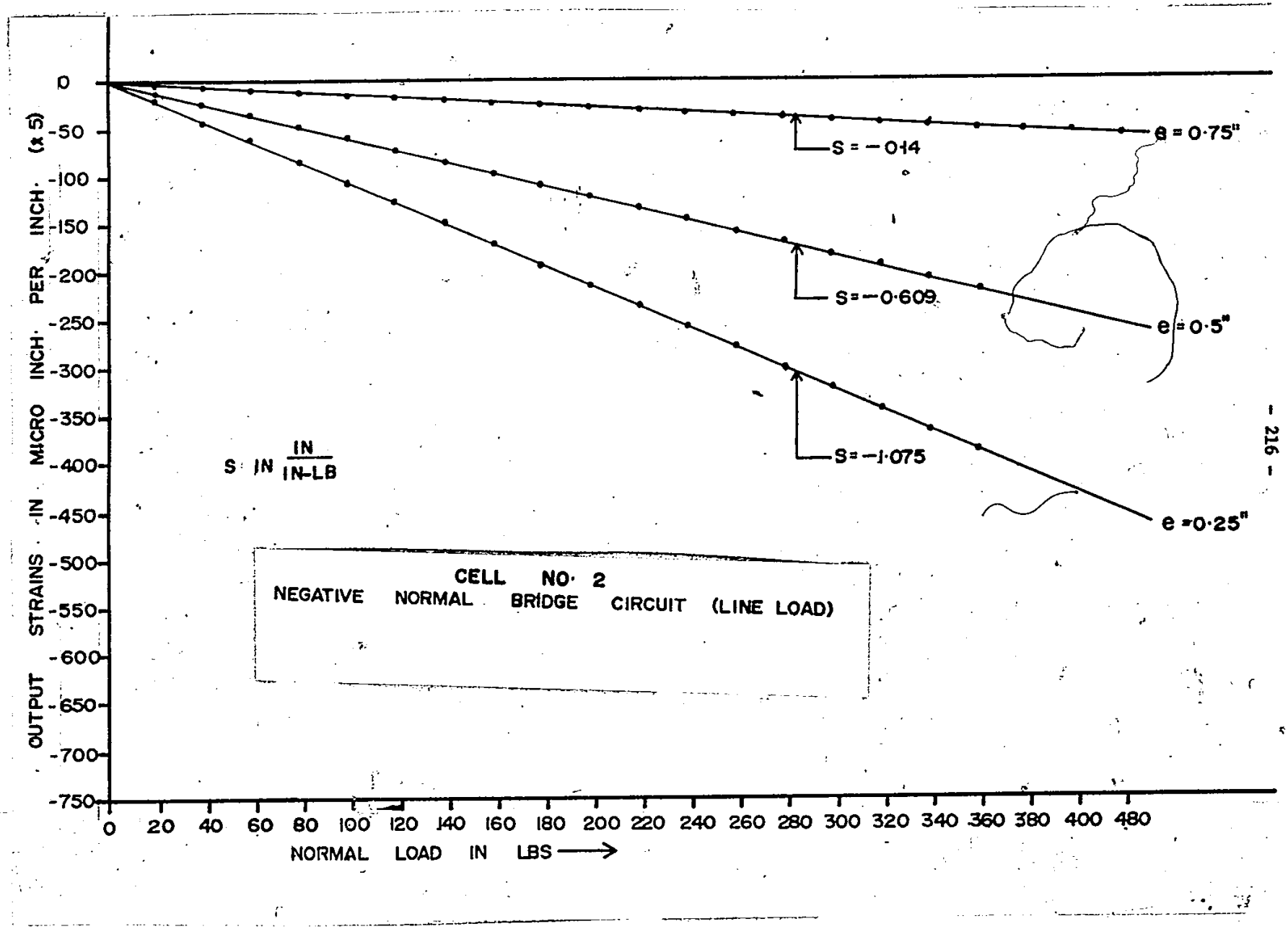
OUTPUT STRAINS IN MICRO INCH PER INCH (x 5)
0
-50
-100
-150
-200
-250
-300
-350
-400
-450
-500
-550
-600
-650
-700
-750
0 20 40 60 80 100 120 140 160 180 200 220 240 260 280 300 320 340 360 380 400 480
NORMAL LOAD IN LBS ⟶
S = −·014
S = −0·609
S = −1·075
e = 0·75"
e = 0·5"
e = 0·25"
S IN IN/IN-LB
CELL NO· 2
NEGATIVE NORMAL BRIDGE CIRCUIT (LINE LOAD)

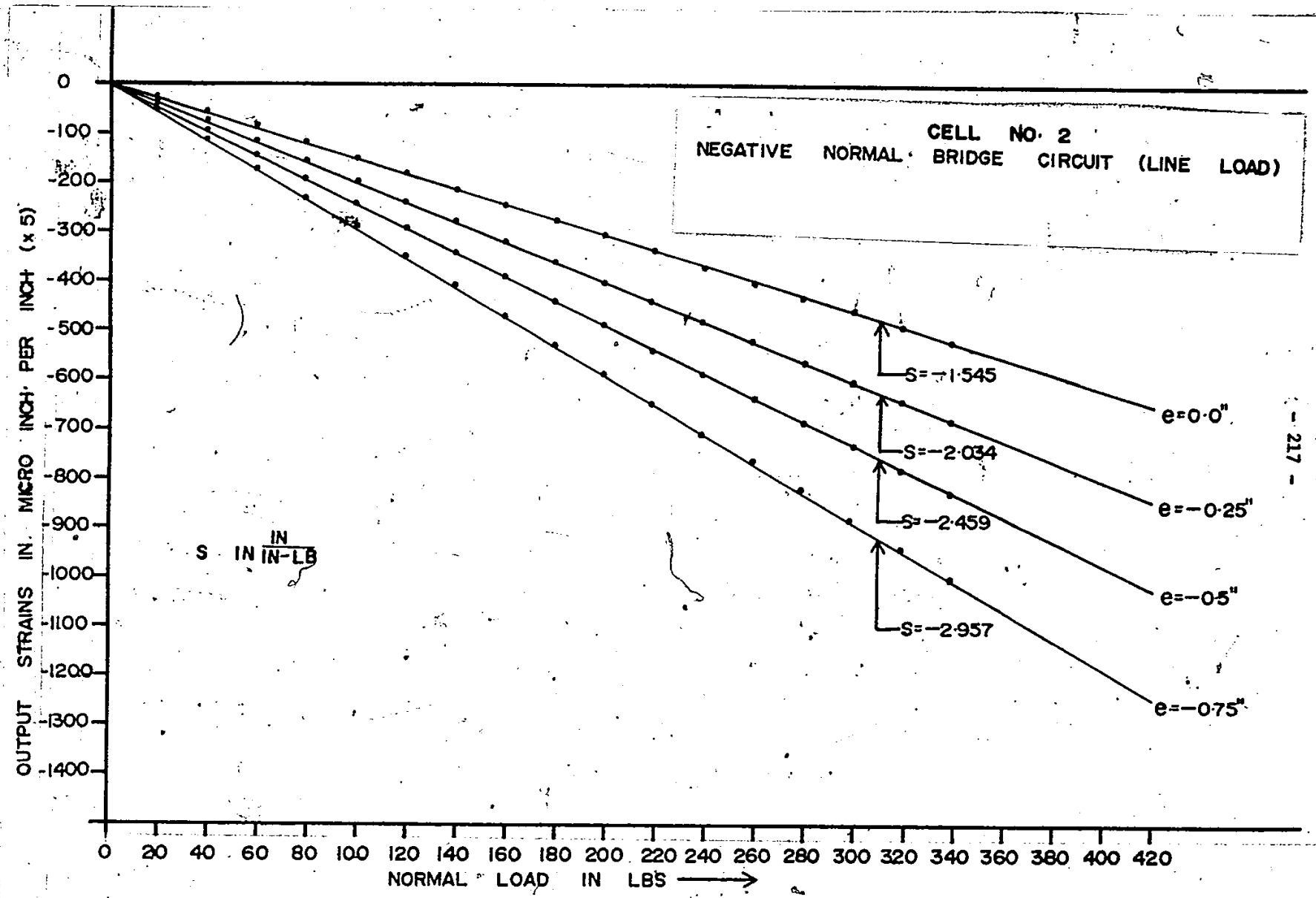
CELL NO. 2
NEGATIVE NORMAL BRIDGE CIRCUIT (LINE LOAD)
OUTPUT STRAINS IN MICRO INCH PER INCH (x 5)
0
-100
-200
-300
-400
-500
-600
-700
-800
-900
-1000
-1100
-1200
-1300
-1400
S IN IN/IN-LB
S=-1·545
S=-2·034
S=-2·459
S=-2·957
e=0·0"
e=-0·25"
e=-0·5"
e=-0·75"
0 20 40 60 80 100 120 140 160 180 200 220 240 260 280 300 320 340 360 380 400 420
NORMAL LOAD IN LBS

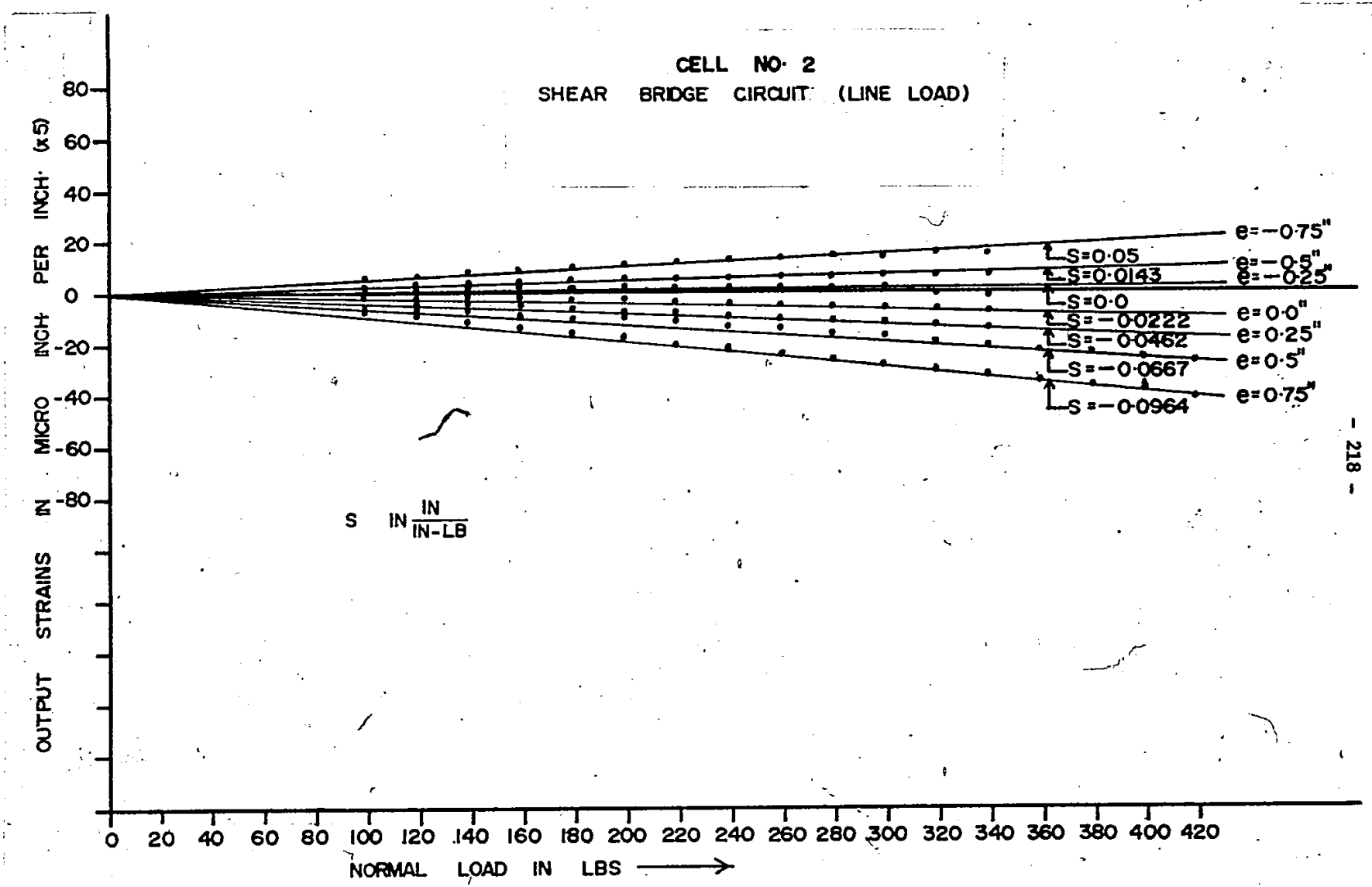
CELL NO. 2
SHEAR BRIDGE CIRCUIT (LINE LOAD)
OUTPUT STRAINS IN MICRO INCH PER INCH (x5)
80
60
40
20
0
-20
-40
-60
-80
S IN $\frac{IN}{IN-LB}$
S=0.05
S=0.0143
S=0.0
S=-0.0222
S=-0.0462
S=-0.0667
S=-0.0964
e=-0.75"
e=-0.5"
e=-0.25"
e=0.0"
e=0.25"
e=0.5"
e=0.75"
0 20 40 60 80 100 120 140 160 180 200 220 240 260 280 300 320 340 360 380 400 420
NORMAL LOAD IN LBS

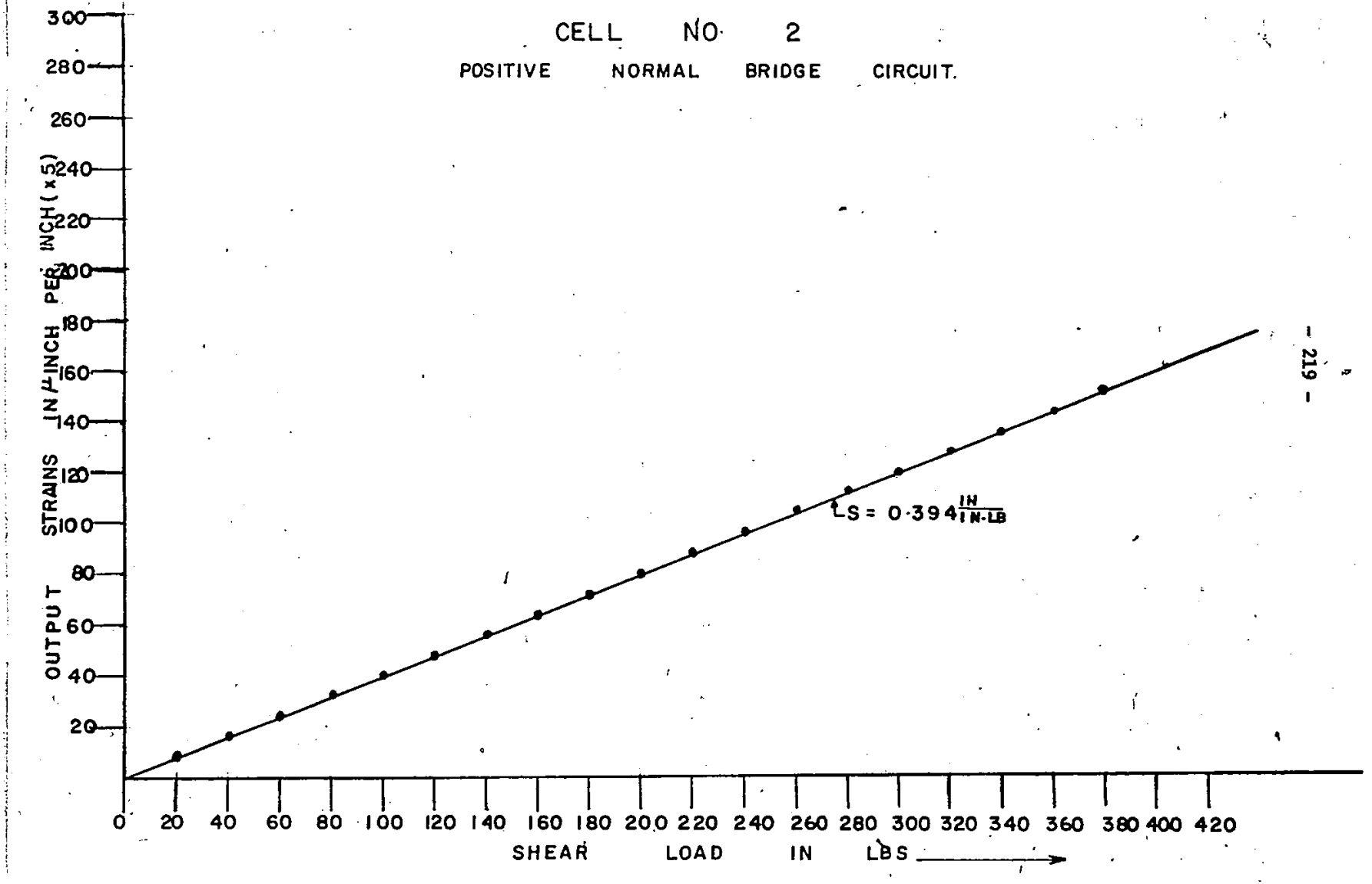
CELL NO 2
POSITIVE NORMAL BRIDGE CIRCUIT.
OUTPUT STRAINS IN μINCH PER INCH (x5)
300
280
260
240
220
200
180
160
140
120
100
80
60
40
20
0
20 40 60 80 100 120 140 160 180 200 220 240 260 280 300 320 340 360 380 400 420
SHEAR LOAD IN LBS
LS = 0·394 IN/IN-LB

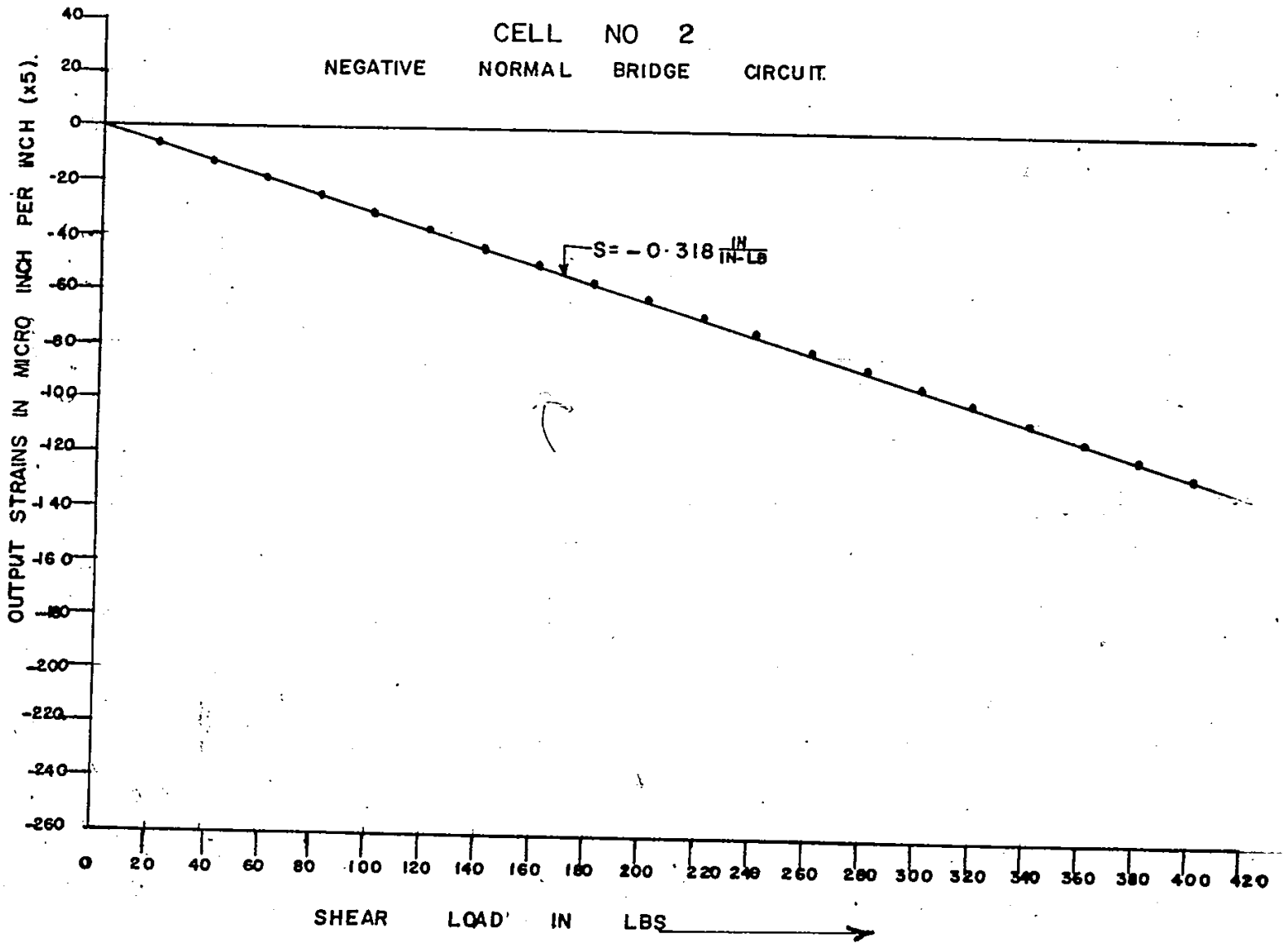
CELL NO 2
NEGATIVE NORMAL BRIDGE CIRCUIT.
S= – 0·318 IN/IN-LB
OUTPUT STRAINS IN MICRO INCH PER INCH (x5).
40
20
0
-20
-40
-60
-80
-100
-120
-140
-160
-180
-200
-220
-240
-260
0 20 40 60 80 100 120 140 160 180 200 220 240 260 280 300 320 340 360 380 400 420
SHEAR LOAD IN LBS

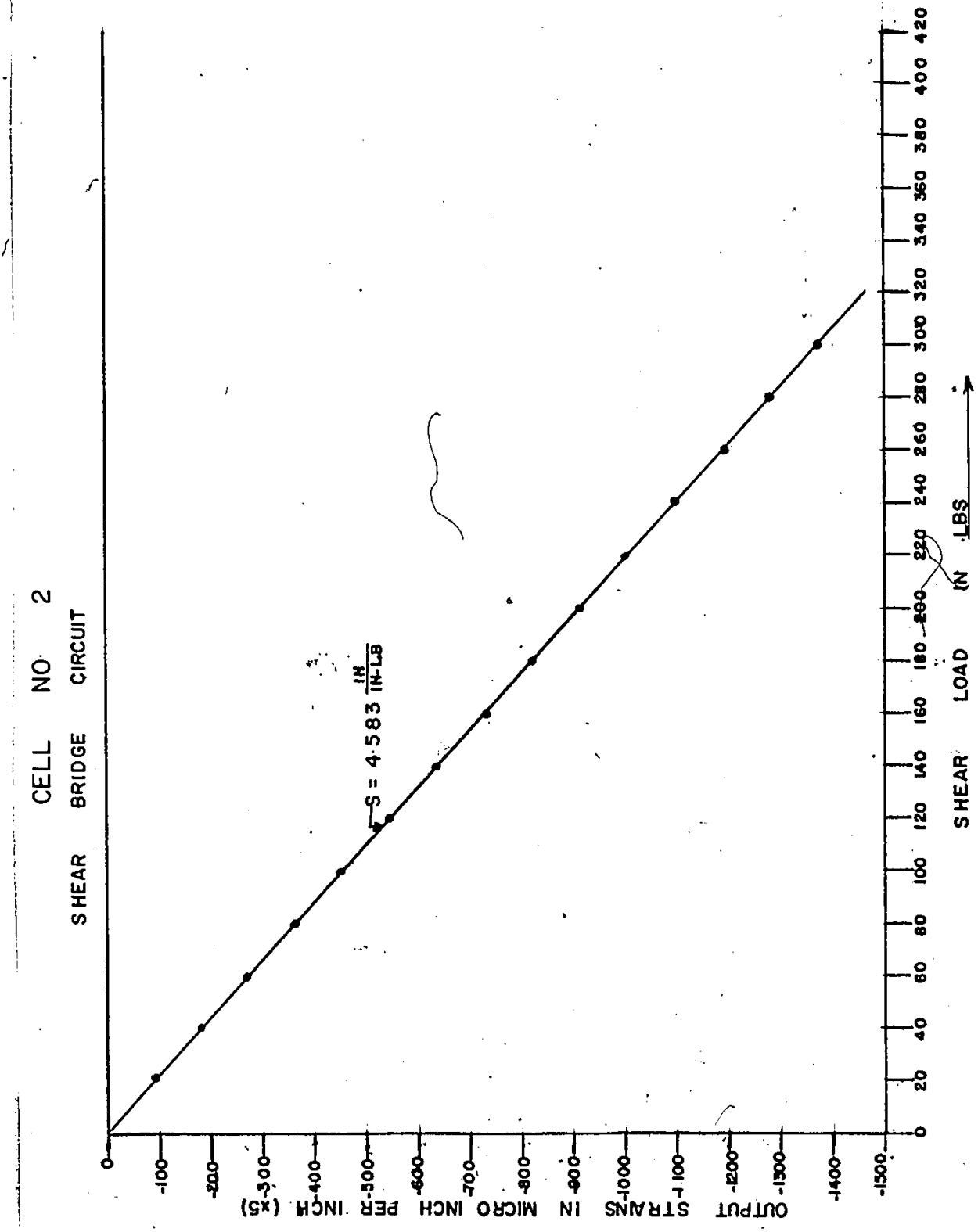
CELL NO 2
SHEAR BRIDGE CIRCUIT
S = 4.583 IN/IN-LB
OUTPUT STRAINS IN MICRO INCH PER INCH (x5)
SHEAR LOAD IN LBS
0
-100
-200
-300
-400
-500
-600
-700
-800
-900
-1000
-1100
-1200
-1300
-1400
-1500
0
20
40
60
80
100
120
140
160
180
200
220
240
260
280
300
320
340
360
380
400
420

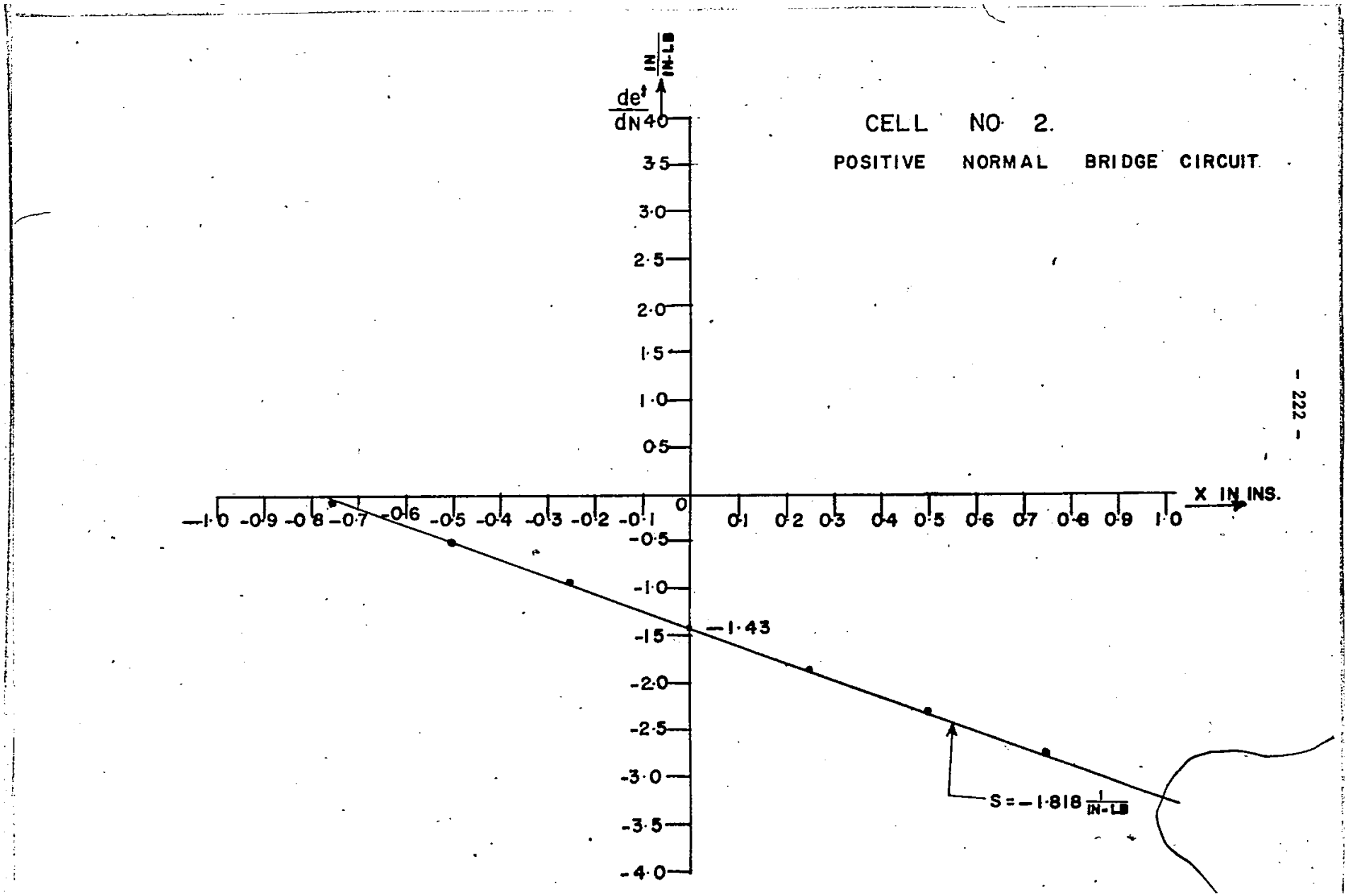
CELL NO. 2.
POSITIVE NORMAL BRIDGE CIRCUIT.
de'/dN IN/IN-LB
X IN INS.
4·0
3·5
3·0
2·5
2·0
1·5
1·0
0·5
-0·5
-1·0
-1·5
-2·0
-2·5
-3·0
-3·5
-4·0
-1·0 -0·9 -0·8 -0·7 -0·6 -0·5 -0·4 -0·3 -0·2 -0·1 0 0·1 0·2 0·3 0·4 0·5 0·6 0·7 0·8 0·9 1·0
-1·43
S = -1·818 1/IN-LB

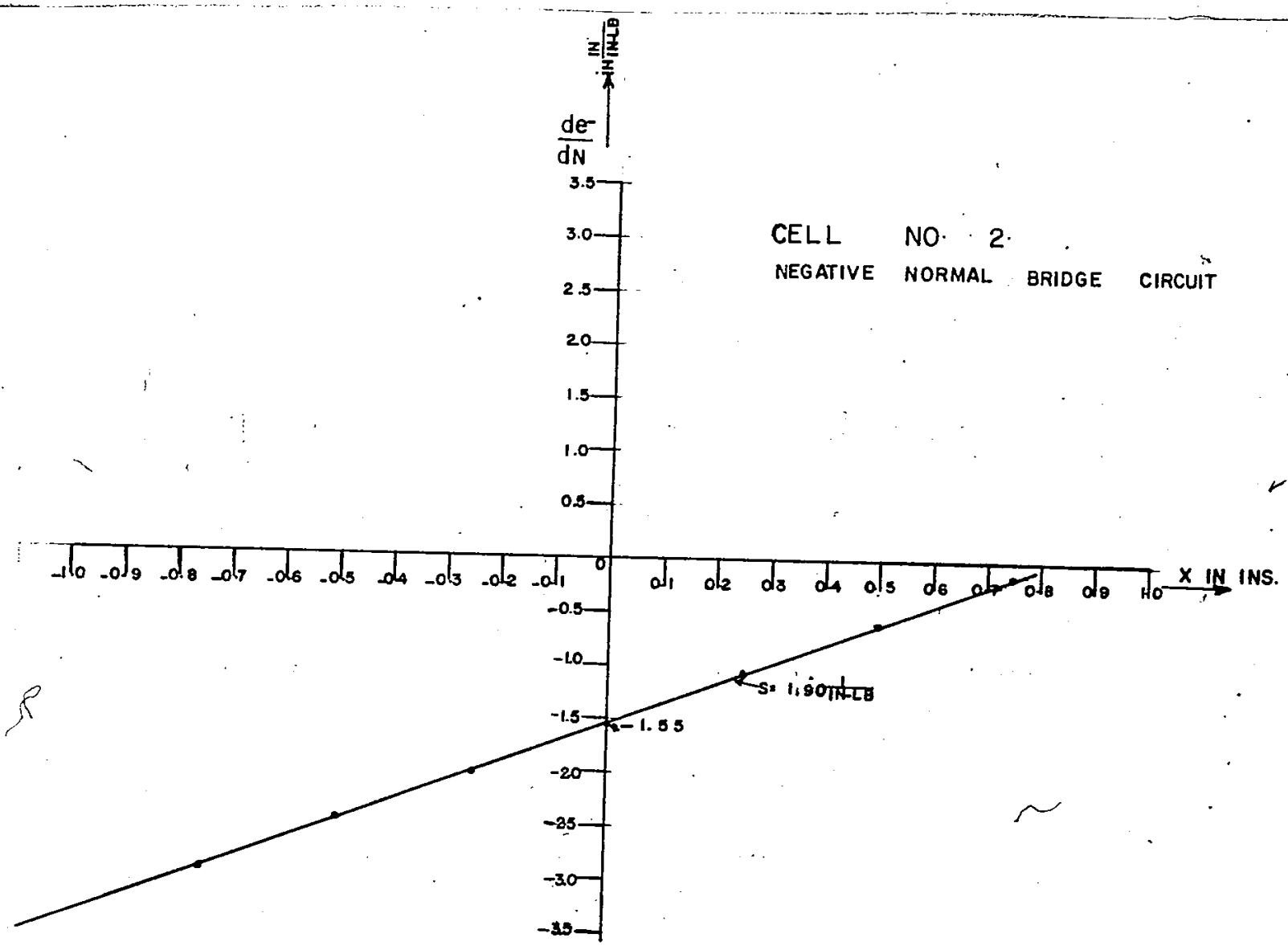

CELL NO. 2.

NEGATIVE NORMAL BRIDGE CIRCUIT

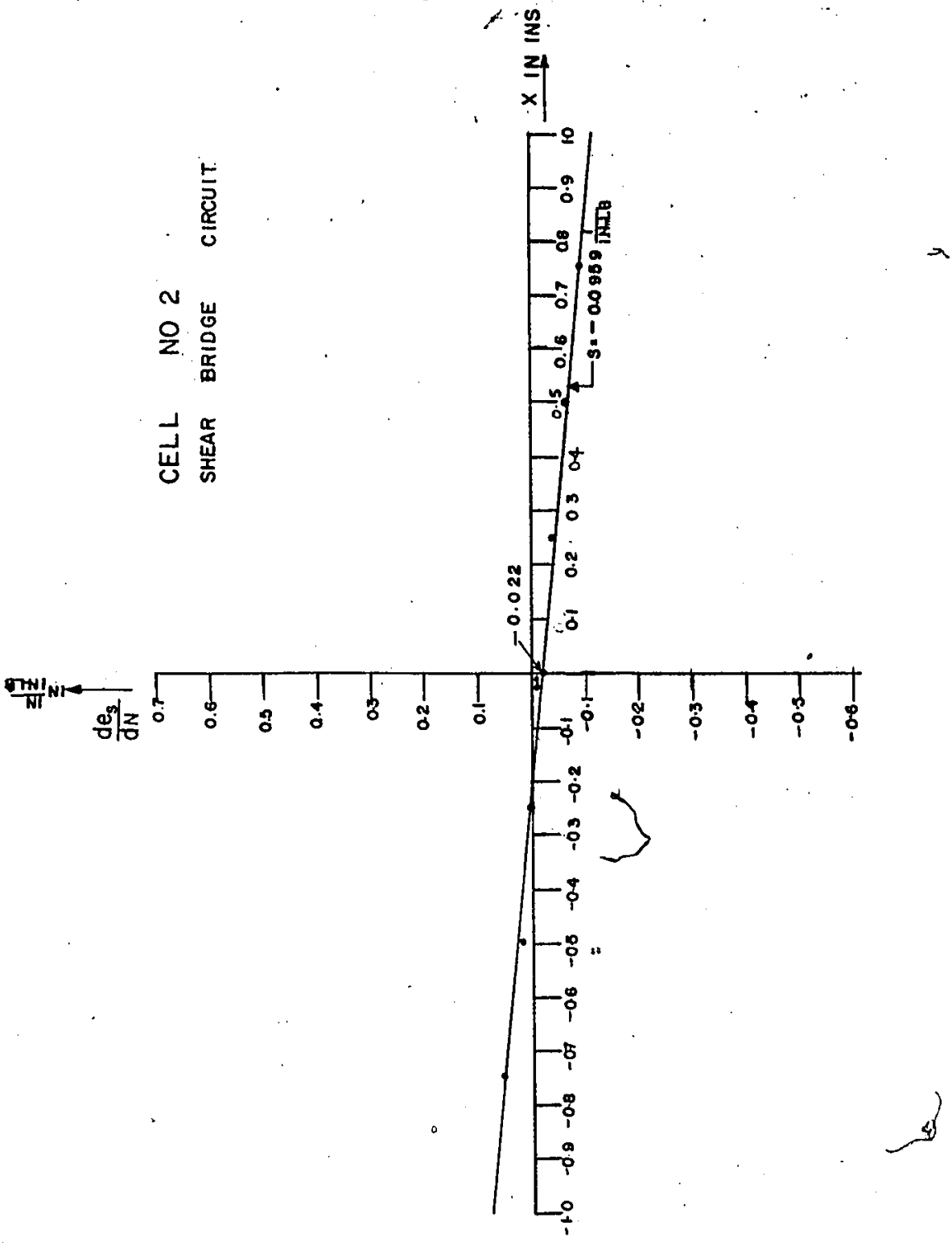
CELL NO 2
SHEAR BRIDGE CIRCUIT
X IN INS
S = - 0.0959 INCH
0.022
$\frac{de_3}{dN}$
$\frac{\text{CHANGE IN N}}{N}$

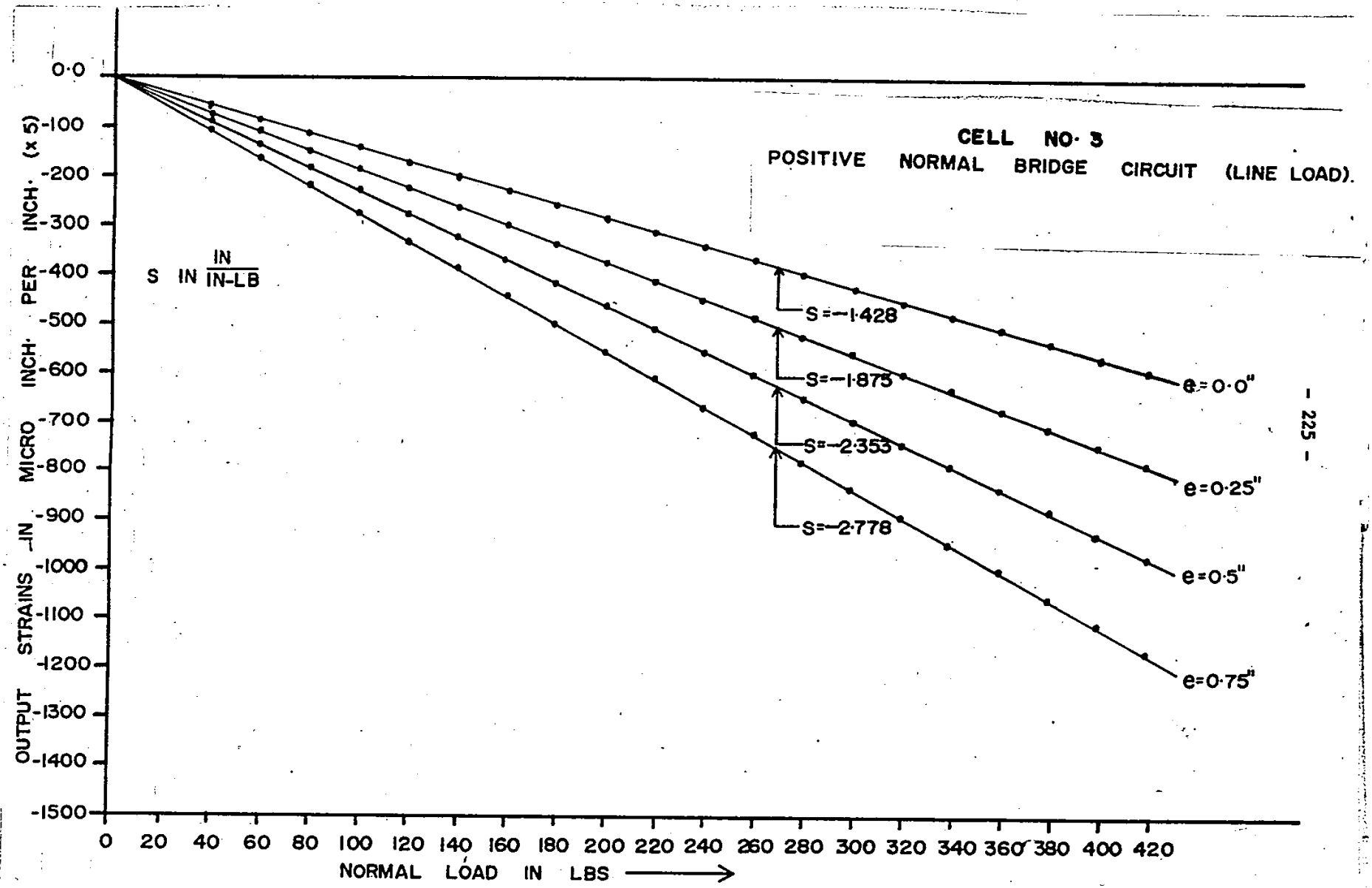
CELL NO. 3
POSITIVE NORMAL BRIDGE CIRCUIT (LINE LOAD).
S IN $\frac{IN}{IN-LB}$
S=-1.428
S=-1.875
S=-2.353
S=-2.778
e=0.0"
e=0.25"
e=0.5"
e=0.75"
OUTPUT STRAINS IN MICRO INCH. PER INCH. (x 5)
0.0
-100
-200
-300
-400
-500
-600
-700
-800
-900
-1000
-1100
-1200
-1300
-1400
-1500
0 20 40 60 80 100 120 140 160 180 200 220 240 260 280 300 320 340 360 380 400 420
NORMAL LOAD IN LBS

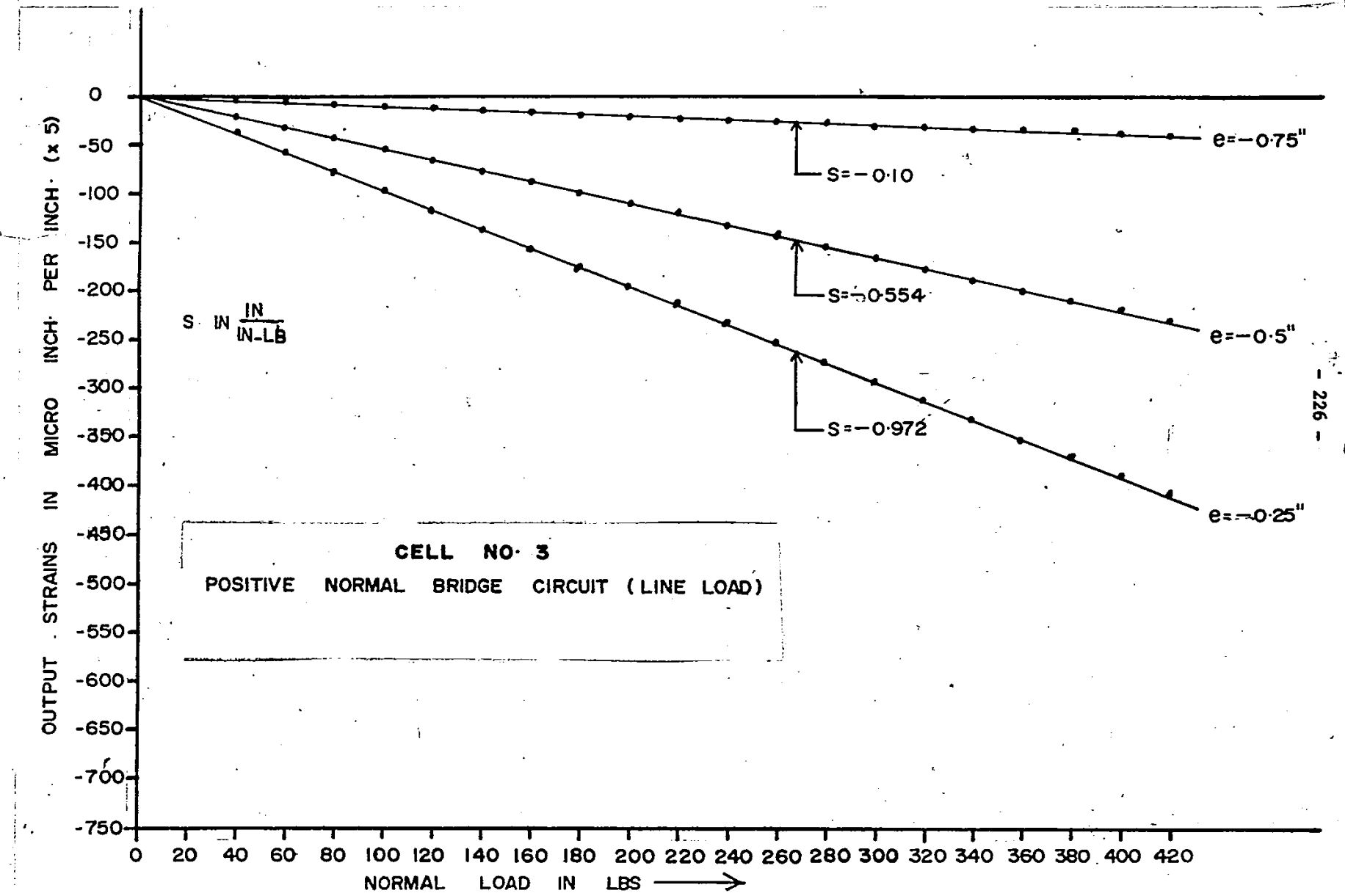
OUTPUT STRAINS IN MICRO INCH PER INCH (x 5)
0
-50
-100
-150
-200
-250
-300
-350
-400
-450
-500
-550
-600
-650
-700
-750
S IN IN/IN-LB
e=-0.75"
S=-0.10
e=-0.5"
S=-0.554
e=-0.25"
S=-0.972
CELL NO. 3
POSITIVE NORMAL BRIDGE CIRCUIT (LINE LOAD)
0 20 40 60 80 100 120 140 160 180 200 220 240 260 280 300 320 340 360 380 400 420
NORMAL LOAD IN LBS

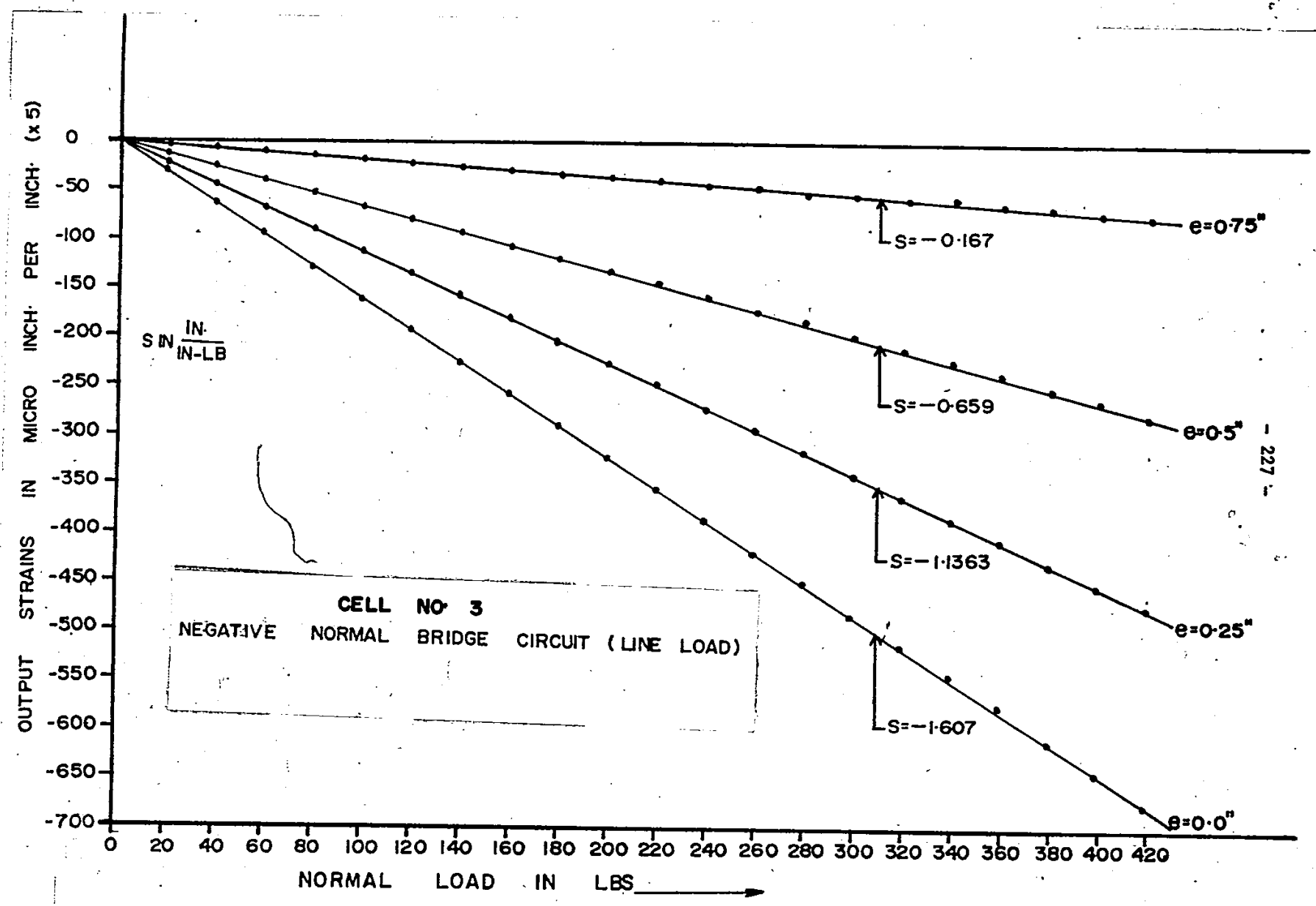
OUTPUT STRAINS IN MICRO INCH PER INCH (x 5)
0
-50
-100
-150
-200
-250
-300
-350
-400
-450
-500
-550
-600
-650
-700
S IN IN./IN-LB
e=0·75"
S=−0·167
e=0·5"
S=−0·659
e=0·25"
S=−1·1363
e=0·0"
S=−1·607
CELL NO· 3
NEGATIVE NORMAL BRIDGE CIRCUIT (LINE LOAD)
0 20 40 60 80 100 120 140 160 180 200 220 240 260 280 300 320 340 360 380 400 420
NORMAL LOAD IN LBS

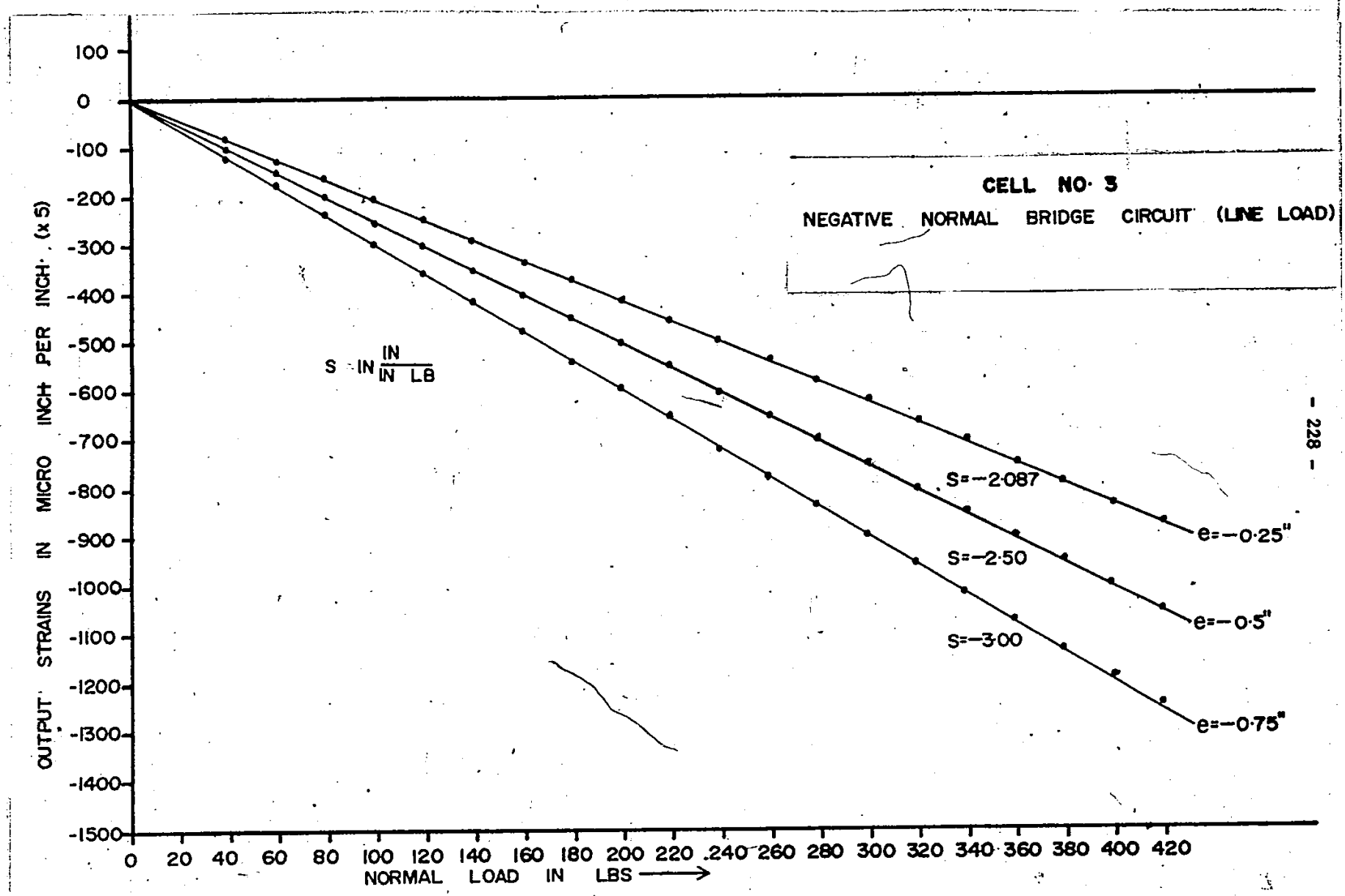
CELL NO. 3
NEGATIVE NORMAL BRIDGE CIRCUIT (LINE LOAD)
S = IN/IN LB
S=-2·087
S=-2·50
S=-3·00
e=-0·25"
e=-0·5"
e=-0·75"
OUTPUT STRAINS IN MICRO INCH PER INCH. (x 5)
100
0
-100
-200
-300
-400
-500
-600
-700
-800
-900
-1000
-1100
-1200
-1300
-1400
-1500
0 20 40 60 80 100 120 140 160 180 200 220 240 260 280 300 320 340 360 380 400 420
NORMAL LOAD IN LBS

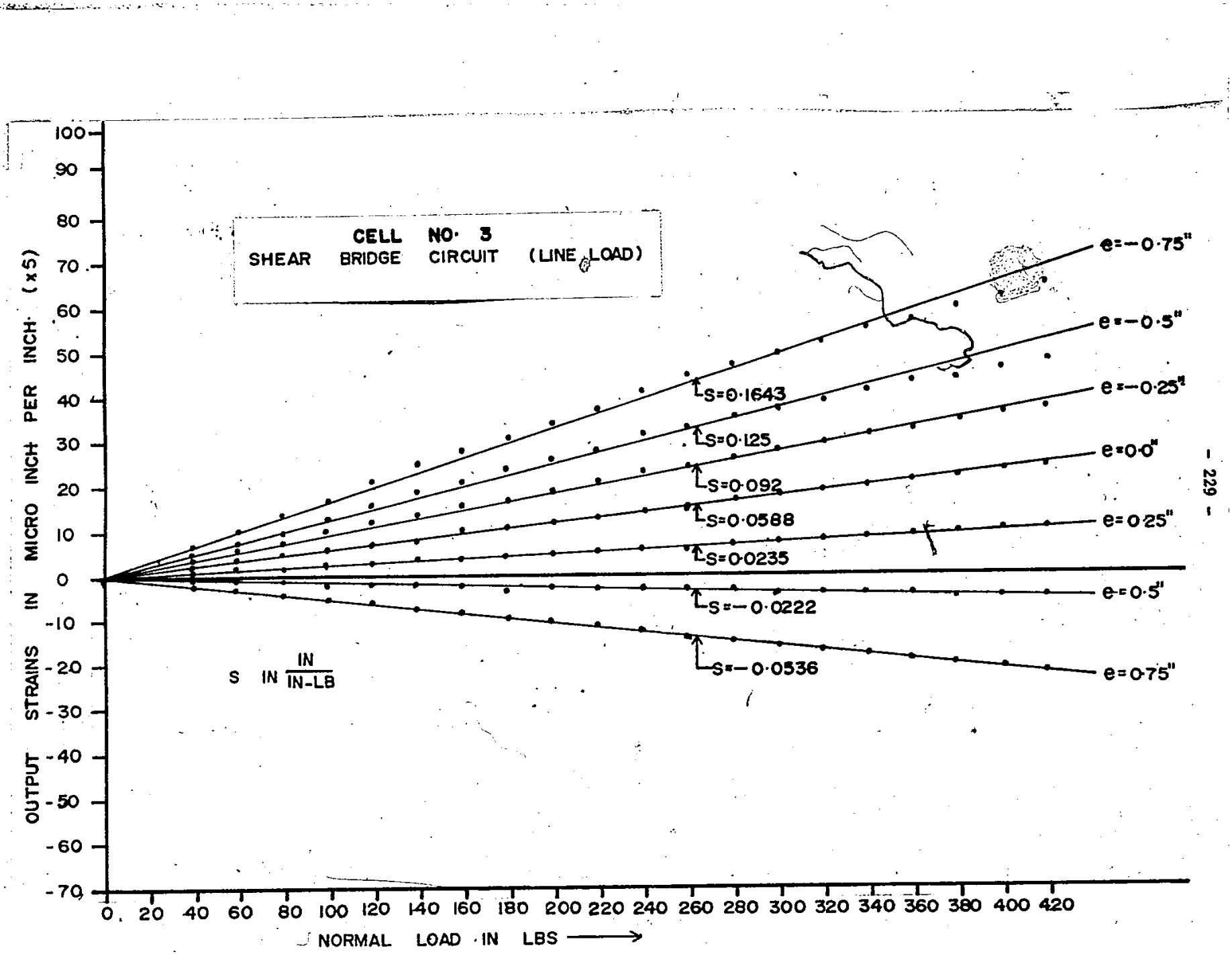
CELL NO. 3
SHEAR BRIDGE CIRCUIT (LINE LOAD)
OUTPUT STRAINS IN MICRO INCH PER INCH (x5)
NORMAL LOAD IN LBS
S IN IN/IN-LB
e=-0.75"
e=-0.5"
e=-0.25"
e=0.0"
e=0.25"
e=0.5"
e=0.75"
S=0.1643
S=0.125
S=0.092
S=0.0588
S=0.0235
S=-0.0222
S=-0.0536
100
90
80
70
60
50
40
30
20
10
0
-10
-20
-30
-40
-50
-60
-70
0 20 40 60 80 100 120 140 160 180 200 220 240 260 280 300 320 340 360 380 400 420

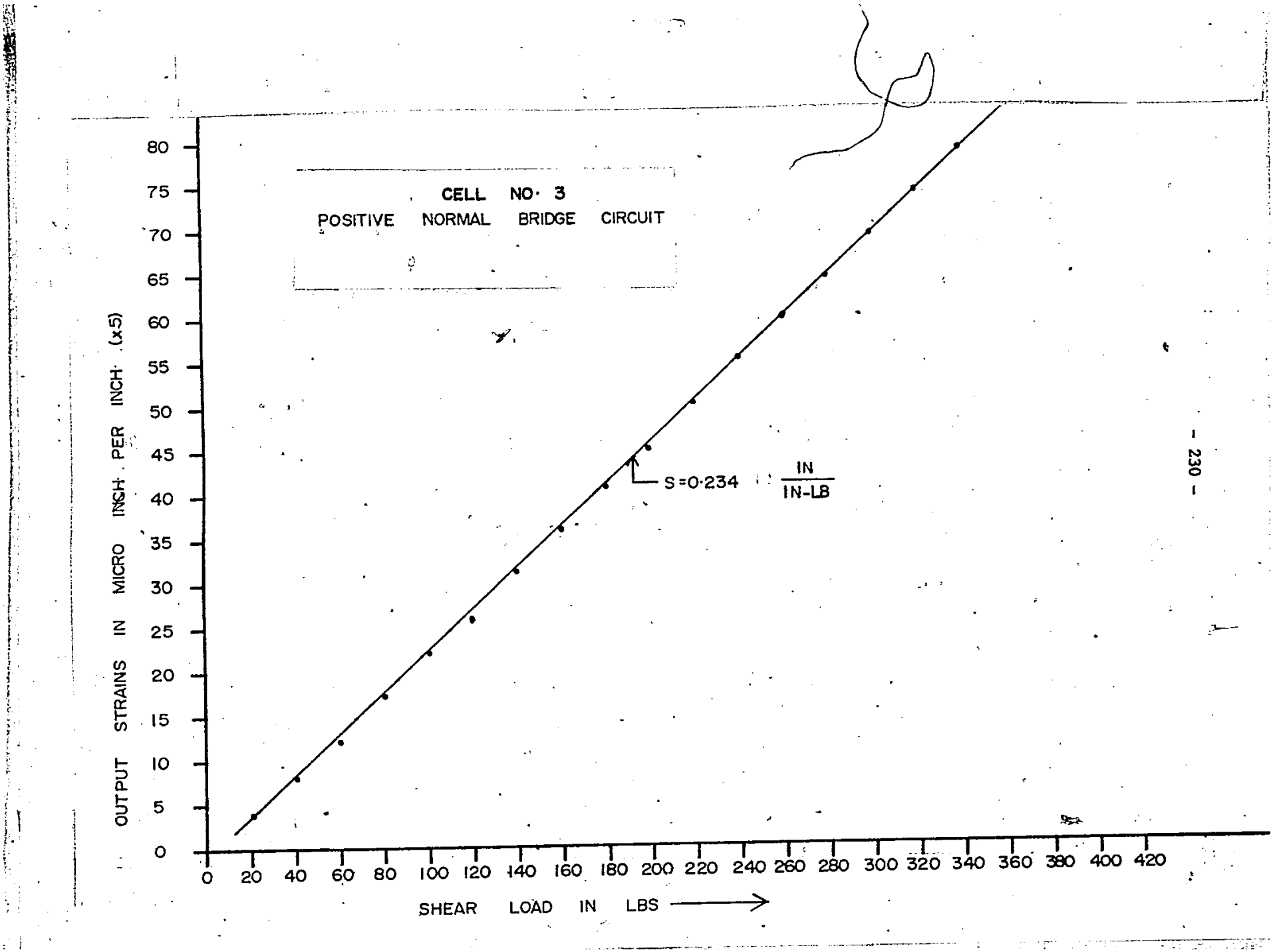
CELL NO. 3
POSITIVE NORMAL BRIDGE CIRCUIT
S=0·234 IN/IN-LB
OUTPUT STRAINS IN MICRO INCH PER INCH (x5)
0 5 10 15 20 25 30 35 40 45 50 55 60 65 70 75 80
0 20 40 60 80 100 120 140 160 180 200 220 240 260 280 300 320 340 360 380 400 420
SHEAR LOAD IN LBS

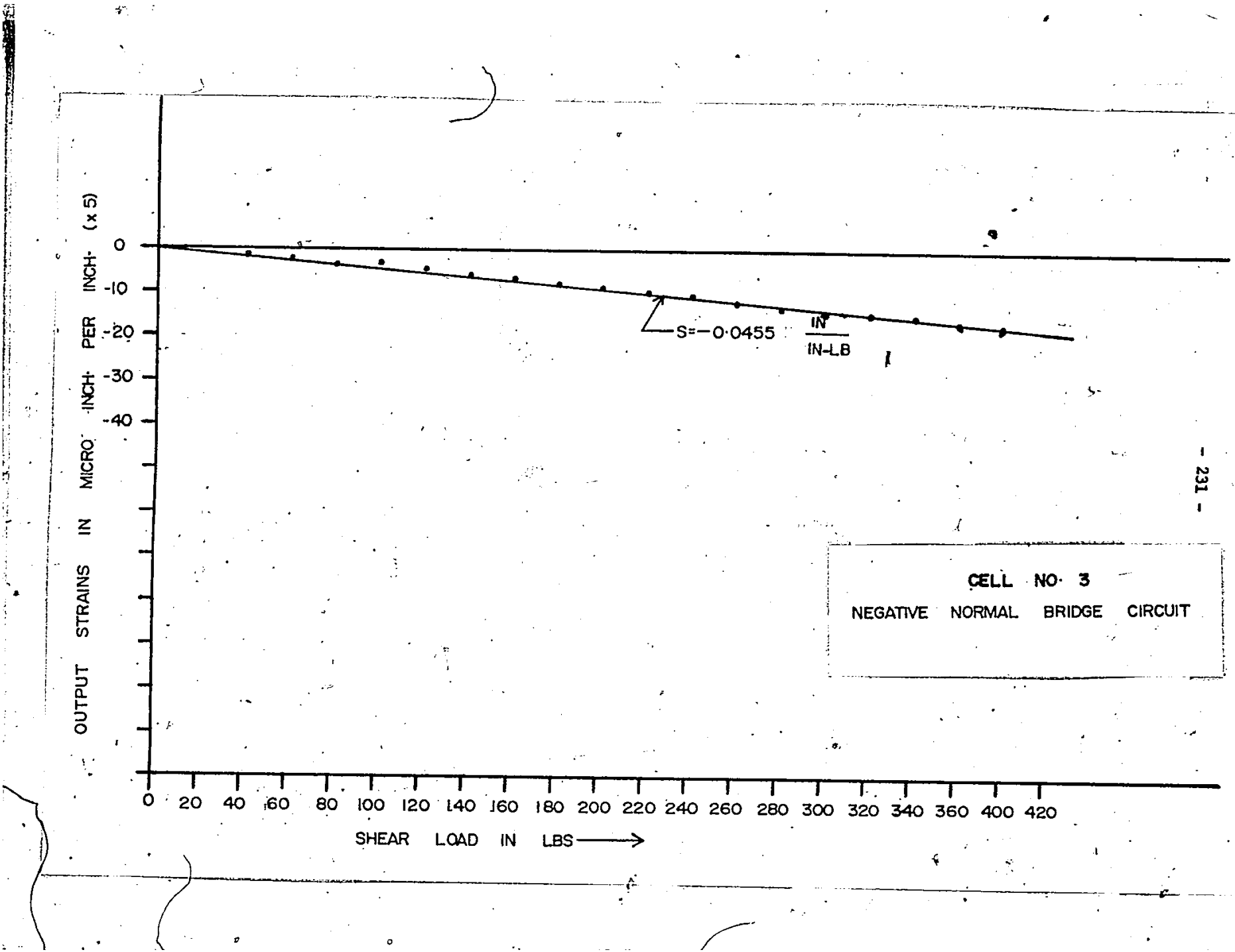
OUTPUT STRAINS IN MICRO INCH PER INCH (x 5)
0
-10
-20
-30
-40
S=-0·0455 IN/IN-LB
0 20 40 60 80 100 120 140 160 180 200 220 240 260 280 300 320 340 360 400 420
SHEAR LOAD IN LBS
CELL NO. 3
NEGATIVE NORMAL BRIDGE CIRCUIT

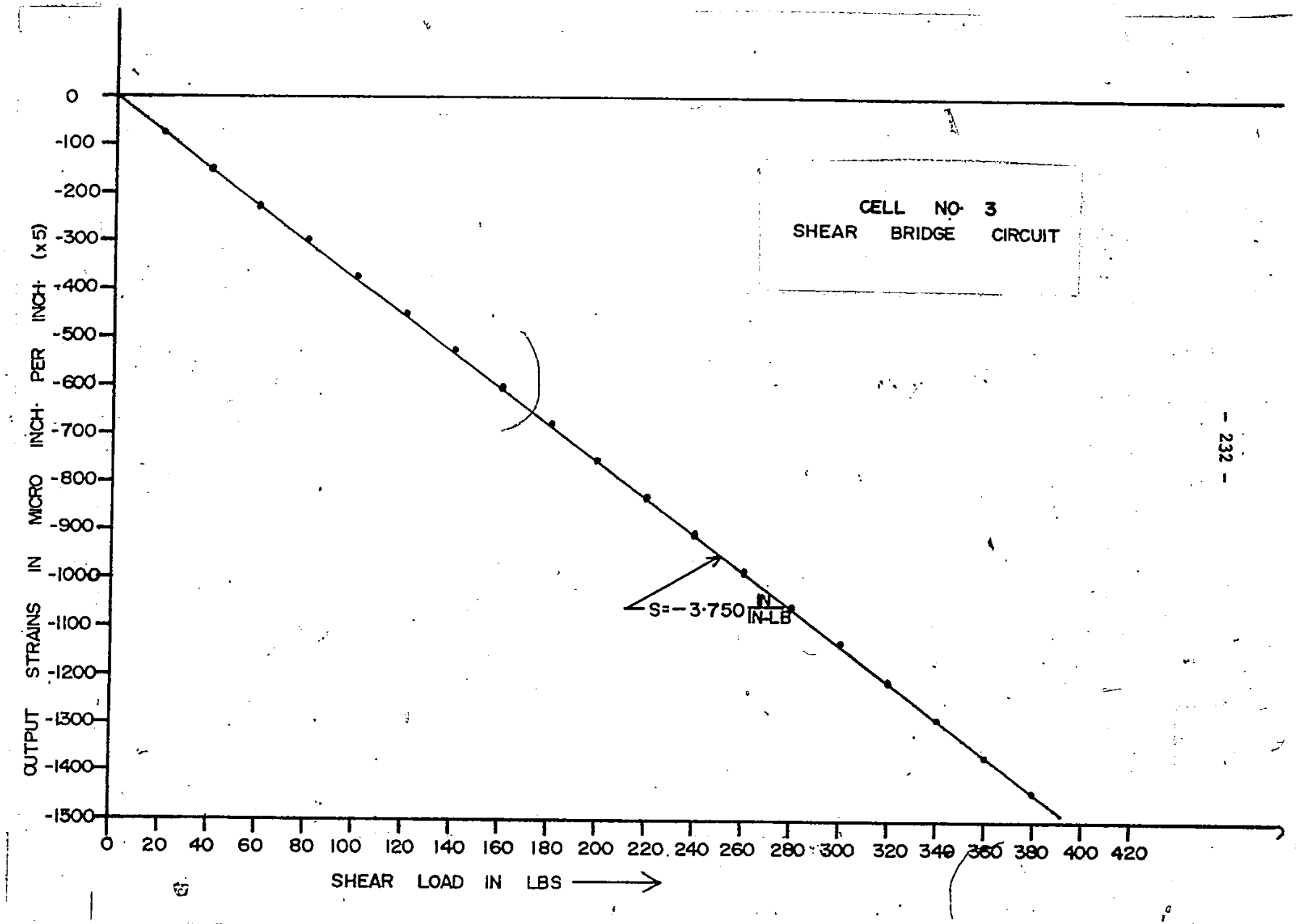
CELL NO. 3
SHEAR BRIDGE CIRCUIT
S=-3·750 μ/IN-LB
OUTPUT STRAINS IN MICRO INCH PER INCH (x5)
0
-100
-200
-300
-400
-500
-600
-700
-800
-900
-1000
-1100
-1200
-1300
-1400
-1500
0 20 40 60 80 100 120 140 160 180 200 220 240 260 280 300 320 340 360 380 400 420
SHEAR LOAD IN LBS

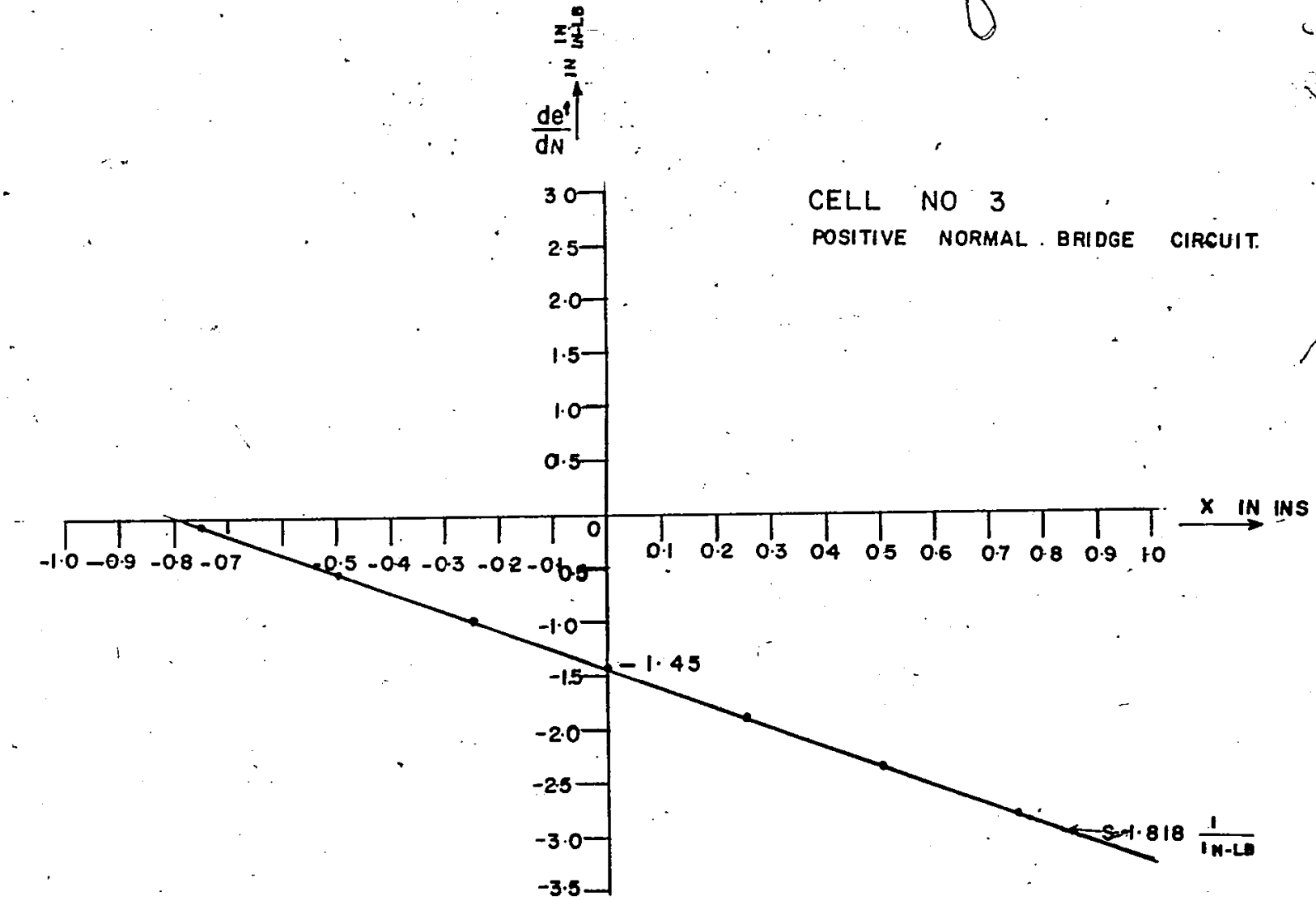
CELL NO 3
POSITIVE NORMAL . BRIDGE CIRCUIT.
$\frac{def}{dN}$ $\frac{IN}{IN-LB}$
X IN INS
3·0
2·5
2·0
1·5
1·0
0·5
0
-0·5
-1·0
-1·5
-2·0
-2·5
-3·0
-3·5
-1·0 -0·9 -0·8 -07
-0·5 -0·4 -0·3 -0·2 -0·1
0·1 0·2 0·3 0·4 0·5 0·6 0·7 0·8 0·9 1·0
-1·45
S=1·818 $\frac{1}{IN-LB}$

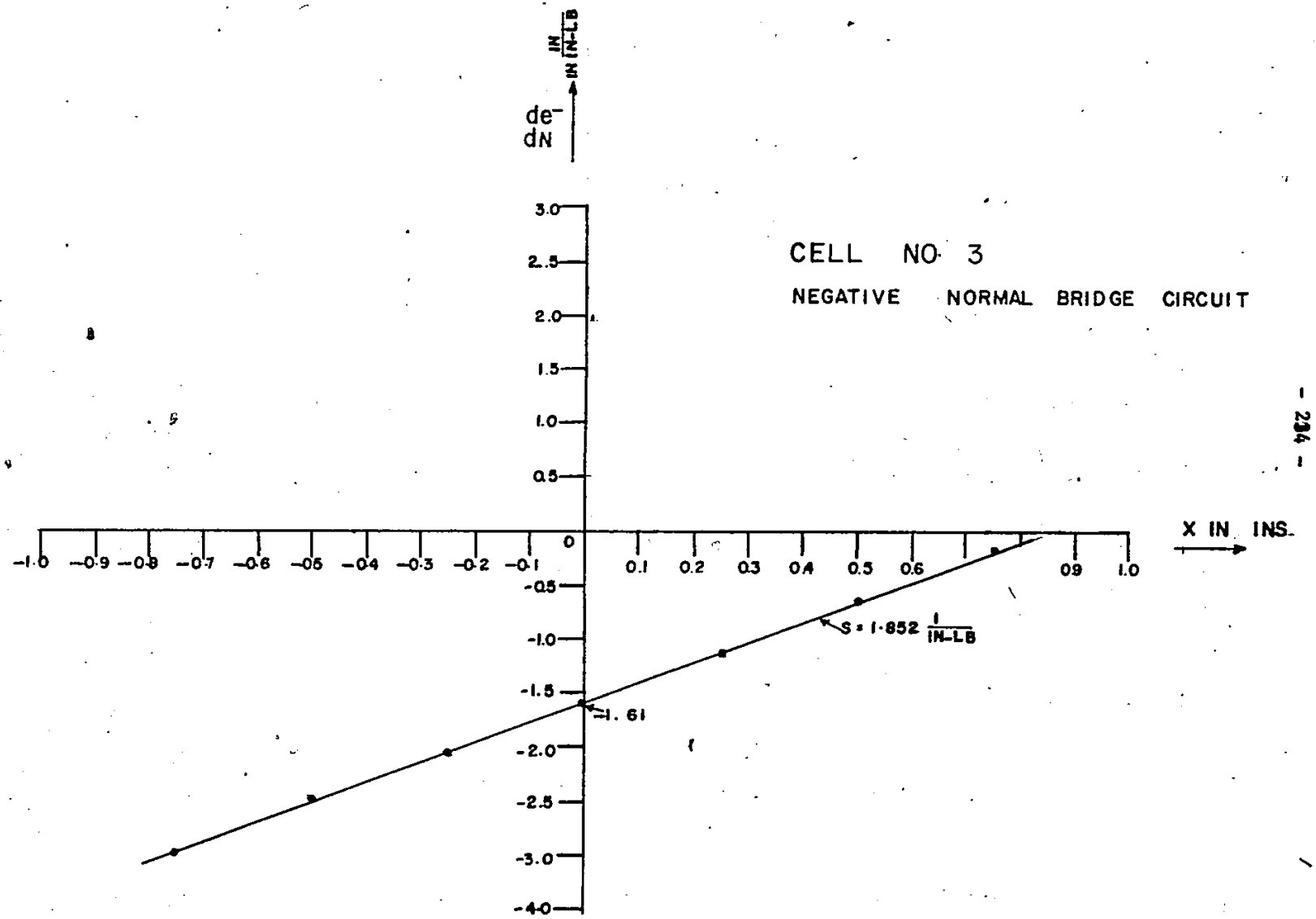
de⁻/dN
IN/IN-LB
CELL NO. 3
NEGATIVE NORMAL BRIDGE CIRCUIT
X IN INS.
3.0
2.5
2.0
1.5
1.0
0.5
0
-0.5
-1.0
-1.5
-2.0
-2.5
-3.0
-4.0
-1.0 -0.9 -0.8 -0.7 -0.6 -0.5 -0.4 -0.3 -0.2 -0.1
0.1 0.2 0.3 0.4 0.5 0.6 0.9 1.0
S = 1·852 1/IN-LB
-1.61

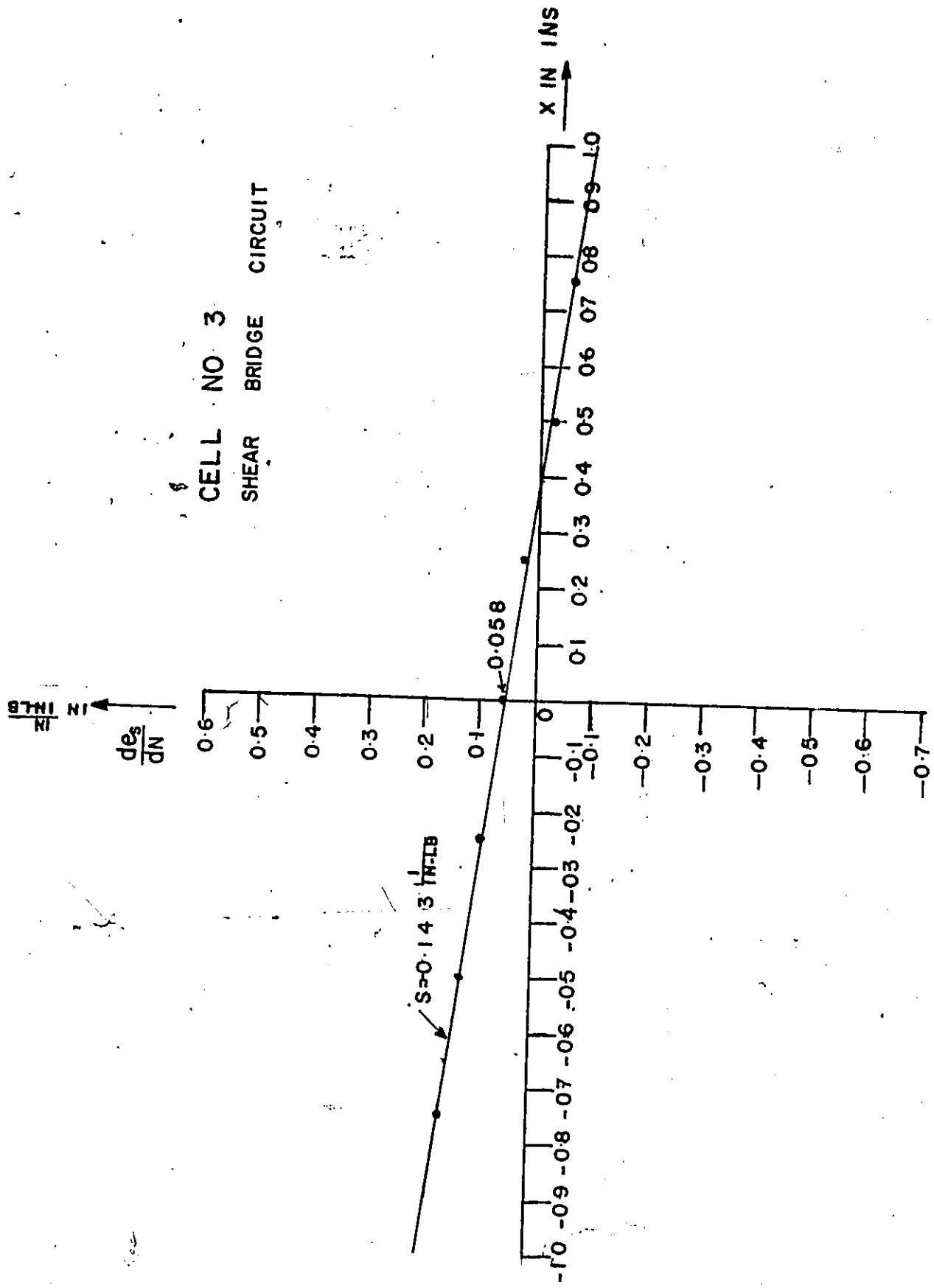
CELL NO 3
SHEAR BRIDGE CIRCUIT
X IN INS
IN / INLB
$\frac{de_s}{dN}$
0·058
S=0·143 IN-LB

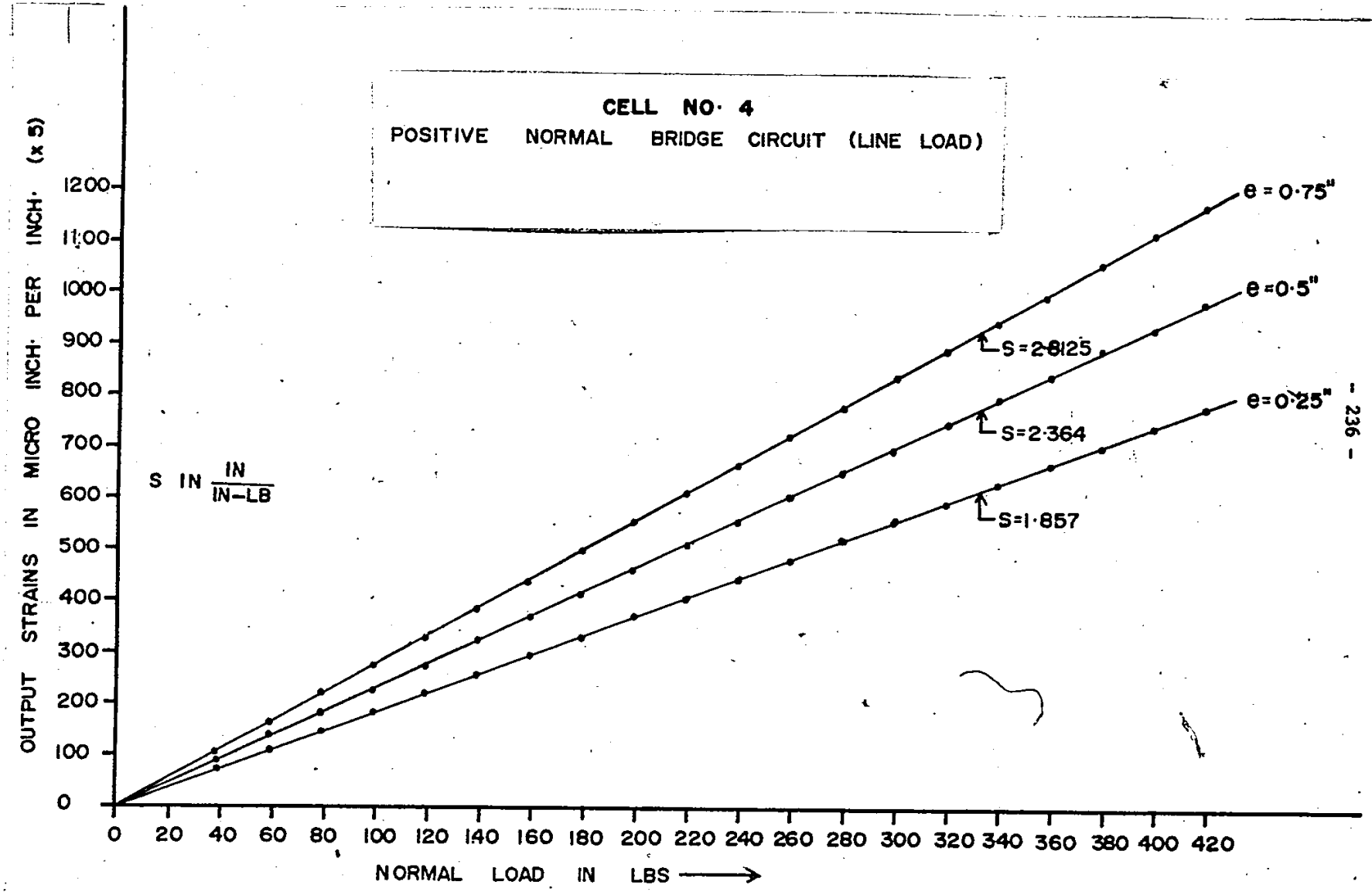
CELL NO· 4
POSITIVE NORMAL BRIDGE CIRCUIT (LINE LOAD)
OUTPUT STRAINS IN MICRO INCH· PER INCH· (x 5)
S IN IN/IN-LB
e = 0·75"
e = 0·5"
e = 0·25"
S = 2·8125
S = 2·364
S = 1·857
0
100
200
300
400
500
600
700
800
900
1000
1100
1200
0 20 40 60 80 100 120 140 160 180 200 220 240 260 280 300 320 340 360 380 400 420
NORMAL LOAD IN LBS

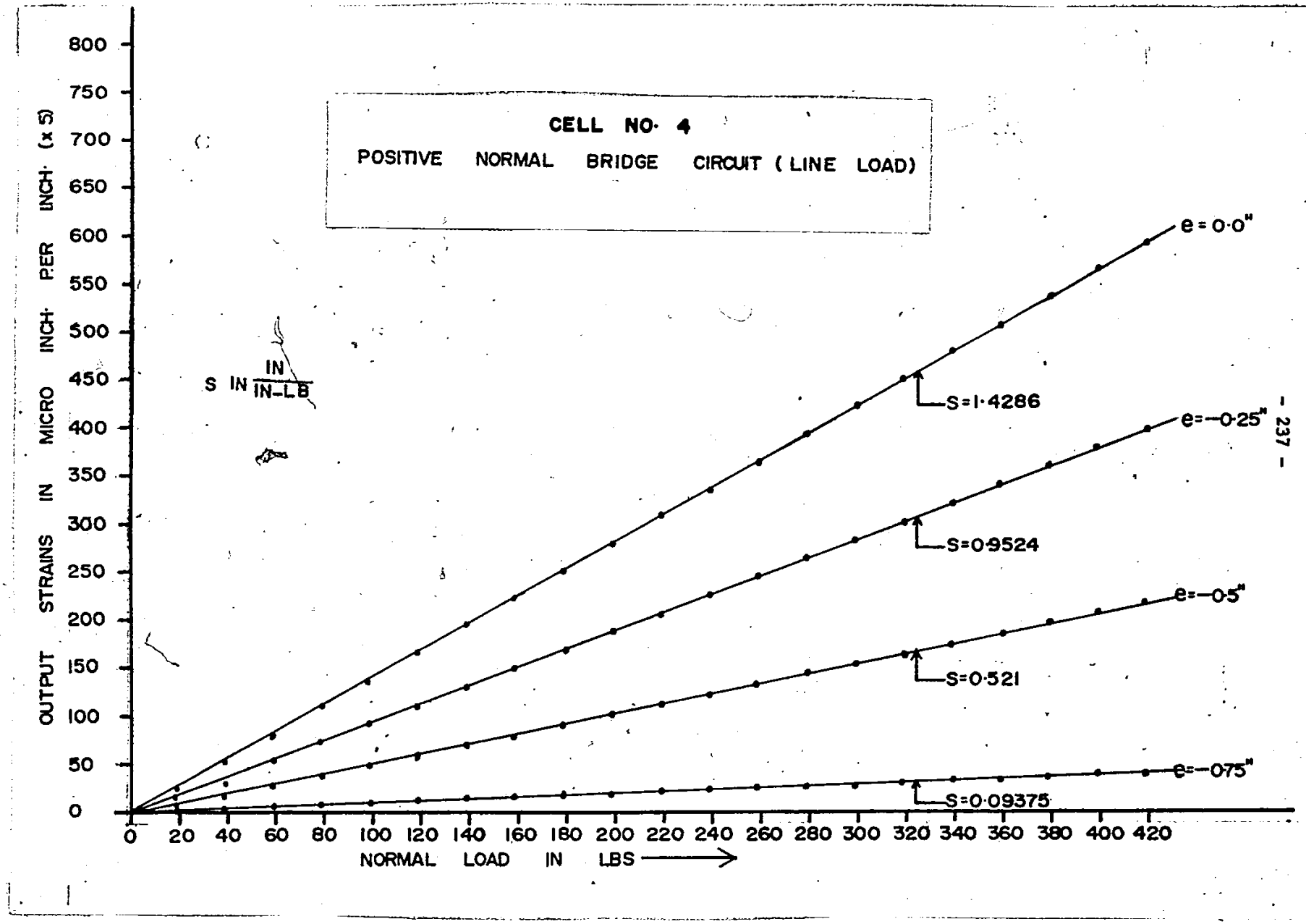
CELL NO. 4
POSITIVE NORMAL BRIDGE CIRCUIT (LINE LOAD)
OUTPUT STRAINS IN MICRO INCH PER INCH (x S)
S IN IN/IN-LB
800
750
700
650
600
550
500
450
400
350
300
250
200
150
100
50
0
0 20 40 60 80 100 120 140 160 180 200 220 240 260 280 300 320 340 360 380 400 420
NORMAL LOAD IN LBS
e = 0·0"
S=1·4286
e=-0·25"
S=0·9524
e=-0·5"
S=0·521
e=-075"
S=0·09375

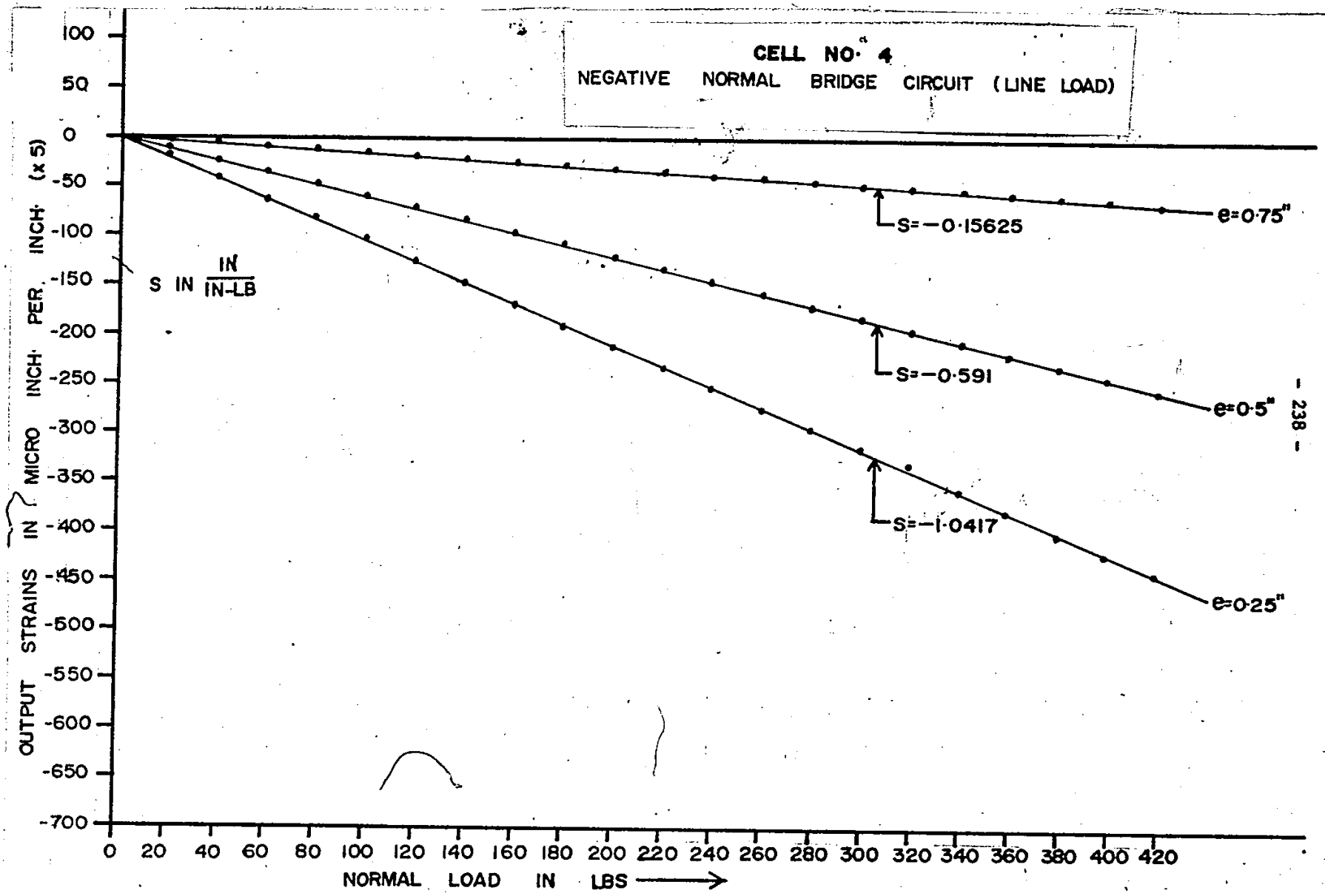
CELL NO. 4
NEGATIVE NORMAL BRIDGE CIRCUIT (LINE LOAD)
S IN IN/IN-LB
S=-0·15625
S=-0·591
S=-1·0417
e=0·75"
e=0·5"
e=0·25"
OUTPUT STRAINS IN MICRO INCH PER INCH (x 5)
NORMAL LOAD IN LBS
100
50
0
-50
-100
-150
-200
-250
-300
-350
-400
-450
-500
-550
-600
-650
-700
0 20 40 60 80 100 120 140 160 180 200 220 240 260 280 300 320 340 360 380 400 420

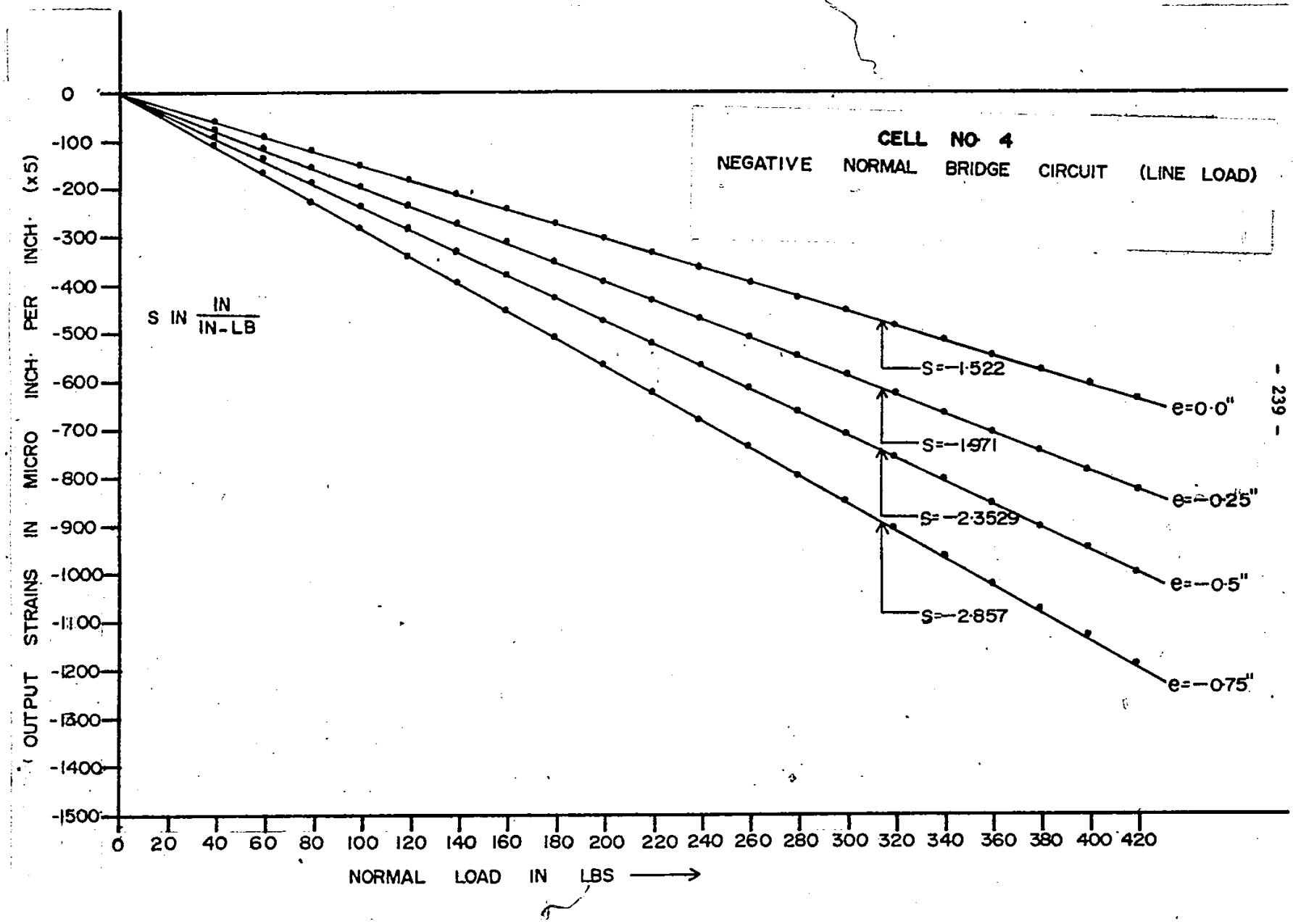
CELL NO 4
NEGATIVE NORMAL BRIDGE CIRCUIT (LINE LOAD)
S IN IN/IN-LB
S=-1·522
S=-1·971
S=-2·3529
S=-2·857
e=0·0"
e=-0·25"
e=-0·5"
e=-0·75"
OUTPUT STRAINS IN MICRO INCH PER INCH (x5)
0
-100
-200
-300
-400
-500
-600
-700
-800
-900
-1000
-1100
-1200
-1300
-1400
-1500
0 20 40 60 80 100 120 140 160 180 200 220 240 260 280 300 320 340 360 380 400 420
NORMAL LOAD IN LBS

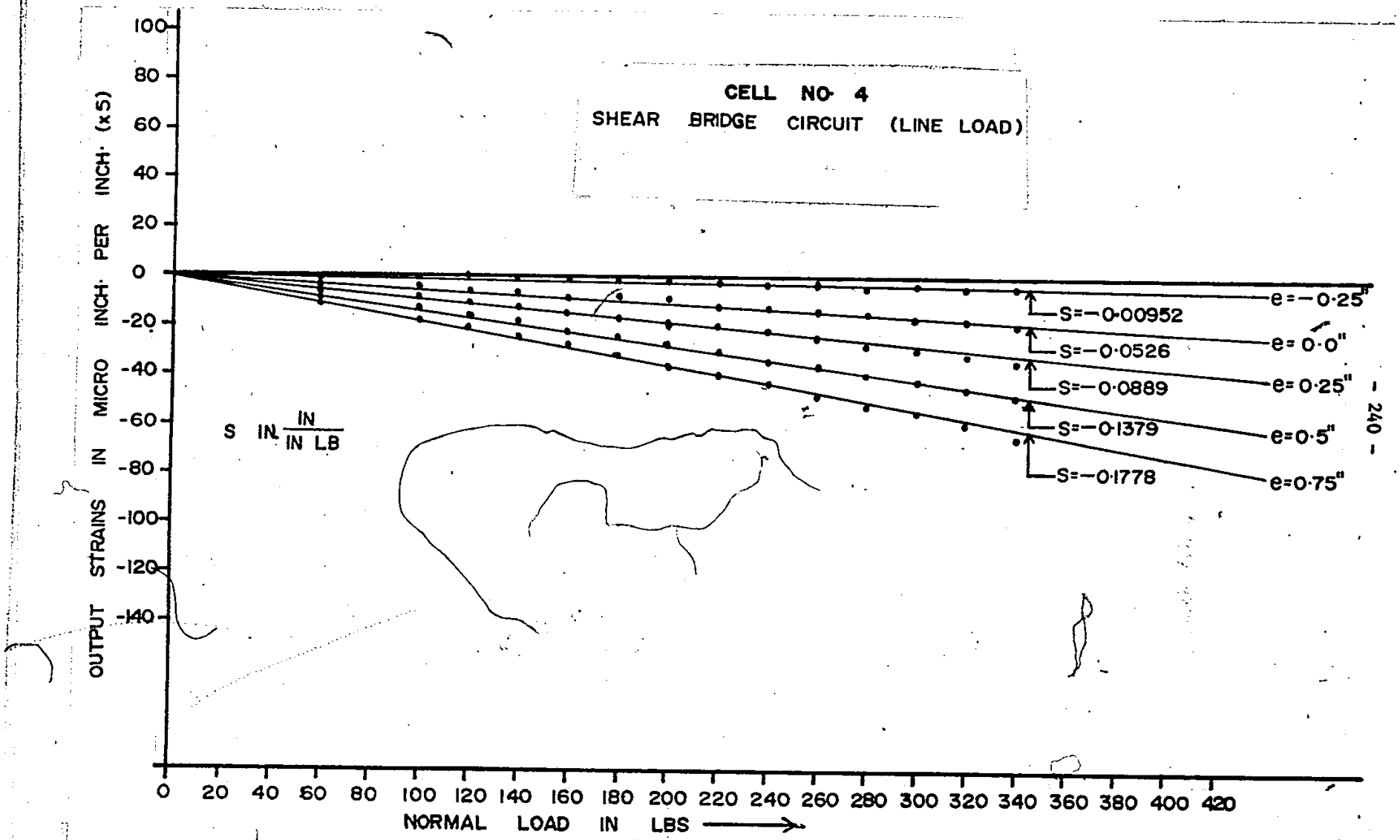
CELL NO. 4
SHEAR BRIDGE CIRCUIT (LINE LOAD)
OUTPUT STRAINS IN MICRO INCH PER INCH (x5)
100
80
60
40
20
0
-20
-40
-60
-80
-100
-120
-140
S IN $\frac{IN}{IN\ LB}$
S=-0·00952
S=-0·0526
S=-0·0889
S=-0·1379
S=-0·1778
e=-0·25"
e=0·0"
e=0·25"
e=0·5"
e=0·75"
0 20 40 60 80 100 120 140 160 180 200 220 240 260 280 300 320 340 360 380 400 420
NORMAL LOAD IN LBS

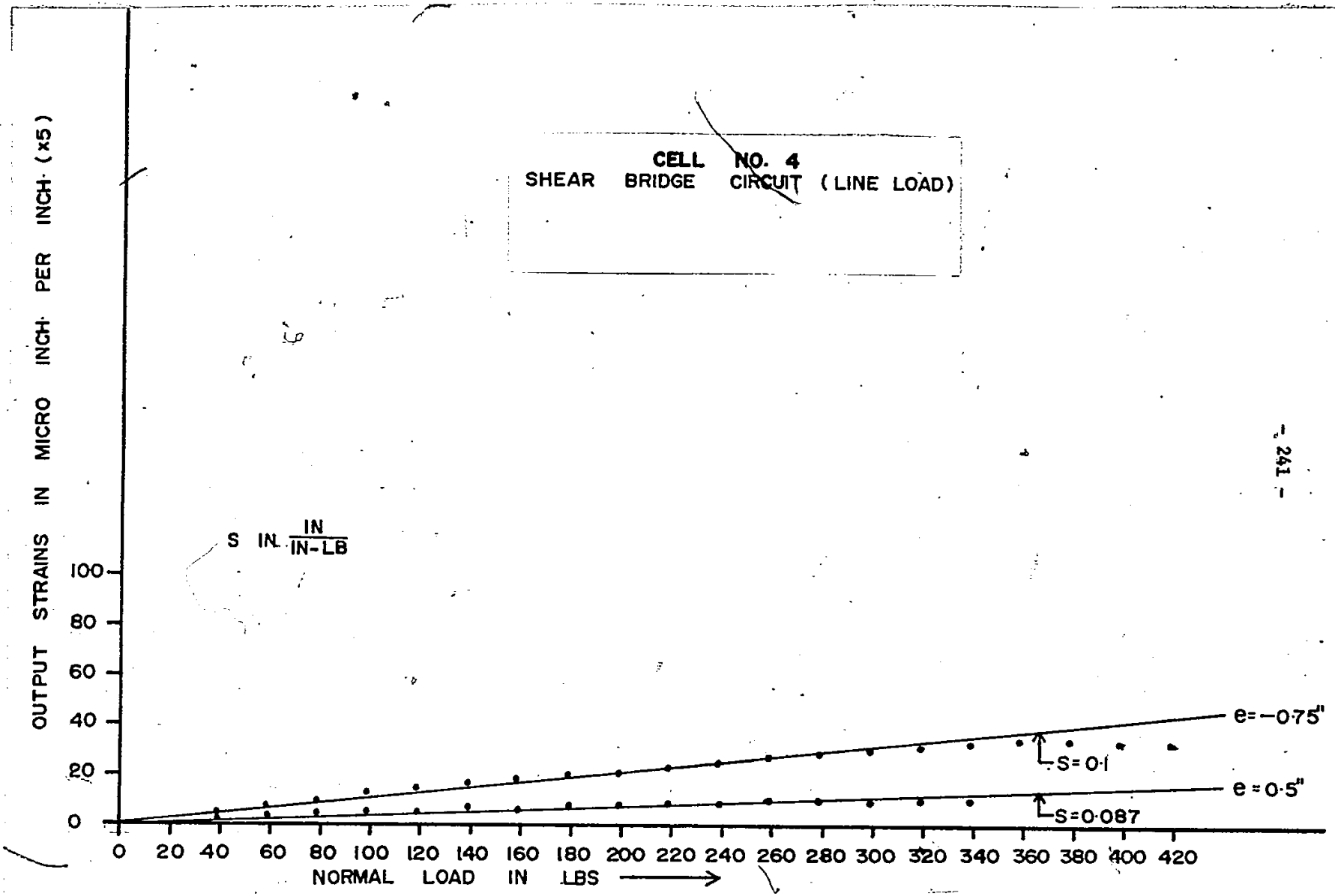
CELL NO. 4
SHEAR BRIDGE CIRCUIT (LINE LOAD)
OUTPUT STRAINS IN MICRO INCH PER INCH (x5)
S IN IN/IN-LB
100
80
60
40
20
0
0 20 40 60 80 100 120 140 160 180 200 220 240 260 280 300 320 340 360 380 400 420
NORMAL LOAD IN LBS
e=-0.75"
S=0.1
e=0.5"
S=0.087

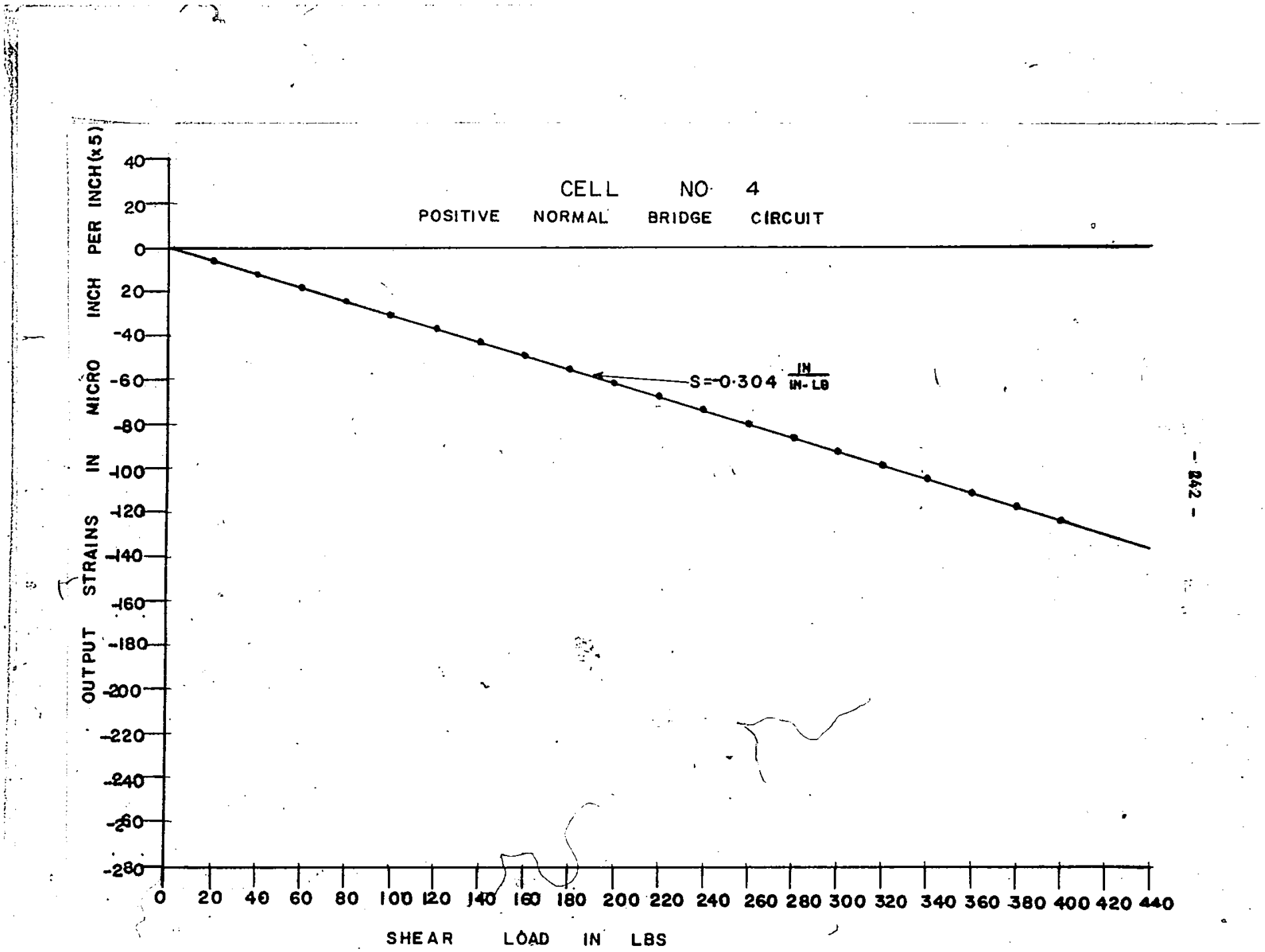
CELL NO 4
POSITIVE NORMAL BRIDGE CIRCUIT
OUTPUT STRAINS IN MICRO INCH PER INCH(x5)
40
20
0
-20
-40
-60
-80
-100
-120
-140
-160
-180
-200
-220
-240
-260
-280
S=-0·304 IN/IN-LB
0 20 40 60 80 100 120 140 160 180 200 220 240 260 280 300 320 340 360 380 400 420 440
SHEAR LOAD IN LBS

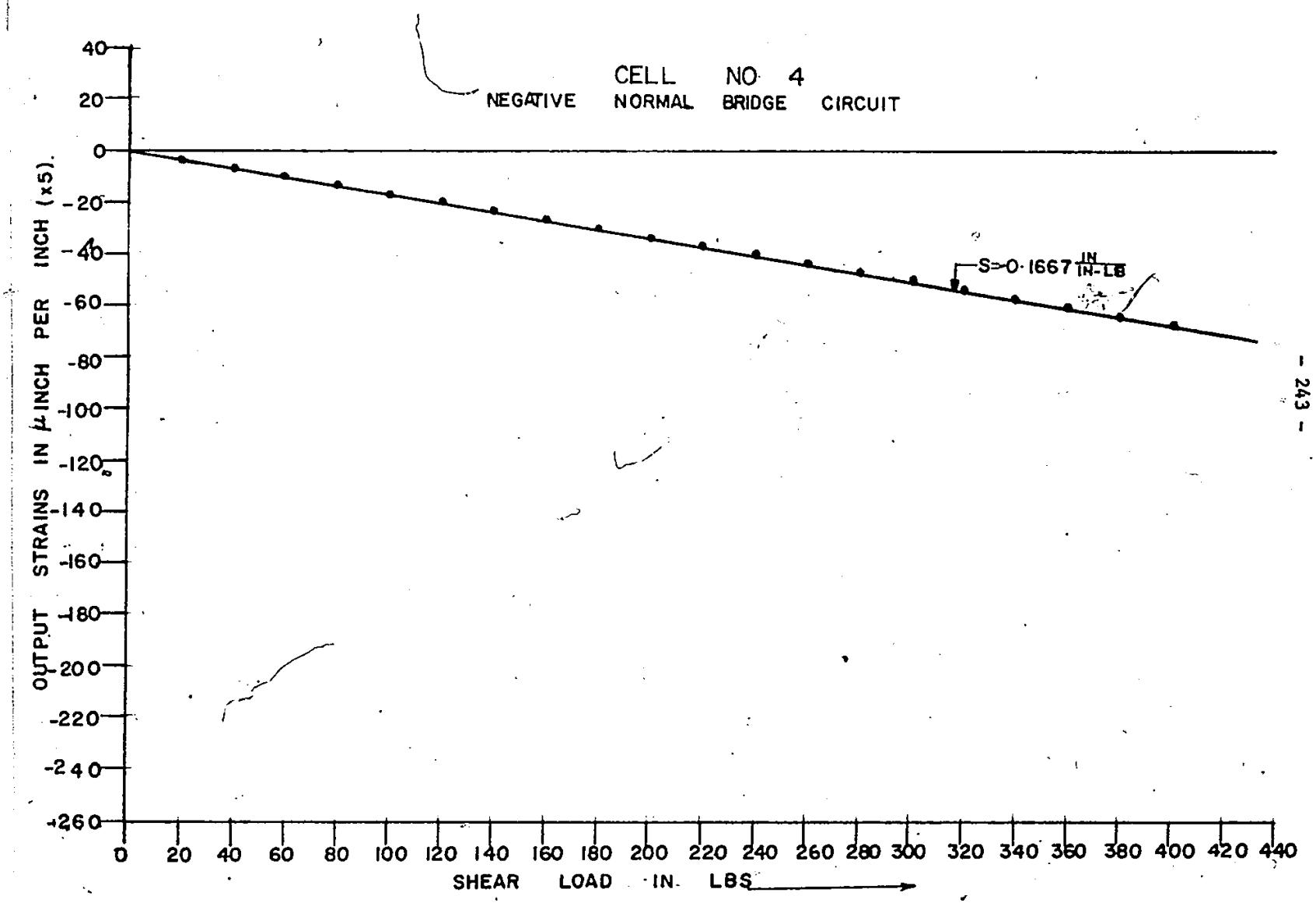
CELL NO 4
NEGATIVE NORMAL BRIDGE CIRCUIT
S=0·1667 IN/IN-LB
OUTPUT STRAINS IN μINCH PER INCH (x5).
40
20
0
-20
-40
-60
-80
-100
-120
-140
-160
-180
-200
-220
-240
-260
0 20 40 60 80 100 120 140 160 180 200 220 240 260 280 300 320 340 360 380 400 420 440
SHEAR LOAD IN LBS

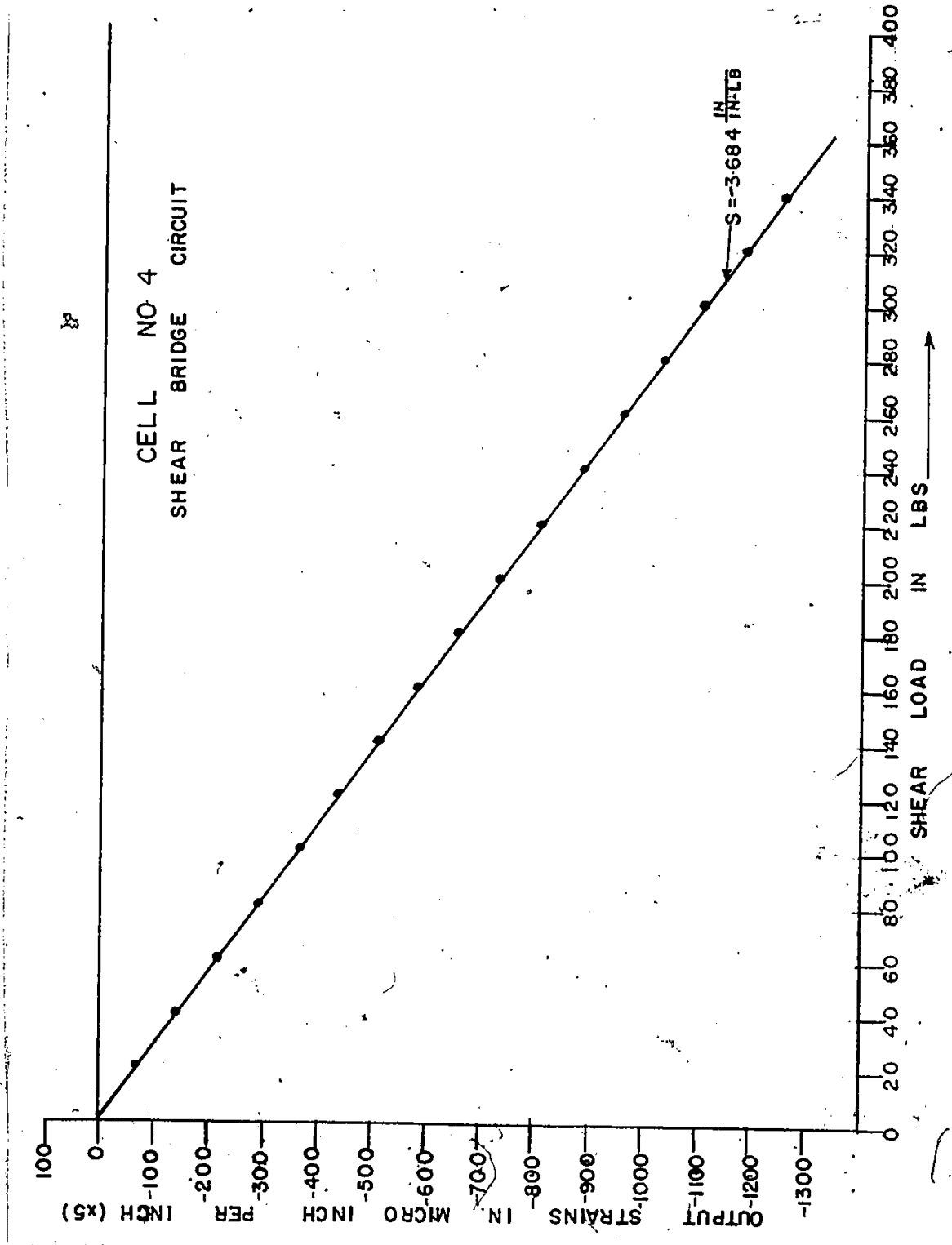
CELL NO 4
SHEAR BRIDGE CIRCUIT
S = -3.684 IN/IN-LB
OUTPUT STRAINS IN MICRO INCH PER INCH (x5)
SHEAR LOAD IN LBS
100
0
-100
-200
-300
-400
-500
-600
-700
-800
-900
-1000
-1100
-1200
-1300
0
20
40
60
80
100
120
140
160
180
200
220
240
260
280
300
320
340
360
380
400

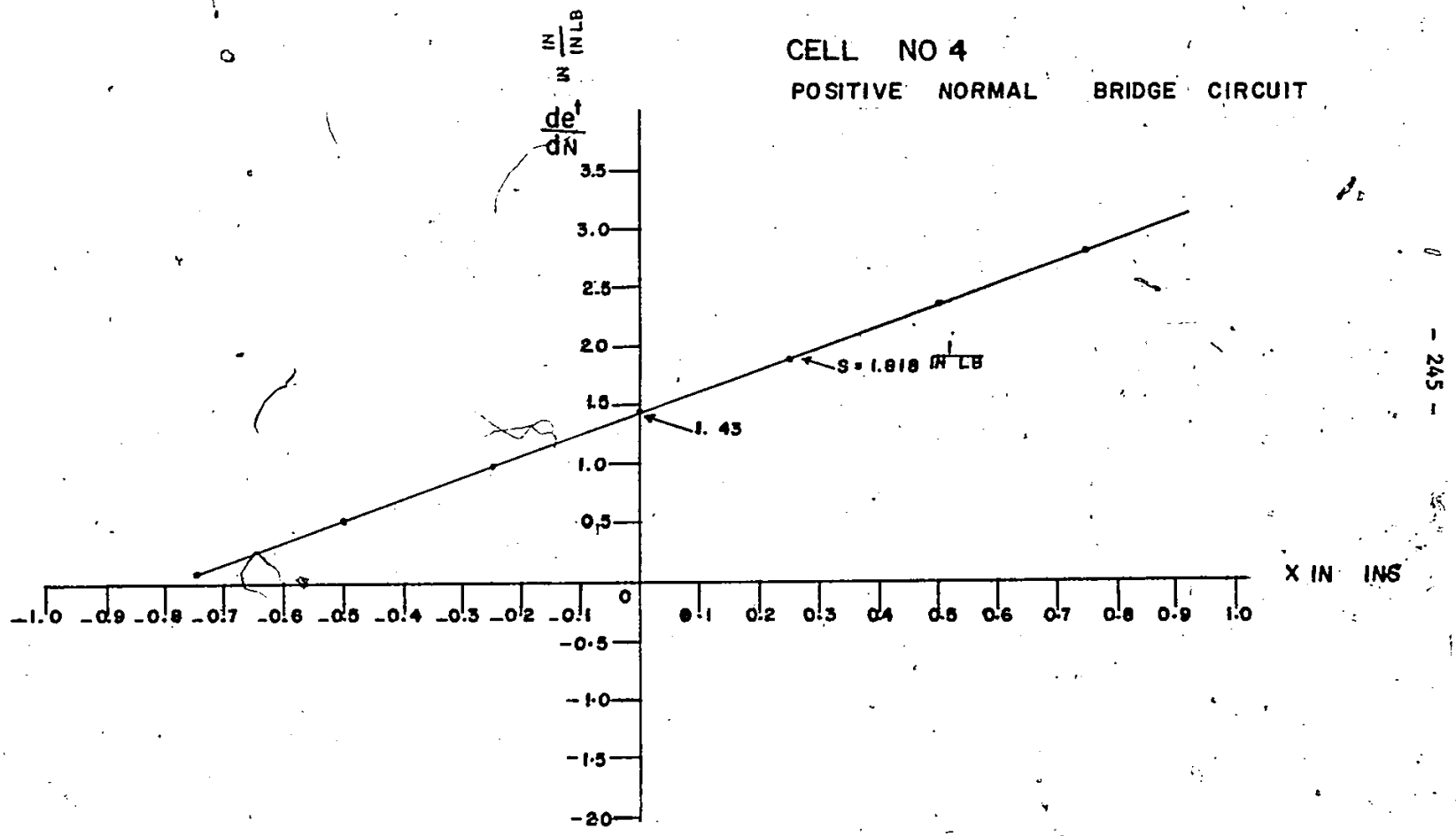
CELL NO 4
POSITIVE NORMAL BRIDGE CIRCUIT
$\frac{de'}{dN}$ $\frac{IN}{IN\,LB}$
3.5
3.0
2.5
2.0
1.5
1.0
0.5
0
-0.5
-1.0
-1.5
-2.0
S = 1.818 $\frac{IN}{IN\,LB}$
1.43
-1.0 -0.9 -0.8 -0.7 -0.6 -0.5 -0.4 -0.3 -0.2 -0.1
0.1 0.2 0.3 0.4 0.5 0.6 0.7 0.8 0.9 1.0
X IN INS

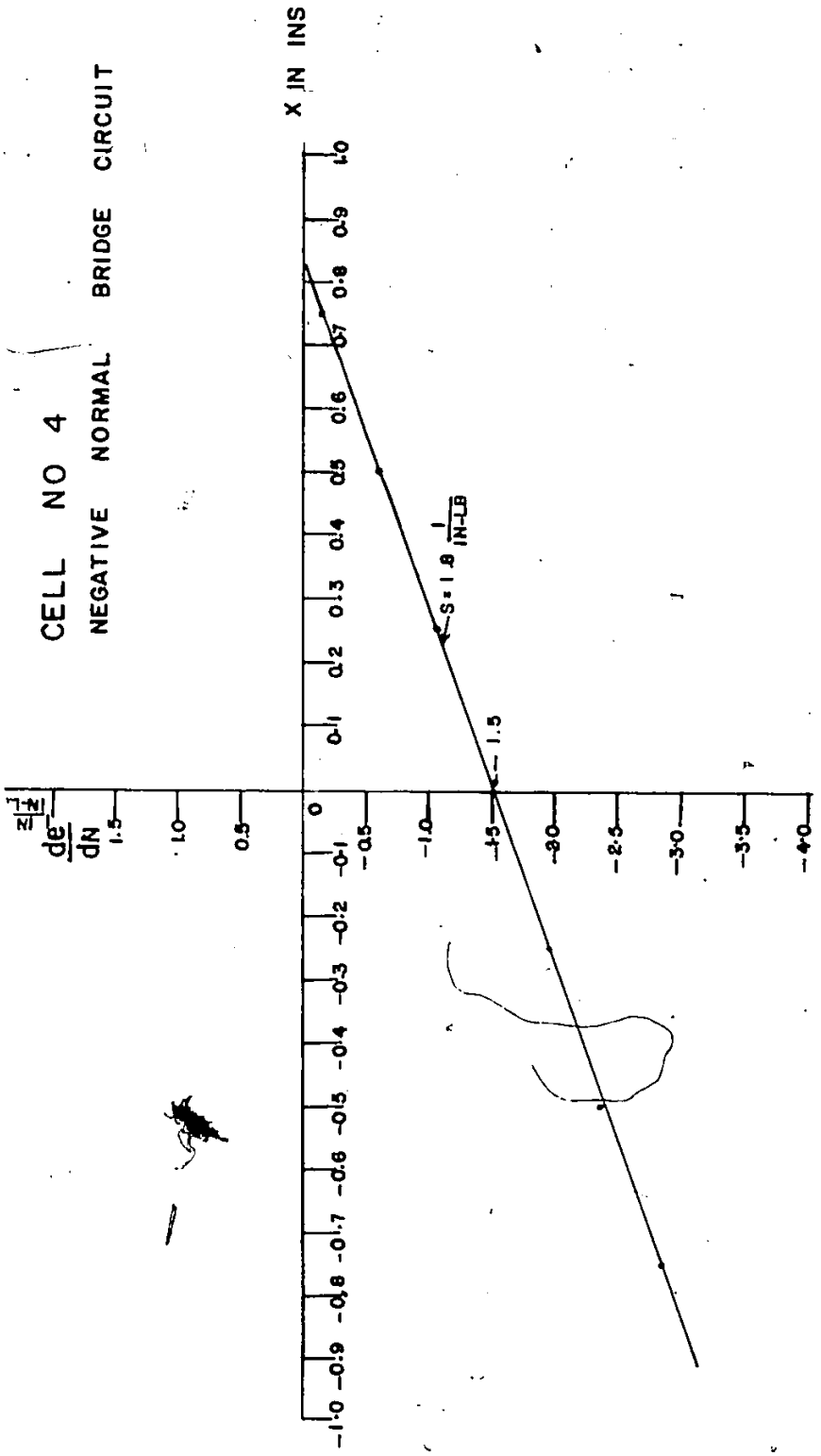
CELL NO 4
NEGATIVE NORMAL BRIDGE CIRCUIT
X IN INS
S = 1.8 1/IN-LB
1.5
de/dN

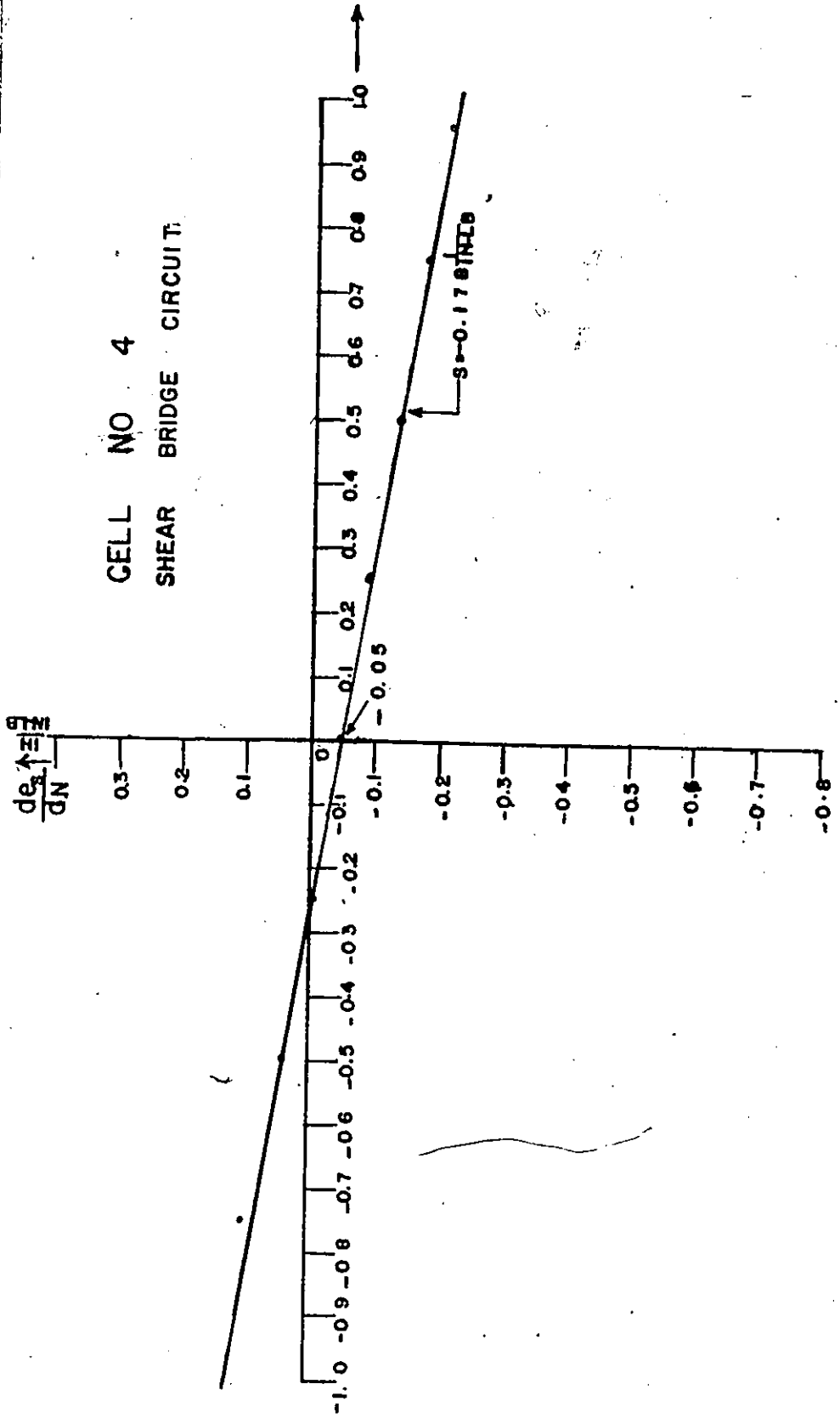
CELL NO 4
SHEAR BRIDGE CIRCUIT
S=-0.178 INCH
-0.05
$\frac{de_s}{dN}$ 수직변형률

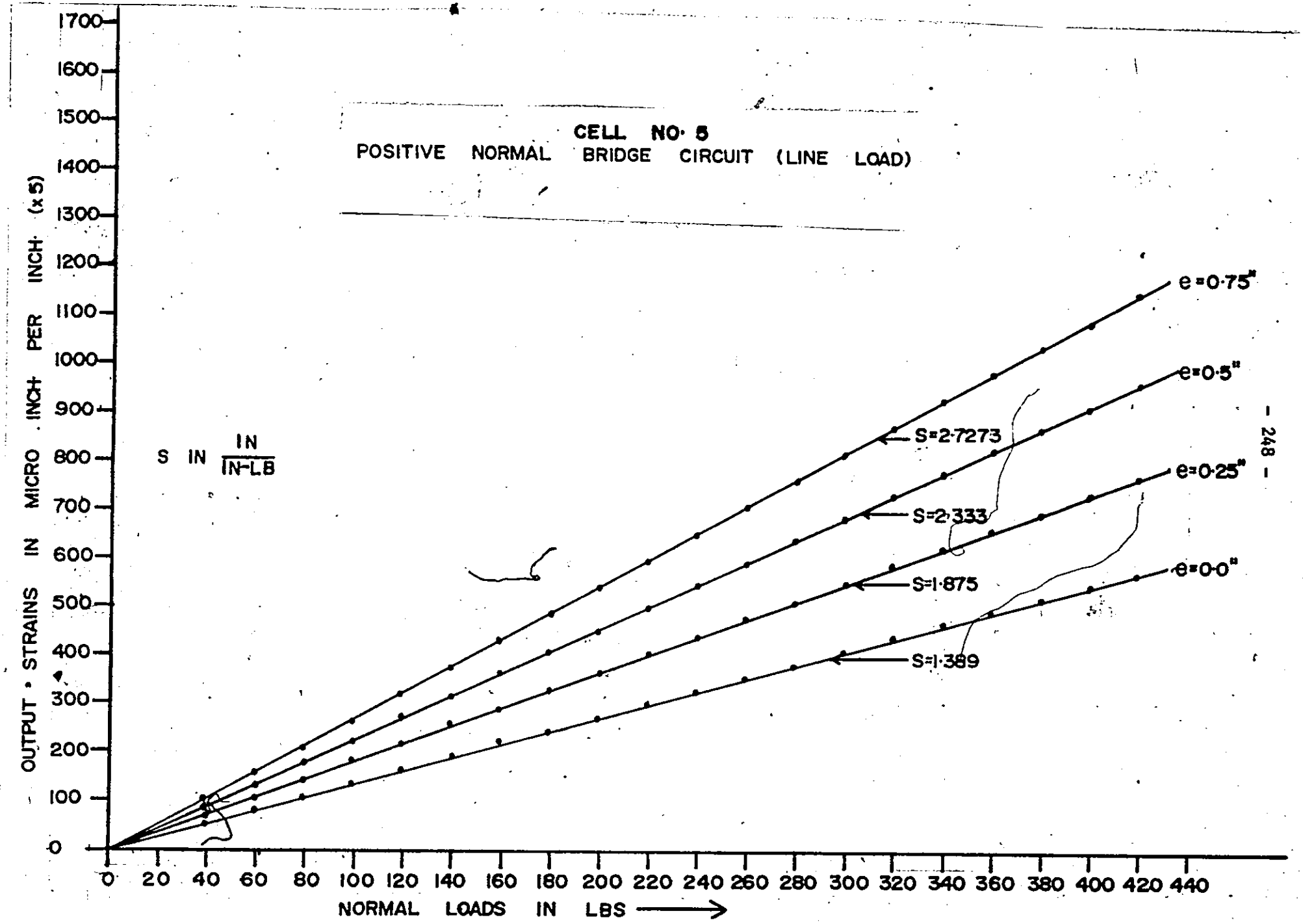
CELL NO. 5
POSITIVE NORMAL BRIDGE CIRCUIT (LINE LOAD)
OUTPUT - STRAINS IN MICRO INCH PER INCH (x5)
1700
1600
1500
1400
1300
1200
1100
1000
900
800
700
600
500
400
300
200
100
0
S IN IN/IN-LB
e=0·75"
e=0·5"
e=0·25"
e=0·0"
S=2·7273
S=2·333
S=1·875
S=1·389
0 20 40 60 80 100 120 140 160 180 200 220 240 260 280 300 320 340 360 380 400 420 440
NORMAL LOADS IN LBS
- 248 -

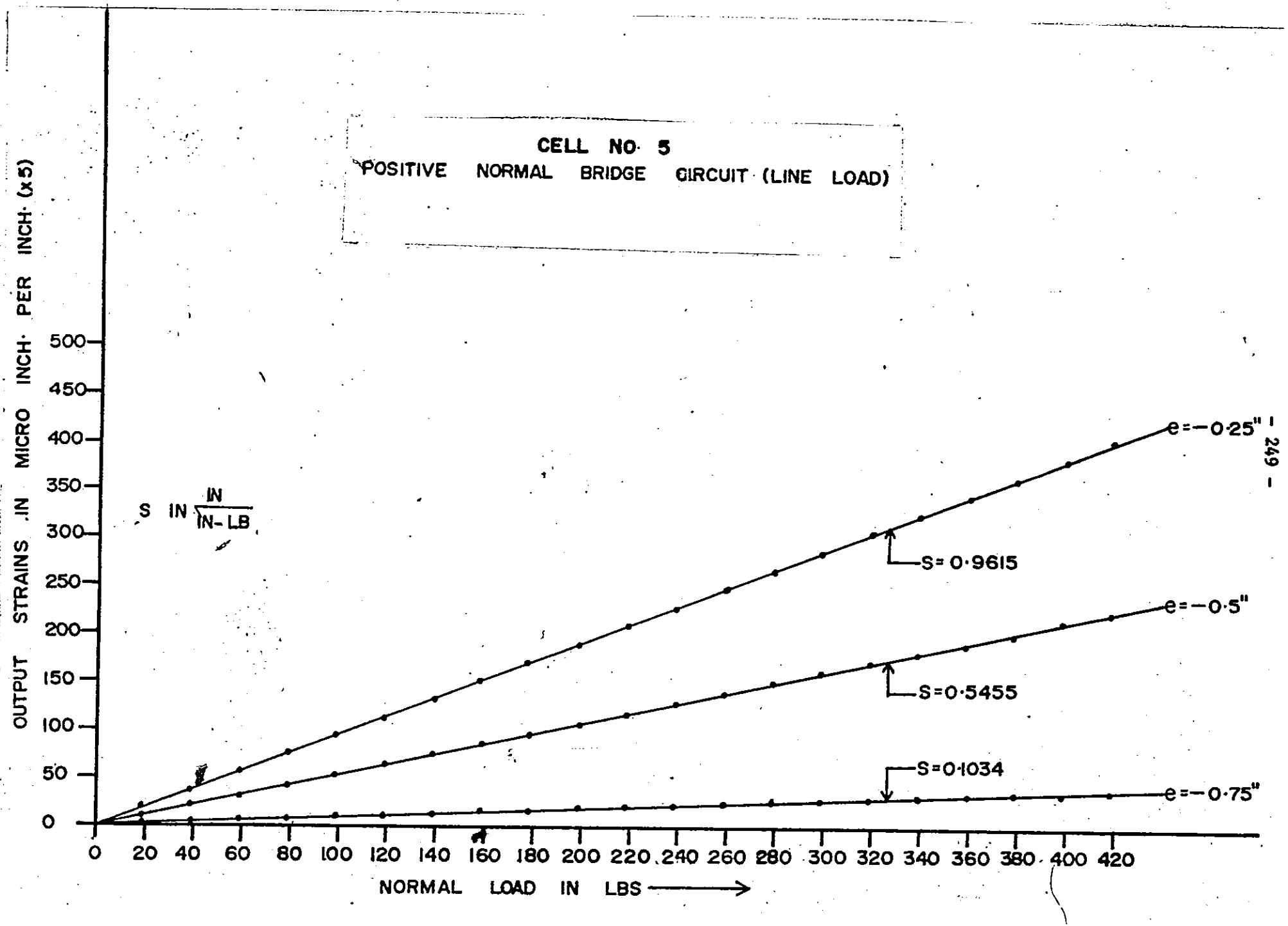
CELL NO. 5
POSITIVE NORMAL BRIDGE CIRCUIT (LINE LOAD)
OUTPUT STRAINS IN MICRO INCH PER INCH (x5)
S IN IN/IN-LB
500
450
400
350
300
250
200
150
100
50
0
0 20 40 60 80 100 120 140 160 180 200 220 240 260 280 300 320 340 360 380 400 420
NORMAL LOAD IN LBS
e=-0.25"
S=0.9615
e=-0.5"
S=0.5455
S=0.1034
e=-0.75"

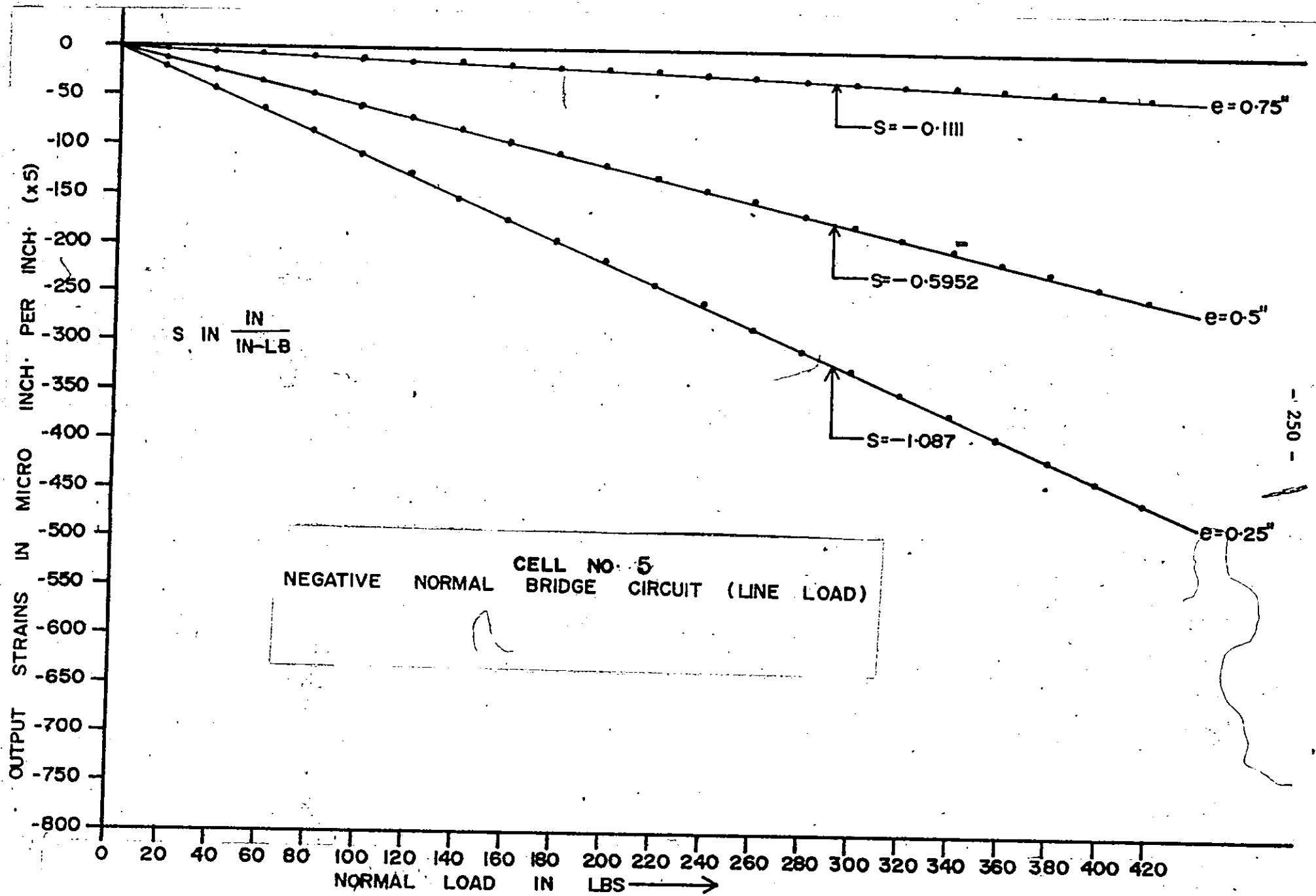
OUTPUT STRAINS IN MICRO INCH PER INCH (x5)
0
-50
-100
-150
-200
-250
-300
-350
-400
-450
-500
-550
-600
-650
-700
-750
-800
S IN IN / IN-LB
e=0.75"
S=-0.1111
e=0.5"
S=-0.5952
e=0.25"
S=-1.087
CELL NO. 5
NEGATIVE NORMAL BRIDGE CIRCUIT (LINE LOAD)
0 20 40 60 80 100 120 140 160 180 200 220 240 260 280 300 320 340 360 380 400 420
NORMAL LOAD IN LBS

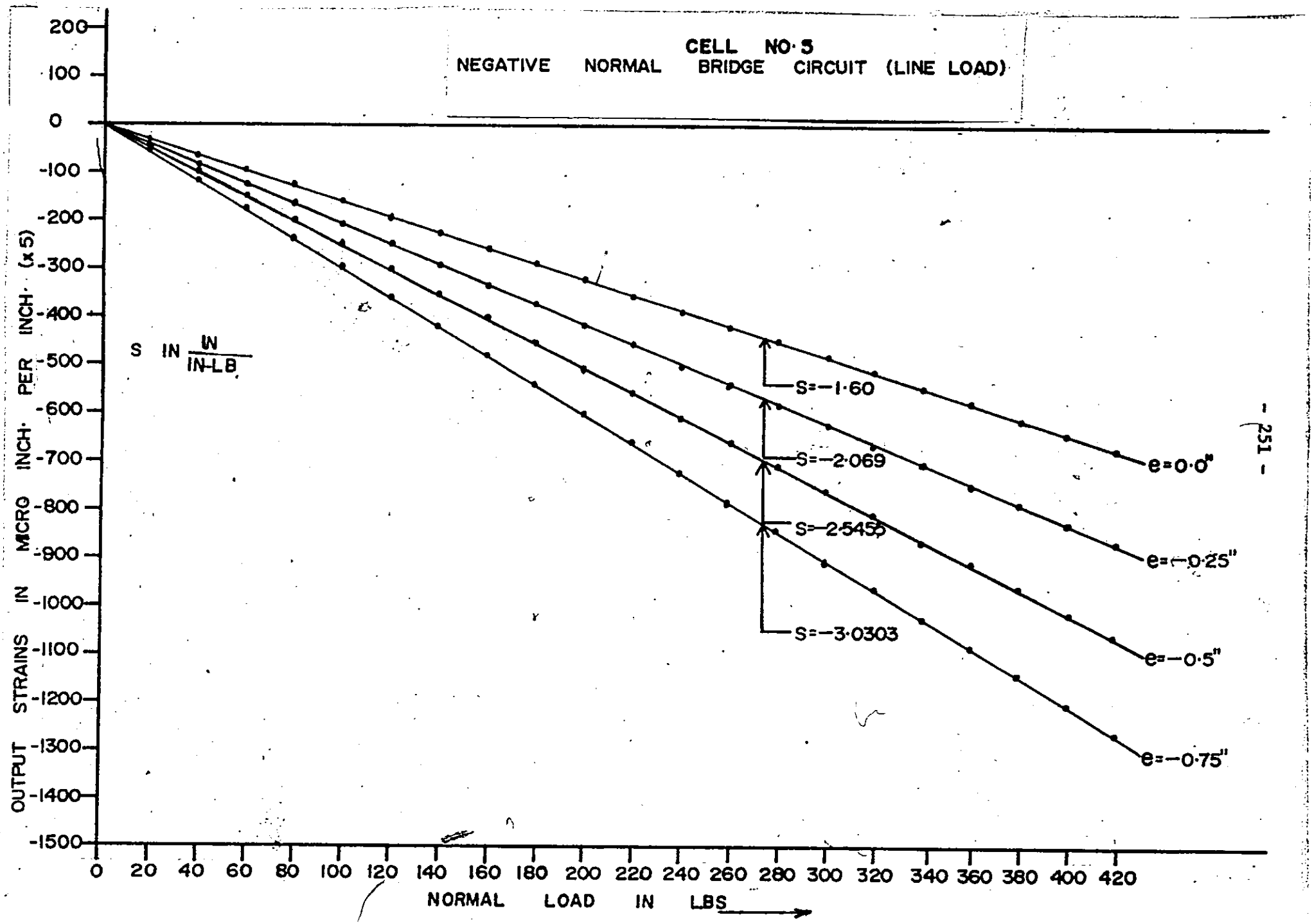
CELL NO·5
NEGATIVE NORMAL BRIDGE CIRCUIT (LINE LOAD)
OUTPUT STRAINS IN MICRO INCH PER INCH (x5)
S IN IN/IN-LB
S=-1·60
S=-2·069
S=-2·5455
S=-3·0303
e=0·0"
e=-0·25"
e=-0·5"
e=-0·75"
NORMAL LOAD IN LBS
200
100
0
-100
-200
-300
-400
-500
-600
-700
-800
-900
-1000
-1100
-1200
-1300
-1400
-1500
0 20 40 60 80 100 120 140 160 180 200 220 240 260 280 300 320 340 360 380 400 420

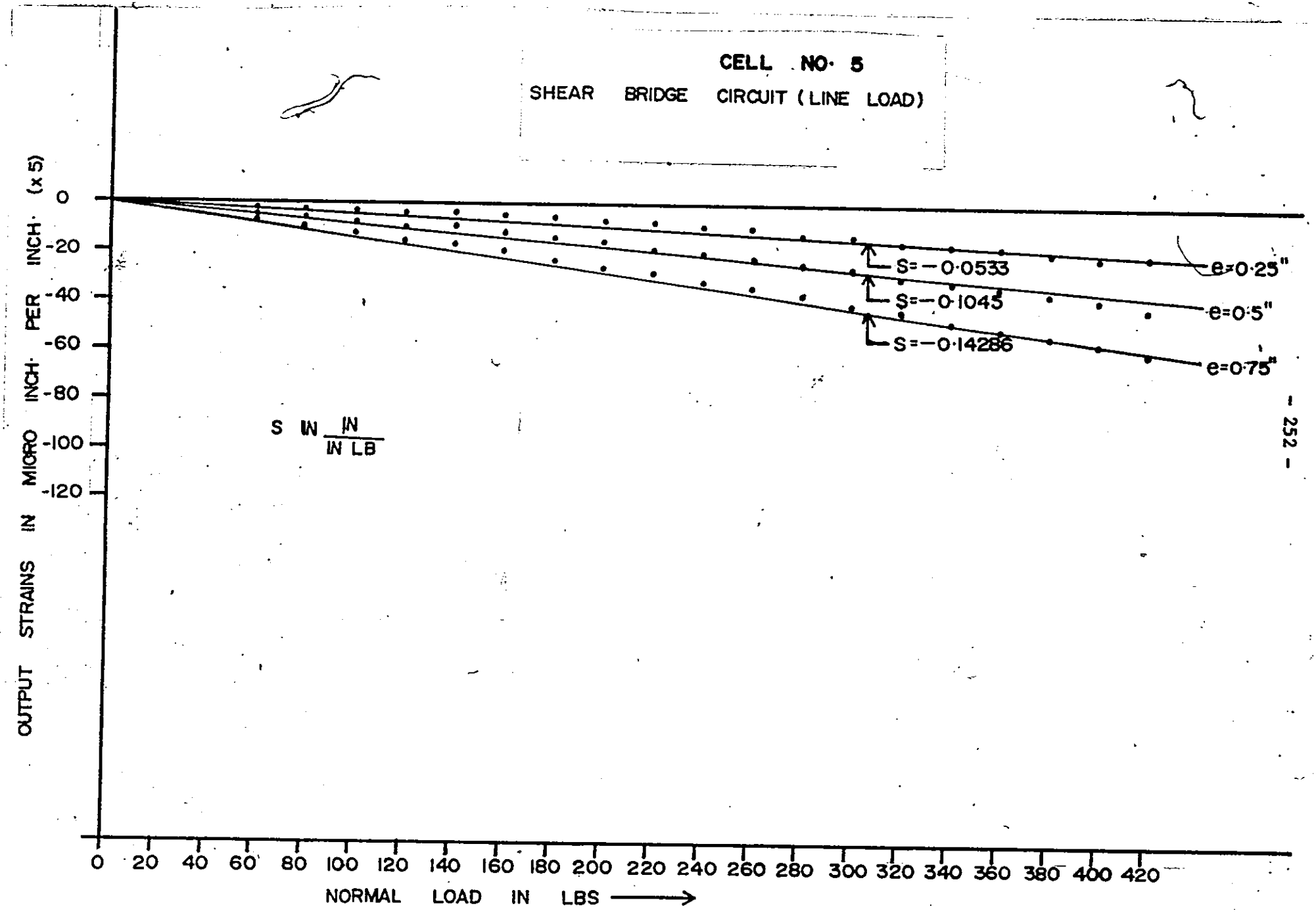
CELL NO. 5
SHEAR BRIDGE CIRCUIT (LINE LOAD)
OUTPUT STRAINS IN MICRO INCH PER INCH (x 5)
0
-20
-40
-60
-80
-100
-120
S IN $\frac{IN}{IN\ LB}$
S=-0.0533
S=-0.1045
S=-0.14286
e=0.25"
e=0.5"
e=0.75"
0 20 40 60 80 100 120 140 160 180 200 220 240 260 280 300 320 340 360 380 400 420
NORMAL LOAD IN LBS ⟶

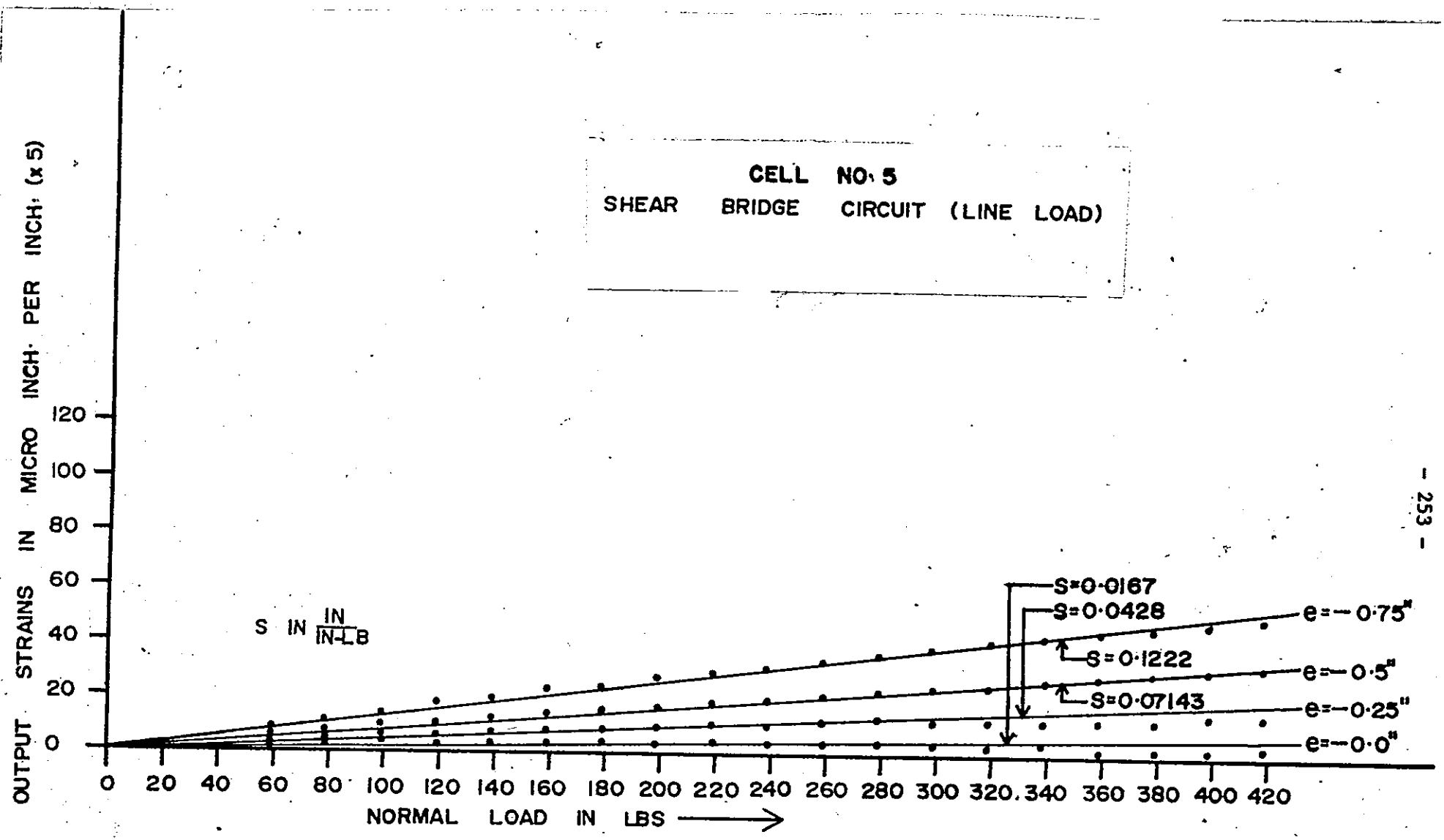
CELL NO. 5
SHEAR BRIDGE CIRCUIT (LINE LOAD)
OUTPUT STRAINS IN MICRO INCH PER INCH (x 5)
0
20
40
60
80
100
120
S IN IN/IN-LB
S=0·0167
S=0·0428
S=0·1222
S=0·07143
e=—0·75"
e=—0·5"
e=—0·25"
e=—0·0"
0 20 40 60 80 100 120 140 160 180 200 220 240 260 280 300 320 340 360 380 400 420
NORMAL LOAD IN LBS

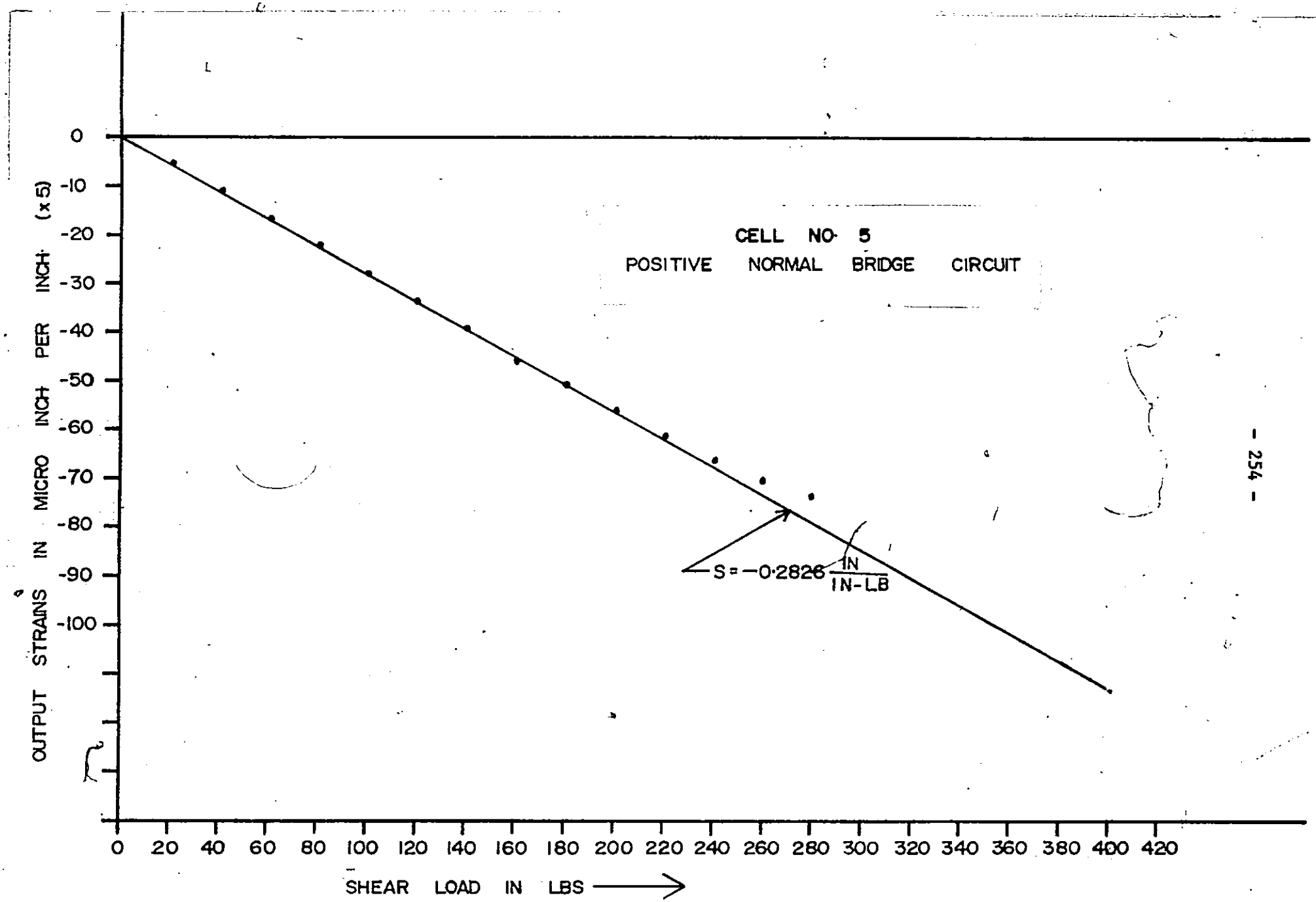
CELL NO. 5
POSITIVE NORMAL BRIDGE CIRCUIT
S = −0·2826 IN/IN-LB
OUTPUT STRAINS IN MICRO INCH PER INCH (x 5)
0
-10
-20
-30
-40
-50
-60
-70
-80
-90
-100
0 20 40 60 80 100 120 140 160 180 200 220 240 260 280 300 320 340 360 380 400 420
SHEAR LOAD IN LBS

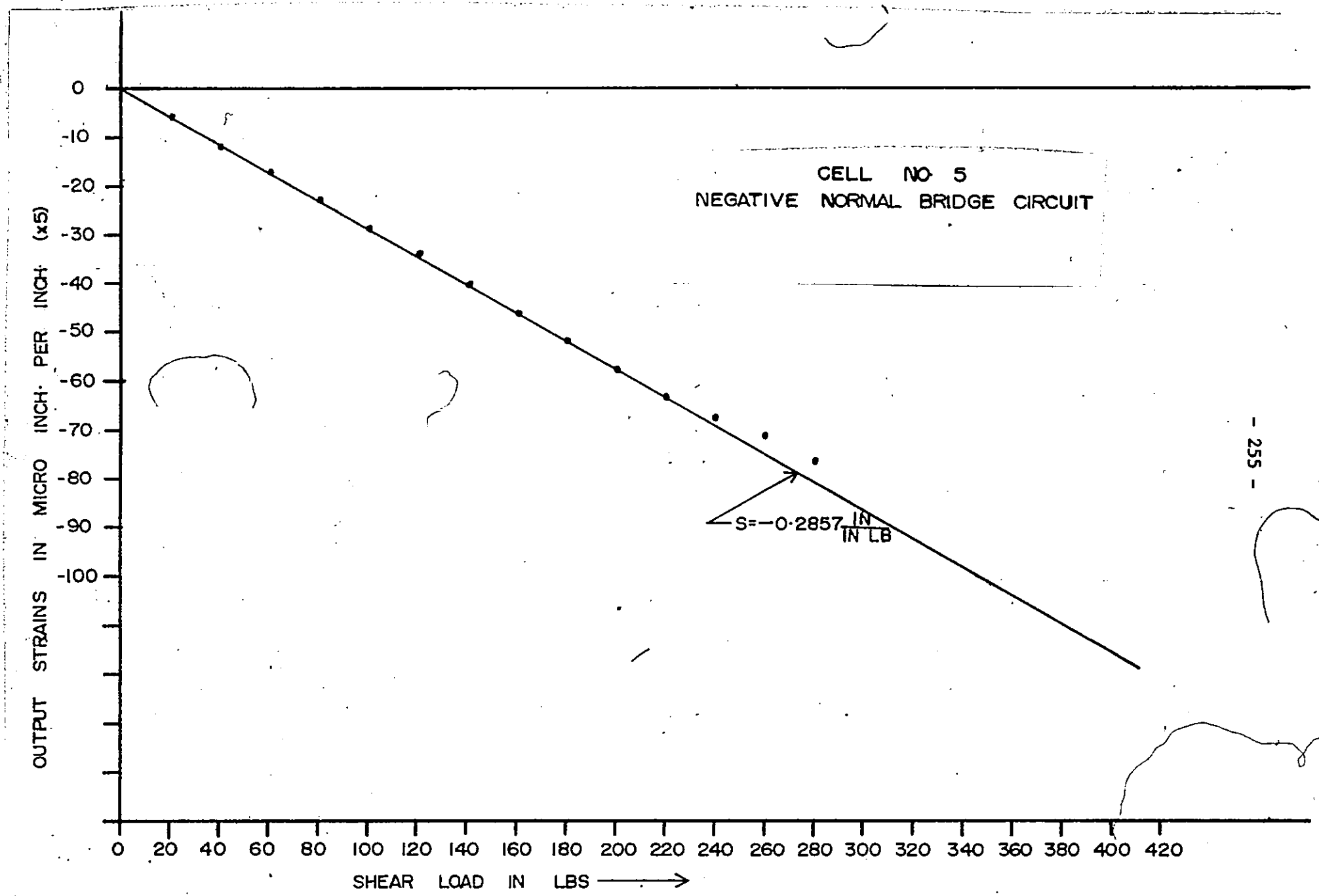
CELL NO 5
NEGATIVE NORMAL BRIDGE CIRCUIT
S=−0·2857 IN/IN LB
OUTPUT STRAINS IN MICRO INCH PER INCH (x5)
0
-10
-20
-30
-40
-50
-60
-70
-80
-90
-100
0 20 40 60 80 100 120 140 160 180 200 220 240 260 280 300 320 340 360 380 400 420
SHEAR LOAD IN LBS

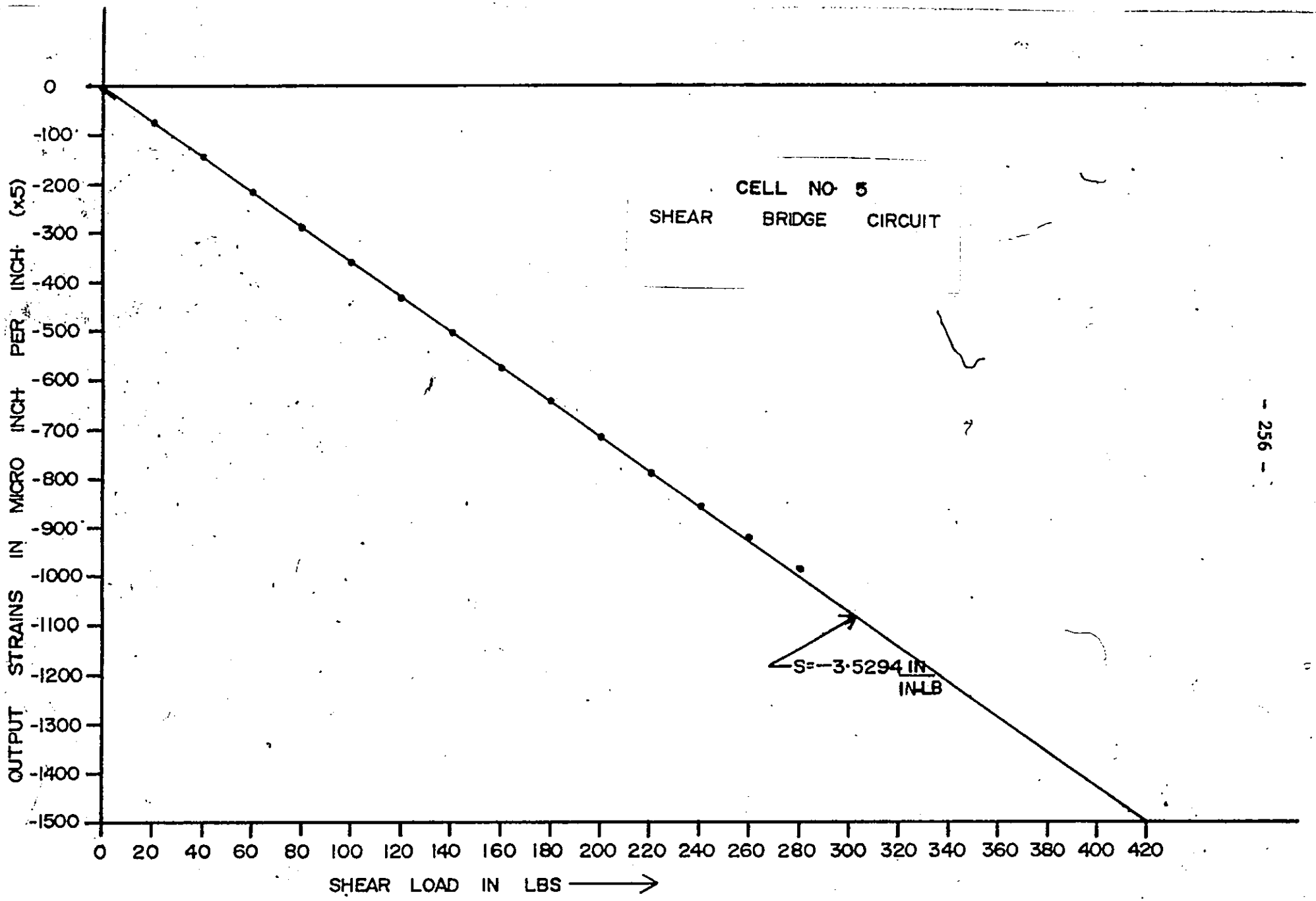
CELL NO 5
SHEAR BRIDGE CIRCUIT
S=-3·5294 IN/IN-LB
OUTPUT STRAINS IN MICRO INCH PER INCH (x5)
0
-100
-200
-300
-400
-500
-600
-700
-800
-900
-1000
-1100
-1200
-1300
-1400
-1500
0 20 40 60 80 100 120 140 160 180 200 220 240 260 280 300 320 340 360 380 400 420
SHEAR LOAD IN LBS

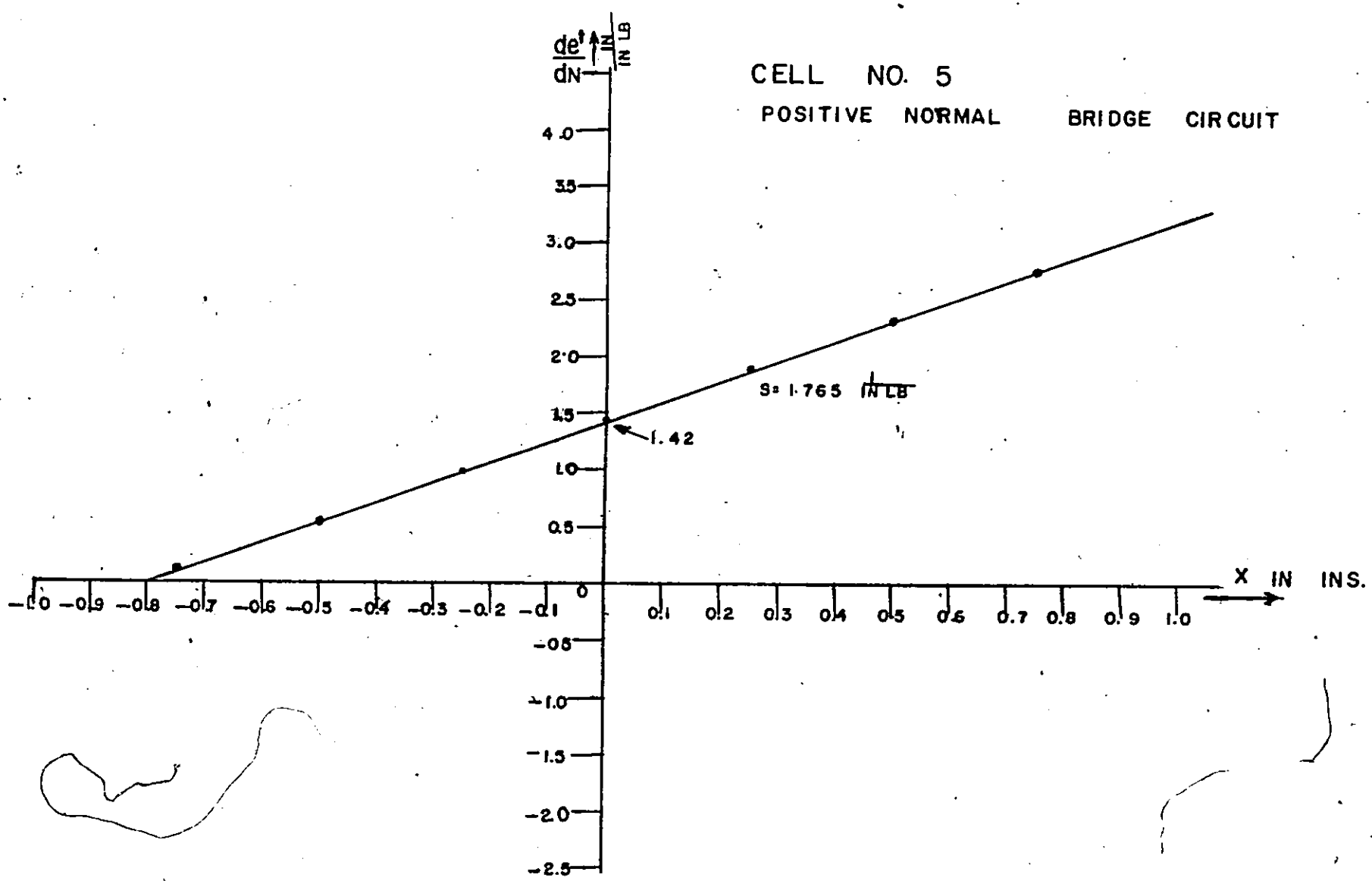
CELL NO. 5
POSITIVE NORMAL BRIDGE CIRCUIT
de'/dN IN/IN LB
4.0
3.5
3.0
2.5
2.0
1.5
1.0
0.5
-0.5
-1.0
-1.5
-2.0
-2.5
1.42
S= 1.765 IN LB
X IN INS.
-1.0 -0.9 -0.8 -0.7 -0.6 -0.5 -0.4 -0.3 -0.2 -0.1 0 0.1 0.2 0.3 0.4 0.5 0.6 0.7 0.8 0.9 1.0

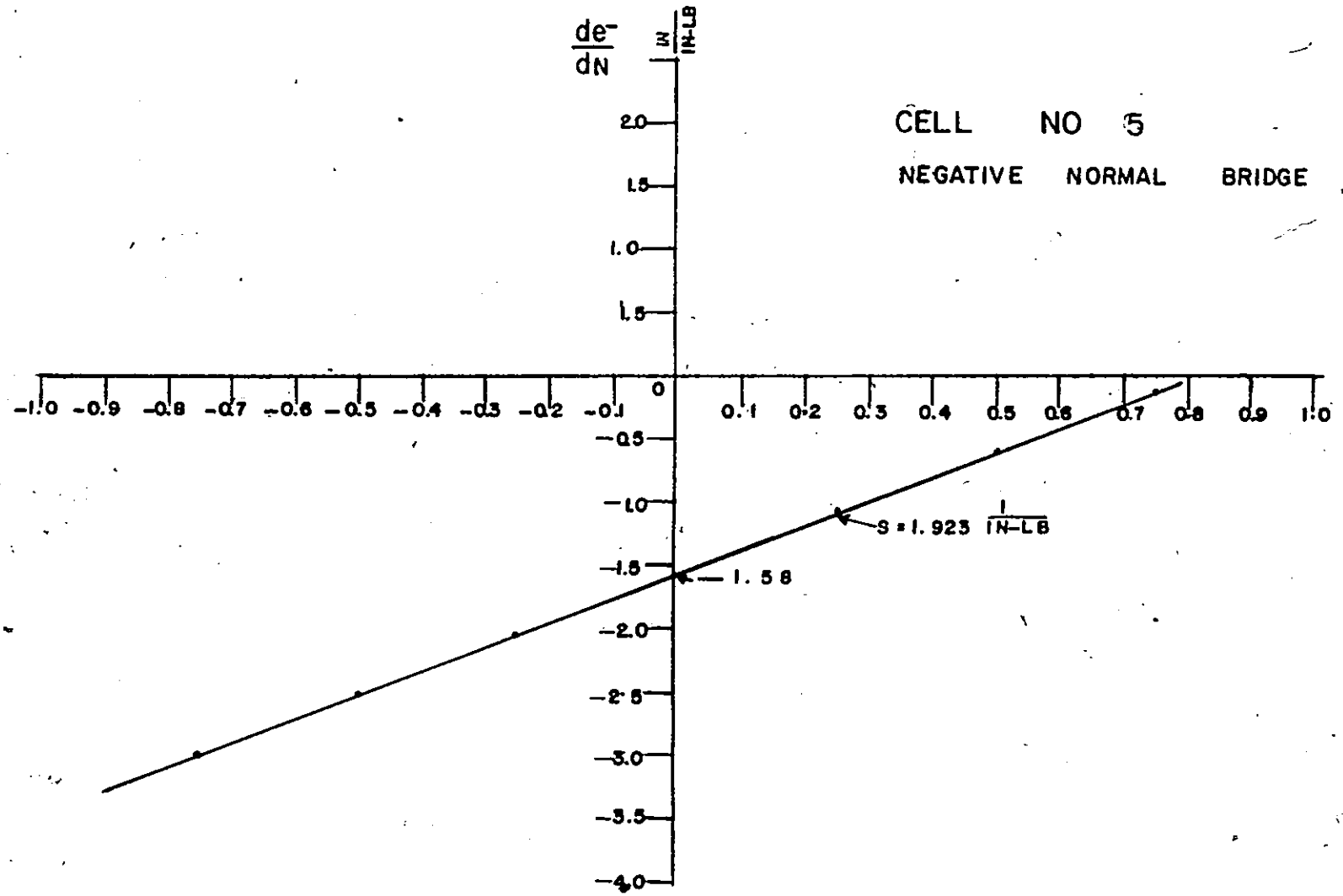
de⁻/dN
IN-LB
CELL NO 5
NEGATIVE NORMAL BRIDGE CIRCUIT
2.0
1.5
1.0
.5
0
-1.0 -0.9 -0.8 -0.7 -0.6 -0.5 -0.4 -0.3 -0.2 -0.1
0.1 0.2 0.3 0.4 0.5 0.6 0.7 0.8 0.9 1.0
-0.5
-1.0
-1.5
-2.0
-2.5
-3.0
-3.5
-4.0
S = 1.923 1/IN-LB
1.58

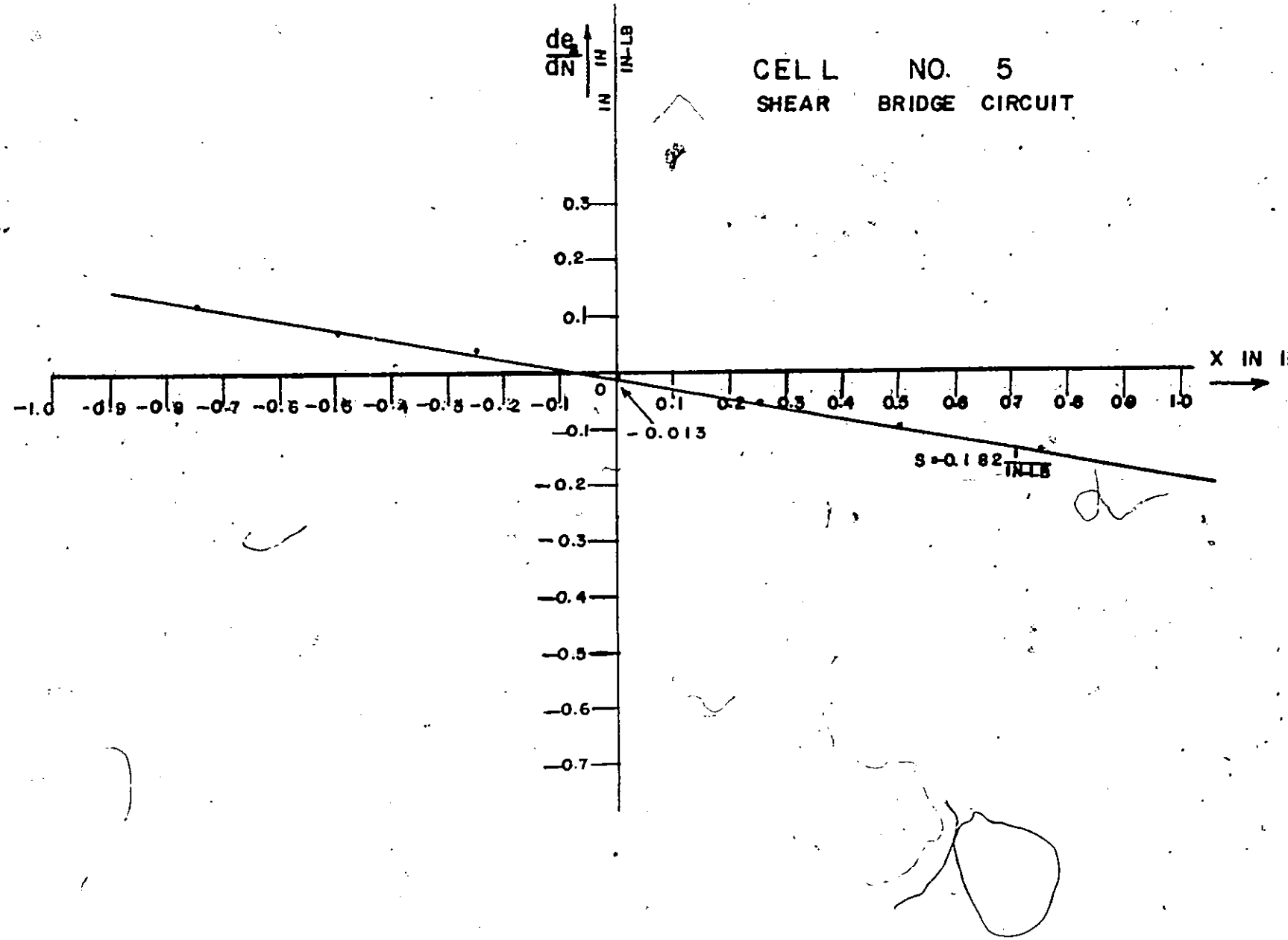
CELL NO. 5
SHEAR BRIDGE CIRCUIT
$\frac{de_s}{dN}$ MV/IN
IN-LB
X IN INS
0.3
0.2
0.1
0
-0.1
-0.2
-0.3
-0.4
-0.5
-0.6
-0.7
-1.0 -0.9 -0.8 -0.7 -0.6 -0.5 -0.4 -0.3 -0.2 -0.1
0.1 0.2 0.3 0.4 0.5 0.6 0.7 0.8 0.9 1.0
-0.013
S=-0.182 IN-LB

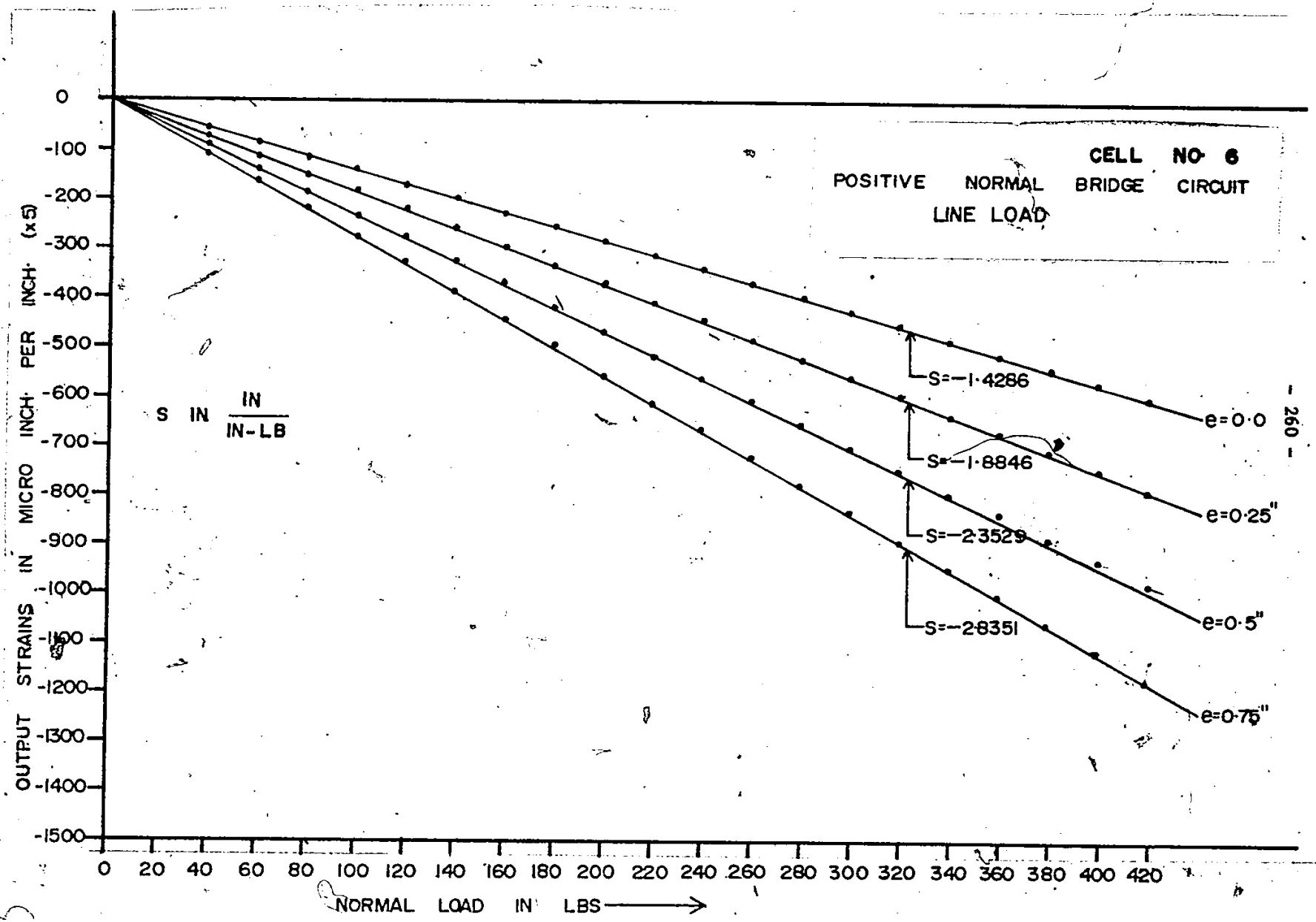
CELL NO. 6
POSITIVE NORMAL BRIDGE CIRCUIT
LINE LOAD
S IN IN / IN-LB
OUTPUT STRAINS IN MICRO INCH PER INCH (x5)
0
-100
-200
-300
-400
-500
-600
-700
-800
-900
-1000
-1100
-1200
-1300
-1400
-1500
0 20 40 60 80 100 120 140 160 180 200 220 240 260 280 300 320 340 360 380 400 420
NORMAL LOAD IN LBS
S=-1·4286
e=0·0
S=-1·8846
e=0·25"
S=-2·3529
e=0·5"
S=-2·8351
e=0·75"

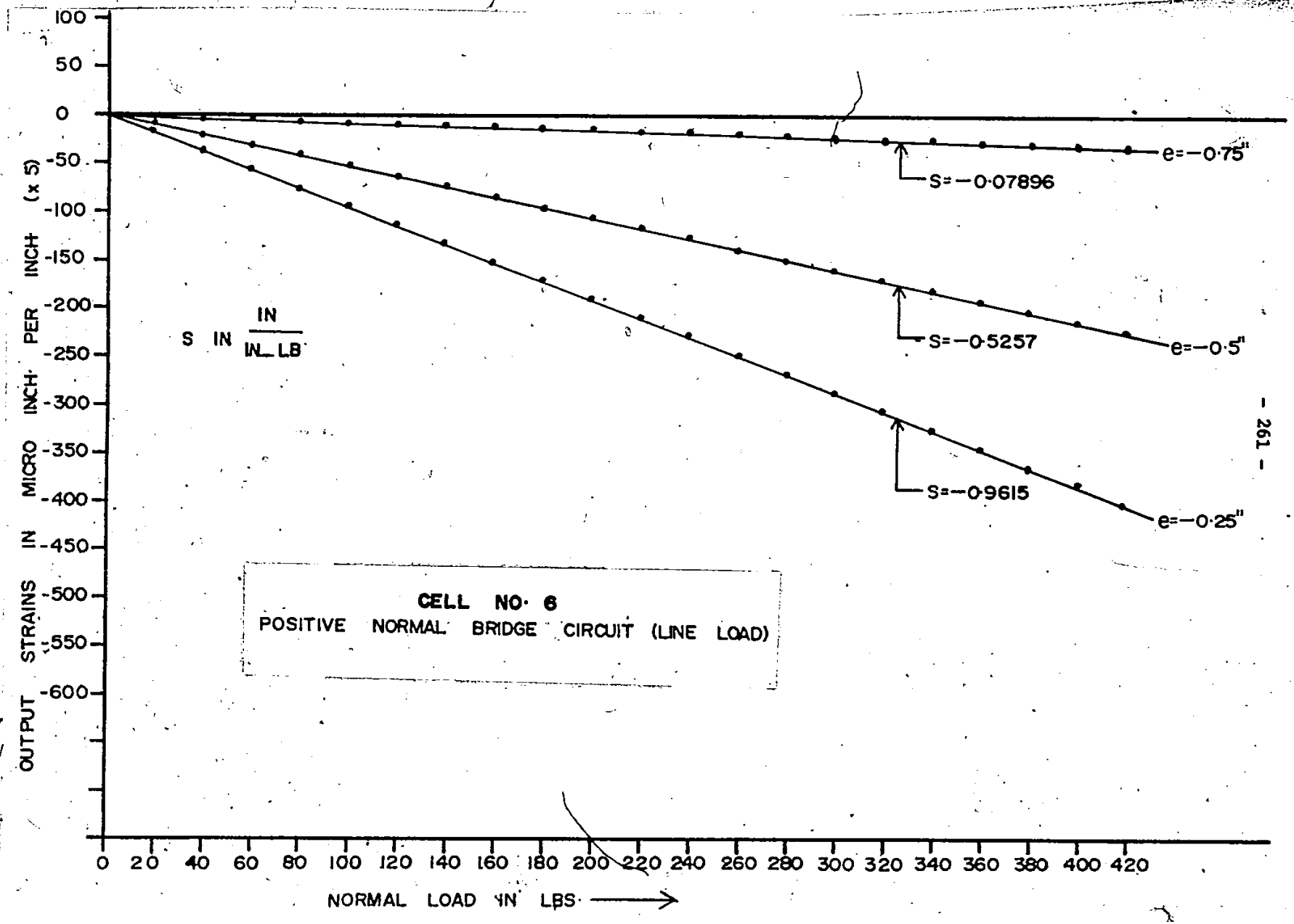
100
50
0
-50
-100
-150
-200
-250
-300
-350
-400
-450
-500
-550
-600
OUTPUT STRAINS IN MICRO INCH PER INCH (x 5)
S IN IN / IN_LB
e=-0·75"
S=-0·07896
e=-0·5"
S=-0·5257
e=-0·25"
S=-0·9615
CELL NO· 6
POSITIVE NORMAL BRIDGE CIRCUIT (LINE LOAD)
0 20 40 60 80 100 120 140 160 180 200 220 240 260 280 300 320 340 360 380 400 420
NORMAL LOAD IN LBS

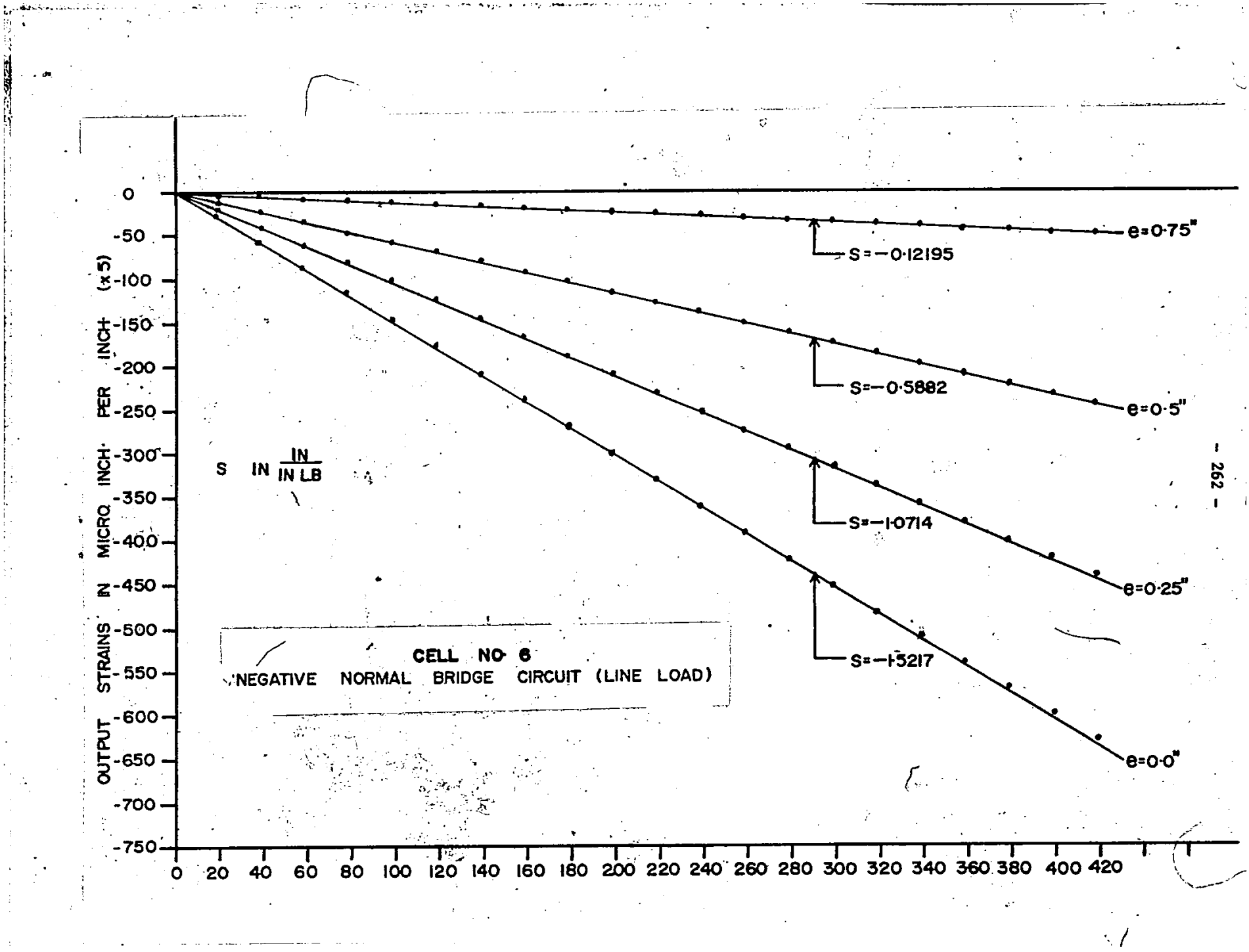
OUTPUT STRAINS IN MICRO INCH PER INCH (x5)
0
-50
-100
-150
-200
-250
-300
-350
-400
-450
-500
-550
-600
-650
-700
-750
0 20 40 60 80 100 120 140 160 180 200 220 240 260 280 300 320 340 360 380 400 420
S IN IN/IN LB
S=-0·12195
S=-0·5882
S=-1·0714
S=-1·5217
e=0·75"
e=0·5"
e=0·25"
e=0·0"
CELL NO 6
NEGATIVE NORMAL BRIDGE CIRCUIT (LINE LOAD)

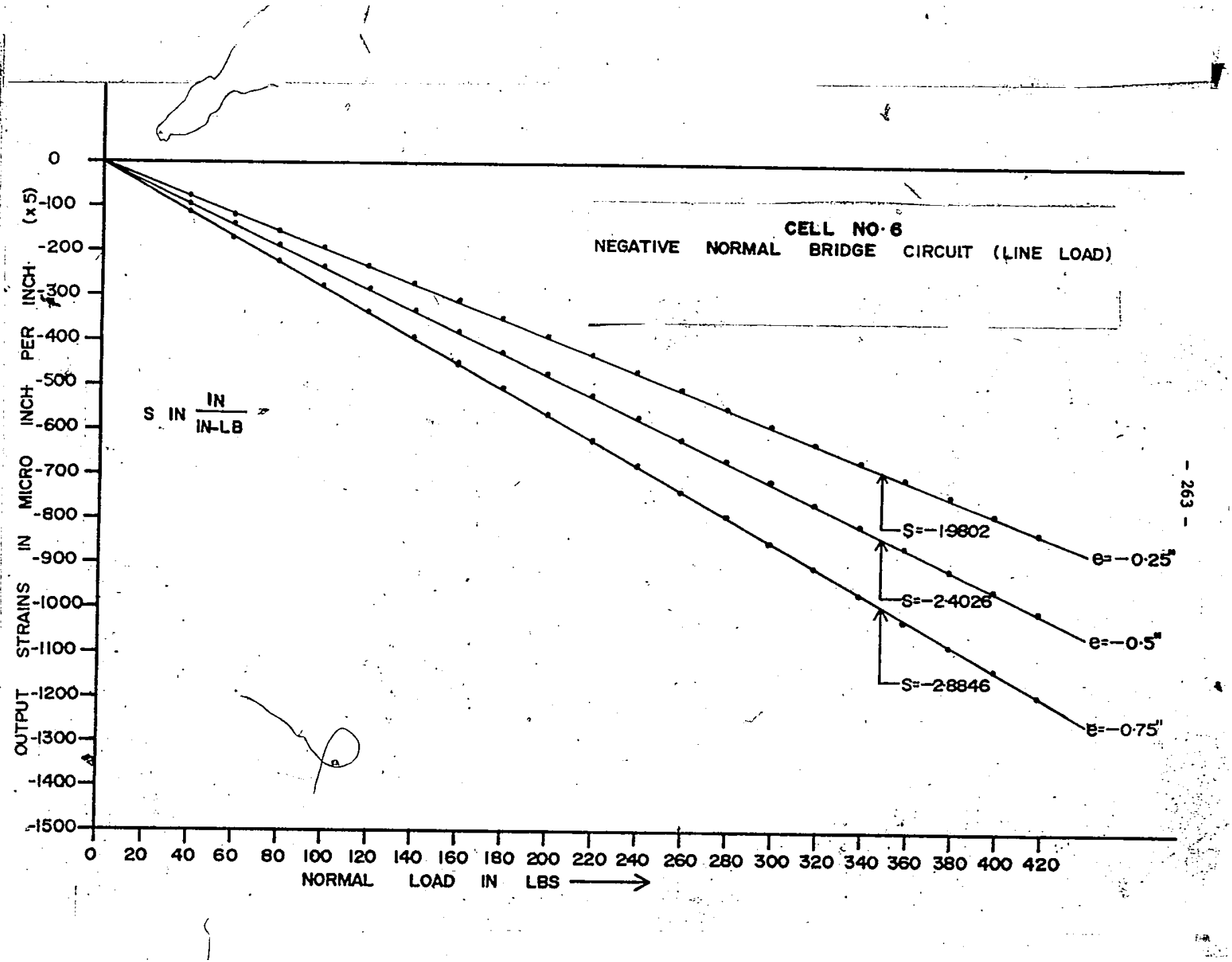
CELL NO·6
NEGATIVE NORMAL BRIDGE CIRCUIT (LINE LOAD)
S IN $\frac{IN}{IN\text{-}LB}$
OUTPUT STRAINS IN MICRO INCH PER INCH (x5)
0
-100
-200
-300
-400
-500
-600
-700
-800
-900
-1000
-1100
-1200
-1300
-1400
-1500
S=-1·9802
S=-2·4026
S=-2·8846
e=-0·25"
e=-0·5"
e=-0·75"
0 20 40 60 80 100 120 140 160 180 200 220 240 260 280 300 320 340 360 380 400 420
NORMAL LOAD IN LBS ⟶

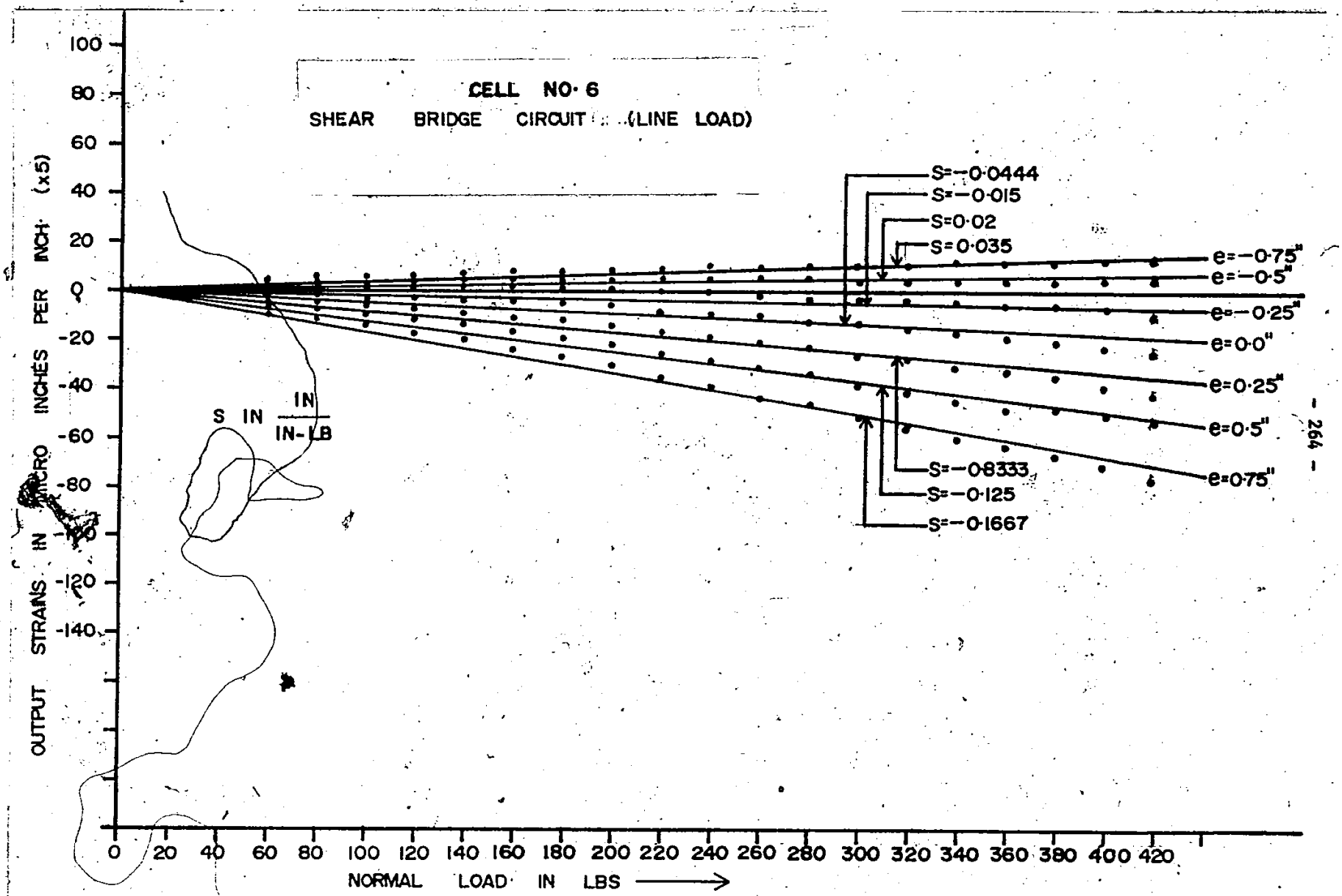
CELL NO. 6
SHEAR BRIDGE CIRCUIT (LINE LOAD)
OUTPUT STRAINS IN MICRO INCHES PER INCH (x5)
100
80
60
40
20
0
-20
-40
-60
-80
-100
-120
-140
S IN IN/IN-LB
S=-0.0444
S=-0.015
S=0.02
S=0.035
e=-0.75"
e=-0.5"
e=-0.25"
e=0.0"
e=0.25"
e=0.5"
e=0.75"
S=-0.8333
S=-0.125
S=-0.1667
0 20 40 60 80 100 120 140 160 180 200 220 240 260 280 300 320 340 360 380 400 420
NORMAL LOAD IN LBS

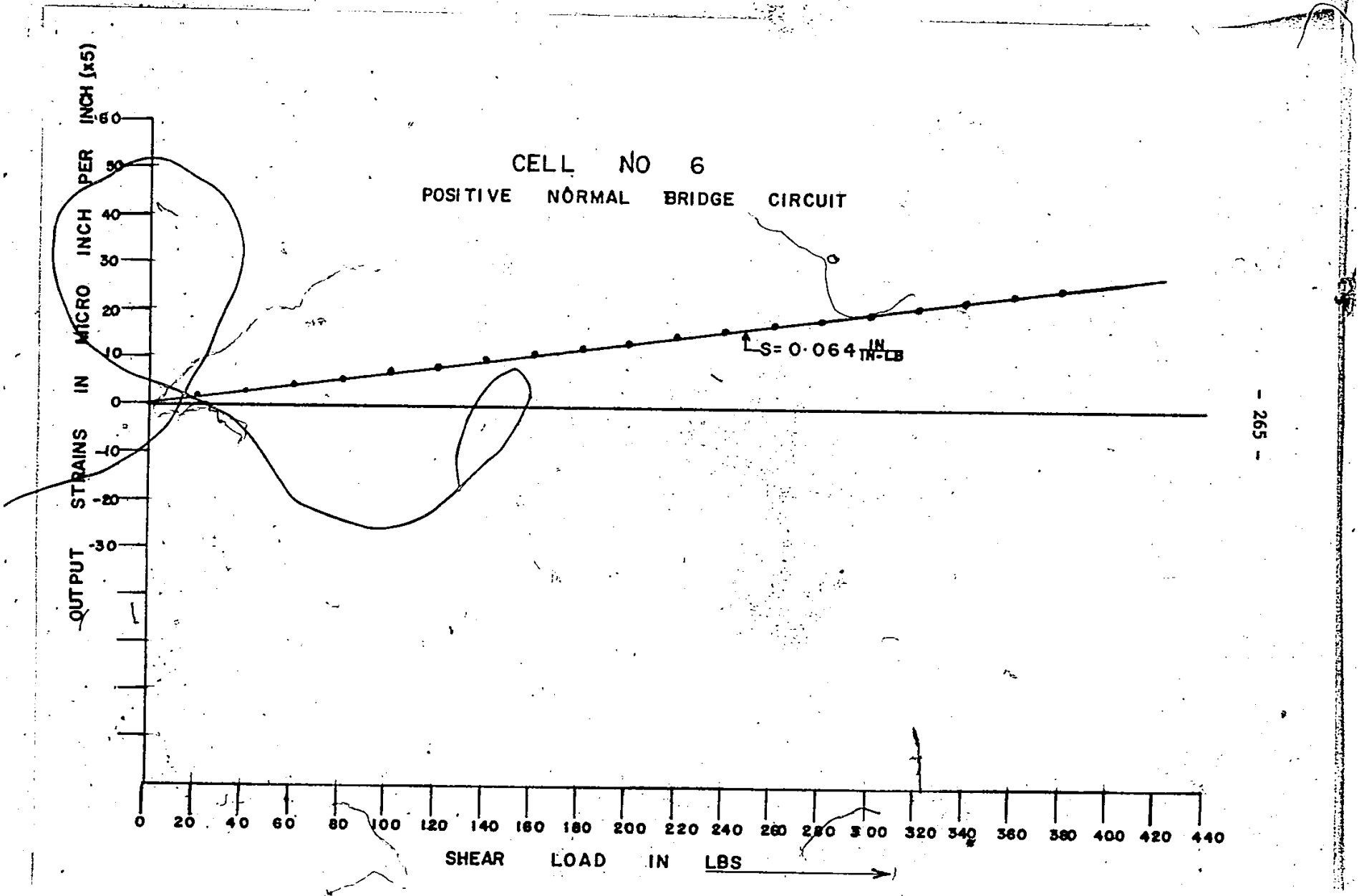
CELL NO 6
POSITIVE NORMAL BRIDGE CIRCUIT
S= 0·064 IN/IN-LB
OUTPUT STRAINS IN MICRO INCH PER INCH (x5)
60
50
40
30
20
10
0
-10
-20
-30
0 20 40 60 80 100 120 140 160 180 200 220 240 260 280 300 320 340 360 380 400 420 440
SHEAR LOAD IN LBS

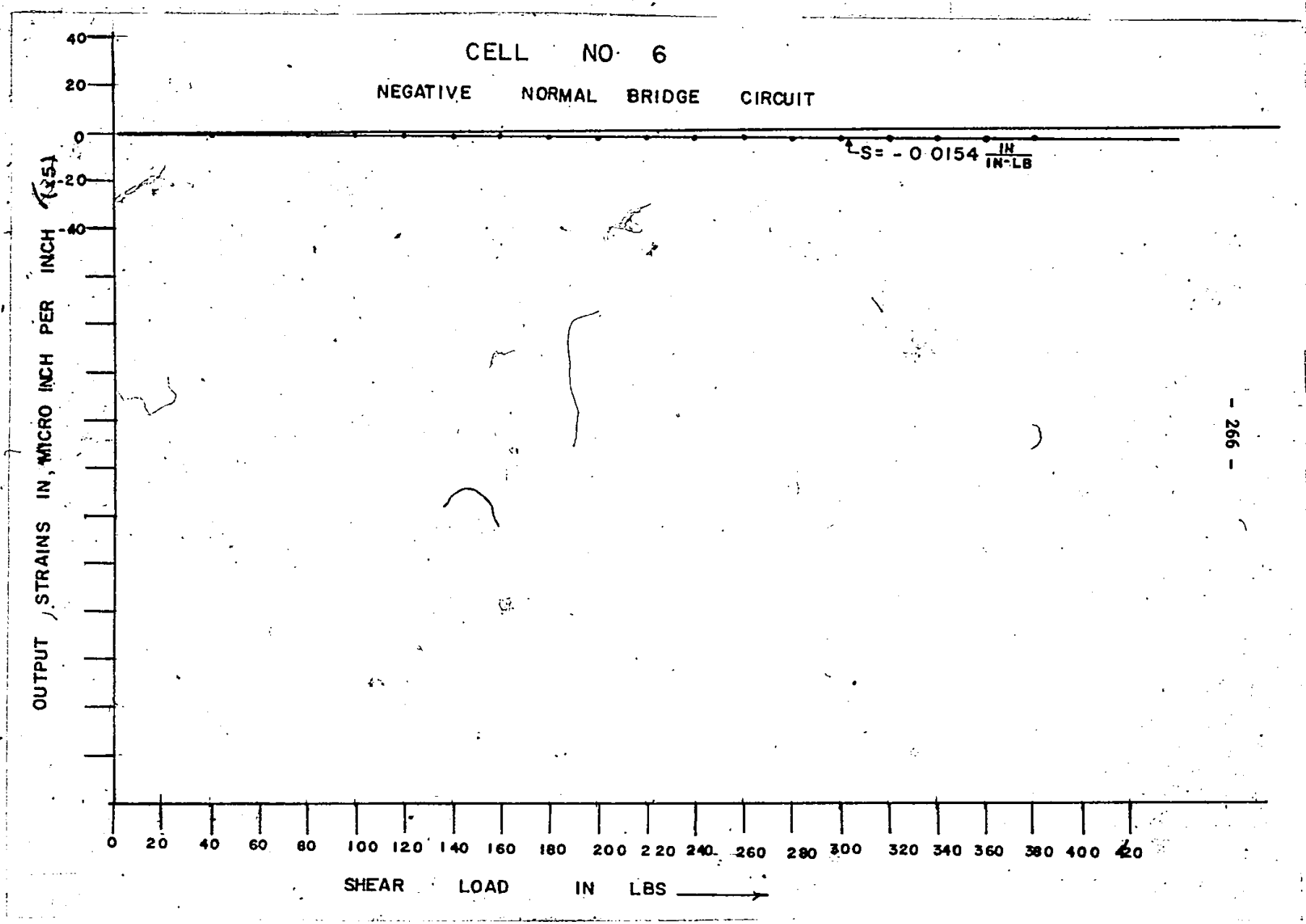
CELL NO. 6
NEGATIVE NORMAL BRIDGE CIRCUIT
S= - 0 0154 IN/IN-LB
OUTPUT STRAINS IN, MICRO INCH PER INCH (x5)
40
20
0
-20
-40
0 20 40 60 80 100 120 140 160 180 200 220 240 260 280 300 320 340 360 380 400 420
SHEAR LOAD IN LBS

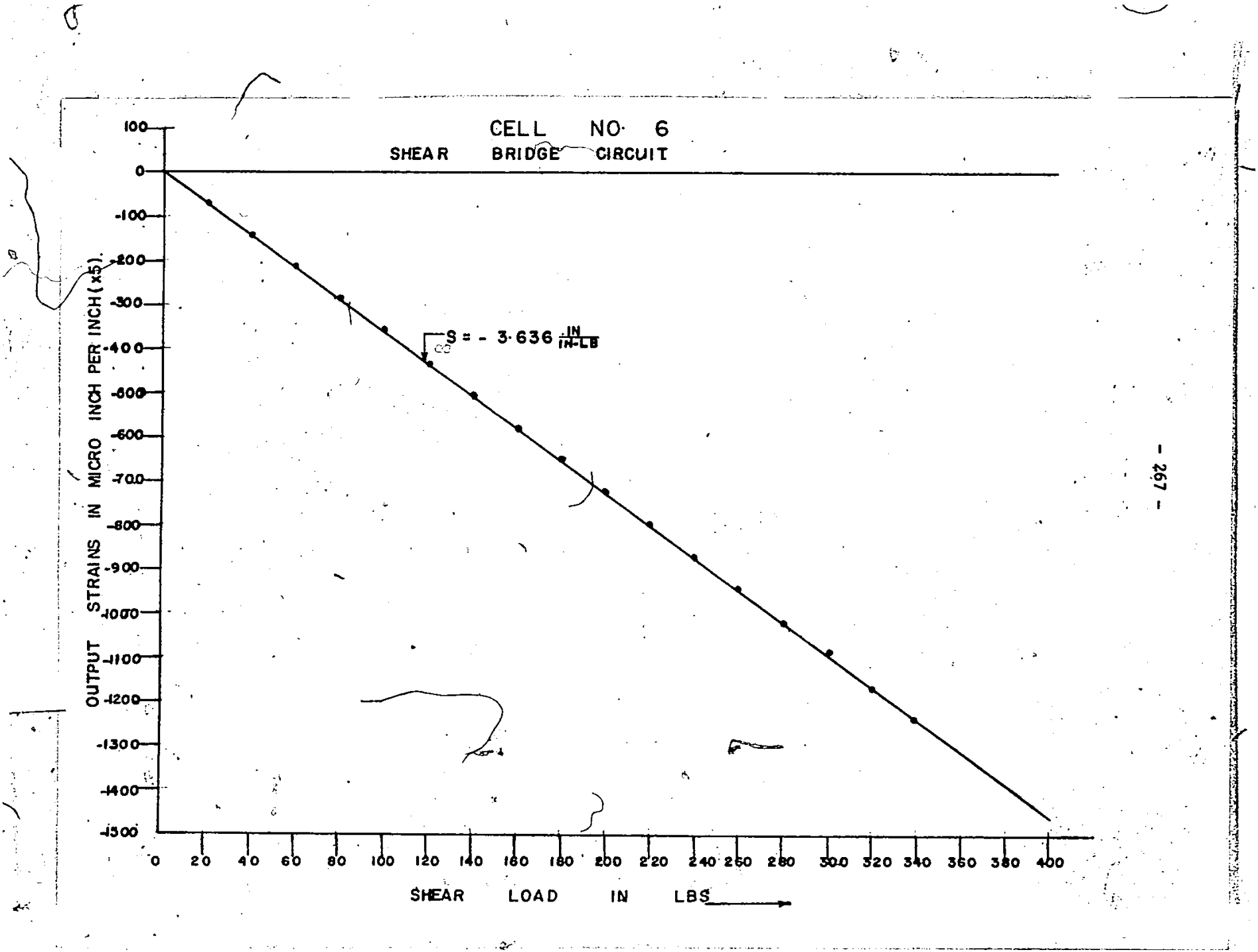
CELL NO. 6
SHEAR BRIDGE CIRCUIT
S = - 3.636 IN/IN-LB
OUTPUT STRAINS IN MICRO INCH PER INCH (x5).
100
0
-100
-200
-300
-400
-500
-600
-700
-800
-900
-1000
-1100
-1200
-1300
-1400
-1500
0 20 40 60 80 100 120 140 160 180 200 220 240 260 280 300 320 340 360 380 400
SHEAR LOAD IN LBS

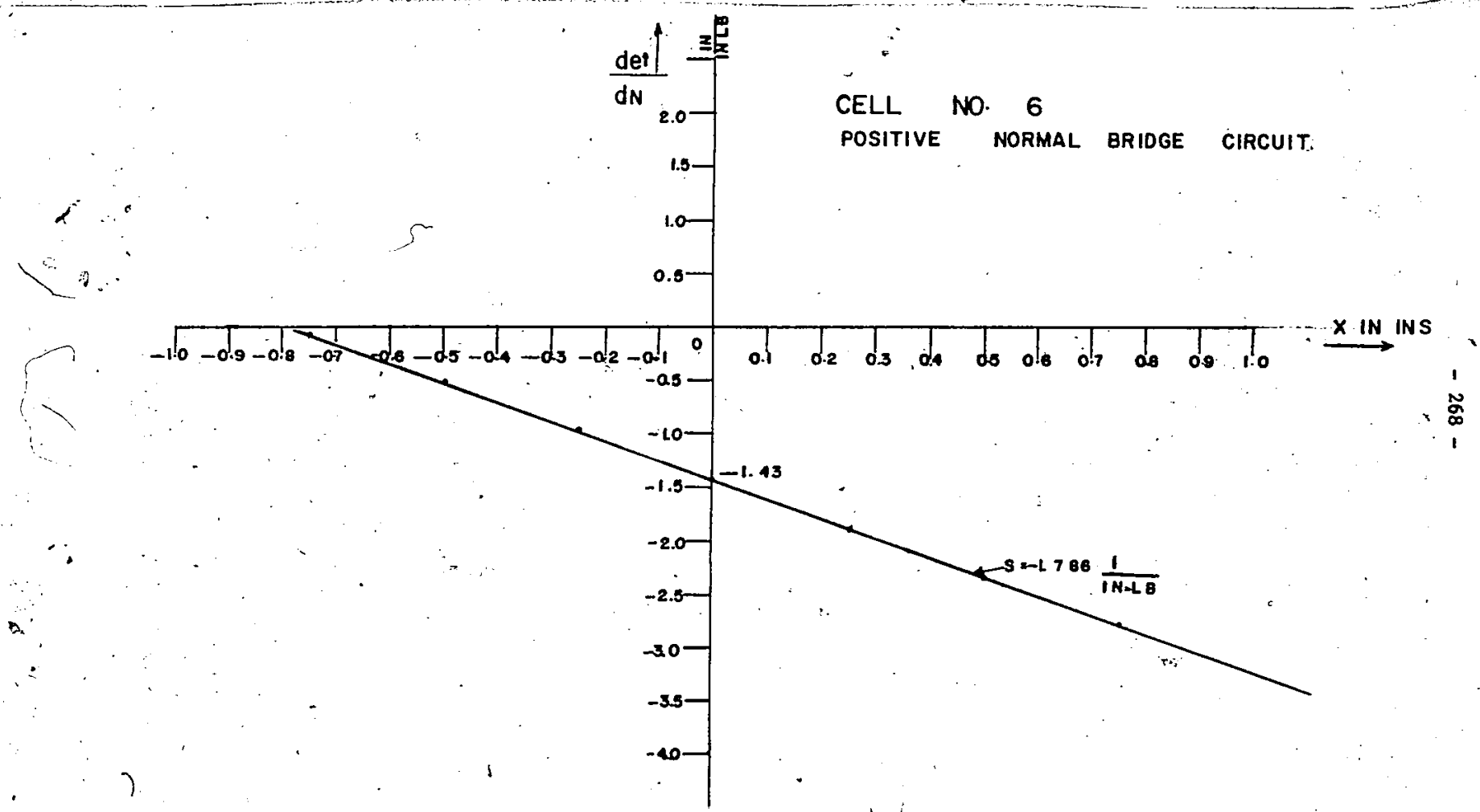
CELL NO. 6
POSITIVE NORMAL BRIDGE CIRCUIT.
det/dN
IN IN-LB
X IN INS
2.0
1.5
1.0
0.5
0
-0.5
-1.0
-1.5
-2.0
-2.5
-3.0
-3.5
-4.0
-1.0 -0.9 -0.8 -0.7 -0.6 -0.5 -0.4 -0.3 -0.2 -0.1
0.1 0.2 0.3 0.4 0.5 0.6 0.7 0.8 0.9 1.0
-1.43
S=-1.786 I/IN-LB

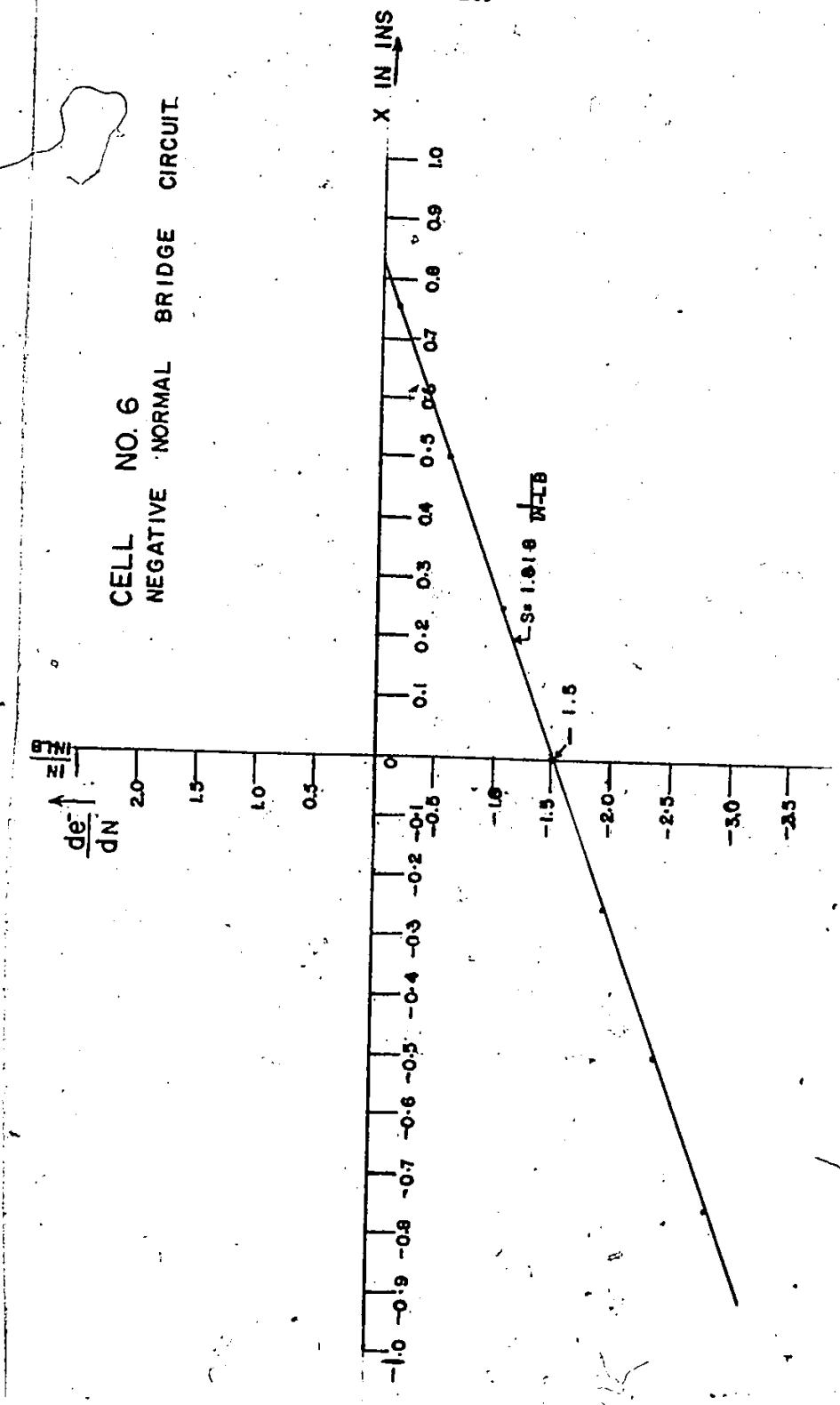
CELL NO. 6
NEGATIVE NORMAL BRIDGE CIRCUIT
X IN INS
de/dN
IN/LB
1.5
S= 1.818 IN-LB

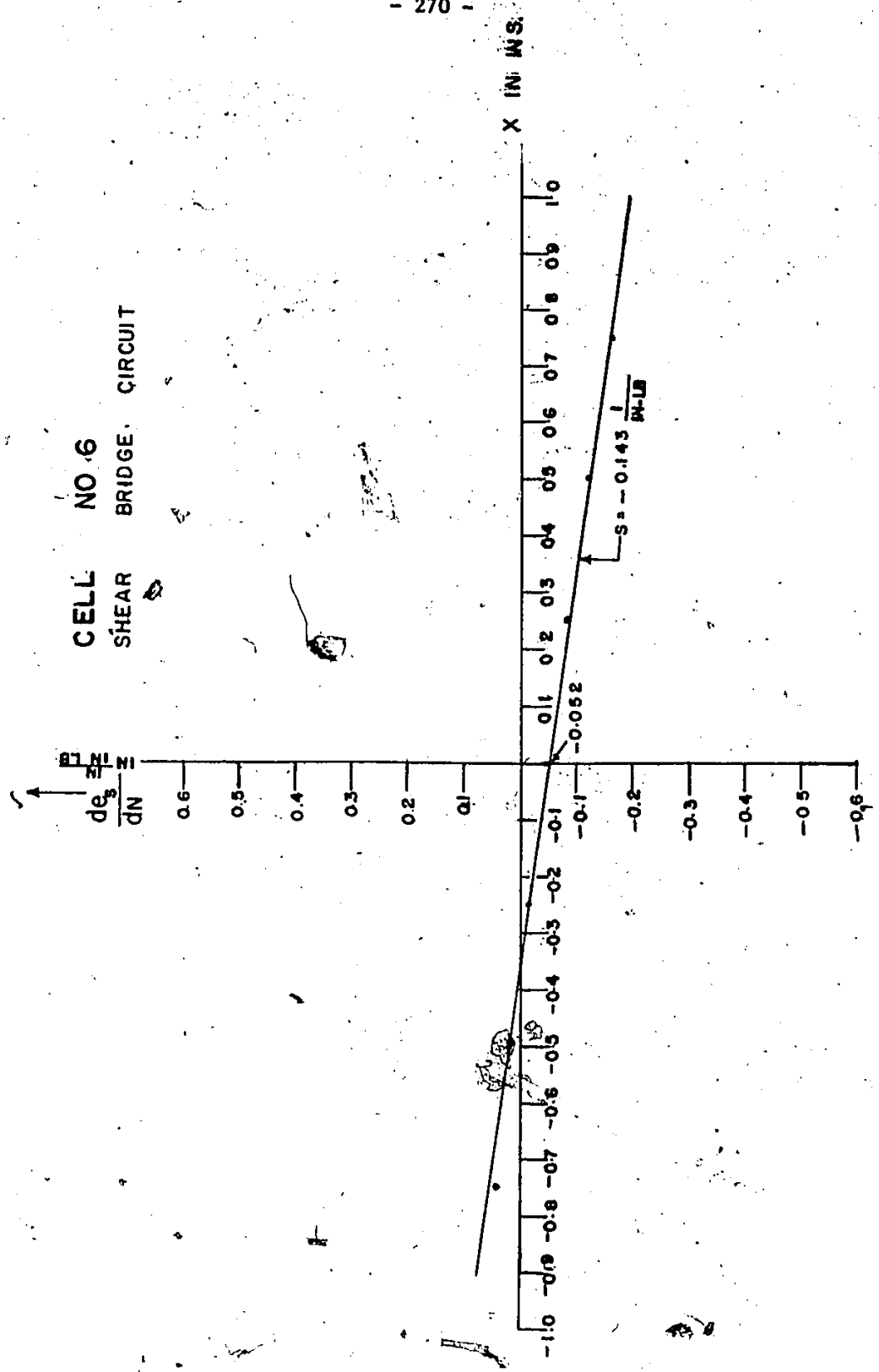
CELL NO 6
SHEAR BRIDGE CIRCUIT
X (IN W.S.)
S = - 0.143 1/IN-LB
-0.052
de_s/dN

APPENDIX B

CALIBRATION GRAPHS (POINT LOAD)

The calibration of the six modified Cambridge load cells under point loads were carried out. For comparison purposes, the calibration curves for a typical load cell, Cell No. 5, under point loads has been presented in this section.

The graphs represent the plot of the output strains from the positive normal bridge circuit, the negative normal bridge circuit and shear bridge circuit at different eccentricities against the normal point loads.

From the slopes of the lines in this appendix and the corresponding lines in Appendix A, it could be concluded that the calibration constants are independent of the nature of loading (whether line loading or point loading).

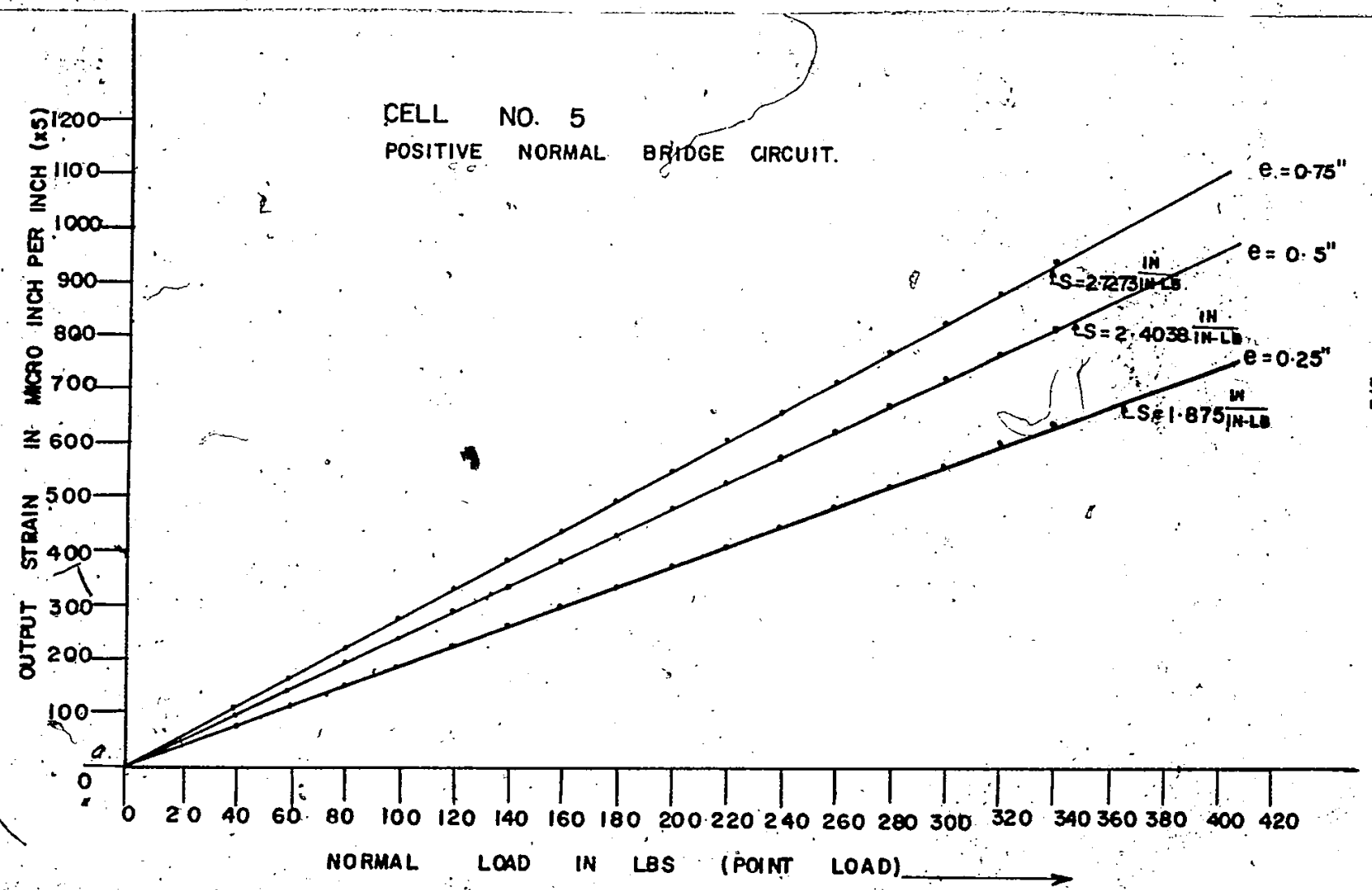
CELL NO. 5
POSITIVE NORMAL BRIDGE CIRCUIT.
e = 0·75"
e = 0·5"
e = 0·25"
LS = 2·7273 IN/IN-LB
LS = 2·4038 IN/IN-LB
LS = 1·875 IN/IN-LB
OUTPUT STRAIN IN MICRO INCH PER INCH (x5)
0
100
200
300
400
500
600
700
800
900
1000
1100
1200
0 20 40 60 80 100 120 140 160 180 200 220 240 260 280 300 320 340 360 380 400 420
NORMAL LOAD IN LBS (POINT LOAD)

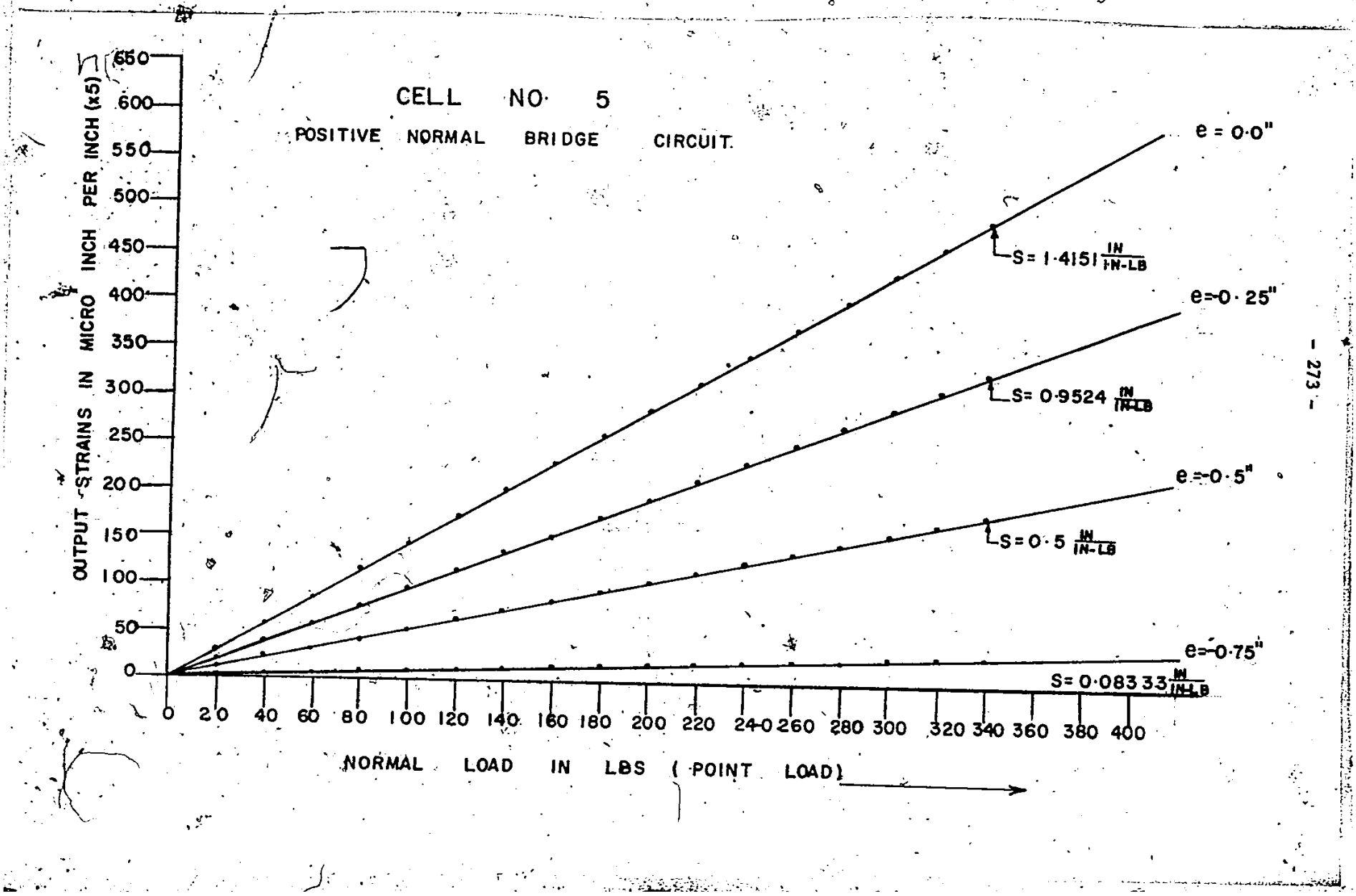
CELL NO. 5
POSITIVE NORMAL BRIDGE CIRCUIT
OUTPUT STRAINS IN MICRO INCH PER INCH (x5)
650
600
550
500
450
400
350
300
250
200
150
100
50
0
e = 0·0"
S = 1·4151 IN/IN-LB
e=-0·25"
S = 0·9524 IN/IN-LB
e=-0·5"
S = 0·5 IN/IN-LB
e=-0·75"
S = 0·08333 IN/IN-LB
0 20 40 60 80 100 120 140 160 180 200 220 240 260 280 300 320 340 360 380 400
NORMAL LOAD IN LBS (POINT LOAD)

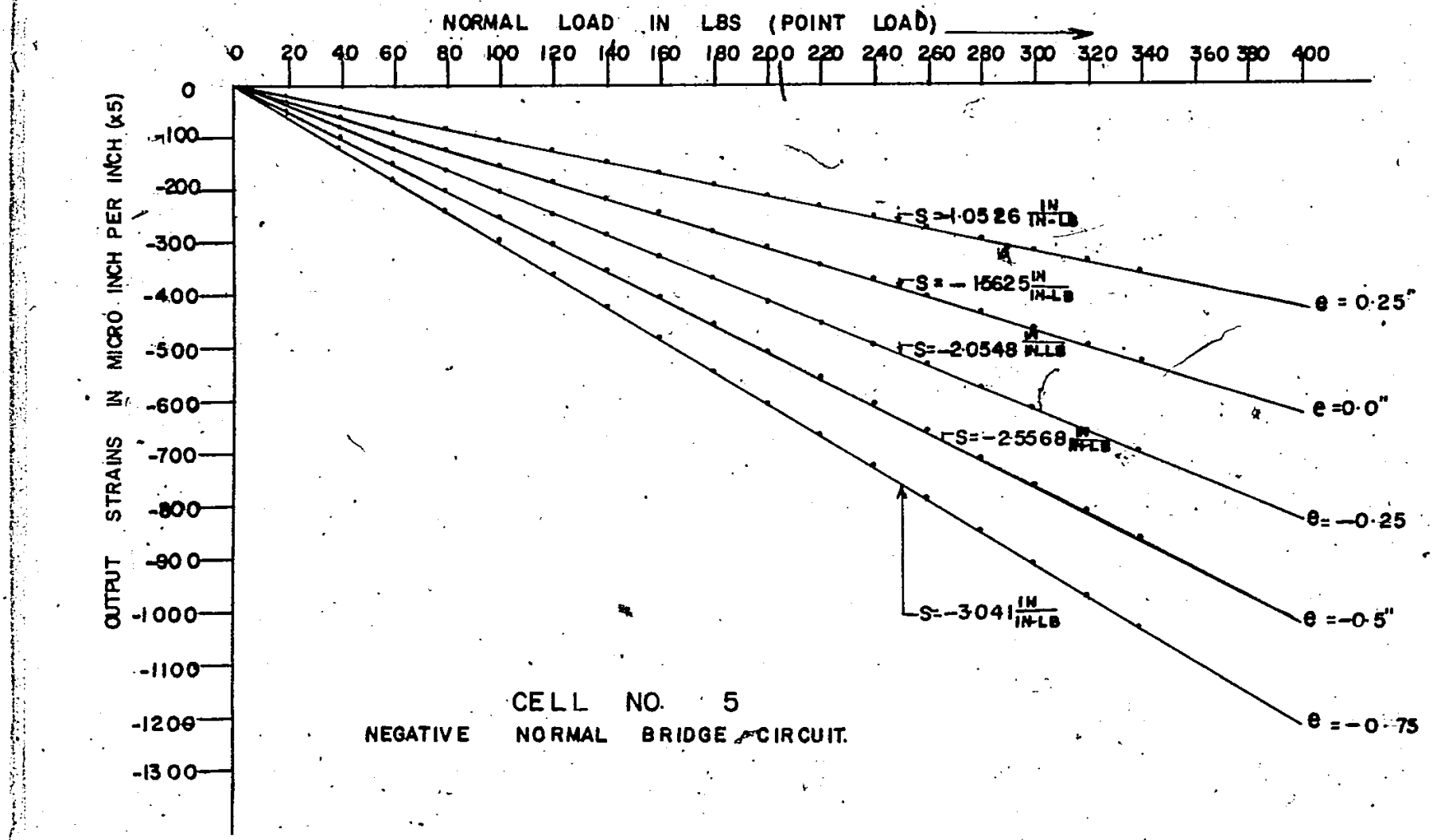
NORMAL LOAD IN LBS (POINT LOAD)
0 20 40 60 80 100 120 140 160 180 200 220 240 260 280 300 320 340 360 380 400
OUTPUT STRAINS IN MICRO INCH PER INCH (x5)
0 -100 -200 -300 -400 -500 -600 -700 -800 -900 -1000 -1100 -1200 -1300
S = -1.0526 IN/IN-LB
S = -1.5625 IN/IN-LB
S = -2.0548 IN/IN-LB
S = -2.5568 IN/IN-LB
S = -3.041 IN/IN-LB
e = 0.25"
e = 0.0"
e = -0.25
e = -0.5"
e = -0.75
CELL NO. 5
NEGATIVE NORMAL BRIDGE CIRCUIT.

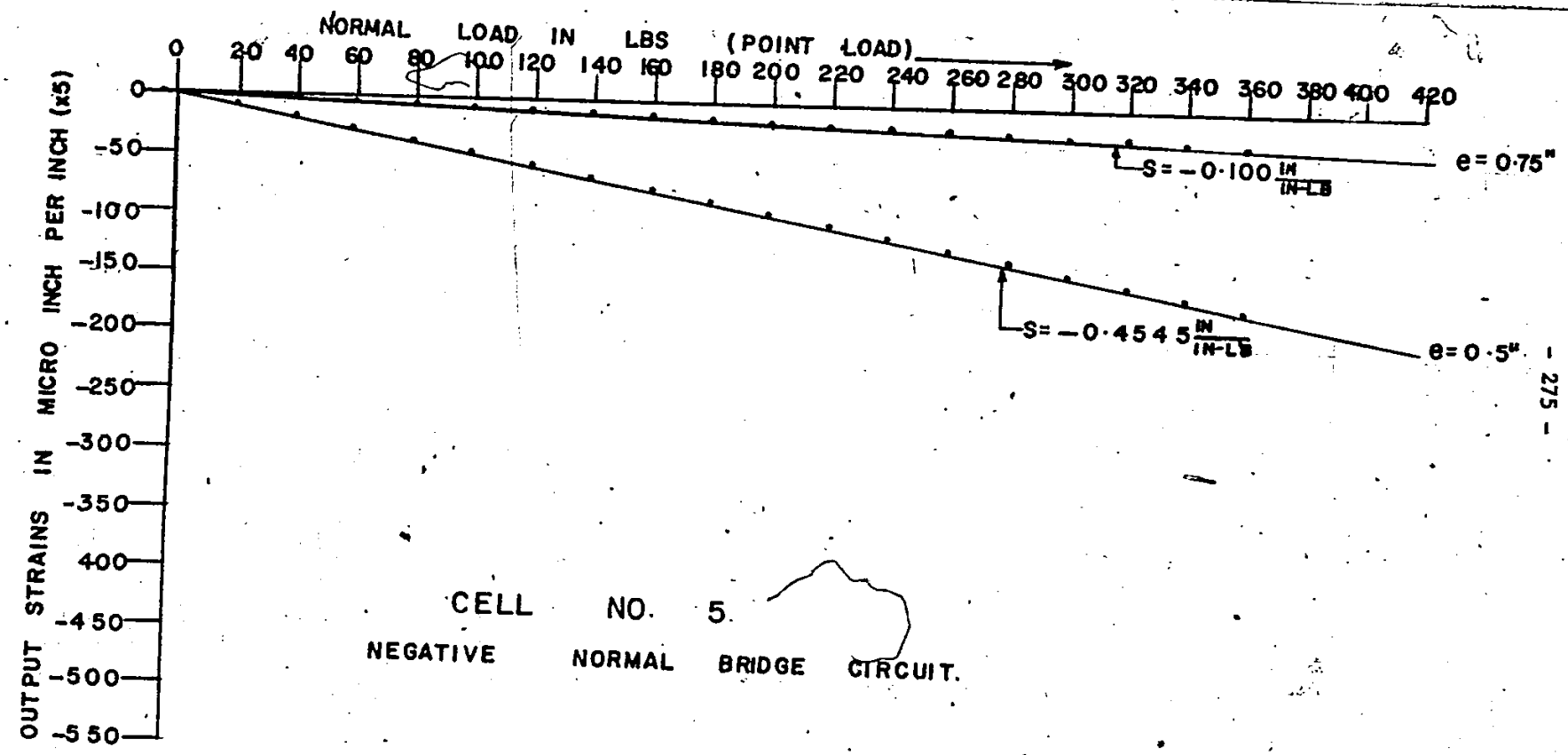

CELL NO. 5.

NEGATIVE NORMAL BRIDGE CIRCUIT.

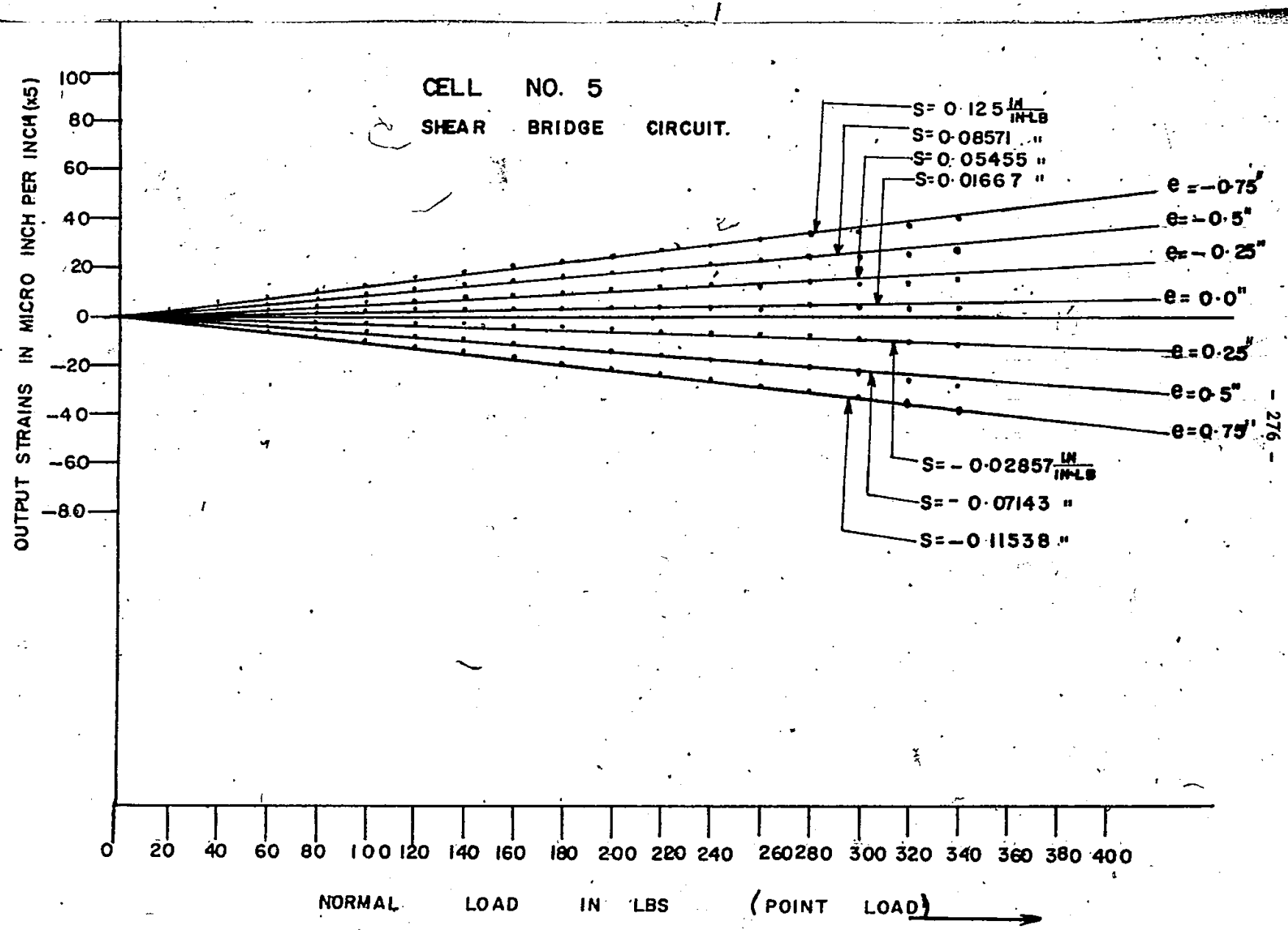
CELL NO. 5
SHEAR BRIDGE CIRCUIT.
OUTPUT STRAINS IN MICRO INCH PER INCH (x5)
100
80
60
40
20
0
-20
-40
-60
-80
S= 0·125 IN/IN-LB
S= 0·08571 "
S= 0·05455 "
S= 0·01667 "
e = -0·75"
e = -0·5"
e = -0·25"
e = 0·0"
e = 0·25"
e = 0·5"
e = 0·75"
S= - 0·02857 IN/IN-LB
S= - 0·07143 "
S= - 0·11538 "
0 20 40 60 80 100 120 140 160 180 200 220 240 260 280 300 320 340 360 380 400
NORMAL LOAD IN LBS (POINT LOAD)

APPENDIX C

STRAINS INDICATED BY BRIDGE CIRCUITS IN LOAD CELLS

An account is given here of the strains indicated by the bridge circuit, the negative normal bridge circuit and the shear bridge circuit, under different magnitudes of loads for the various tests.

The loads were allowed to act for the time intervals stipulated.

TABLE C.1

Strains Indicated by the Bridge Circuits in the Load Cells for Test One

Duration of Load Application in Mins	Load	Cell Nos.	Positive Normal Bridge Circuit	Negative Normal Bridge Circuit	Shear Bridge Circuit
			Output Strains in Micro Inch per Inch		
		1	-33	-22	-3
		2	-27	-28	-15
5	805.03 lb	3	-23	-30	0
	[3.58 KN]	4	22	-28	-13
		5	3	-17	-16
		6	4	-15	-3
		1	-107	-94	-22
		2	-114	-96	-6
5	3239.8 lb	3	-83	-99	-5
	[14.42 KN]	4	89	-92	-20
		5	24	-65	-28
		6	-38	-61	-16
		1	-148	-142	-27
		2	-172	-144	0
5	6185.0 lb	3	-133	-154	-10
	[27.52 KN]	4	142	-142	-19
		5	52	-107	-36
		6	-69	-115	-23
		1	-193	-176	-36
		2	-206	-178	+3
5	8541.2 lb	3	-166	-192	-20
	[38.0 KN]	4	183	-180	-24
		5	67	-137	-48
		6	-90	-158	-36
		1	-219	-203	-46
		2	-216	-198	5
5	10465.43 lb	3	-186	-221	-29
	[46.57 KN]	4	218	-213	-30
		5	74	-157	-60
		6	-105	-189	-50

TABLE C.2

Strains Indicated by the Bridge Circuits in the Load Cells for Test Two

Duration of Load Application in Mins	Load	Cell Nos.	Positive Normal Bridge Circuit	Negative Normal Bridge Circuit	Shear Bridge Circuit
			Output Strains in Micro Inch per Inch		
		1	-34	-39	-5
		2	-35	-35	-6
5	2770.0 lb	3	-24	-30	-3
	[12.33 KN]	4	19	-23	-13
		5	15	-27	-14
		6	-13	-15	-8
		1	-83	-98	-12
		2	-77	-81	-16
5	4853.0 lb	3	-73	-81	-12
	[21.60 KN]	4	51	-54	-28
		5	46	-78	-42
		6	-27	-35	-24
		1	-222	-253	-45
		2	-187	-200	-40
5	11275.0 lb	3	-216	-225	-54
	[50.17 KN]	4	150	-138	-67
		5	110	-214	-126
		6	-68	-107	-74
		1	-297	-331	-59
		2	-242	-264	-52
5	14520.0 lb	3	-292	-305	-82
	[64.61 KN]	4	207	-187	-87
		5	115	-263	-169
		6	-91	-151	-103
		1	-339	-374	-72
		2	-272	-300	-59
5	16250.0 lb	3	-325	-343	-104
	[72.3 KN]	4	234	-212	-102
		5	121	-282	-196
		6	-101	-169	-120
		1	-469	-503	-124
		2	-344	-385	-97
		3	-383	-454	-183
5	18510 lb	4	328	-269	-163
	[82.37 KN]	5	151	-335	-280
		6	-118	-219	-173

TABLE C.3

Strains Indicated by Bridge Circuits in the Load Cells for Test Three

Duration of Load Application in Mins	Load	Cell Nos.	Positive Normal Bridge Circuit	Negative Normal Bridge Circuit	Shear Bridge Circuit
			Output Strains in Micro Inch per Inch		
		1	-53	-42	-2
		2	-40	-45	+2
17	2000 lbs	3	-52	-73	-1
	[8.9 KN]	4	31	-42	-3
		5	24	-43	-25
		6	-22	-38	-7
		1	-89	-73	-9
		2	-71	-77	+5
16	4000 lbs	3	-89	-123	-13
	[17.8 KN]	4	63	-77	-10
		5	47	-78	-51
		6	-45	-70	-19
		1	-118	-97	-15
		2	-102	-105	+6
17	6000 lbs	3	-125	-169	-24
	[26.7 KN]	4	93	-110	-18
		5	70	-111	-72
		6	-65	-100	-35
		1	-173	-150	-24
		2	±162	-161	+5
17	10000 lbs	3	-189	-246	-40
	[44.5 KN]	4	154	-172	-36
		5	116	-178	-107
		6	-110	-163	-64
		1	-227	-204	-38
		2	-224	-224	-2
17	13000 lbs	3	-243	-316	-67
	[57.85 KN]	4	219	-229	-69
		5	133	-227	-149
		5	-135	-212	-101

TABLE C.4

Strains Indicated by Bridge Circuits
in the Load Cells for Test Four

Duration of Load Application in Mins	Load	Cell Nos.	Positive Normal Bridge Circuit	Negative Normal Bridge Circuit	Shear Bridge Circuit
			Output Strains in Micro Inch per Inch		
15	3000 lbs [13.35 KN]	1	-62	-62	-6
		2	-48	-66	-14
		3	-61	-63	-6
		4	45	-38	-15
		5	40	-62	-32
		6	-23	-40	-20
15	4000 lbs [17.8 KN]	1	-83	-87	-12
		2	-70	-94	-20
		3	-74	-85	-16
		4	60	-53	-20
		5	45	-74	-44
		6	-33	-60	-33
15	5000 lbs [22.25 KN]	1	-96	-100	-15
		2	-85	-109	-16
		3	-89	-103	-21
		4	75	-69	-24
		5	46	-84	-50
		6	-37	-71	-43
15	6500 lbs [28.93 KN]	1	-114	-117	-18
		2	-102	-127	-17
		3	-106	-122	-25
		4	86	-87	-28
		5	65	-102	-47
		6	-48	-83	-45
15	7500 lbs [33.38 KN]	1	-124	-130	-20
		2	-114	-142	-20
		3	-116	-134	-29
		4	97	-97	-32
		5	76	-117	-52
		6	-63	-97	-50
15	9000 lbs [40.05 KN]	1	-139	-146	-19
		2	-129	-158	-26
		3	-129	-151	-29
		4	110	-107	-34
		5	92	-136	-52
		6	-75	-113	-54

TABLE C.5

Strains Indicated by the Bridge Circuits in the Load Cells for Test Five

Duration of Load Application in Mins	Load	Cell Nos.	Positive Normal Bridge Circuit	Negative Normal Bridge Circuit	Shear Bridge Circuit
			Output Strains in Micro Inch per Inch		
15	1000 lbs [4.45 KN]	1	-15	-15	-3
		2	-24	-27	+2
		3	-20	-21	-2
		4	21	-22	0
		5	13	-19	-9
		6	-14	-23	-11
15	2000 lbs [8.9 KN]	1	-35	-33	-4
		2	-43	-48	-2
		3	-44	-47	-6
		4	46	-45	-5
		5	27	-46	-25
		6	-26	-46	-24
15	3000 lbs [13.35 KN]	1	-61	-58	-2
		2	-58	-69	-13
		3	-69	-78	-18
		4	66	-57	-14
		5	37	-69	-47
		6	-49	-72	-33
15	4000 lbs [17.8 KN]	1	-79	-73	0
		2	-68	-82	-13
		3	-91	-103	-17
		4	74	-65	-6
		5	62	-99	-53
		6	-72	-85	-18
15	4500 lbs [20.03 KN]	1	-87	-82	0
		2	-77	-90	-10
		3	-101	-112	-16
		4	84	-74	-2
		5	74	-115	-52
		6	-80	-97	-18

APPENDIX D

LOAD AND SETTLEMENT TESTS RESULTS

In this section, the settlements of the 1' x 2' (30.48 cm x 60.96 cm) footing for the various tests under different magnitudes of load are tabulated.

These results have been duly plotted and are shown in Figures 6.2.1, 6.2.2, 6.2.3, 6.2.4 and 6.2.7.

TABLE D.1

Load and Settlement Test Results for Test One

Pressure Indicated by Hydraulic Jack Gauge		Load		Settlement of Footings	
in psi	in kPa	in lbs	in KN	in inches	in cm
0.0	0.0	0.0	0.0	0.0	0.0
41	282.9	805.03	3.58	0.3125	0.794
165	1138.5	3239.8	14.42	0.375	0.953
315	2173.5	6185.0	27.52	0.4375	1.111
435	3001.5	8541.2	38.00	0.5	1.27
533	3677.7	10465.43	46.57	0.5625	1.429
560	3864.0	10999.6	48.95	0.625	1.588
630	4347.0	12370.0	55.05	0.75	1.905
730	5037.0	14333.515	63.78	0.875	2.223
830	5727.0	16297.01	72.52	1.125	2.858
850	5865.0	16689.7	74.27	1.4375	3.651

TABLE D.2

Load and Settlement Test Results for Test Two

Duration of Load Application in Mins.	Load Indicated by Hydraulic Jack Pressure Gauges	Load Indicated by Load Cell		Settlement			
				Dial Gauge A	Dial Gauge B	Average	
	in psi	in lb	in KN	in inches	in inches	in inches	in cms
0	0	0	0	0	0	0	0
0	0	230	1.024	0.003	0.004	0.0035	0.0089
5	0	1045	4.65	0.030	0.034	0.032	0.0813
5	0	1860	8.28	0.067	0.068	0.0675	0.172
5	0	2770	12.33	0.107	0.117	0.112	0.285
5	150	4853	21.60	0.217	0.235	0.226	0.574
5	500	11275	50.17	0.374	0.394	0.384	0.975
5	500	11460	51.0	0.478	0.499	0.489	1.241
5	700	14520	64.61	0.726	0.737	0.732	1.858
5	800	16200	72.31	0.848	0.862	0.855	2.172
5	800	17190	76.50	0.955	0.971	0.963	2.446
5	850	18180	80.90	1.152	1.207	1.195	3.034
5	900	18510	82.37	1.308	1.306	1.312	3.333
5	900	18720	83.30	2.361	2.372	2.367	6.01
30	900	19936	88.72	3.195	3.203	3.199	8.126

TABLE D.3

Load and Settlement Test Results for Test Three

Duration of Load Application	Load in lbs	Load in KN	Settlement in inches	Settlement in cm
0.0	0.0	0.0	0.0	0.0
16	1000	4.45	0.0394	0.1
17	2000	8,90	0.059	0.15
14	3000	13.35	0.12	0.30
16	4000	17.8	0.197	0.50
17	5000	22.25	0.256	0.65
17	6000	26.7	0.315	0.80
16	7500	33.375	0.374	0.95
17	10000	44.5	0.57	1.45
18	12000	53.4	0.689	1.75
17	13000	57.85	0.748	1.90
20	14000	62.3	0.827	2.10
15	15000	66.75	0.886	2.25
17	16000	71.2	0.945	2.40

TABLE D.4

Load and Settlement Test Results for Test Four

Duration of Load Application in Mins.	Load		Settlement			
			Dial Gauge A	Dial Gauge B	Average	
	in lbs	in KN	in ins.	in ins.	in ins.	in cm
0	0	0	0	0	0	0
15	1000	4.45	0.054	0.069	0.0615	0.156
15	2000	8.9	0.134	0.135	0.1345	0.342
15	3000	13.35	0.482	0.457	0.4695	1.193
15	4000	17.8	0.782	0.768	0.775	1.969
15	5000	22.25	1.211	1.211	1.211	3.076
15	5500	24.48	1.937	2.026	1.982	5.033
15	6000	26.7	2.454	2.448	2.451	6.226
15	6500	28.93	3.071	3.074	3.0725	7.804
15	7000	31.15	3.240	3.226	3.233	8.212
15	7500	33.38	3.824	3.927	3.8755	9.844
15	8000	35.6	4.395	4.385	4.39	11.151
15	9000	40.05	5.181	5.171	5.176	13.47
15	9500	42.28	5.621	5.618	5.6195	14.274
15	10000	44.50	6.001	6.000	6.0005	15.241

TABLE D.5

Load and Settlement Test Results for Test Five

Duration of Load Application in Mins.	Load		Settlement	
	in lbs	in KN	in ins	in cm
0	0	0	0	0
15	1000	4.54	0.356	0.904
15	2000	8.9	0.943	2.395
15	3000	13.35	2.322	5.898
15	3500	15.573	3.645	9.258
15	4000	17.8	4.642	11.791
15	4500	20.03	5.512	14.00